IAEA HUMAN HEALTH REPORTS No. 8

Development of Procedures for In Vivo Dosimetry in Radiotherapy

IAEA
International Atomic Energy Agency

IAEA HUMAN HEALTH SERIES PUBLICATIONS

The mandate of the IAEA human health programme originates from Article II of its Statute, which states that the "Agency shall seek to accelerate and enlarge the contribution of atomic energy to peace, health and prosperity throughout the world". The main objective of the human health programme is to enhance the capabilities of IAEA Member States in addressing issues related to the prevention, diagnosis and treatment of health problems through the development and application of nuclear techniques, within a framework of quality assurance.

Publications in the IAEA Human Health Series provide information in the areas of: radiation medicine, including diagnostic radiology, diagnostic and therapeutic nuclear medicine, and radiation therapy; dosimetry and medical radiation physics; and stable isotope techniques and other nuclear applications in nutrition. The publications have a broad readership and are aimed at medical practitioners, researchers and other professionals. International experts assist the IAEA Secretariat in drafting and reviewing these publications. Some of the publications in this series may also be endorsed or co-sponsored by international organizations and professional societies active in the relevant fields.

There are two categories of publications in this series:

IAEA HUMAN HEALTH SERIES

Publications in this category present analyses or provide information of an advisory nature, for example guidelines, codes and standards of practice, and quality assurance manuals. Monographs and high level educational material, such as graduate texts, are also published in this series.

IAEA HUMAN HEALTH REPORTS

Human Health Reports complement information published in the IAEA Human Health Series in areas of radiation medicine, dosimetry and medical radiation physics, and nutrition. These publications include reports of technical meetings, the results of IAEA coordinated research projects, interim reports on IAEA projects, and educational material compiled for IAEA training courses dealing with human health related subjects. In some cases, these reports may provide supporting material relating to publications issued in the IAEA Human Health Series.

All of these publications can be downloaded cost free from the IAEA web site:

http://www.iaea.org/Publications/index.html

Further information is available from:

Marketing and Sales Unit
International Atomic Energy Agency
Vienna International Centre
PO Box 100
1400 Vienna, Austria

Readers are invited to provide their impressions on these publications. Information may be provided via the IAEA web site, by mail at the address given above, or by email to:

Official.Mail@iaea.org.

DEVELOPMENT OF PROCEDURES FOR IN VIVO DOSIMETRY IN RADIOTHERAPY

The following States are Members of the International Atomic Energy Agency:

AFGHANISTAN
ALBANIA
ALGERIA
ANGOLA
ARGENTINA
ARMENIA
AUSTRALIA
AUSTRIA
AZERBAIJAN
BAHRAIN
BANGLADESH
BELARUS
BELGIUM
BELIZE
BENIN
BOLIVIA
BOSNIA AND HERZEGOVINA
BOTSWANA
BRAZIL
BULGARIA
BURKINA FASO
BURUNDI
CAMBODIA
CAMEROON
CANADA
CENTRAL AFRICAN REPUBLIC
CHAD
CHILE
CHINA
COLOMBIA
CONGO
COSTA RICA
CÔTE D'IVOIRE
CROATIA
CUBA
CYPRUS
CZECH REPUBLIC
DEMOCRATIC REPUBLIC OF THE CONGO
DENMARK
DOMINICA
DOMINICAN REPUBLIC
ECUADOR
EGYPT
EL SALVADOR
ERITREA
ESTONIA
ETHIOPIA
FIJI
FINLAND
FRANCE
GABON
GEORGIA
GERMANY
GHANA
GREECE
GUATEMALA
HAITI
HOLY SEE
HONDURAS
HUNGARY
ICELAND
INDIA
INDONESIA
IRAN, ISLAMIC REPUBLIC OF
IRAQ
IRELAND
ISRAEL
ITALY
JAMAICA
JAPAN
JORDAN
KAZAKHSTAN
KENYA
KOREA, REPUBLIC OF
KUWAIT
KYRGYZSTAN
LAO PEOPLE'S DEMOCRATIC REPUBLIC
LATVIA
LEBANON
LESOTHO
LIBERIA
LIBYA
LIECHTENSTEIN
LITHUANIA
LUXEMBOURG
MADAGASCAR
MALAWI
MALAYSIA
MALI
MALTA
MARSHALL ISLANDS
MAURITANIA
MAURITIUS
MEXICO
MONACO
MONGOLIA
MONTENEGRO
MOROCCO
MOZAMBIQUE
MYANMAR
NAMIBIA
NEPAL
NETHERLANDS
NEW ZEALAND
NICARAGUA
NIGER
NIGERIA
NORWAY
OMAN
PAKISTAN
PALAU
PANAMA
PAPUA NEW GUINEA
PARAGUAY
PERU
PHILIPPINES
POLAND
PORTUGAL
QATAR
REPUBLIC OF MOLDOVA
ROMANIA
RUSSIAN FEDERATION
RWANDA
SAN MARINO
SAUDI ARABIA
SENEGAL
SERBIA
SEYCHELLES
SIERRA LEONE
SINGAPORE
SLOVAKIA
SLOVENIA
SOUTH AFRICA
SPAIN
SRI LANKA
SUDAN
SWAZILAND
SWEDEN
SWITZERLAND
SYRIAN ARAB REPUBLIC
TAJIKISTAN
THAILAND
THE FORMER YUGOSLAV REPUBLIC OF MACEDONIA
TOGO
TRINIDAD AND TOBAGO
TUNISIA
TURKEY
UGANDA
UKRAINE
UNITED ARAB EMIRATES
UNITED KINGDOM OF GREAT BRITAIN AND NORTHERN IRELAND
UNITED REPUBLIC OF TANZANIA
UNITED STATES OF AMERICA
URUGUAY
UZBEKISTAN
VENEZUELA
VIET NAM
YEMEN
ZAMBIA
ZIMBABWE

The Agency's Statute was approved on 23 October 1956 by the Conference on the Statute of the IAEA held at United Nations Headquarters, New York; it entered into force on 29 July 1957. The Headquarters of the Agency are situated in Vienna. Its principal objective is "to accelerate and enlarge the contribution of atomic energy to peace, health and prosperity throughout the world".

IAEA HUMAN HEALTH REPORTS No. 8

DEVELOPMENT OF PROCEDURES FOR IN VIVO DOSIMETRY IN RADIOTHERAPY

INTERNATIONAL ATOMIC ENERGY AGENCY
VIENNA, 2013

COPYRIGHT NOTICE

Marketing and Sales Unit, Publishing Section
International Atomic Energy Agency
Vienna International Centre
PO Box 100
1400 Vienna, Austria
fax: +43 1 2600 29302
tel.: +43 1 2600 22417
email: sales.publications@iaea.org
http://www.iaea.org/books

Printed by the IAEA in Austria
December 2013
STI/PUB/1606

IAEA Library Cataloguing in Publication Data

Development of procedures for in vivo dosimetry in radiotherapy. — Vienna : International Atomic Energy Agency, 2013.
p. ; 30 cm. — (IAEA human health reports, ISSN 2074–7667 ; no. 8)
STI/PUB/1606
ISBN 978–92–0–141610–0
Includes bibliographical references.

1. Radiation dosimetry. 2. Radiotherapy — Measurement. 3. Radiotherapy — Safety measures 4. Radiotherapy — Equipment and supplies — Quality control. I. International Atomic Energy Agency. II. Series.

IAEAL 13–00856

FOREWORD

In vivo dosimetry is a direct method of measuring radiation doses to cancer patients receiving radiation treatment. The purpose of in vivo dosimetry is to verify that the treatment is carried out as prescribed. Together with other treatment verification tools used in radiotherapy, in vivo dosimetry constitutes a part of the quality management system in a radiotherapy department. It is a suitable method both to monitor treatment delivery and to detect various errors early in the course of treatment. It may help to limit the escalation of an error to subsequent treatment sessions for a particular patient and to avoid systematic errors affecting many patients. At the same time, monitoring the dose delivery constitutes a safety measure, being a part of the patient radiation protection programme required by several national regulatory bodies. Even if no errors are detected, the in vivo measurement provides a treatment record confirming that the dose was delivered correctly within the expected tolerance.

There is no general consensus among radiotherapy centres on the cost effectiveness of in vivo dosimetry, and until recently its routine implementation was not widespread. Arguments are made that most treatments are carried out in a correct manner and that only a small fraction of patients actually benefit from rectifying errors, because very few are detected. However, a recent series of major accidents in radiotherapy, which would have been prevented if in vivo dosimetry systems had been in place, has strengthened the reasoning in favour of in vivo dosimetry. It is now more broadly considered that preventing the severe consequences of serious errors justifies the effort and costs of in vivo dosimetry programmes. This has generated an increasing interest among radiotherapy centres in the methodology for in vivo dosimetry.

The IAEA initiated a coordinated research project (CRP) entitled “Development of Procedures for In Vivo Dosimetry in Radiotherapy” in 2005. The emphasis of the CRP was on patient dose studies, both evaluating the clinical value of in vivo dosimetry and comparing different techniques for in vivo dosimetry in a clinical setting. Phantom studies to characterize the dosimeters used in this CRP and to develop the relevant methodology were performed prior to patient studies. The focus was on dose delivery verification at the beam axis (entrance dose) for stationary techniques. Well established dosimetry methods based on thermoluminescent dosimetry and semiconductor diodes were compared with those of newer devices based on metal oxide field effect transistor and optically stimulated luminescence technologies.

This publication reports on the in vivo dosimetry methodology developed and tested within the CRP and summarizes the results of the dosimeter characterization and in vivo measurements on patients conducted by the participants up until 2010. A set of written guidelines for clinical use of in vivo dosimetry systems with a list of possible restrictions and special considerations has been developed. The experience of this CRP may serve as a reference for a radiotherapy centre seeking to establish a well devised in vivo dosimetry programme and may be helpful for the selection of appropriate in vivo dosimetry systems suitable for particular clinical situations.

This CRP has been supported by in-kind contributions by Landauer (OSL), Thomson-Nielsen (MOSFET) and PTW (diodes), which provided equipment used by the CRP participants. These contributions are gratefully acknowledged. The IAEA is grateful for contributions by P. Mayles (United Kingdom). The IAEA officer responsible for this publication was J. Izewska of the Division of Human Health.

EDITORIAL NOTE

This report (including the figures, tables and references) has undergone only the minimum copy editing considered necessary for the reader's assistance.

This report does not address questions of responsibility, legal or otherwise, for acts or omissions on the part of any person. Although great care has been taken to maintain the accuracy of information contained in this publication, neither the IAEA nor its Member States assume any responsibility for consequences which may arise from its use.

The use of particular designations of countries or territories does not imply any judgement by the publisher, the IAEA, as to the legal status of such countries or territories, of their authorities and institutions or of the delimitation of their boundaries.

The mention of names of specific companies or products (whether or not indicated as registered) does not imply any intention to infringe proprietary rights, nor should it be construed as an endorsement or recommendation on the part of the IAEA.

The authors are responsible for having obtained the necessary permission for the IAEA to reproduce, translate or use material from sources already protected by copyrights. Material prepared by authors who are in contractual relation with governments is copyrighted by the IAEA, as publisher, only to the extent permitted by the appropriate national regulations.

The IAEA has no responsibility for the persistence or accuracy of URLs for external or third party Internet web sites referred to in this book and does not guarantee that any content on such web sites is, or will remain, accurate or appropriate.

CONTENTS

1. OVERVIEW OF IN VIVO DOSIMETRY IN RADIOTHERAPY

In vivo dosimetry involves the measurement of radiation doses to patients during their radiation treatment in order to ensure that the treatments are carried out as they were intended. For many years, it has been common practice to use in vivo dosimetry to check doses to organs at risk (e.g. skin, eye or rectum). The primary goal of in vivo dosimetry, however, is quality assurance (QA) of the radiotherapy process. It is considered an important part of quality management of a radiotherapy department. Following recommendations by the World Health Organization (WHO), the International Commission on Radiological Protection (ICRP), the IAEA [1–3] and other bodies [4–6], the use of in vivo dosimetry has become more widespread.

In vivo dosimetry is used for the overall verification of the chain of treatment preparation and delivery. As such, it measures the radiation dose to the patient, which can be affected by many variables in the overall radiotherapy process. The global results of measurements of patient doses provide the information necessary for assessment of the accuracy and precision in dose planning and delivery for a specific treatment site, or by a given radiotherapy machine. In vivo dosimetry can also be used for the estimation of uncertainties in radiation treatment at a given institution.

In vivo dosimetry is also a tool for the detection of systematic errors and the prevention of unintended exposures of patients undergoing radiotherapy. Although it may not prevent the misadministration of a single dose, it will minimize the possibility of escalating such an event to many treatments or many patients. In vivo dosimetry can detect radiation under- or overdosing early in the course of treatment, so that corrections can be made in subsequent irradiation sessions. For example, the radiotherapy accident in Panama [2] involved a calculation error in the treatment planning process. If in vivo dosimetry had been used on these patients, the escalation of the mistreatment consequences would have been eliminated and many patients would not have suffered as a result of this error. In this context, in vivo dosimetry constitutes an important component of a radiation safety system of a radiotherapy department and should be used for all patients undergoing radiation treatments.

The methodology is well established for in vivo patient entrance dose measurements [4, 5, 7–11] using solid state dosimeters, mainly semiconductor diodes. Entrance dose measurements enable the detection of errors in beam calibration, machine output instability and use of incorrect accessories as well as patient set-up errors such as the use of incorrect treatment distance. In vivo exit dose measurements detect most of the errors found by the entrance dose measurements; in addition, they provide information about differences in radiological patient thickness and heterogeneities in the patient's anatomy. Entrance and exit dose measurements give results for a specific point, whereas the in vivo dosimetry technique based on the electronic portal imaging device (EPID) is a two dimensional, image based method [12]. It provides a direct relationship between the measured dose values and the beam and patient geometries. It is particularly useful for dynamic treatment delivery techniques such as intensity modulated radiation therapy (IMRT). Since this method utilizes an imaging system, information on the dose distribution relative to the patient's anatomy and the beam axis is obtained. EPID in vivo dosimetry and patient set-up verification complement each other in the verification of correct treatment execution. The current interest in EPID based in vivo dosimetry is mainly from the research point of view, and there is limited routine clinical use. This is due to the fact that developmental work is still ongoing in academic centres, and adequate software is not yet commonly available.

In spite of the availability of the various in vivo dosimetry systems, the routine clinical implementation of such systems remains quite limited, even in industrialized countries. This is partially related to the implementation of record and verify (RV) systems and the general belief in their usefulness in detecting patient set-up errors, as well as beam energy, treatment accessory and geometry errors. Indeed, RV systems provide on-line verification of treatment parameters that have been entered into the system during treatment planning, and therefore they ensure direct error free data transfer to the treatment delivery. However, if mistakes are made at the treatment planning and data input stages of the treatment preparation, these mistakes will be transferred to the treatment execution. Some errors in treatment planning may be detected by a systematic verification of the planned dose using the independent monitor unit calculation method [9, 13–18]. However, a recent series of radiotherapy accidents in advanced radiotherapy centres [19, 20] led to the conclusion that only the direct measurement of the dose actually delivered to the patient gives the information as to whether the treatment was carried out as it was intended. Therefore in vivo dosimetry is recommended for routine verification of the dose delivery for all groups of patients undergoing

radiotherapy. The methodology for characterization and clinical implementation of in vivo dosimetry systems is the subject of this report.

2. OVERVIEW OF THE COORDINATED RESEARCH PROJECT

The coordinated research project on "Development of Procedures for In Vivo Dosimetry in Radiotherapy" was proposed by a group of international consultants in 2003. The goal was to assist participating Member States in developing and evaluating procedures for in vivo dosimetry to make them potentially available to radiotherapy centres in various countries. The ultimate goal was to contribute to the improvement of radiation dosimetry practices and increased precision of dose delivery to cancer patients.

A group of CRP participants was formed in 2004 representing the following countries: Brazil, Canada, China, Colombia, Croatia, Pakistan, Poland and the United Kingdom. The participants were medical physicists working in radiotherapy centres and research institutions, who had adequate equipment, staffing and knowledge levels to carry out the research proposed within this CRP. The centres participating in the measurements on patients already had some experience with in vivo dosimetry systems and access to a sufficient number of patients to be monitored. The main part of research work done under this CRP was completed in 2008, but participants continued to collect measurements on patients in subsequent years. The participants from Colombia and Pakistan took part in the initial part of the CRP only; therefore, their reports are not included in this report. The main contributions of the Canadian and UK participants were to the development of the common methodology used within the CRP for the dosimeter characterization, tests on phantoms and the procedure for the introduction of routine in vivo dosimetry in clinics.

This CRP was supported by in-kind contributions from manufacturers of in vivo dosimetry systems, which provided the equipment used by the CRP participants. These were: Landauer (USA), Thomson-Nielsen (Canada) and PTW (Germany). The IAEA Dosimetry Laboratory contributed to this CRP by providing technical support to the participants.

The purpose of this CRP was to evaluate the state of the art of in vivo dosimetry using point dose measurements. Various characteristics of in vivo dosimetry systems were evaluated, either based on existing knowledge or through experimental investigations leading to new developments where a methodology was currently lacking for emerging in vivo dosimetry methods.

In vivo dosimetry systems under study in this CRP can be divided into two categories: established (i.e. thermoluminescence dosimeters (TLDs) and semiconductor diodes), and recently developed or emerging (i.e. metal oxide semiconductor field effect transistor (MOSFET) and optically stimulated luminescent dosimetry (OSLD)).

TLD is a well established technique used for several applications in radiotherapy such as mailed dosimetry [21–24], inter-institution dose comparisons, measurements in phantoms and in vivo dosimetry on patients. TLDs are also useful for those applications in which small dosimeters are required (e.g. in the areas of high dose gradients, to record the dose to critical organs or for in vivo dose verification in brachytherapy). TLD equipment needed for in vivo dosimetry such as readers, annealing ovens and dosimeters are available in many radiotherapy hospitals in developing countries. A disadvantage of TLDs is that there is no on-line readout available during treatment delivery.

Semiconductor dosimeters or diodes were introduced in the early 1980s. Since then, a growing interest in their use has been observed in the medical physics community. There are a large number of papers addressing their basic characteristics as well as practical considerations for the clinical use of this type of dosimeter. This has resulted in a number of review documents presenting the state of the art of in vivo dosimetry with diodes [4, 5]. Diodes have the advantage of instantaneous readout of measured doses. A disadvantage might be the need to handle the cables which connect the diodes on the patient to the electrometer located outside of the treatment room.

MOSFET dosimeters provide for a fast readout of the dose. In addition, the information is permanently stored in the MOSFET. Therefore, a measurement of total accumulated dose over the treatment course can be obtained. Their main advantage is their small size. This makes them very useful for measurements in high dose gradient regions, typical, for example, in brachytherapy. It also allows them to be easily inserted inside body cavities without causing too much discomfort to the patient. They do not require connection to the reader during the irradiation

time, which eliminates the need for cables running across the treatment room. Their disadvantage is their limited lifetime. MOSFET dosimeters are relatively new in radiotherapy compared with TLDs and diodes. Their accuracy has been reported to be similar to that of diodes and somewhat better than that of TLDs when used under controlled laboratory conditions.

OSLD using aluminium oxide (Al_2O_3) was developed in an industrial environment and is in use in personal dosimetry worldwide. Al_2O_3 based dosimetry systems have not been characterized for clinical applications in radiotherapy to the same extent as other systems [25–28]. Complete dosimetric characterization of the material in terms of energy and angular dependence, dose–response linearity and response to different radiation beam qualities are just a few of the areas that have been evaluated under this CRP. The dosimeters used in the study were made of Al_2O_3 powder coated on a substrate in the form of 'dots'. They were used in a passive mode registering an integrated dose, similar to TLDs. Since the method of reading uses optically stimulated luminescence (OSL), the reading process is much simpler and less time consuming than that for TLDs. In addition, the Al_2O_3 material can be read multiple times, which may prove advantageous in the case of measurements that may appear suspect. The main advantage of OSLDs is that they can be reused after optical bleaching; however, their sensitivity depends on the accumulated dose [29], which limits their useful lifetime.

2.1. WORK DONE UNDER THE CRP

The emphasis of the CRP was on patient studies, both to evaluate the clinical value of in vivo dosimetry and to compare different techniques for in vivo dosimetry in a clinical setting. Phantom studies to characterize new dosimeters and to develop the relevant methodology complemented the patient studies. MOSFET and OSLDs were investigated and compared with established techniques (i.e. TLD and diodes for use under the local conditions in the CRP participating institutions).

Clinical evaluation and development of the various techniques for in vivo dosimetry started with studies of patients treated with ^{60}Co or high energy X rays for pelvic tumours. From a technical point of view, in vivo dosimetry is most straightforward for this patient group. The accuracy achievable for in vivo dosimetry for the pelvic site has been well documented in industrialized countries [4, 11, 30, 31], and it was of interest to compare their results with those from selected institutions in developing countries. Depending on the time and resources available, participating institutions continued with other treatment sites or studied the use of in vivo dosimetry for special techniques such as total body irradiation (TBI), IMRT and field matching.

For external beam therapy, the initial focus was on dose delivery verification at the beam axis (entrance dose).

Initially, the clinical studies were primarily aimed at gathering data, which were displayed as histograms of dose deviations. These histograms have been used to establish action levels and action protocols for non-conforming results. The clinical research has also resulted in recommendations on how to avoid and deal with false positive warnings and on the required frequency of patient measurements.

Simultaneously with patient dose measurements using TLD and diodes, a group of CRP participants started characterizing MOSFETs for in vivo dosimetry using phantom studies. The other institutions characterized OSLDs. For TLDs and diodes, the required corrections for the dosimeter readings are generally well known. For MOSFETs and OSLDs, several correction factors have been investigated. The investigations included dosimeter intrinsic characteristics (i.e. energy and angular dependence, fading, non-linearity and dose rate dependence) as well as environmental corrections (i.e. temperature dependence and clinically related corrections, such as wedge factors, field size dependence and source–skin distance (SSD) dependence).

For all in vivo dosimetry techniques, procedures were developed and documented to obtain adequate measurement accuracy and precision.

The use of an appropriate buildup cap is of crucial importance for in vivo dosimetry with TLDs, diodes, MOSFETs and OSLDs. For diodes, some work has already been done, and the published data were made available to the participants of the CRP [4, 5]. For MOSFETs, buildup caps were provided by the manufacturer. Studies of buildup caps were conducted for TLD and OSL dosimeters by the IAEA. Special attention was paid to the selection of the appropriate materials for buildup caps, taking into account the impact of low energy radiation and attenuation of the beam. In general, beam attenuation behind the in vivo dosimeter equipped with the buildup cap should not exceed 5%.

Finally, each institution performed clinical comparisons of its selected established technique with the new technique that it has characterized. For this purpose, parallel in vivo dose measurements were performed on patients using the two systems. Selected participants compared TLDs with MOSFETs, TLDs with OSLDs, diodes with MOSFETs, and diodes with OSLDs.

The results of the measurements using TLD and diodes were compared to the measurements performed with MOSFETs and OSLDs, and this led to development of guidelines for their clinical use.

2.2. CRP RESULTS

The scientific yield of the CRP is at the level of the research radiotherapy centres in developing countries with the potential transfer of knowledge to other centres. A new methodology and procedures for in vivo dosimetry, developed with active input of all participants, have contributed to the improvement of dose delivery to cancer patients treated with radiotherapy in participating centres.

Based on the results of the measurements performed within the CRP involving the new dosimeters' characterization, a comparative analysis has been done indicating dosimeter properties particularly suitable for use in specific clinical situations. A set of written guidelines for a given in vivo dosimetry system with a list of possible restrictions and special considerations has been developed that was adapted to the local circumstances of each institution participating in the CRP. In addition, based on the series of patient dose measurements, this report describes the accuracy and precision of the various in vivo dosimetry systems in routine clinical use in a developing country scenario. Once sufficient data for in vivo dosimetry had been collected, data on the distribution of patient doses was obtained. As a spin-off of the CRP, the origin of the systematic deviations in the participating institutions was traced.

A set of extensively tested buildup caps for TLD and OSLD needed for patient dose measurements was made available through this CRP.

The detailed results of the CRP are presented in this report, including the description of the methodology for the characterization of in vivo dosimetry systems and their introduction to a clinical practice. Work performed by individual participants is given in the annexes. This report may serve as reference material for a radiotherapy centre seeking to introduce in vivo dosimetry and may be helpful for the selection of the appropriate in vivo dosimetry systems suitable for local conditions.

The research outputs of this CRP will contribute to the overall increase in radiation dosimetry expertise and to reducing the number of misadministrations of doses to radiotherapy patients which might have occurred without in vivo dosimetry.

3. DOSIMETRY SYSTEMS EVALUATED IN THE CRP

This section describes the characteristics of the four dosimetry systems which were evaluated in this CRP. The text should provide sufficient information to enable readers to understand the dosimetry system in question, but for an in-depth understanding, readers are referred to the extensive literature on the subject, some of which is cited below. All of these dosimetry systems produce some form of relative dosimetry signal for which a dose conversion factor must be derived by a process of calibration. The calibration procedures followed in this CRP are covered in Section 4.3.

For in vivo dosimetry, the aim is to measure the dose at the depth of dose maximum on either the entry or exit surface of the patient while minimizing the perturbation of the beam. If electronic equilibrium has not been reached by the sensitive part of the dosimeter, the results can be very dependent on factors which may affect the buildup of the dose on entering the patient, such as the field size, the use of wedges and trays, and the energy of the beam. For this reason it is standard practice to use buildup materials surrounding the dosimeter. Diode dosimeters (see Section 3.2) are usually supplied by the manufacturer with built-in buildup material, but the requirement for such buildup is not unique to diodes. If dosimeters are to be used without buildup, extensive measurements are required to characterize the influence of any factors that may affect the amount of dose buildup. This can make the

use of such dosimeters very complex, and for this reason, buildup caps have been used for all dosimeters in this CRP.

3.1. THERMOLUMINESCENT DOSIMETERS

3.1.1. Basic principles

Thermoluminescent dosimetry, or TLD, relies on the fact that in certain materials, electrons, when provided with sufficient energy, may be trapped in metastable states. By heating the material, these electrons may be given sufficient energy to escape from their unstable state. In the process of reverting to a stable state, they emit an optical photon. The optical photons can be detected by a photomultiplier and the light output measured. The readout process partly restores the dosimeter to its original state, and, with further heating to a high temperature, it is possible to eliminate any residual metastable electrons. This heating treatment is called annealing and allows the dosimeters to be reused almost indefinitely. For annealing and calibration, dosimeters are usually grouped together in batches.

This section and Section 4 cover similar topics to Chapter 11 of 'Radiotherapy Physics in Practice' by Mayles et al. [32], to which the reader is referred for more detail. Another recommended account of in vivo dosimetry with diodes and TLD is given by Marinello in the 'Handbook of Radiotherapy Physics' edited by Mayles, Nahum and Rosenwald [33].

3.1.2. Choice of TLD material

TLD materials come in many physical and chemical forms. The most commonly used material in radiotherapy is lithium fluoride doped with traces of magnesium and titanium (LiF:Mg,Ti). The production process was originally patented by Harshaw (patent now held by ThermoElectron) who manufactured the material as extruded ribbons which were then cut into chips approximately 3 mm square and 0.9 mm thick. This material is available as TLD 100 containing lithium with natural abundance (i.e. 92.5% ^{7}LiF and 7.5% ^{6}LiF). The two isotopes of lithium have different sensitivities to thermal neutrons and by using different proportions of ^{7}LiF and ^{6}LiF, a useful dosimeter for the differential detection of thermal neutrons can be produced. Other suppliers now provide a similar material in different shapes and sizes. A newer material, lithium fluoride, doped with about 2% of phosphorus and traces of magnesium and copper (LiF:Mg,Cu,P) [34], is more sensitive than LiF:Mg, Ti and is also said to have a lower sensitivity dependence on the energy of the radiation. LiF:Mg,Cu,P is very sensitive to incorrect thermal treatment [35], so for routine radiotherapy, use of LiF:Mg,Ti still has advantages. Other thermoluminescent materials are sometimes used but are outside the scope of this CRP.

LiF was originally used in powder form, and this is the form used by the IAEA/WHO/ TLD postal dose audit service [36–38]. Subsequently, other physical forms have been developed. Discs of LiF mixed with Teflon are widely used in radiation protection dosimetry, but the variability of sensitivity within a batch and the upper limit of 300°C on the temperature at which the discs can be annealed limit their use in radiotherapy. The two most useful forms are the chips already described: sintered discs and microrods. The latter are made of extruded material which is formed into rods 1 mm in diameter and 6 mm long. Chips (or sintered discs) are possibly easier to handle, but for some applications, microrods are particularly convenient as they can be accurately inserted into small cylindrical holes. In this report, the word 'chip' is used for any compressed form of dosimeter.

3.1.3. Readout

The two requirements to read out the dose given to a TLD sample are: a reliable form of heating and a method of measuring the light output. In one form of reader, the dosimeter is placed on a planchette and then pushed into the reader. A heater is then brought into contact with the underside of the planchette. Another form of reader uses hot gas to heat the dosimeter. Both types of reader are available with automatic sample changers. The advantages of the heated tray method are that any form of dosimeter, including powder, can be read, and the heating cycle can be controlled more precisely. The hot gas method is faster, and there is no dependence on the degree of thermal contact with the dosimeter or the reflectivity of the tray.

The light output of the dosimeter is measured with a photomultiplier. As the temperature of the dosimeter is increased, the light output will vary (see Fig. 1). The area under the so-called 'glow curve' (i.e. the total light output) is proportional to dose. The reading will be affected by the voltage applied to the photomultiplier. The integration of the area under the curve is carried out automatically and produces an arbitrary number which must then be converted into dose by a calibration process.

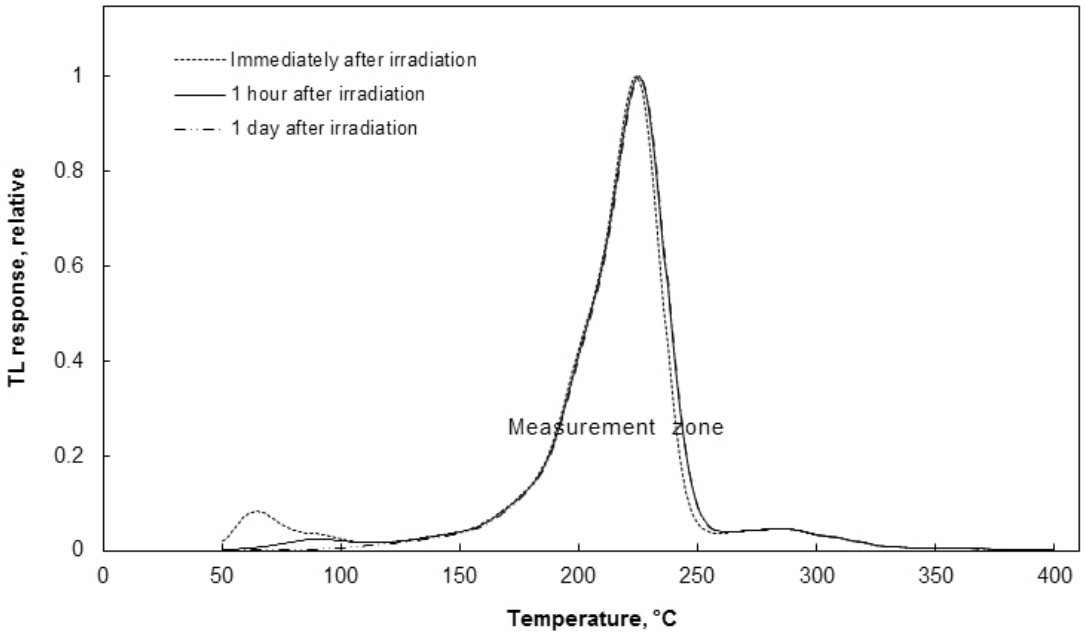

FIG. 1. TLD 100 glow curve. Readings are taken immediately after the TLD irradiation (dots), one hour after the irradiation (solid line) and one day after the irradiation (dash-dot line).

3.1.4. Linearity

The light output of LiF:Mg,Ti is linearly related to dose up to approximately 1 Gy, but after that, it becomes supralinear. The response of LiF:Mg,Cu,P is linear up to approximately 10 Gy [39], after which its response becomes sublinear. The necessary correction can be established by plotting the TL reading against dose for LiF:Mg,Ti as in Fig. 2. For a given TLD material with a consistent annealing cycle, the characteristic linearity curve will remain stable throughout its life, but it is wise to confirm this from time to time.

3.1.5. Energy and beam quality dependence

Horowitz [40] gives a useful review of the extensive and often contradictory literature on the energy dependence of LiF. The theoretical foundation is the Burlin formula for the ratio of the photon dose, D_{det}, recorded by a radiation dosimeter, to the dose D_{med} to the medium in which it is placed:

$$D_{det} = D_{med} [d\{\text{mass stopping power ratio}\} + (1-d)\{\text{mass energy absorption coefficient ratio}\}] \quad (1)$$

where d is a factor to allow for attenuation of secondary electrons in the dosimeter. For a small dosimeter (compared to the secondary electron range) $d = 1$ and for a large dosimeter $d = 0$ (see Ma and Nahum [41] for further details). For an electron beam, only the first term in equation (1) applies, and d may be regarded as a perturbation correction [42]. For energies between 200 keV and 3 MeV, both the stopping power ratio and the mass energy absorption coefficient ratio for LiF are almost unchanged. Mobit et al. have shown that, as expected, the differences in sensitivity of LiF at different megavoltage energies are small, both for photons [43] and for electrons [44], and

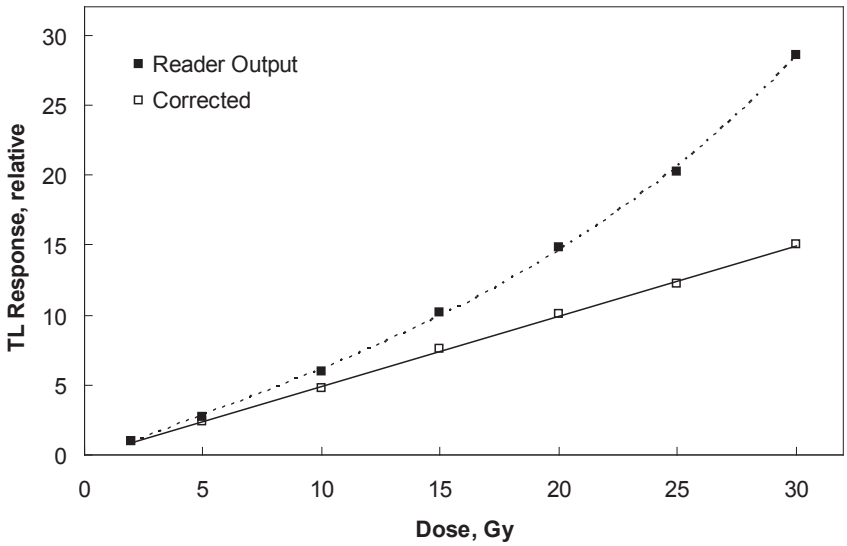

FIG. 2. TLD linearity graph for TLD 100 (LiF:Mg,Ti).FIG. 2. TLD linearity graph for TLD 100 (LiF:Mg,Ti).

in many situations, LiF measurements may be easier to convert to dose than ion chamber measurements. The following conclusions may be drawn:

(a) The simplest approach is to calibrate the chips against an ionization chamber using the beam quality that is to be used for the measurements.
(b) If a ^{60}Co beam is used for calibrations, the measured doses will need to be multiplied by a factor ranging from 1.01 for 6 MV X rays to 1.025 for 25 MV X rays [43] and from 1.04 for 2 MeV electrons to 1.03 for 20 MeV electrons [44]. The necessary correction increases towards the end of the electron range [45].
(c) If thicker TLD materials are used, or if dosimeters are stacked up, the correction factors will increase.
(d) For X ray energies below 300 kV, it is essential to calibrate the TLDs in the relevant beam. The calibration coefficient will be expected to follow the variation in the mass energy absorption coefficient ratio. LiF:Mg,Cu,P is a better dosimeter for use at these energies.
(e) The widely varying results obtained by different workers illustrate the need for careful consideration when the energy spectrum of the radiation is changing. Some of these differences may be accounted for by poor ionization chamber reference dosimeter measurements.

3.1.6. Angular dependence

The angular dependence of TLD is only a problem in so far as the orientation of the chips can affect the size of the cavity. This is more important for electrons and in brachytherapy, where the dose gradient may be high. However, it is always sensible to irradiate normal to the flat face of chips or to the long axis of microrods. However, for in vivo dosimetry where buildup caps are used, the angular dependence results from the attenuation and scatter in the buildup cap as well as the angular response of TLD.

3.1.7. Fading

Fading is the term applied to the decrease in the thermoluminescent signal between irradiation and readout. This is caused by electrons in the lower energy traps moving into the stable state and mainly affects the lower temperature traps. It is important, therefore, that the readout process excludes the low temperature thermoluminescent signal (see Fig. 1). Fading can be reduced by waiting for an hour or more before reading the TLDs, but this should be unnecessary if an appropriate readout cycle is used.

3.1.8. Background signals

Some doses will be recorded even if the dosimeters have not been irradiated. Under normal circumstances, background signals will be no more than 1 mGy. The background signal comes from the dark current of the photomultiplier and from the residual signal from previous irradiations. The dark current increases following exposure to light (i.e. if the equipment is opened for servicing) and after switch-on, the amplifier may take some time to stabilize, so the reader should therefore be left on all the time, unless a rapid warm up facility is built in to the reader (e.g. a cooled photomultiplier). Residual signals from previous irradiations should not be a problem if an adequate annealing cycle is used.

TLD materials naturally produce a small luminescence signal in the absence of radiation. This may be associated with chemical reactions on the surface of the dosimeters (called chemiluminescence) or, especially with powder, with movement in the crystal lattice (called tribothermoluminescence). This can be minimized by carrying out the readout in an atmosphere of high purity nitrogen, although this should not be necessary at radiotherapy doses. Reader associated background and the inherent TLD background can be distinguished by running the read cycle without a dosimeter and with an unirradiated dosimeter.

3.1.9. Annealing

The residual signal after the dosimeter has been read out is removed by heating the dosimeter to a temperature above the readout temperature. A facility to do this is built into some readers. However, this increases the readout time and is not fully effective, particularly if the dosimeters have been submitted to large doses; therefore, in this case, it is better to use a separate annealing oven. The annealing cycle should follow the recommendations of the manufacturer of the TLD material as it can be different for different materials.

Annealing involves maintaining the dosimeters at a high temperature and then allowing them to cool in a controlled way. The time taken to cool from the high temperature to the low temperature is a determinant of the sensitivity of the dosimeter, with faster cooling leading to higher sensitivity. The annealing cycle should therefore be as reproducible as possible. It is particularly important that any one batch of chips should be given identical treatment. This can be achieved by putting all the dosimeters together into an oven in a tray made of stainless steel, glass or anodized aluminium. Ordinary aluminium may contaminate the dosimeters and should not be used. Metal trays have the advantage of conducting heat and therefore contributing to the uniformity of the heat treatment. Trays made in house should have their holes counterbored so that the surface is smooth and flat, and it is especially important to remove all traces of oil.

3.1.10. Glow curves

The glow curve as shown in Fig. 1 is a plot of the output of the photomultiplier against the temperature of the dosimeter. Most modern readers have a built-in computer interface that permits storage and display of the glow curves. This is a useful facility as it allows retrospective analysis of the glow curve in the event of unexpected readings.

The heating cycle typically has three phases: a low-temperature pre-readout anneal to eliminate the low temperature peaks, the measurement phase when the light output from the main peak is integrated, and a high temperature post-readout anneal. The duration and temperature of each of these phases can usually be adjusted by the user to conform to the cycle recommended by the reader manufacturer for that particular type of material.

The glow curve is important as a method of determining whether the readout cycle is appropriate for the dosimeter used. The low temperature peaks should not be included in the integration; however, the higher temperature dosimetry peaks (see Fig. 1) should be fully included. If the start point of integration is too soon, fading will increase and if the upper cut-off point occurs before the readout of the dosimetry peak is completed, the variability of the results will increase.

3.1.11. Calibration

The calibration technique used depends on the form of the dosimeter and the accuracy required. A detailed description of the calibration process used in this CRP is given in Section 4.3. With careful calibration and appropriate replication of the measurements, it is possible to achieve between 1% and 3% accuracy. It should be realized that the process shows inherent statistical variability, and that the uncertainty will be related to the number of photomultiplier counts. It is essential that the physicist in charge of the system has a full understanding of these issues, as without proper care, it is possible for TLD results to show very large variations. It is especially important to realize that both the measurement and the calibration exposures contribute to the uncertainty of the final result.

The use of powder is described in detail by several authors [21, 23, 38, 46–50]. Equal quantities of powder are dispensed into sachets or capsules before irradiation using a special dispenser. After irradiation, the powder from each capsule is transferred to the planchette and read out. For the greatest accuracy, portions of powder sufficient for several readouts are put in the capsule and then dispensed in sequence onto the planchette after irradiation.

3.1.12. Packaging and handling

UV radiation can have an effect in increasing both the background and fading. Neither effect is likely to be a problem with LiF for therapeutic doses, but it is advisable to avoid exposure to UV light and to store the dosimeters in the dark.

It is essential that TLD materials do not become contaminated, especially with grease. They must therefore not be touched by hand. The only really satisfactory method of handling rigid materials is to use vacuum tweezers. If chips become contaminated, they should be washed in pure alcohol and rinsed in deionized water. However, it is not recommended that this should be a frequent procedure. Severely contaminated dosimeters should be discarded. Planchettes should be cleaned in a similar way.

Planchette reflectivity may change the measured light output by several per cent, and cleaning should be done at regular intervals. Variation in reflectivity between planchettes is a problem for automatic multi-planchette readers. Higher precision can be achieved in manual mode with only one planchette or by associating specific chips with specific planchettes [51]. Similar problems may occur with automatic readers using measuring cupels, unless the cupels receive special thermal treatment before use that reduces reflectivity.

3.2. DIODES FOR DOSIMETRY

Semiconductor diodes are useful in radiation dosimetry because of their high radiation sensitivity relative to the ionization volume. Therefore, the measuring volume can be very small, leading to good spatial resolution. Semiconductor diodes offer many advantages for clinical dosimetry: high sensitivity, real time readout, simple instrumentation, robustness and air pressure independence. However, diodes are subject to influence from a number of factors, including temperature dependence and, for a rigorous system, consideration needs to be given to all of these. Many publications on the properties of diodes are available (see, for example, Refs [4, 5, 52–54]).

3.2.1. Theory of operation

Most semiconductor diodes are made from silicon that is either n type (silicon doped with group V material, e.g. phosphorus) or p type (silicon doped with group III material, e.g. boron). To form a dosimeter, a p–n junction must be created.

During irradiation, electron hole pairs are created. These charge carriers are collected under the action of the field that exists across the depletion region. In this way, a current is generated, flowing in the reverse direction to normal diode current flow. The rise time can be fast enough to see individual pulses of a linear accelerator, but this is dependent on the way the dosimeter is operated.

Diodes for dosimetry are operated without an external reverse bias voltage to minimize leakage. Without external bias, the output signal of the diode can be measured in short circuit mode (current) or open circuit mode (voltage). A simple electrometer can be used in each case. Short circuit mode is the mode of choice since it has the advantage of producing a linear relationship between the charge generated in the diode and the dose. In short circuit

mode, shown in Fig. 3, the electrometer must have a low dynamic input impedance, as is provided by an operational amplifier with a feedback loop and a low offset voltage. As the diode signal is quite high, the electrometer used only needs to have moderate gain. It is usual for diode systems to have a multichannel electrometer.

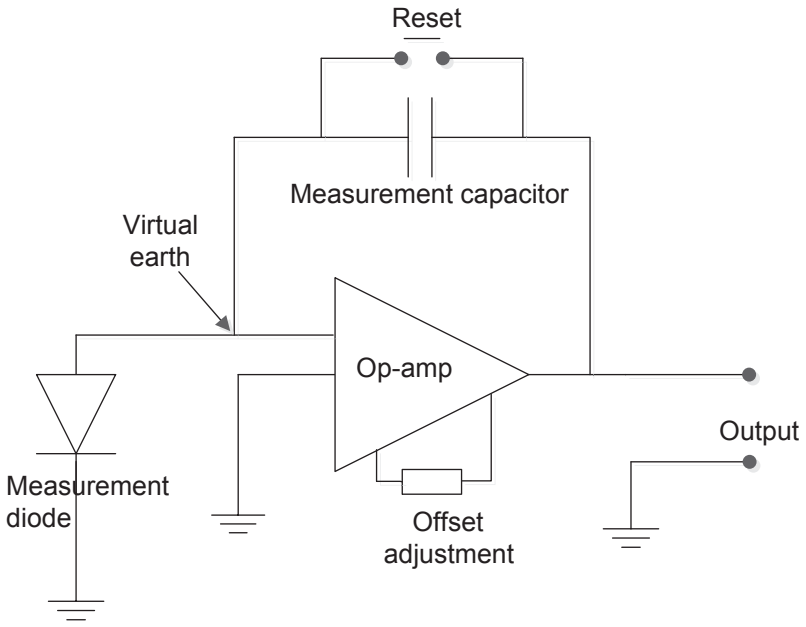

FIG. 3. Diode measurement circuit.

3.2.2. Diode encapsulation

Diodes are fragile and need to be encapsulated. As described in the introduction to Section 3, the encapsulation usually includes the necessary material to achieve full buildup (domed diodes), although sometimes the amount of buildup is inadequate for the quoted energy [4, 5, 52, 55]. If unit density material were used, it would be inconveniently bulky. To reduce the bulk, metallic buildup caps are usually used.

3.2.3. Temperature effects

The internal resistance of a diode decreases as the diode temperature increases. This property can be used to measure the temperature of the diode before each measurement, and this facility is incorporated into some commercial systems. The sensitivity usually increases with temperature (although an anomalous decrease in sensitivity has been reported). This is due to changes in parameters such as carrier mobility and the number of traps in the dosimeter crystal. The variation of sensitivity with temperature depends on the accumulated dose received by the diode. Typically, the sensitivity will increase with temperature by less than 0.1% per °C when the diode has not been irradiated, but after a dose of 6 kGy with 20 MeV electrons (more with photons), this may increase to 0.4% per °C [4, 56]. The sensitivity and temperature dependence of an unirradiated diode varies quite rapidly with the dose it has received and for this reason many manufacturers preirradiate diodes before sale in order to produce a more stable product, albeit with a higher temperature dependence. When a diode is placed on a patient, its temperature will rise by approximately 10°C from room temperature in 2 to 3 minutes and then reach a steady state. If the sensitivity variation is found to be significant, the diodes should be left to reach body temperature for at least 3 minutes before the measurement is begun and a correction made for the difference in temperature between calibration and measurement. Diodes can be calibrated at body temperature using a water phantom containing warm water. Alternatively, as recommended in this CRP, a thin layer of expanded polystyrene insulator can be placed between the diode and the patient so that the diode remains at room temperature.

3.2.4. Background signal

Even in the unbiased mode of operation, a diode will generate a dark current due to thermally generated charge carriers. This is only a problem when low doses and dose rates are being measured and if the input offset voltage of the electrometer is not zero. The background signal is strongly temperature dependent, and some diodes generate increasingly high currents as the temperature rises, even at reasonably low accumulated doses. The background signal can change by 4 mGy/min between room temperature and body temperature. The effect appears to be greater for n type diodes than for p type diodes. Although the current can be zeroed out before measurements are taken, several minutes are necessary to obtain a satisfactory background measurement, and any subsequent change in temperature will upset the balance of the circuit and cause a change in diode response.

3.2.5. Radiation damage

Radiation damage occurs when silicon atoms are displaced from their lattice sites. This introduces recombination centres which capture charge carriers leading to the reduction in sensitivity mentioned in Section 3.2.3 and to an increase in dose rate dependence. P type diodes are generally less affected by radiation damage than are n type diodes, which show a pronounced drop in sensitivity with accumulated radiation doses. The amount of damage for a given dose is dependent on radiation quality. For example, 20 MeV electrons are 20 times more damaging than 8 MV photons [53]. When subjected to radiation damage, the n type diode response becomes non-linear with dose rate. Therefore, the more expensive p type diodes are recommended for general use as they show a linear response with dose rate even after very high dose irradiation, and have a smaller sensitivity drop with accumulated doses. N type diodes can be used in ^{60}Co beams.

3.2.6. Energy dependence

Silicon is far from being tissue equivalent, especially for low energy radiation. For this reason energy compensated diodes are used for water phantom dosimetry in photon beams. The stainless steel used to provide the buildup material for surface dose measurements also has the effect of shielding the diode from low energy scattered radiation. Care must be taken when making measurements at depth in a phantom (for which diodes supplied for in vivo dosimetry were not designed) or in TBI fields where low energy scattered radiation contributes a substantial fraction of the dose.

3.2.7. Angular dependence

For domed diodes, directional dependence is not expected to be a significant factor until the radiation is angled greater than 30° from a line perpendicular to the diode baseplate. The actual dependence is related to the shape and construction of the diode. In most applications, the diodes will be placed on a surface perpendicular to the radiation beam axis, and thus correction factors can be neglected. However, the diodes do exhibit an asymmetry of calibration that can be as much as 15% when irradiated from the flat side compared to irradiation from the domed side [32]. Cylindrical diodes have a cylindrically symmetrical response, but the response reduces by about 15% towards the tip [32].

3.2.8. Calibration

Calibration of diodes is in two parts: calibration against an ionization chamber in a standard set-up to establish the diode calibration coefficient for absorbed dose to water $N_{w,diode}$ and the establishment of a series of correction factors to account for calibration differences when measurements are performed under various experimental conditions. The values of $N_{w,diode}$ for individual diodes may vary widely, but the correction factors will usually be close to 1.0 and will be similar for diodes of the same type. The techniques used for calibration in this CRP are described in Section 4.3.

3.3. DOSIMETRY USING MOSFETs

MOSFET dosimeters were introduced into radiation dosimetry in the early 1980s [57] and into radiation therapy dosimetry in the early 1990s [58, 59]. Since then, MOSFET use has expanded in both external beam and brachytherapy, as well as in diagnostic radiology. MOSFETs are particularly useful in high dose gradient radiation fields because of their small size. This feature provides a good spatial resolution of measurements, especially important in IMRT, radiosurgery and brachytherapy. MOSFETs offer some other advantages for clinical dosimetry such as the possibility of real time readout, simple instrumentation and robustness. In addition, dual MOSFET dual voltage dosimeters are temperature independent, which is an advantage in clinical dosimetry. MOSFETs also allow for permanent dose storage, since there is little fading of the signal with time.

However, MOSFETs have a limited lifetime, which depends on the thickness of the silicon oxide layer and the mode they are used in. Many publications on the properties of MOSFETs are available (see for example Soubra et al. [58], Ramaseshan et al. [60], Scalchi et al. [61, 62] and Jornet et al. [63]).

3.3.1. Theory of operation

As depicted in Fig. 4, a MOSFET is a transistor with three electrical connections (terminals): source, drain and gate. The type shown is called a p channel enhancement MOSFET, which is built on a negatively doped (n type) silicon substrate. Two terminals, the 'source' and 'drain', are situated on top of a positively doped (p type) silicon substrate region. The terminal known as the 'gate' is situated on top of a thin silicon oxide (SiO_2) layer which is in contact with the n type region of the silicon substrate. This n type region immediately below the SiO_2 layer is known as the 'channel' region. When a sufficiently large negative (in respect to the substrate) voltage, V_g, is applied to the gate, a number of minority carriers (holes in this case) is attracted to the silicon–silicon oxide interface from other regions of the silicon substrate, and the n type material immediately under the SiO_2 layer is gradually converted into a p type material. Thus a conduction channel (p type in this case) is formed allowing for the current, I_{ds}, to flow between the source and the drain, if they are biased [64]. The value of V_g, above which a certain predetermined I_{ds} current is attained, is called the 'threshold voltage', V_{TH}. The thickness of the channel is <0.1 µm. V_T is the main electrical parameter of a MOSFET.

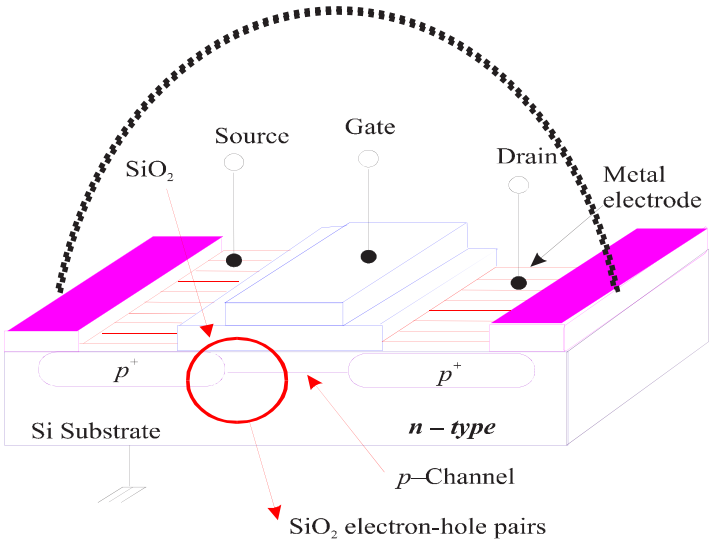

FIG. 4. Construction of a MOSFET.

For dosimetry purposes, MOSFET dosimeters can operate either in 'active' or in 'passive' mode. A MOSFET with a setting of $V_g > 0$ during irradiation is said to operate in the active mode, while an unbiased MOSFET ($V_g = 0$) is said to operate in the passive mode. When operating in the passive mode, the MOSFET does not require any bias

supply, which improves portability but at a cost of reduced sensitivity. In this project, only dual MOSFET dual bias dosimeters operating in active mode were used, and therefore the rest of the discussion will be mostly concerned with this type of dosimeter.

When the MOSFET is exposed to ionizing radiation, electron hole pairs are created in the SiO_2 layer. If $V_g > 0$ during irradiation, holes are pushed away from the gate towards the Si/SiO_2 interface, where they become trapped. As a consequence, the previous V_{TH} value can no longer switch the MOSFET on. An increase of V_{TH} by ΔV_{TH} (voltage shift) is required for the same I_{ds} current to pass through the drain to the source as before the irradiation (see Fig. 5). The resulting ΔV_{TH} is proportional to the absorbed dose.

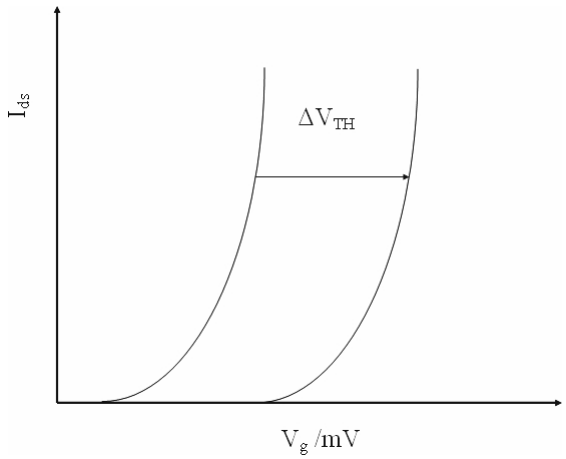

FIG. 5. Voltage shift ΔV_{TH} during MOSFET operation.

3.3.2. MOSFET encapsulation

MOSFETs are fragile and need to be encapsulated. Encapsulation may cause a non-uniform dosimeter response with respect to the irradiation beam angle. Such anisotropy of dosimeter response may also depend on the energy of the radiation.

3.3.3. Temperature dependence

For a single MOSFET dosimeter, the relationship between V_{TH} and I_{DS} can be especially susceptible to temperature. Temperature changes can affect V_{TH} by as much as 4 to 5 mV per °C [65]. Some MOSFETs showed a high temperature coefficient variation (40 mV or 8 cGy for 15 °C variation, which is equivalent to a dose of 8 cGy), and great care needs to be taken if used on a patient [66]. A 1.5% decrease in response at 37 °C in comparison with the response at 20 °C was reported for another type of MOSFET, although no value was indicated for the temperature coefficient (mV/°C) [67]. Dual bias dual MOSFET dosimeter circuits were devised to limit these dependencies [58]. They have been shown to have a negligible temperature dependence (0.015 mV/°C) in the range 0 to 80 °C [58, 60, 68].

3.3.4. Radiation damage

MOSFETs have a limited lifetime due to the increase of trapped charge in the oxide layer. Saturation occurs after a specific amount of dose, depending on the thickness of the oxide layer, and MOSFET dosimeters stop working.

3.3.5. Energy dependence

Silicon and silicon oxide are not tissue equivalent, especially for low energy radiation. For this reason, the sensitivity of MOSFET dosimeters depends on the energy of the ionizing radiation. The response of MOSFETs has been shown to be energy independent within ± 2–3% over a wide range of electron (5 MeV to 21 MeV) and photon (4 MV to 25 MV) therapy beams [60, 68].

Below 0.6 MeV, the MOSFET response increases with decreasing energy. Indeed, for quasi-monoenergetic low X ray energies (12 keV to 208 keV), MOSFET sensitivity was found to be 4.3 times higher at 33 keV than at 6 MV [69]. Similarly to diodes, this has been attributed to the secondary electron stopping power ratios of silicon to water, producing peak sensitivity at an incident energy of approximately 30 keV.

3.3.6. Angular dependence

The angular dependence of the MOSFET dosimeter is related to its shape and construction. Since the shape of the MOSFET dosimeter is not spherical and its structure is not homogeneous, the dosimeter may have a different response for different beam directions.

In general, full buildup set-ups where charged particle equilibrium exists (e.g. the sensor is positioned inside a cylinder [70] or hemisphere [60, 68, 71]) give more isotropic results than surface set-up or in air measurements [61, 62].

The angular dependence of MOSFET dosimeters for orthovoltage beam energy was evaluated by Cygler et al. [72].

In addition, angular dependence of MOSFET response is a function of beam energy. Therefore it should be evaluated before using the dosimeters for patient measurements.

3.3.7. Calibration

Calibration of MOSFETs is similar to that of other dosimeters used for in vivo dosimetry (i.e. calibration against an ionization chamber in a standard set-up to establish the MOSFET calibration coefficient for absorbed dose to water $N_{w,MOSFET}$ and the determination of a series of correction factors when measurements are performed under various experimental conditions different from the standard set-up). The methodology used in this CRP for MOSFET calibration is described in Section 4.3.

3.4. OPTICALLY STIMULATED LUMINESCENCE DOSIMETERs (OSLDs)

OSLDs have been routinely used as passive personal dosimeters for almost a decade, following the successful introduction and development of carbon doped aluminium oxide (Al_2O_3:C) [73, 74]. Although the OSLD principle of operation is similar to the principle of operation of TLDs, the OSLD readout is done by simply illuminating the dosimeters. Heating prior to or after irradiation is generally not necessary.

OSLDs and TLDs share some similar features: they work mostly as passive dosimeters, require no power or cable, can be made very small for spatial resolution, are not subject to electromagnetic interference or atmospheric pressure effects, and can be used for measurements of a wide range of doses, from environmental to radiotherapy levels. However, the high sensitivity of Al_2O_3:C and the all optical nature of the OSL technique combined provide additional convenient features such as almost non-destructive readouts with readout periods under 1s [75]. OSLDs can also be used for imaging or as probes in optical fibre dosimetry [76, 77].

In addition to the literature available on OSL dosimetry in general [78, 79], recent articles have started to explore the potential advantages of OSLDs for medical dosimetry [80–83]. However, best practices are not yet established. Recent reviews on OSL applied to medicine include Akselrod et al. [84] and Yukihara and McKeever [25].

3.4.1. Theory of operation

There are two main processes responsible for the dosimetric properties of OSLDs: the trapping of electrons and holes created by ionizing radiation in defects of the crystal and optical stimulation of the trapped charges during readout, leading to electron hole recombination and luminescence. The luminescence detected during readout is proportional to the initial concentration of trapped charges, which in turn is proportional to the absorbed dose in the dosimeter.

Figure 6(a) shows the elements of an OSL reader schematically, including a light source (light emitting diodes, lasers, lamps, etc.) for stimulation and a photomultiplier tube (PMT) for light detection. For optimum discrimination between the luminescence and stimulation light, the stimulation wavelength should be shifted with respect to the dosimeter's main luminescence band. Optical filters with transmission coinciding with the dosimeter luminescence band are placed in front of the PMT to block the stimulation light. In most cases, these detection filters are not sufficient to completely block the photons coming from broadband light sources. Therefore, additional optical filters are placed in front of the light source to block the wavelength components that would pass through the detection filters.

Figure 6(b) shows a typical OSL curve (i.e. the intensity of an irradiated Al_2O_3:C as a function of the stimulation time). The OSL intensity is highest during the initial stimulation owing to the large concentration of trapped charges and the consequent large number of charges stimulated out of the traps. However, it decreases with 'exponential-like' behaviour as the traps are emptied. The OSL intensity and total area under the curve (total light emitted) are proportional to the absorbed dose, but the shape of the OSL curve also depends on the stimulation intensity and wavelength [85]. By controlling the stimulation time, intensity and wavelength, it is possible to increase or decrease the amount of trapped charges stimulated during each OSL readout (i.e. the amount of depletion of the OSL signal). OSL signals with sufficient intensity for dosimetry purposes can be produced by short stimulation times with low light intensity, leaving most of the trapped charges intact for future readouts.

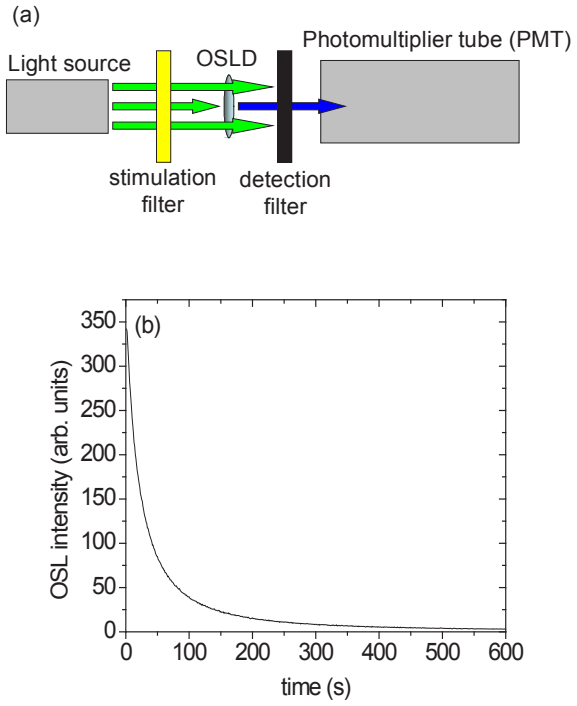

FIG. 6. (a) Schematics of the main elements in an OSL reader; (b) Typical OSL curve of an irradiated Al_2O_3:C dosimeter under green stimulation.

Control over the stimulation intensity provided by light emitting diodes (LEDs) and lasers enables different readout approaches. In the most simple and convenient approach, the so-called continuous wave OSL (CW-OSL), the dosimeter is illuminated with constant intensity with simultaneous detection of the luminescence. Another approach is the pulsed OSL (POSL) technique, which consists of stimulating the dosimeter with light pulses while detecting the luminescence asynchronously [74]. Because of the long luminescence lifetime of the luminescence centres in Al_2O_3:C, an appropriate choice of timing parameter allows most of the luminescence to be detected in between the stimulation pulses. This time based discrimination between stimulation and luminescence reduces the requirements in terms of optical filters, allowing higher signal-to-noise ratios to be achieved by using optical filters more appropriate for the dosimeter's emission. This is particularly convenient for low dose measurements but not particularly necessary for the dose levels in radiotherapy.

3.4.2. Readers and dosimeters

There are currently two types of OSL readers commercially available: multipurpose automated research readers [86] and readers that are part of Landauer's InLight™ dosimetry system [87], which includes the portable microStar™ reader. Some laboratories have also set up their own OSL readers [88].

The InLight readers use an array of green LEDs operating in CW-OSL mode as the stimulation source. The dosimeters are stimulated only for a short time (1 s). The luminescence is detected using a PMT protected by Hoya B-370 filters (bandpass filter with 50% transmission limits at 320 nm and 420 nm). The InLight readers can operate in two readout modes, depending on the dose. At low doses, the maximum stimulation intensity is used to produce a high OSL signal, but as a result, each readout depletes the OSL signal by ~0.2–0.3%. At high doses, the reader can operate with lower stimulation intensity, resulting in a depletion per readout of less than 0.1%. The exact value of depletion rates may vary with reader unit. In the current software, the user can choose between the two readout modes using the 'hardware test' or 'calibration' mode. Otherwise, the choice is made automatically by the reader using a short 0.1 s stimulation test prior to the measurement. The crossover between the low dose and high dose range is of the order of 0.1 Gy from caesium-137 gamma rays, so for most of the measurements in radiotherapy, the high-dose range (low beam intensity) is selected automatically by the reader.

The InLight readers work with the same type of dosimeters used in Landauer's Luxel™ dosimetry system: Al_2O_3:C powder incorporated in a polymer tape of ~0.3 mm total thickness and cut to the desired size, depending on the application. The InLight badges contain four dosimeter elements, each one ~7 mm in diameter, from which an area of ~5 mm of diameter is exposed for readout. For medical applications, Landauer have introduced the InLight dot dosimeter, a carrier containing a one element dosimeter identical to those used in the InLight badge that can be read using a microStar reader with an adapter. The InLight dosimeter holders also protect against room light exposure that can erase part of the OSL signal.

General properties of Al_2O_3:C have been discussed in the literature review mentioned earlier. For radiotherapy applications, the main complicating factors can be the presence of transient signals originating from shallow trapping centres, sensitivity changes caused by previous irradiations, and non-linearity in the OSL signal for doses above a few grays. Sensitivity changes and supralinearity are related aspects caused by the filling of deep traps in the crystal [89, 90]. The influence of these factors on the precision and accuracy of dose estimates in radiotherapy will depend on the calibration protocol and still needs to be investigated, although calibration procedures have been proposed to account for the sensitivity changes and non-linearities using automated research readers [82, 91].

Other materials for OSL dosimetry are also currently under development [92, 93].

3.4.3. OSLD preparation

If necessary, the radiation induced signal accumulated by the Al_2O_3:C OSLDs can be reset by exposure to light. Due to the possibility of inducing an OSL signal by UV, short wavelengths should be avoided. Typically, any broadband light source with a UV blocking filter or longpass glass filter can be used. The exposure time required to reset the signal depends on the light intensity and dose history of the dosimeter. Typically, the signal can be reduced to less than 1% of the original value by exposure to fluorescent light filtered by a longpass Schott OG-515 glass filter (yellow), with an intensity of ~5 mW/cm^2 at the dosimeter position. Although the dosimeters can be reset, previous doses can cause sensitivity changes depending on the dose levels involved.

4. CHARACTERIZATION OF DOSIMETRY SYSTEMS

A common set of procedures for the characterization of in vivo dosimetry systems for clinical use was developed under this CRP. Before the dosimeters were used for patient measurements, a process was established to characterize the dosimeters and to determine a calibration coefficient that would enable the dose to be derived from dosimeter readings. Before carrying out measurements on patients, this system of dose assessment was tested using an Alderson Rando anthropomorphic phantom. This section describes the measurements carried out to prepare for the patient measurements.

4.1. PROCEDURES FOLLOWED ON RECEIPT OF DOSIMETERS PRIOR TO CALIBRATION

The procedures carried out to verify that a particular dosimeter was satisfactory for use were different depending on the dosimeter and are described in Sections 4.1.1–4.1.5.

4.1.1. TLD

A new batch of TLD dosimeters was first cycled 5 times without reading the results (i.e. the TL dosimeters were irradiated to about 100 cGy and then annealed). The annealing cycle followed the manufacturer's recommendations, e.g. for Harshaw TLD 100 it was 400ºC for 1 hour followed by 80ºC for 24 hours (or alternatively 400ºC followed by 100ºC for 2 hours). The annealing cycle used was recorded. The chips were allowed to stand at room temperature for at least 12 hours before use.

4.1.2. Diodes

The reproducibility and stability of new diodes were checked before calibrating them. The diode was positioned on top of a calibration phantom and irradiated 10–15 times with the same reference field. The standard deviation of the resulting signals should be within 0.5%. The measurements were repeated on different days over two weeks (at least four times). The measurement procedure, including the measurement equipment, the phantom set-up and diode positioning, was considered reliable and stable, if all measurements were within 1%, i.e. ±0.5% of the mean (assuming that the beam output of the treatment unit was stable as monitored by the ionization chamber) [4].

4.1.3. MOSFET

Because of the limited radiation life of MOSFET dosimeters, the amount of dose delivered during acceptance tests must be kept to a minimum. Three exposures of 50 cGy were recommended to check MOSFET response reproducibility before calibration. The three readings should be within 4%. A period of 2 minutes after irradiation was allowed before reading the dosimeter.

4.1.4. OSLD

Experience with OSLD is limited but the issues are similar to those of using MOSFETs. Because of the limited radiation life of the dosimeters, the amount of dose delivered during acceptance tests must be kept to a minimum. One exposure of 50 cGy was recommended, and then the dosimeter was read out 10 times to check reproducibility before calibration. The 10 readings should be within 4%. A period of 10 minutes after irradiation was allowed before reading the dosimeter. This period was based on the results of measurements which showed that there was very rapid fading of the signal in the first few minutes after irradiation (see Section 4.4.1.3 and Annex Sections I–5.1.6, III–5.4.1 and VI–3.1).

4.1.5. Dose rate dependence for diodes, MOSFET and OSLD

The quantity corresponding to dose rate that is relevant on a linear accelerator is dose per pulse. The dosimeter should be rejected if there is a dose rate dependence greater than 0.5% over the range of doses per pulse (or dose rate for ^{60}Co). The dose rate dependence should be checked by measuring the calibration coefficient as in Section 4.3.5 at the standard SSD and at the standard SSD + 30cm. For this purpose, it is necessary to know the percentage depth dose at the extended SSD. This may be calculated using the Burns formula (see Knight and Mayles [94]). The dose rate dependence may change with the accumulated dose, so the tests should be repeated regularly.

4.2. ENCAPSULATION OF DOSIMETERS

All measurements with all dosimeters used for teletherapy were made using a buildup cap (except when deriving the individual factors for TLD — see below). For diodes, this is usually provided by the manufacturer as part of the encapsulation of the diode. For MOSFETs, buildup caps can be provided by the manufacturer or made locally. For TLD and OSL dosimeters, buildup caps were designed within this CRP and provided by the IAEA (Fig. 7). Two buildup caps were manufactured, one for ^{60}Co (2 mm Al) and one for 6 MV and above (2 mm stainless steel).

FIG. 7. TLD buildup caps of aluminium (left bottom) used for measurements in a ^{60}Co beam and of stainless steel (left top) used for TLD measurements in 6 MV and 15 MV high energy photon beams. A 1 mm thick PMMA baseplate used for TLD encapsulation is also shown (right).

Verification of the water equivalent depth has been performed for buildup caps in which dosimeters were encapsulated. For this purpose, the dosimeter was placed on the surface of a solid phantom (10 × 10 cm, standard SSD) and measurements were taken adding slabs on top of the dosimeter until its reading reached the maximum. Air gaps need to be avoided when making this measurement, so the first plate was fabricated with an opening for a dosimeter (this slab was treated as providing zero additional buildup). Knowing the depth of the maximum dose for each beam and the water equivalent thickness of the slabs above the dosimeter, the water equivalent thickness of the buildup cap was calculated.

The perturbation of the radiation field caused by the dosimeter with a buildup cap was measured using a radiographic film placed at d_{max} and at 5 cm or 10 cm depth (depending on the photon beam quality) beneath the dosimeter.

For diodes, it was proposed to address the need (if it exists) for a temperature correction when placed on the patient's skin by separating the diode from the patient by a 2 mm thickness of styrofoam. This was also used throughout the calibration process.

4.3. CALIBRATION PROCEDURE

4.3.1. Introduction

The procedure for all in vivo dosimeters was to set them up on a phantom surface as shown in Fig. 8. For each beam and dosimeter, the appropriate buildup caps were used.

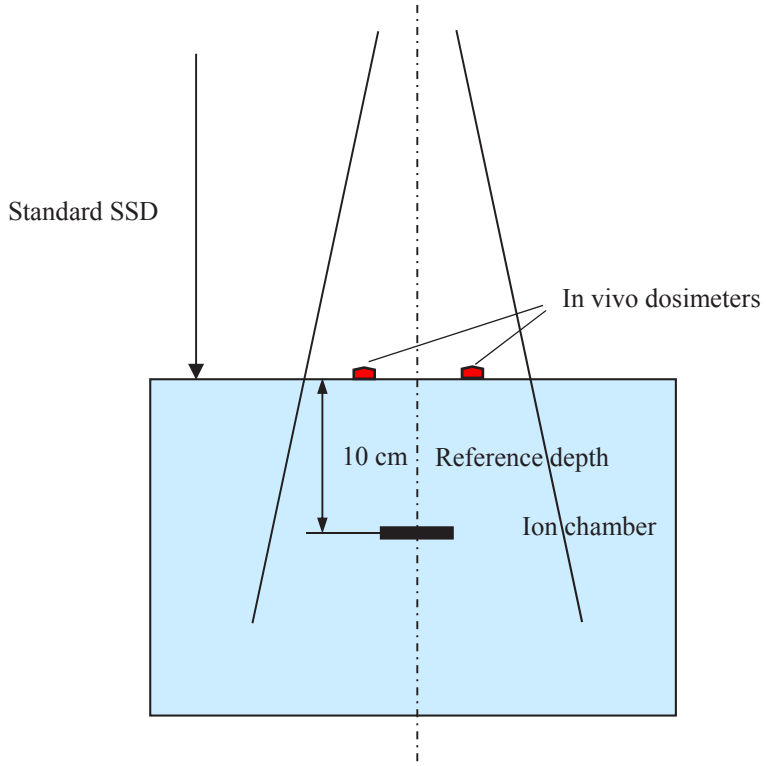

FIG. 8. Set-up of in vivo dosimeters for calibration.

The calibration was carried out with the ionization chamber at the reference depth used for the beam calibration. It was recommended that a solid water phantom be used, but if this was not available, a plastic phantom could be used provided that a correction factor was derived by measurement as described below. The calibration was to the dose at d_{max} in water with the phantom surface at the isocentre (SSD set-up), and the dose measured by the ionization chamber must therefore be increased according to the percentage depth dose at the measurement depth. The field size used for calibration was 10 cm × 10 cm. In order to minimize any subsequent SSD correction factor, a specific SSD correction to the position of the dosimeter was made both at calibration and for use on patients. For the calibration, the dosimeter reading was therefore multiplied by:

$$\left(\frac{SSD - d_s}{SSD + d_{\max}}\right)^2 \tag{2}$$

where SSD is the distance to the surface of the phantom and d_s is the distance from the surface of the phantom to the centre of the sensitive volume of the dosimeter. Note that this correction was also made when making measurements as described below.

The frequency of calibration depends on the dosimeter. For TLD, the factor must be established after each annealing. For diodes, monthly calibration was recommended, unless the calibration coefficient was found to change significantly between monthly calibrations. For MOSFETs, repeat calibration would be considered if patient measurements exceeded the action level. For OSL, the procedure was to irradiate each dosimeter to 50 cGy and to read it 5 times. If all the 5 readings were not within 4 %, the rejection of the dosimeter should be considered.

4.3.2. Individual calibration factors for TLD

TLD is different from the other solid state dosimeters in having a built-in statistical uncertainty between dosimeters, which cannot be measured non-destructively. For this reason, individual 'chip' factors were applied. If desired, subbatches from a much larger group of chips could be selected in order to minimize the sensitivity variation, but this was not essential. To establish the individual factors, the entire batch (the recommended size is 100–120 chips) that was to be annealed together was irradiated to the same dose (approximately 100 cGy) and then read out. This was carried out by laying all the chips side by side on a clean sheet of paper at an appropriate depth in a slab phantom or in a dedicated plastic phantom. Alternatively, but less satisfactorily because dose uniformity is harder to achieve, the chips could be irradiated in plastic trays supplied by the manufacturer. The fundamental requirement is that all the dosimeters receive the same dose. This may be conveniently carried out in a ^{60}Co beam using a field size that provides a margin of at least 3 cm around the chips. It is important to check the uniformity of the beam at the chosen depth (beams are often more uniform at a depth of between 4 cm and 7 cm than at d_{max}, and an extended SSD could also be used). If the beam non-uniformity over the area of the chips was greater than 0.5%, a correction should be applied. This process was repeated at least 3 times (following the preparation process described in Section 4.1.1). The chips were kept in trays supplied by the manufacturer or fabricated in house. Care should be taken if using metal trays as these could have non-uniform chemical composition or could become contaminated.

To calculate the individual factors, the average reading of all chips was calculated, and this was then divided by the reading of each chip to provide the 'chip factor', k_{chip}. There were therefore 3 subsequent measurements of each chip factor, and the factor to be used for all future measurements was the average of these 3. If the difference between the maximum and minimum measurement of the chip factor for an individual chip (taken in 3 subsequent sessions) exceeded 3%, it was recommended to reject it. Typically, not more than 5% of chips would need to be rejected. If a large percentage of chips needed to be rejected, it would be necessary to review the reader stability, chip handling and annealing process. Additionally, two further repeat measurements need to be carried out in order to see whether the variability of the TL response remained high. The variation of individual factors within a batch in the same reading session can range up to about 10%. A spreadsheet was produced to assist with this. For convenience, chips were individually labelled (e.g. A1–10, B1–10). The chips were irradiated in pairs and kept together so that if they were inadvertently exchanged, the effect would be minimal, although every effort was made to maintain their individual identity to facilitate monitoring of the variability.

4.3.3. Batch calibration for TLD

Following each irradiation of a TLD, it was annealed in accordance with the recommendations of the manufacturer of the chips. Following each annealing, the batch of chips was recalibrated using 5 IAEA buildup caps containing 2 chips each, which were selected from the batch at random. The calibration coefficient was the average of the outcome of the calibration measurements. At each calibration, the standard deviation of the 10 readings was calculated to monitor the reliability of the chips. If this standard deviation increased by a factor of 2 compared to the initial measurement, it was recommended that the entire batch should be recalibrated following remeasurement of the individual chip factors (see Section 4.3.2).

4.3.4. Verification of MOSFET and OSL reproducibility at different dose levels

The calibration dose initially selected for MOSFET dosimeters was 50 cGy. In order to verify that this did not compromise accuracy, a procedure was established whereby a dosimeter was set up on a calibration phantom, and doses of 50 cGy and 100 cGy delivered (5 times each). The standard deviation of each dose group was calculated.

If the 100 cGy standard deviation had been smaller by more than 20% than that of the 50 cGy group, 100 cGy would have been used (see Section 4.3.5). For OSL dosimeters, the calibration dose was 50 cGy.

4.3.5. Generic calibration process

The process for deriving the calibration coefficient for each individual dosimeter was essentially the same as outlined in Section 4.3.1. The dosimeters were placed at a point close to the central axis in a beam. The dosimeter calibration was performed for each beam to be used for in vivo dosimetry (a ^{60}Co beam and photon beams from a linear accelerator). The irradiation time was set to deliver D_0 = 100 cGy at d_{max} (for MOSFETs and OSL, D_0 = 50 cGy was used in order to extend the dosimeter lifetime, but see Section 4.3.4). The actual delivered dose D was measured with the ionization chamber at the reference depth. The dose delivered to the ionization chamber was calculated following the established protocol used in the country where the research was taking place (usually the IAEA TRS-398 Code of Practice [95]).

The calibration coefficient N_{cal} is given by:

$$N_{cal} = \frac{D_0}{M}\left(\frac{SSD - d_s}{SSD + d_{\max}}\right)^{-2} \cdot k_{pl} \tag{3}$$

where

D_0 = D/(PDD/100);
PDD is the percentage depth dose;
M is the in vivo dosimeter reading;

and k_{pl} is the plastic to water correction. k_{pl} is defined in Eq. (4).

For diodes, the irradiation was repeated 5 times (unless identical readings were obtained for 3 exposures). For MOSFETs, the irradiation was performed 3 times and for OSLD, 5 repeat readings were performed for each single exposure. As discussed in Section 4.3.3, for TLD, the calibration coefficient was averaged over the 10 chips used.

If a solid non-water phantom was used for measurements, the effect of this had to be measured. The general equation for the plastic-to-water correction factor, k_{pl}, is given by:

$$k_{pl} = \frac{\left[\frac{M_w}{D_w}\right]}{\left[\frac{M_{pl}}{D_{pl}}\right]} \tag{4}$$

where M_w, M_{pl} are the chamber readings corrected for influence quantities (temperature and pressure, and humidity if it is not in the range of 20% to 80%), and D_w and D_{pl} are the absorbed dose to water at d_{max} as measured in water and in plastic, respectively.

The procedure was as follows: The water tank was set up with the chamber at the depth used for standard calibration. D_0 = 100 cGy absorbed dose was delivered to water at d_{max} (100 MU or appropriate setting for cobalt to deliver 100 cGy). The chamber reading, M'_w, and the temperature, T_w, of the chamber in water (which should be close to room temperature) and room air pressure, P_w, at the time of measurement was recorded. The procedure was repeated 5 times. The average value and standard deviation was calculated. The solid phantom was set up in the same way as the water phantom with the chamber at the same depth. The same number of MU (or the same time period) was used. The chamber reading, M'_{pl}, and the corresponding temperature, T_{pl}, and pressure, P_{pl} was recorded.

As the same number of MU (or time period) was set for both water and plastic measurements, the doses cancel out, but the uncorrected readings M'_w and M'_{pl} have to be corrected for the influence quantities. The resulting formula is given by:

$$k_{pl} = \frac{M'_w}{M'_{pl}} \times \frac{P_{pl}}{P_w} \times \frac{T_w + 273}{T_{pl} + 273} \tag{5}$$

4.4. MEASUREMENT OF CORRECTION FACTORS

Correction factors intrinsic to the dosimeter, such as dose response non-linearity, energy, fading, angle of incidence and dose rate, as well as those which are beam dependent, such as SSD, field size, beam modifiers or wedge, were measured as described below. If the correction factor for the range of readings expected in clinical use was less than 1%, the factor would be set to 1.0 for all clinical measurements. However, the measured factors were recorded to allow retrospective data analysis.

4.4.1. Correction factors intrinsic to the dosimeter

4.4.1.1. Non-linearity dose response correction

Dosimeters were placed on the surface of the solid phantom, as for calibration, with the ionization chamber in position. They were given the following doses: 20, 50, 100, 150, 200, 300 and 400 cGy. If higher doses needed to be delivered in clinical practice, additional doses at 200 cGy steps were also measured.

The non-linearity dose response correction factor is defined as the ratio of the dosimeter response M per unit dose measured at the dose D_0 (corresponding to the dose at the calibration, see Section 4.3.5) to the dosimeter response per unit dose measured at the dose D.

$$k_{lin} = \frac{\left[\frac{M_{D_0}}{D_0}\right]}{\left[\frac{M_D}{D}\right]} \tag{6}$$

A graph was plotted of k_{lin} vs. the dose derived from the ionization chamber reading. If this graph showed that any correction was within 0.99–1.01, no further action was required. However, for TLD and OSLD, there was the necessity for a correction. A graph plotted of k_{lin} against dose can be converted into a formula (see the example in Mayles et al. [33]) or can be used as a lookup table.

4.4.1.2. Energy correction

The energy correction factor is defined as the ratio of the dosimeter response M to the delivered dose D_0 in a ^{60}Co γ ray beam to the ratio of dosimeter response to the delivered dose D_0 in the X ray beam of the beam quality D_{20}/D_{10}.

$$k_{engy} = \frac{\left[\frac{M}{D_0}\right]_{^{60}\mathrm{Co}}}{\left[\frac{M}{D_0}\right]_{X\,ray}} \tag{7}$$

The calibration coefficient, N_{cal}, was determined for ^{60}Co and for each high energy linear accelerator photon beam that was to be used for in vivo dosimetry. The calibration procedure is described in Section 4.3.5. The

ionization chamber has to be placed at the appropriate reference depth for each beam quality. The energy correction factor is the ratio of the calibration coefficient at the relevant energy to that for a ^{60}Co beam. However, it was recommended that the measured N_{cal} for each energy should be used. The measurement of the energy correction factor was to ensure the consistency of the in vivo dosimetry system. Typical values of the energy correction factor for LiF would be about 1.02–1.03 for 6 MV and 1.03–1.04 for 15–18 MV beams.

4.4.1.3. Fading correction

The fading correction factor is the ratio of the dosimeter reading taken with the reference delay Δt_{ref}, for which no fading is assumed, to the dosimeter readout taken with the delay Δt,

$$k_{fad} = \frac{\left(\frac{M}{D}\right)_{\Delta t_{ref}}}{\left(\frac{M}{D}\right)_{\Delta t}} \tag{8}$$

For TLD, it usually is a ratio of the response of a dosimeter irradiated and read on the day t_1 to the response of the dosimeter irradiated on the day t_1 and read on the day t_2. However, fading will not be relevant for TLD unless there is a significant variation in time between the irradiation and reading for different TLDs. The time delay should always be kept approximately constant. Also, TLDs should not be read out within 30 minutes of irradiation to avoid short-time fading. TLDs should be kept in the dark for most of their life.

Diodes are read out immediately, and fading is not therefore a consideration.

For MOSFETs, fading is only relevant if they are to be used to store measurements for an individual patient. It was not intended that this would be done in this project. It was recommended that readouts of MOSFETs should be performed 2 minutes after exposure.

For OSLD, fading is rapid in the first few minutes after irradiation, and therefore it was recommended that the dosimeters should be read after a constant time delay (e.g. 10 minutes after irradiation).

4.4.2. Beam dependent correction factors

The beam dependent correction factors described below were measured for each photon beam quality to be used for in vivo dosimetry, both for ^{60}Co and linear accelerators. For each beam, the appropriate buildup caps were used.

4.4.2.1. Angle of incidence correction

The dosimeter was placed on the surface of the solid phantom with the sensitive volume at the isocentre, and readings were taken for 100 MU (or equivalent for ^{60}Co) with the gantry at –60º, –45º, –30º, –15º, 0º, 15º, 30º, 45º, 60º. If M_{ang} is the reading at each angle, then the correction factor k_{ang} is given by:

$$k_{ang} = \frac{\left(\frac{M}{D}\right)_{0^\circ}}{\left(\frac{M}{D}\right)_{ang}} = \frac{M_{0^\circ}}{M_{ang}} \tag{9}$$

k_{ang} is not normally needed except when measuring areas such as the breast and larynx. The primary measurement of this factor was carried out at the middle energy to be used clinically (e.g. 6 MV). It was checked at 45º for each energy being used. If the factor differed by more than 1.0% from the primary measurement, then it would be necessary to carry out a full set of measurements for each energy.

4.4.2.2. SSD correction

In general, the SSD correction originates from three effects. Firstly, there is the geometric effect of the different distances from source to ionization chamber and from source to in vivo dosimeter. Secondly, there is the dose rate dependence pertaining to diodes and MOSFETs (see Section 4.1.5). The third effect is relevant for dosimeters with insufficient buildup and relates to the contribution to the dosimeter signal from contaminant electrons.

For dosimeters with appropriate buildup caps exhibiting low dose-rate dependence (tested as described in Section 4.1.5), the need for an SSD correction should be obviated by the specific inverse square correction between the depth of dose maximum and the position of the active volume of the dosimeter. However, it is necessary to verify that, in practice, no correction is required. The procedure was to place the dosimeter on the surface of the phantom as for the dosimeter calibration (Section 4.3.5) and perform measurements at 70, 80, 90, 100 and 110 cm with a fixed collimator opening (the same as for the reference conditions). The dose D_0 = 100 cGy at d_{max}, (corresponding to 100 MU or the equivalent time for ^{60}Co) was set for each distance. For this purpose, it was necessary to calculate the predicted dose at the extended SSD. This was calculated using the Burns formula as already described in Section 4.1.5. The dosimeter reading must be corrected for SSD to the depth dose maximum using the formula in Section 4.3.1.

The resulting formula is given by:

$$k_{SSD} = \frac{\left[\frac{M_0}{D_0} \times \left(\frac{(SSD_0 - d_s)}{(SSD_0 + d_{max})}\right)^2\right]}{\left[\frac{M_{SSD}}{D_{SSD}} \times \left(\frac{(SSD - d_s)}{(SSD + d_{max})}\right)^2\right]} \tag{10}$$

where SSD_0 corresponds to the standard treatment distance (as used for the dosimeter calibration), and SSD is the distance of interest.

The corrected dosimeter readings were then plotted against the SSD. If the graph implied that the correction needed for the range of SSDs to be used was greater than 1%, it would be necessary to include a correction.

4.4.2.3. Field size correction

The field size correction factor may be needed if the dosimeter is used for a wide range of beam sizes and the buildup thickness is insufficient as the changes in dose response originate from contaminant electrons, and the dosimeter is exposed to varying scatter conditions depending on the field size. The field size correction factor is defined as

$$k_{field} = \frac{\left[\frac{M}{D_0}\right]_{10\times10}}{\left[\frac{M}{D}\right]_{X\times X}} \tag{11}$$

D_0 refers to the absorbed dose to water at d_{max}, and ion chamber measurements should be converted from the reference depth in water to d_{max}. If both the dosimeter and ion chamber measurements were made in plastic, an appropriate conversion to derive absorbed dose to water at d_{max} should be used. Alternatively, ion chamber measurements could be made in water, while the measurements for the in vivo dosimeter were made on a solid phantom. For convenience, the formula describing k_{field} can be converted to group in vivo dosimeter measurements in the numerator and ion chamber measurements in the denominator.

$$k_{field} = \frac{\frac{(M)_{10\times10}}{(M)_{X\times X}}}{\frac{(D_0)_{10\times10}}{(D)_{X\times X}}} \tag{12}$$

4.4.2.4. Wedge correction

The wedge correction factor is sometimes needed because of the change in the beam energy spectrum associated with introducing a wedge into the beam. For virtual wedges, obtained by moving the linac jaws, this is unlikely to be necessary.

The wedge correction factor is defined as the ratio between the wedge transmission factor (*WF*) for a 10 cm × 10 cm open field, measured with an ionization chamber at the reference depth and converted to d_{max}, and the wedge transmission factor for the same field size, measured with the in vivo dosimeter placed on the surface of the solid phantom.

$$k_{wedge} = \frac{\left[\frac{M}{D}\right]_{open}}{\left[\frac{M}{D}\right]_{wedge}} = \frac{\frac{D_{wedge}}{D_{open}}}{\frac{M_{wedge}}{M_{open}}} = \frac{WF_{ic}}{WF_{det}} \tag{13}$$

where the wedge transmission factor is defined by:

$$WF = \frac{Dose\,at\,d_{max}\ for\,100MU\ with\,wedge}{Dose\,at\,d_{max}\ for\,100MU\ without\,wedge} \tag{14}$$

The measurement was carried out as follows. The solid phantom was set up as for calibration, but with the dosimeter accurately placed on the beam's central axis. D_{open} = 100 cGy, i.e. 100 MU (or 100cGy in a cobalt-60 beam) was delivered without a wedge. The MUs were then divided by the wedge factor, WF, in order to give the same dose at d_{max} as for the open field, MU_{wedge} = 100/WF and the relevant number of monitor units delivered. Under the measurement conditions ($D_{open} = D_{wedge}$), the wedge correction formula is simplified to:

$$k_{wedge} = \frac{M_{open}}{M_{wedge}} \tag{15}$$

If M_{open} and M_{wedge} differ by more than 1%, a correction will be needed. However, if the correction does appear to be significant, the value of WF as defined here should be carefully checked. If k_{wedge} is large for a 10 cm × 10 cm field size, it may be necessary to repeat the measurements for different field sizes, depending on the clinical use.

4.4.2.5. Block and tray correction

If in vivo dosimetry is used for blocked fields, the block and tray correction may be needed. Measurements of the correction factors are performed similarly as for wedge factors (see Section 4.4.2.4).

4.5. CLINICAL USE OF THE MEASURED CORRECTIONS

Once the corrections, as defined above, have been measured, it is possible to use the dosimeters clinically. Before use with patients, the measurement procedure needs to be verified using the Alderson Rando anthropomorphic phantom.

4.5.1. Calculation of entrance dose at d_{max} from dosimeter reading

For a patient measurement, the 'entrance dose', D, is defined as the dose at the depth of maximum dose. From the in vivo dosimeter reading, this is calculated as the product of the dosimeter reading, the calibration coefficient and correction factors for each individual beam:

$$D = M \cdot N_{cal} \cdot \prod_i k_i \tag{16}$$

where k_i are the relevant correction factors applicable for a given dosimeter in a specific clinical set-up. For example, for measurement at an angle, in a wedged beam geometry at an extended SSD and a small field size, the entrance dose calculation requires the following corrections:

$$D = M \cdot N_{cal} \cdot \left(\frac{SSD - d_s}{SSD + d_{\max}} \right)^2 \cdot k_{lin} \cdot k_{ang} \cdot k_{SSD} \cdot k_{wedge} \cdot k_{field} \tag{17}$$

N_{cal} refers to a dosimeter calibration in a given high energy photon beam. If TLD is used for this measurement, k_{chip} (see Section 4.3.2) would also be applied.

4.5.2. Calculation of expected dose

The expected dose was calculated using the treatment planning system (TPS) by placing a calculation point at the depth of d_{max} for each beam[1]. Some TPS will automatically calculate this. The contribution to the dose at the point from each beam separately is required, and all in vivo measurements are made measuring only one beam at a time. For the purposes of this calculation, the TPS should be used in absolute dose mode, and the calculated expected dose should be the dose that the TPS calculates for the exact number of monitor units that are to be used for the measurements.

The expected dose will be as calculated by the TPS and also using a 'manual' independent method. If the results of these calculations are different by more than 2%, the reason for the difference should be investigated. The manual independent dose calculation must enable a calculation of the dose expected at d_{max} relative to the dose that is required to be delivered from that beam to the centre of the target volume. This will enable an estimate of the target dose to be made based on the measured dose to the dosimeter on the surface.

4.5.3. Alderson Rando phantom measurements

Measurements were made on an Alderson Rando phantom before any measurements were made on patients. The tests described below are for the pelvis, head and neck, and breast. They were performed for each beam energy to be used in measurements on patients.

Alderson Rando phantom measurements were considered satisfactory if the measured dose did not differ from the TPS dose by more that 3% ($0.97 < D_{mes}/D_{TPS} < 1.03$) for the pelvis, and head and neck, and by more than 5% ($0.95 < D_{mes}/D_{TPS} < 1.05$) for the breast.

[1] The depth of d_{max} varies with field size, but for this purpose, it is proposed that a fixed value be used.

4.5.3.1. Pelvis

Entrance dose measurements were made for a three field beam arrangement (anterior and two opposing lateral fields), making measurements for one beam at a time. Two plans were created.

For the first plan, all three fields were 20 cm × 20 cm in size without wedges (see Fig. 9). Doses were calculated by the TPS to deliver 50 cGy to the isocentre, which was at the centre of one of the phantom slices (i.e. not at a slice junction). If the agreement between the measurement and calculation was not within 3%, the measurements were repeated. If the measurements do not agree within 5%, this suggests a problem with the system which would need to be investigated before making patient measurements.

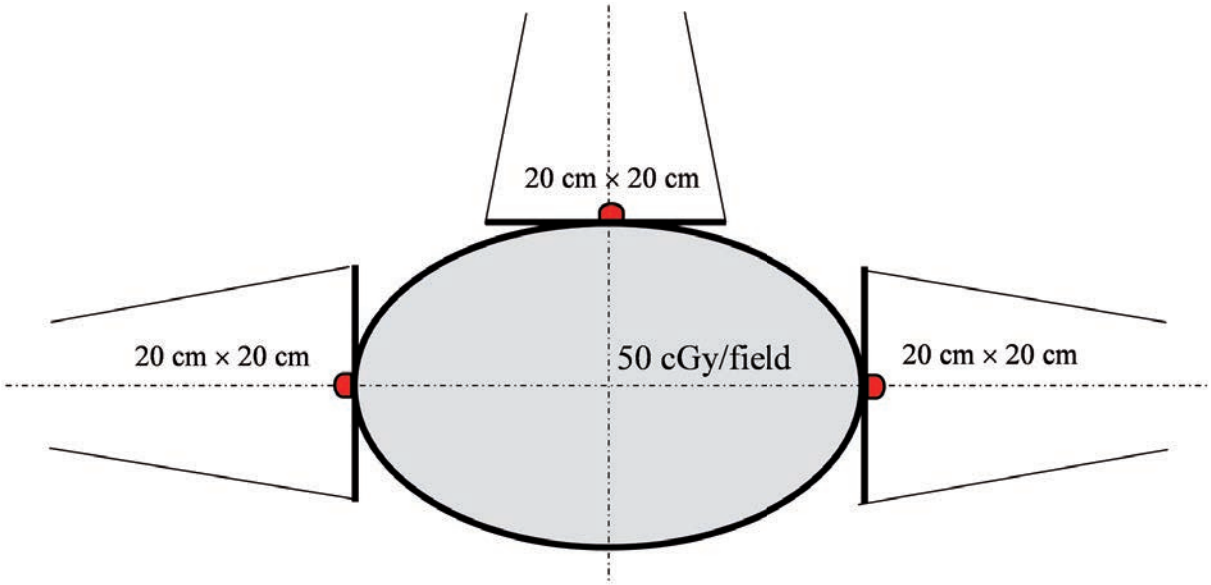

FIG. 9. Irradiation geometry for pelvis with open beams. Entrance dose measurements are performed in sequence for each of three fields using a Rando phantom. Note that only one dosimeter is present for each field.

The second plan used a 20 cm × 20 cm anterior field and two opposing lateral fields of 10 cm × 10 cm with 30º wedges and with the thin end of the wedge positioned posteriorly (see Fig. 10).

4.5.3.2. Head and neck

Two parallel opposed 6 cm × 6 cm fields without wedges were used (Fig. 11). The centre of the field was again at the centre of a phantom slice in the region of the junction of the neck and the chin. 100 cGy was delivered to the isocentre for each field. These measurements were performed on an Alderson Rando phantom without an immobilization mask.

The measurements were then repeated with the immobilization mask. The inverse square correction would be expected to be different for these two situations.

If the measured dose differed by more than 3% from the calculated dose, the measurements would need to be repeated, as before.

4.5.3.3. Breast

Entrance dose measurements were made for two (medial and lateral field) opposed tangential fields (length of the field between 18 cm and 20 cm, width 10 cm) with a 30° wedge. The position of the field was adjusted to have approximately 1 cm difference between the phantom surface and the upper edge of the field (see Fig. 12).

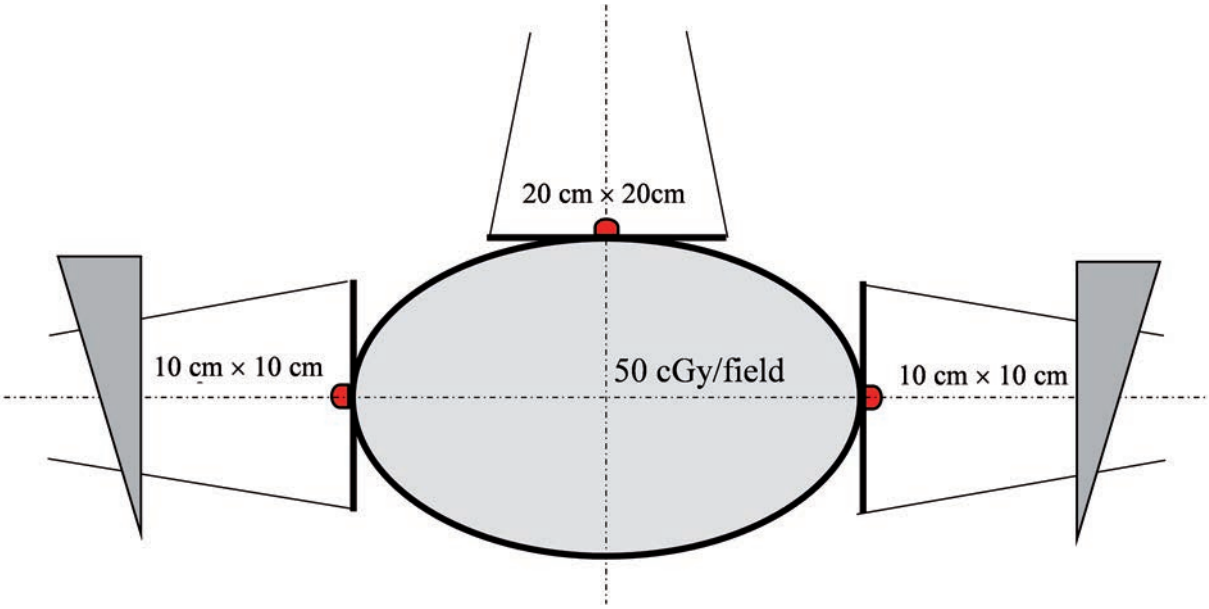

FIG. 10. Irradiation geometry for pelvis with wedged beams. Entrance dose measurements were performed in sequence for two fields using an Alderson Rando phantom.

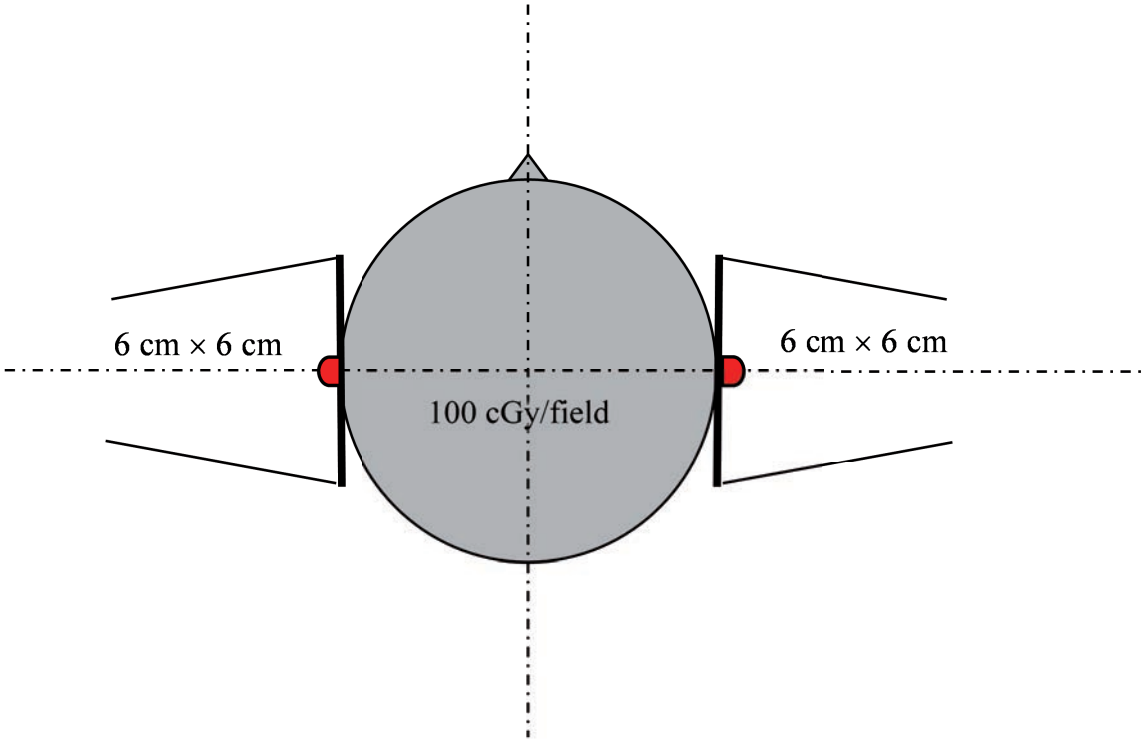

FIG. 11. Irradiation geometry for head and neck irradiation. Entrance dose measurements were performed in sequence for two fields using a Rando phantom.

The technique applied was identical to that routinely used in clinical practice in the radiotherapy department (fixed SSD or isocentric set-up, asymmetric jaws, etc.).

Doses were calculated by the TPS to deliver 100 cGy to the isocentre (or to the point of intersection of two beams), depending on the technique used. The point of beam intersection was placed at the centre of one of the phantom slices (i.e. not at a slice junction).

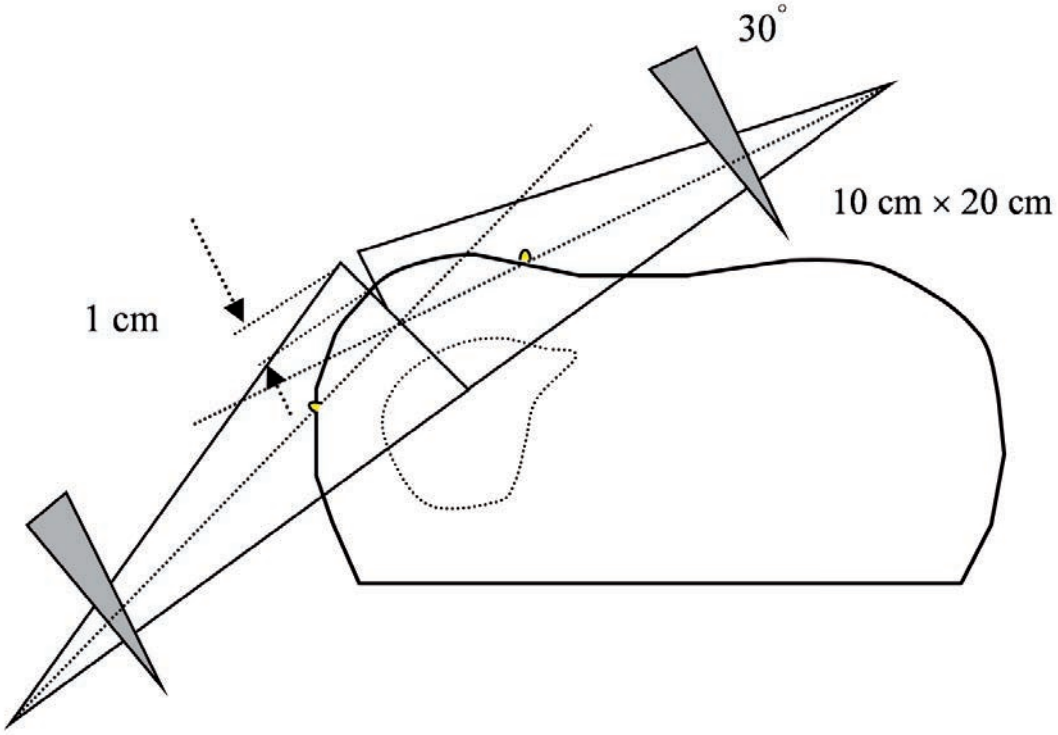

FIG. 12. Irradiation geometry for breast irradiation. Entrance dose measurements are performed in sequence for two fields using a Rando phantom.

The measurements were made for one field at a time. If the agreement between measurement and calculation was not within 5%, the measurements would need to be repeated. If the measurements did not agree within 7%, this suggested a problem with the system, which required investigation before making patient measurements.

4.6. EXIT DOSE MEASUREMENTS

Exit dose measurements were not carried out as part of the CRP. However, the following suggests how they would ideally be carried out.

4.6.1. Calibration

The calibration process involves placing the dosimeter on the exit surface of a water phantom using a lateral beam so that the dosimeter is exposed on one side to a lack of backscatter (due to air). Because treatment planning systems do not normally compensate for this lack of backscatter, it was proposed that the reference dose should be the dose calculated by the TPS since any 'error' in the calculation could be expected to be repeated in the clinical situation and does not influence the outcome of the measurement. The calculation point would be at the depth of d_{max} for the relevant energy towards the radiation source measured from the phantom exit surface. The $N_{cal,exit}$ would be calculated using:

$$N_{cal,exit} = \frac{D_{calc}}{M}\left(\frac{SDD}{SDD - d_{max} - d_s}\right)^2 \quad (18)$$

where SDD is the distance from the source to the sensitive volume of the dosimeter. From this, it is possible to calculate k_{exit} as follows:

$$k_{exit} = \frac{N_{cal,exit}}{N_{cal,entrance}} \tag{19}$$

The measurement would then allow calculation of the exit dose.

However, there are several issues specific for exit dosimetry, including the use of correction factors for exit dose determination. It is advisable to refer to the relevant literature discussing this topic [4].

4.7. IN VIVO MEASUREMENTS IN BRACHYTHERAPY

Within this CRP, measurements for brachytherapy were made with MOSFET dosimeters. Calibration measurements were made inside the phantom to have a similar geometry as for the patient measurements.

4.7.1. Calibration in a ^{60}Co beam

Reference conditions were: ^{60}Co beam, water phantom, SSD = 80 cm, reference depth = 10 cm, at the central axis of the beam, dose 100 cGy. In these conditions, three readings of the ionization chamber were taken. With the same geometry, the MOSFET was positioned with its flat side towards the beam. Five measurements were taken. The measurements were repeated with the MOSFET with the bubble side facing towards the beam. The calibration coefficients for each MOSFET orientation were calculated using the formula below:

$$N_{Co\text{-}60} = D/M \text{ [cGy/mV]} \tag{20}$$

4.7.2. Calibration for ^{192}Ir brachytherapy source

Reference conditions were as follows: the dosimeter was placed in the acrylic cylindrical afterloading phantom, 1 cm away from the ^{192}Ir source, on the central axis of the source.

Using the current source activity, the dwell time to deliver dose 100 cGy at 1 cm was calculated. Both TPS and manual calculations were made, according to the TG-43 recommendations [96].

$$D = S_K \Lambda \tag{21}$$

where S_K is air kerma strength of the ^{192}Ir source and Λ is dose rate constant.

The calibration coefficient was defined as follows

$$N_{Ir\text{-}192} = D/M \text{ [cGy/mV]} \tag{22}$$

In order to compare the dosimeter response with that in a ^{60}Co beam, $k_{en} = N_{Ir\text{-}192}/N_{Co\text{-}60}$ was used.

4.7.3. Measurement of angular response of the dosimeter

The dosimeter angular response was checked for several angles around 360°. A cylindrical phantom accommodating the catheters with the radioactive source and the dosimeter was made to allow such measurements. Only dosimeters with an isotropic angular response were used for in vivo dosimetry in brachytherapy.

4.7.4. Catheter correction factor, k_c

Two series of three measurements were performed for the same dwell time with the dosimeter positioned inside the catheter and without the catheter. The average was calculated for each situation. The catheter correction factor, k_c, was calculated from the following formula:

$$k_c = M_{no\text{-}cath}/M_{cath} \tag{23}$$

For in vivo measurements, which should be preceded by phantom measurements, the dose was calculated using the formula:

$$D = M \cdot N_{Ir\text{-}192} \cdot k_c \tag{24}$$

4.7.5. Phantom measurements

A simple water equivalent phantom was developed. The treatment catheters were inserted in the phantom. The dosimeter used for in vivo measurements was positioned in a well defined location. The same phantom as for the angular response measurements was used. CT images were taken in order to allow reconstruction of the geometrical positions of catheters and dosimeters. Orthogonal films are a suitable alternative, depending on usual clinical practice. Dose points were created at the position of the dosimeters. A treatment plan was generated, and dose values at the specified points were calculated and reported. The treatment as per plan was then delivered to the phantom, and the in vivo measurement was performed. The measured dose values were compared with the calculated doses. The procedure was repeated five times.

If the agreement between the measurement and calculation was not within 5% (1 SD), the measurements would be repeated with a different MOSFET dosimeter. If the repeated measurements agreed with the first within 5%, this suggests a problem with the system, which should be investigated before delivering patient treatment and taking in vivo measurements.

4.7.6. Patient measurements

Rectum dose measurements were performed for 50 patients. Special care was taken to ensure that the dosimeters did not move during the treatment. The measured dose values were compared with the calculated ones. The results were carefully analysed taking into account uncertainties due to high dose gradients.

5. IN VIVO DOSIMETRY ON PATIENTS

5.1. USES OF IN VIVO DOSIMETRY

In vivo dosimetry can be carried out at several levels. Two different goals can be identified: the measurement of doses to organs at risk that are difficult to calculate (such as the dose to eyes and gonads) and the verification of the delivered dose in order to improve treatment accuracy and to minimize the risk of dose misadministrations. Although the use of in vivo dosimetry for the assessment of doses to organs at risk is an important use of the system, this report does not consider the issues associated with such measurements nor does it consider the possibilities of dosimetry with portal imaging systems.

The simplest form of in vivo dosimetry for dose verification is to carry out an entrance dose measurement. For this reason, it is recommended that an in vivo dosimetry programme should begin with entrance dose measurements. However, in order to get closer to the goal of an independent verification of the prescribed dose, entrance and exit measurements are required. Setting up a satisfactory system for exit dose measurements is more complex, and for this reason, it was decided that exit dose measurements would not be included in this CRP until the centre has a fully functional and validated system for entrance dose measurements.

It is necessary to be realistic about what can be achieved with in vivo dose measurements. It should also be noted that in vivo measurements only relate to the treatment session at which the doses are measured, and it is possible that an undetected error may occur at another fraction. One can expect to detect at least the types of errors listed below.

For entrance dose measurements:

— Equipment related errors;
— Changes in the dose delivered per monitor unit;
— Incorrectly aligned wedge filter or other accessories;
— Beam parameters out of tolerance (e.g. flatness, energy);
— Human errors in data generation, data transfer and treatment set-up;
— Incorrect setting of monitor units;
— Missing or incorrectly positioned wedge filter (but not a reversed wedge);
— Wrong choice of energy;
— Positioning discrepancies between treatment planning and delivery (e.g. SSD, beam geometry, the use of a wrong table height when applying wedged lateral fields);
— Treatment data for the wrong patient selected;
— Miscalculation of the entrance dose by the TPS.

For entrance and exit dose measurements:

— Discrepancies in the thickness and composition of the patient between planning and treatment;
— Errors in the TPS dose calculation algorithms.

It must be emphasized that entrance dose measurements alone will not identify errors associated with patient composition or geometry, nor will they detect errors in the treatment planning system algorithm. However, with entrance dose measurements, it will be possible to detect most human errors in treatment set-up and errors in the treatment equipment, which represent the majority of serious errors. Entrance dose measurements can also trace errors in the dose calculation (e.g. in the use of wrong beam data, a wrong wedge factor or a systematic error in a complicated algorithm).

In vivo dosimetry is easier to implement in sites with regular body contours such as the pelvis and for simple techniques not involving high dose gradients. For this reason, it is recommended that implementation begin with such sites and techniques. Once the system has been established and validated for these sites, more complex areas should be considered.

It is also possible to carry out dose measurements in natural body cavities such as the rectum and the oesophagus. One of the problems here is that it may be very difficult to ensure that the dosimeter is correctly positioned at the point of interest and not moving. It is helpful if radiographic evidence of the position of the dosimeter can be obtained. Even when the position is accurately known, it may nevertheless be the case that the dosimeter is in an area of high dose gradients (such as in brachytherapy measurements in the rectum), and practically useful action levels may be hard to achieve so that only serious misadministrations can be detected. There may, however, be a place for such measurements where access to a body cavity in which the dose rate is reasonably uniform can be achieved.

5.2. ESTABLISHING AN IN VIVO DOSIMETRY PROGRAMME

5.2.1. Staff roles and responsibilities

The following professionals should be part of the in vivo dosimetry implementation team:

— Clinically qualified medical radiation therapy physicist;
— Radiation oncologist;

— Dosimetrist/physics assistant;
— Radiation therapist (RTT, radiographer).

Overall scientific control of the in vivo dosimetry programme must be in the hands of a competent and fully trained expert in radiotherapy physics. However, it is appropriate and cost effective to ensure that the treatment staff are fully involved in the routine delivery of the programme, and they should be part of the process of managing the logistics of the system. It is important to establish clear definitions of responsibilities for different staff groups.

These should be as follows:

— Radiotherapy physicist(s): Has overall responsibility for the in vivo dosimetry programme, including acceptance, commissioning, periodic QA and establishing action levels (in consultation with physician(s)). Designs measurements and results reporting forms and provides in-service training for other personnel. Shares (with dosimetrists) responsibility for checking the calculations that will be compared with in vivo measurements. Reviews or supervises review of the measurement results. Investigates measurements that fall outside the action levels and notifies the physician if treatment errors occur or if the cause of the discrepancy is not understood and discusses remedial actions. TG-62 [5] suggests that one physicist should have primary responsibility for the in vivo dosimetry programme and that at least one qualified backup person be designated.
— Dosimetrist(s): Calculates the quantities for comparison with dosimeter readings, prepares the worksheet and assists physicists in investigating measurements outside of action levels. Shares other responsibilities as designated by the physicist(s).
— Therapists(s): Places dosimeters, records the results, performs simple calculations to compare measured with expected results, and informs the physicist if a result exceeds tolerance.
— Physician(s): Formally requests in vivo dosimetry and reviews each patient's in vivo dosimetry record after the physics review is completed. Works with the physicist to establish the types of cases to measure, the measurement frequency and the action levels. Determines the remedies when treatment errors are found.

5.2.2. Training of staff

The training should consist of an education session for the radiotherapy staff outlining the philosophy and rationale for in vivo dosimetry. This should be followed by practical training sessions for each group of staff on how to perform the patient measurements and the use of the on-line dosimetry system at the treatment machine (RTTs and physics assistants), use of the TLD reader (physics assistants), etc.

At this point, it would be useful to provide the staff with a draft of the in vivo dosimetry protocol and ask for their input. This document should therefore be produced before the commencement of training.

5.2.3. Encapsulation of dosimeters

Encapsulation of dosimeters should be applied in the same way as for the Rando-Alderson phantom measurements. It is important to use the correct buildup for the energy being used.

5.2.4. Positioning of the dosimeters

The standard position of the dosimeters is on the central axis of the beam. This point is easily identified, and the dose at this point is easily calculated.

It is important that the dosimeter is firmly attached to the patient. This can be done with adhesive tape. Body hair can make it difficult to attach the dosimeter. In this case it may be appropriate to choose a part of the field not on the beam axis where there is less hair, but the dosimeter should not be more than 2 cm from a beam edge. Occasionally, it may be necessary to ask the patient's permission to shave a small area for the dosimeter.

In the case of a head and neck patient being treated in a thermoplastic shell (immobilization mask), there is an issue as to whether the dosimeter should be placed on top of or underneath the shell. It is recommended that it should be placed on top of the shell, but care must be taken that the dose is calculated for the correct position (i.e. the inverse square correction between the dose calculation point and the dosimeter position should be applied).

For breast treatments, the issue of the angle of incidence of the beam is a potential source of uncertainty, as already discussed. For more complex techniques for breast treatment, it may be appropriate to place the dosimeter at a standard distance (e.g. 2 cm) from the edge of the field closest to the lung.

There are some situations where it is not appropriate to place the dosimeter at the centre of the field. Some examples of these are half-blocked fields, fields with extensive blocking, fields where the centre of the beam is in air or in an area where it is difficult to calculate the expected dose (e.g. due to loss of scatter). In these cases, it is important to find a measurement point which can be unambiguously defined and at which the expected dose can be calculated. When the centre of the field is close to the edge of a block, it may also be appropriate to place the dosimeter 2 cm away from the block edge.

If for some reason the dosimeter cannot be placed on the beam axis and a wedge is being used, it is suggested to move the dosimeter away from the beam axis in the unwedged direction so that the effect of the wedge can be more easily calculated.

5.2.5. Prevention of cross-infection

The use of the same dosimeter on different patients may lead to cross-infection, which must be avoided. Diodes and MOSFETs can usually be cleaned with alcohol swabs, but manufacturer recommendations should be followed. Alternatively, a thin plastic film/foil could be placed on the surface of the patient.

5.2.6. Instructions for the measurements

Short instructions for the use of the equipment should be written and be available to the staff using the equipment. A regular QA programme of the in vivo dosimetry system is essential as described in the section on dosimetry (refer also to AAPM No. 87 [5], chapter 7, and ESTRO booklet No. 5 [4]).

Measurements should be made during the first or second fraction of treatment and whenever a significant change is made to the treatment.

An in vivo measurement should be analysed as soon after the treatment as possible and in any case before half the treatment course has been delivered. In the event that the in vivo measurement exceeds the action level, the treatment should be interrupted and the cause identified. For techniques that involve single fractions, there is a strong preference for an in vivo dosimetry system that allows real time display of the dose.

5.2.7. Documentation of the results

The result of an in vivo dosimetry measurement is expressed as the percentage difference between measured and expected dose for each individual field divided by the expected dose:

$$\Delta = \frac{(Measured\ Dose - Expected\ Dose) \times 100}{Expected\ Dose} \tag{25}$$

The measured dose is calculated from the dosimeter reading using the method described in Section 4.5.1. The expected dose is the dose calculated at the depth of dose maximum at the point chosen for measurement. The calculation may be performed by the TPS for planned treatments or can be calculated by hand. The calculation needs to include only the contribution for the single field being measured. Where manual methods are used to check the TPS calculation, the TPS calculated dose should preferably be used.

A form needs to be designed to document the results. An example is given in Fig. 13. It is also useful to develop a database to record the data.

5.2.8. Calculation of expected dose

The expected dose should be calculated both using the TPS and by a manual method as described in Section 4.5.2. The estimate of the target dose based on the measured doses to the dosimeters on the surface of the patient should be compared directly to the physician's prescription.

IN VIVO CHART (ENTRANCE DOSE) # _____
SURNAME/NAME: _____
PATIENT ID NUMBER: _____
IRRADIATION TECHNIQUE (isocentric/SSD) : _____
TREATMENT SITE : _____
CT (Y/N): _____
TREATMENT UNIT: _____

To be completed by dosimetrist/physicist.

	Field 1	Field 2	Field 3	Field 4	Field 5
FIELD IDENTIFICATION					
BEAM (MV)					
GANTRY ANGLE					
SSD (cm)					
EQUIV. FIELD SIZE (cm)					
BLOCKS (Y/N)					
DOSIMETER ANGLE					
WEDGE					
REFERENCE DOSE (Gy)					

DATE: _____
TREATMENT TIME:_____
To be completed by the physicist (shadowed). To be filled in by RTT at treatment unit.

	Field 1	Field 2	Field 3	Field 4	Field 5
FIELD IDENTIFICATION					
DOSIMETER					
EXPECTED READING					
TOLERANCE LIMITS					
SSD (cm)					
READING					

If any reading is out of tolerances, indicate possible causes:
Energy ☐ Wedges ☐
Field size ☐ Reading system problems ☐
MU ☐ Mistake in the type of diode, buildup cap, etc. ☐
Blocks ☐ Dosimeter placement problems ☐
Not known ☐ Other ☐ Details …….

FIG. 13. Example of an in vivo dosimetry patient record form.

5.2.9. Definition of tolerance levels

During the development of the in vivo dosimetry procedures, it is necessary to define an acceptable level for the percentage difference between the expected and measured dose. In this report, this is referred to as the tolerance level. Until further evidence is accumulated, a tolerance level of 5% was considered appropriate during the pilot study.

In extending in vivo dosimetry more widely into more complex techniques and routine use, the tolerance levels will need to be reviewed. It is important that tolerance levels are not set too low, thereby generating a high number of false alarms due to the dosimetry system. The pilot study should identify the proportion of measurements

for which a repeat measurement is required. If the tolerance levels are set so that interventions are needed for most patients, the system will rapidly fall into disrepute. The following guidance is offered:

— If the rate of measurements outside tolerance is 2–3% or lower, the tolerance level can be set lower;
— If the rate of measurements outside tolerance is 15–20%, the tolerance level can be set higher.

As stated above, one of the outcomes of in vivo dosimetry should be to improve the accuracy of treatment, and it is therefore to be expected that, with the increased experience gained over time, it will be possible to reduce the tolerance levels, both as a result of improved treatment accuracy and as a result of improvements to the in vivo dosimetry system. An appropriate goal is to be able to use a tolerance level of 5% for simple treatments, with a level of 7% for situations such as breast treatments where measurement complications exist. However, once the number of measurements exceeding this limit has been reduced below 2%, it would be appropriate to consider whether the limit could be lowered further as part of a continuous improvement programme. It is inappropriate to seek to reduce the tolerance level below that determined by the intrinsic uncertainty of the measurement system. It is considered that the best achievable measurement uncertainties (standard deviation of an individual measurement) for the in vivo dosimetry systems considered in this report are as follows:

— TLD 3%;
— Diodes 2%;
— MOSFETs 3%;
— OSL 3%.

As part of the continuous improvement of an in vivo dosimetry programme, the introduction of exit dose measurements may be considered. The benefit of this is likely to be greater than reducing the entrance dose tolerances below 5% or 7%.

Although in the initial stages of the introduction of in vivo dosimetry the tolerance levels may need to be higher, every effort should be made to achieve tolerance levels of about 5% by a process of progressive elimination of identified causes of dose differences. This process should be under the supervision of a qualified expert in radiotherapy physics.

5.2.10. Actions to be taken if the in vivo measurements are out of tolerance

When a measurement is outside tolerance, it is necessary to take action. If a real time dosimeter reading is available, it is appropriate that the immediate action is to check the set-up of the patient. If the dose measurement is not available while the patient is in the treatment position or if no set-up error can be detected, it is necessary to plan steps in the discrepancy analysis process. When there is an unexplained error, the situation must be brought to the attention of the medical physicist in charge of the in vivo system. The physicist will then establish whether the error can or cannot be explained. Once the facts have been established, a decision must be made on what further action to take. This decision is the responsibility of the physician in charge of the patient in discussion with the medical physicist.

The first step is to check the treatment plan, the monitor unit calculation and the calculation of the expected dose. The possibility of an incorrect initial reading should also not be discounted. A second in vivo measurement should then be carried out. If the likely cause of the error has been identified, it should first be corrected. At the second measurement, a medical physicist should be present to check the set-up and dosimeter positions.

If the tolerance level is exceeded by a factor of 2, treatment should not proceed unless the cause has been identified. This is termed the ‘action level’. The physician in charge of the patient must immediately be informed and should be involved in decisions about further action. Consideration should also be given to the possibility that there is a significant problem with the output of the treatment machine, and that a check of the machine output should be made before other patients are treated.

Investigations of situations where the tolerance level has been exceeded should include measurements with a phantom and a reference dosimeter (i.e. an ionization chamber) both to check the output of the treatment machine and to check the particular set-up for the patient. If the dose difference is close to the tolerance level, it is acceptable to wait until after the repeat measurement.

If the tolerance level is exceeded for several successive patients, this is an indication that the treatment machine is at fault or that there is a problem with the in vivo dosimetry system. A check of the output and of the in vivo dosimetry system should therefore be made.

A flow chart of a system for taking action is given in Fig. 14. During the development of the in vivo dosimetry programme, confidence will be built in the reliability of the measurements. Large dose differences at the beginning are likely to be due to deficiencies in the measurements, but measurement problems should soon be eliminated, and deviations will then be more likely to be related to errors in treatment. It is particularly important at the early stages of the project that there is close involvement of a senior medical physicist who will be able to make an informed judgement about the likely cause of deviations.

In some circumstances, it will not be possible to identify a specific cause for a deviation. Such cases may be due to random variation or to the treatment technique requiring calculations beyond the limits for which the commissioning measurements were made. A record should be kept of such cases and a review carried out periodically to ensure that there is not a systemic cause.

If it is necessary to make more than two measurements for a given patient treatment, consideration needs to be given to the shielding effect of the dosimeters. One possibility is to place the dosimeter in a slightly different position.

For techniques which involve single fractions, there is a strong preference for an in vivo dosimetry system that allows real time display of the dose. An in vivo measurement should be analysed before half the treatment has been delivered. In the event that the in vivo measurement exceeds the action level, the treatment should be interrupted and the cause identified. In any event, the dosimeter should not be left in place for a significant part of a single fraction because of the shielding effect.

5.2.11. Feedback on in vivo dosimetry results

The results of in vivo dosimetry should be routinely reported both to the medical staff and to the staff who treat the patients. Commitment from the treatment staff is essential to the success of in vivo dosimetry, and demonstration of improvements resulting from the programme will have a good effect. Conversely, it is important to be sensitive about reporting poor results, especially to avoid a culture of blame.

5.3. PILOT STUDIES

The introduction of in vivo dosimetry should be in two stages. Firstly, a pilot study should be carried out including a limited number of patients for a couple of simple techniques under the close supervision of the qualified expert in medical physics. After completion of the pilot study, the routine in vivo dosimetry programme should become part of the quality management system.

The aim of the pilot study is to establish the clinical entrance dose measurement protocol and to train participating staff.

In this CRP, two pilot studies have been carried out with each dosimetry system under study: the first with pelvic treatments where the dosimetry technique is straightforward and the second with head and neck patients. An additional aim of the pilot study was to familiarize staff with the second dosimetry system being tested in this CRP.

Before starting pilot studies with patients, phantom measurements should have been satisfactorily completed for a particular energy and the selected treatment technique.

5.3.1. Application by the CRP participants

Measurements on patients were done with one dosimeter at a time[2] in order to avoid too much dose attenuation caused by the dosimeter and the buildup cap. Typically, these measurements were performed on the same treatment machines. A minimum of ten patients was included for each treatment technique and each of the two dosimetry systems under study. The aim was to carry out at least 20 patient measurements to provide sufficient confidence in the system.

[2] A TLD dosimeter comprised two TLD chips in one buildup cap.

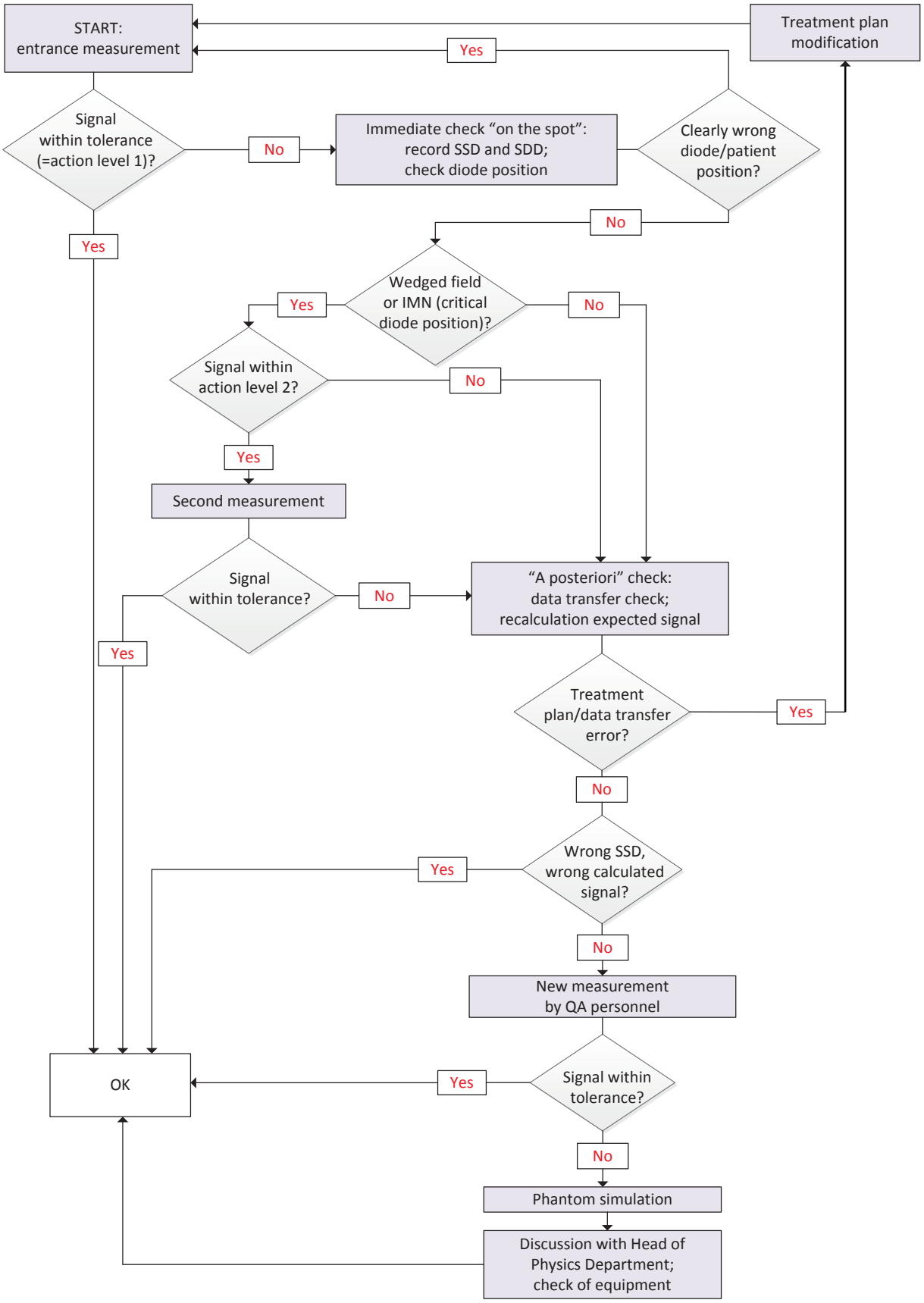

FIG.14. Example flow chart indicating a possible sequence of actions to be taken in the event of a patient measurement exceeding the action level. Figure courtesy of ESTRO [4].

During the pilot study, a medical physicist was present for the patient set-up, the dosimeter positioning and reading. This assured proper training of the technical staff routinely involved in the patient's treatment. It also allowed fine tuning of the clinical in vivo dosimetry protocol. Copies of this protocol should be available at the treatment unit, treatment planning system and in the in vivo dosimetry laboratory.

In order to be able to assess the ergonomic factors associated with an in vivo dosimetry programme, during the pilot study, several additional parameters relating to the time taken were recorded:

— Time involved in the calibration and the ongoing QA of the in vivo system;
— Extra time per patient needed to perform in vivo measurements at the treatment unit;
— Time needed to complete the in vivo record chart before and after the treatment session;
— Extra time needed to analyse the dosimeter reading and/or recycle TLD chips.

5.3.2. In vivo dosimetry protocol

A qualified expert in medical physics is needed to set up and supervise the in vivo dosimetry programme in the clinic. In order to introduce in vivo dosimetry into routine use, a detailed clinical protocol is required that specifies the responsibilities of the staff involved, describes the in vivo measurements, including dosimeter related issues, tolerance levels and actions to undertake when tolerance levels are exceeded. Such a protocol should include:

— The roles and responsibilities of different staff groups (medical physicists, radiation therapists, radiation oncologists);
— Details of positioning of the dosimeters on patients;
— Guidance on the prevention of cross infection when using the same dosimeter for different patients;
— Instructions for measurements;
— How results should be documented;
— Forms for recording the results;
— Actions to be taken if the in vivo measurements are out of tolerance;
— Guidance on who should take these actions.

The in vivo dosimetry implementation team should write the in vivo dosimetry protocol to be used in the clinic. For on-line dosimeters such as diodes and MOSFETs, the flow chart presented in Fig. 14 can be used as a general guideline for actions to be taken after entrance dose measurements. An example of an in vivo dosimetry record form is shown in Fig. 13. All record forms should be stored to allow statistical studies. Preparing a database for this purpose beforehand can be very useful and save a lot of time.

The in vivo implementation team should also prepare the training programme for the rest of the staff involved in the in vivo dosimetry procedures.

5.4. ROUTINE IN VIVO DOSIMETRY

The simple techniques defined in the pilot study were chosen so that centres can develop a reproducible technique for in vivo dosimetry. When they are confident that this has been achieved, it will be possible to extend it to more complex situations. Some considerations that may need to be taken into account were described in Section 5.2. At this stage, most of the work will be transferred to RTTs and physics assistants, and the involvement of the physicists should be at the supervisory level.

In this CRP, the in vivo dosimetry programme was not designed to be used for IMRT treatments or for treatments with very small fields except as part of a specific ethically approved research project. In such cases, it has not yet been demonstrated that useful accuracy levels can be achieved, and the disruption of treatment is therefore not justified.

Unless every treatment fraction of every patient is monitored with an in vivo measurement, there will inevitably be situations where a treatment error will escape detection. However, it is strongly recommended that entrance dose measurements not be made on every fraction because the requirement to use a buildup cap means that the dose beneath the dosimeter is significantly attenuated. The best method to ensure that all treatment fractions are

delivered in the same way is to install an RV system. In vivo dosimetry measurements associated with RV systems have been found to detect fewer errors. With an RV system, an in vivo measurement at the start of treatment should give the maximum benefit. However, since random errors are single events by definition, their effect on the total dose may be of less consequence because they can be averaged over the whole treatment period. For these reasons, the recommendation is to carry out in vivo dosimetry on all treatment beams at one of the first fractions (and following any change to the treatment set-up) and to repeat this if the measurement is out of tolerance before taking corrective action[3].

5.4.1. Priorities for in vivo dosimetry in a clinic

While initially the programme should be directed to simple techniques, it is important that more complex techniques are included as soon as practicable. Where staffing or the availability of equipment means that it is not possible to make measurements on every patient, priority should be given to:

— The introduction of new treatment protocols or techniques;
— Changes to equipment or software such as:
  • Introduction of a new treatment machine;
  • Software updates to the planning system or linear accelerator control software;
  • Any modifications to network communication of patient data;
  • Other changes to equipment or software;
— Total body irradiation or total skin irradiation;
— Single fraction treatments (but see Section 5.2.10);
— Treatments with curative intent where the dose is potentially close to normal tissue tolerance;
— Participation in clinical trials.

5.4.2. Introduction of new treatment protocols or techniques

It is important to identify what constitutes a new treatment protocol or technique. A new treatment technique is considered to be one in which the treatment planning system has been used in a new way. Examples are given below:

— Changing from SSD to isocentric treatment;
— New procedures for treatment plan generation;
— Introducing blocked or multileaf collimator (MLC) limited fields;
— Changing from physical to MLC defined blocks;
— Introducing a half-block technique (changing from an isocentre at the centre of the target volume to a half-blocked technique);
— A change in the policy on the use of bolus in different treatment techniques;
— A new method of patient dose or MU/treatment time calculation (e.g. change or upgrade of TPS, MU calculation method, etc.).

When a new treatment technique is introduced, it is recommended that the first action should be to make measurements with an ionization chamber in a phantom. Once the technique has been verified in this way, measurements should be made on the phantom with the in vivo dosimetry system (as in the pilot study). Only when the technique has been verified in this way should it be introduced for patients.

5.4.3. Comparison of two in vivo dosimetry systems

A comparative analysis was performed by each CRP participant to review dosimeter properties particularly suitable for use in specific clinical situations. It involved the comparison of dosimeter characteristics such as dose

[3] In the absence of an RV system, exit measurements, which avoid the problem of shadowing by the detector, or portal dosimetry as a constancy check, may be an alternative if there is concern that consistent set-ups are not being achieved.

response non-linearity, effect of energy, fading, angle of incidence correction, SSD correction, field size correction, wedge correction, and block and tray correction. Next, the results of Alderson Rando phantom measurements were compared in terms of convenience of use of a particular dosimeter as well as the precision, reproducibility and possible problems with set-up.

Once the pilot study for a particular site and for both dosimetry systems had been completed in a satisfactory way, comparative measurements were carried out between the two dosimetry systems. In order to compare the results for both types of dosimetry systems, two equal groups of patients were required. At least one hundred patient measurements needed to be carried out with each measurement system using the same treatment machine and the same treatment sites. Note that this was envisaged as a parallel study. Two dosimeters were not simultaneously placed on the same field.

Histograms of the in vivo dosimetry results were prepared for each dosimetry system and treatment site. The study generated sufficient statistical information to compare the number of out-of-tolerance readings (beyond 5%) within the two systems. These data were used to compare results between centres and among treatment sites, as well as among machines within a centre. Results of in vivo dosimetry were compared and reported in an anonymized way.

A set of written guidelines for clinical use of a given in vivo dosimetry system with a list of possible restrictions and special considerations has been developed by each institution participating in the CRP. In addition, based on the series of patient dose measurements, the accuracy and precision of the various in vivo dosimetry systems were assessed in routine clinical use. Possible restrictions and special considerations for the clinical use of dosimeters were listed by participants.

6. SUMMARY OF MEASUREMENTS BY CRP PARTICIPANTS

The results obtained by different countries are contained in the annexes. In this section, important common aspects are brought together. For more detail of individual results, the reader is referred to the appropriate annex. Reference is also made to Sections 4 and 5 describing the methodology developed and adopted under this CRP.

6.1. DOSIMETER CHARACTERIZATION

6.1.1. Reproducibility

6.1.1.1. Reproducibility of diode and MOSFET measurements

When a new measurement instrument of any sort is received, it is necessary to check that it is possible to achieve reproducible results. For diodes, it can be expected that repeat measurements made at one measurement session will have a standard deviation of less than 0.5 %. Measurements made over a number of different sessions should be within 1% of each other. Indeed, the measurement data presented in Section III–5.1.1 supports this assessment. For MOSFETs, repeat measurements are more difficult to make as each measurement reduces the life of the dosimeter. However, it was shown in Section IV–2.2.5 that there was no need to correct for non-linearity of MOSFET response with dose, and using the results from multiple dosimeters, it can be inferred that the standard deviation is less than 0.6%.

6.1.1.2. Reproducibility of TLD measurements

If a number of TLDs are irradiated from the same batch, it is expected that there will be a spread of results, and the variation will depend on whether an attempt has been made by the manufacturer or the user to select dosimeters with similar sensitivity. It was recommended that chips for a batch should be selected to have sensitivities within ±3% of each other. For the material used in China, 3.5% of the original batch was outside this range (see Annex IV, Fig. IV–3), whereas for the material used in Brazil, 49% was outside the range (see Annex I, Fig. I–6). Therefore,

almost half of TLD chips provided by the manufacturer had to be rejected in the latter case. Using individual chip factors, the effect of the variation between chips can be substantially reduced, and this was the practice recommended. Data from Brazil (Annex I) show that if individual chip factors are applied, the standard deviation of repeat readings can be reduced from 5.0% to 1.9%. By using two chips for each reading and applying individual chip factors to each chip, the uncertainty of an individual measurement was only 1.3%.

6.1.1.3. Reproducibility of OSL measurements

At the start of the CRP, the reproducibility of the OSL measurements was found to be unsatisfactory in some centres while being acceptable in others. The problems were found to be related to the operation of the OSL readers (newly introduced in the market) that were made available by the manufacturer (Landauer) for this CRP. The speed with which the knob could be used to operate the reader was a sensitive point in the readout process, it being very important to turn the knob slowly to avoid affecting the operation of the optical system of the reader. An additional problem related to the shutter, which prevents the OSL material from being subjected to ambient light. When the reader is operated, this shutter is supposed to be fully withdrawn by the mechanism. It was found that, on occasions, the shutter was either not opened at all or was only partially opened, resulting in a low reading. These problems generated a large spread of readings; in particular, sets of low readings were obtained (see Annexes I, III, VI). Feedback was given to the manufacturer, and the initial problems were resolved. As a result, modifications of the reader were considered by the manufacturer.

The readout process is in principle non-destructive to the OSL signal, and it is possible to make several readings and to reject any low results. It was found to be appropriate to repeat each reading 5 times. It should be pointed out that the readout process is only partially non-destructive, and the reduction in signal associated with each reading was measured as 0.04% in Croatia (Annex III, Fig. III–10), 0.03% in Brazil (Annex I, Section I–5.1.1) and 0.06% in the United Kingdom (Annex VI, Section VI–4.1.2).

There is no general consensus on best practices regarding the use of OSL in medical applications. At the start of the CRP, it was thought that the dosimeters could be used repeatedly, taking into account their previous exposure in a similar way to MOSFETs. The advice from Landauer was that erasing the signal from the dosimeters (bleaching) by exposure to a bright light was possible but not recommended. However, it was found that with progressive irradiation, the sensitivity of the dosimeter changed and the reproducibility was reduced. It was determined that bleaching the dosimeters in a manner similar to the TLD annealing process gave satisfactory reproducibility while allowing the dosimeters to be reused several times. In carrying out the bleaching process, it was important to avoid the heat from the lamp increasing the temperature of the plastic holder of the OSL material. Two methods of doing this were devised as described in Annex I (Section I–5.1.3) and Annex III (Section III–4.1).

When a single exposure was carried out and the dosimeter was then bleached after readout, the standard deviation of repeat measurements with an individual dosimeter was found to be 1.5% (Annex III, Section III–3.4.1). However, the variation in the sensitivity within a batch of dosimeters was only 1.6%, and there was little to be gained by maintaining individual factors for the OSL dosimeters (dots).

6.1.2. Dose rate dependence

As described in Section 4.1.5, the dosimeters under study (i.e. diodes, MOSFET and OSL) were investigated for dose rate dependence in the range of dose rates of interest for in vivo dosimetry. None of them were found to have a dose rate dependence with the dose rates encountered in this CRP. As discussed in Section 3.1, there was no need to repeat this exercise for TLD as evidence exists in the literature [97] that TLD does not exhibit dose rate dependence in the range of interest.

6.1.3. Dosimeter calibration in terms of absorbed dose to water

All the dosimeters used in this CRP are relative dosimeters and must be calibrated to give the dose at the depth of dose maximum. Some dosimeter manufacturers (e.g. OSL) provide a calibration coefficient. However, it was found that for the accuracy required in radiotherapy, calibration against an ionization chamber was essential. The calibration process also allowed the variability of the dosimetry system to be monitored. For TLD, it was

important to include the individual chip factor for each dosimeter in order to achieve a clear understanding of the variability.

6.1.4. Dose response non-linearity correction

The non-linearity of the response of dosimeters for exposures from a few cGy up to 4 Gy was measured as these represent the single exposures likely to be experienced in clinical use. Some participants extended the range of investigation up to 6 or 8 Gy.

6.1.4.1. Non-linearity of MOSFETs and diodes

Neither MOSFETs nor diodes showed significant dose response non-linearity over the range of doses measured. However, for both types of dosimeter, sensitivity changes were observed with the total dose received. There was a more marked effect with MOSFETs for which the dosimeters have a maximum total dose beyond which they can no longer be used.

6.1.4.2. Non-linearity of TLDs

The dose response non-linearity of TL dosimeters is significant, as shown in Fig. 15. However, for doses up to 1.2 Gy, the calibration coefficient measured with an exposure of 1 Gy can be used without further correction. If this correction is not made for doses of 4 Gy, the measured dose may be in error by up to 9%.

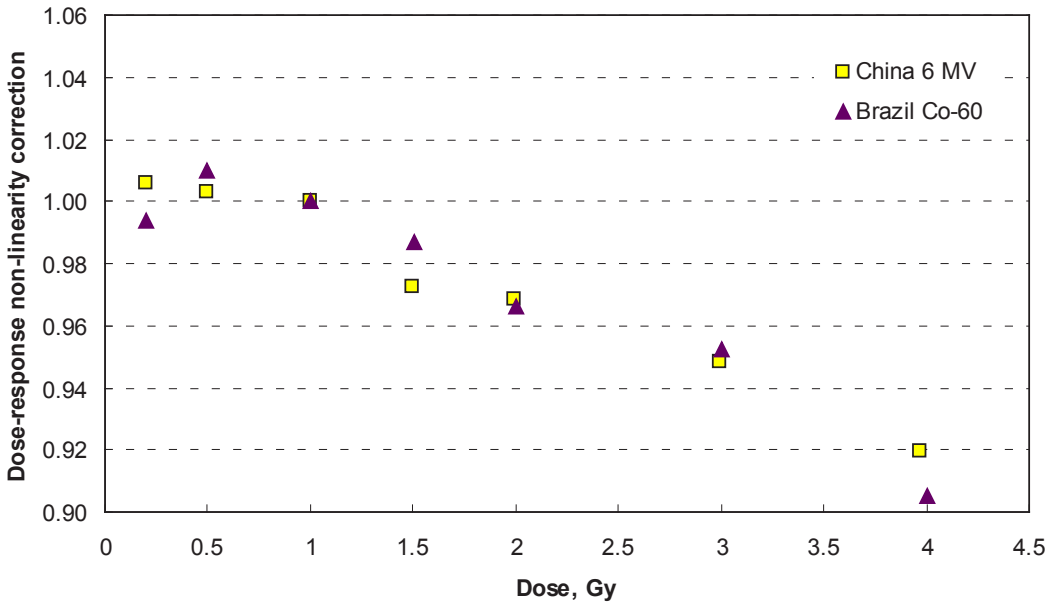

FIG. 15. The variation of the measured correction factor for non-linearity of the TL signal with dose. The uncertainty of the individual measured values is about 1%.

6.1.4.3. Non-linearity of OSLDs

The non-linearity of OSLDs is complex and depends on whether an individual dot calibration of the OSL dots is carried out or whether a single calibration coefficient is used for the whole batch. This can be seen in Fig. 16 where different results were obtained depending on whether the dosimeters were calibrated with 50 cGy before or after the exposure for the actual measurement. This exercise was performed without bleaching the dosimeters

between the calibration and measurement exposures. For the datapoints marked as uncalibrated, no individual calibration exposure was performed with the assumption that all dosimeters have the same calibration coefficient.

In general, there are differences between the two sets of data from Brazil and Croatia, indicating that different dosimeter batches show different dose response results. No major difference was found for dosimeters calibrated with 50 cGy before or after their use in the range up to 6 Gy.

In Fig. 16, potential effects of the reader performance on the results can also be seen. In particular, large scatter of measurements was observed for the dose of 20 cGy by the Brazilian participant, possibly reflecting a sub-optimal OSL reader performance for the low dose range. This may be related to the automatic switch of the reading mode from low to high sensitivity. It was found that the crossover parameters did not provide a continuous smooth transition between the modes, thus generating high reading uncertainties that are not acceptable for radiotherapy applications. Such effects were not found in the results by the Croatian participant whose reader was adjusted so that only the low sensitivity mode was used for the whole range of doses without automatic switching to the high sensitivity mode.

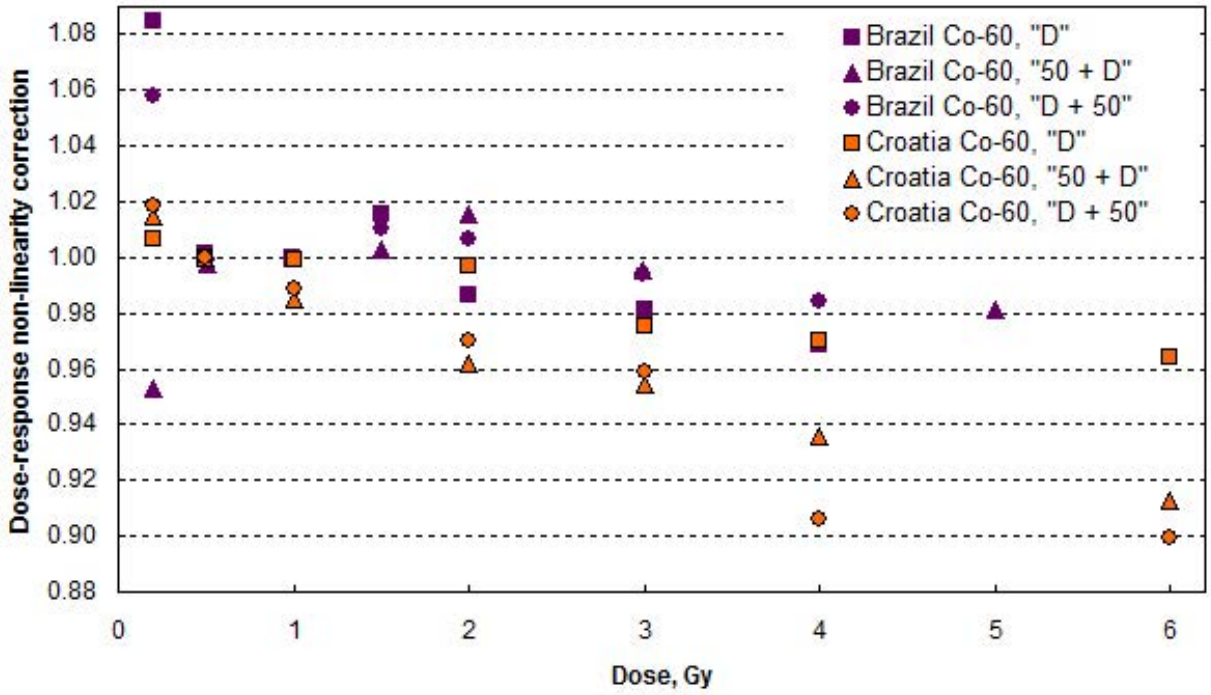

FIG. 16. Graph showing the variation of the measured correction factor for non-linearity of the OSL signal with dose. The uncertainty of the individual measured values is about 1.6%. The linearity depends on whether a calibration irradiation of 50 cGy is made before (50 + D) or after (D + 50) the measurement exposure. For the data labelled as uncalibrated (D), no calibration exposure was performed as the assumption was made that all dosimeters have the same calibration coefficient.

If dosimeters are given a single dose after each bleaching session, the non-linearity is significantly reduced. For clarity, these results are shown separately in Fig. 17.

OSLDs can be reused several times without significant changes of sensitivity (above 3%) until a certain dose has been accumulated. This is illustrated in Fig. 18 where the relative dose response for a group of OSL dots is shown following their irradiation history without bleaching. The dots were irradiated in ^{60}Co beams in Brazil (4 dots) and Croatia (6 dots) with various doses up to an accumulated dose of 4 Gy. After each irradiation, the dots were read out and bleached before the next use. As can be seen in Fig. 18, the upper dose limit is about 2.5–3 Gy for the dots under investigation. After having accumulated such a dose, the dots should no longer be used due to the significant changes of sensitivity. This finding is consistent with previous publications [25, 80]. When signal bleaching is not performed in between the subsequent OSL exposures, the results show higher uncertainties and more scatter (see Annexes I and III).

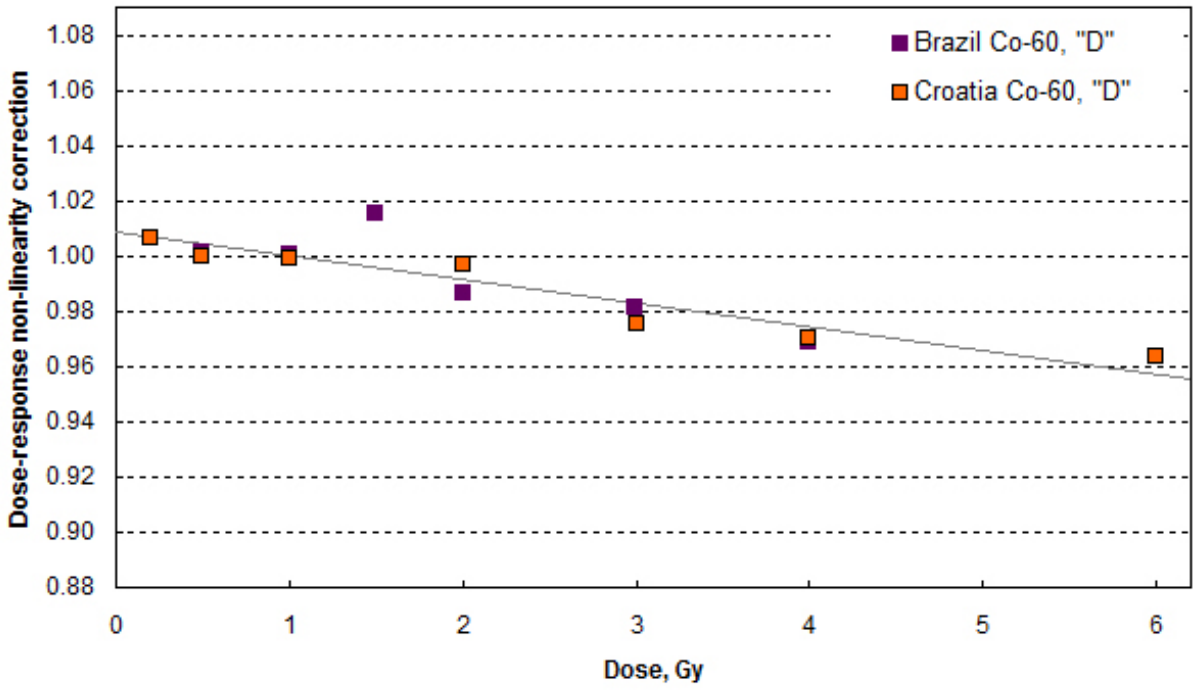

FIG. 17. Extract from Fig. 16 showing the effect of not individually calibrating the OSL dosimeters without bleaching.

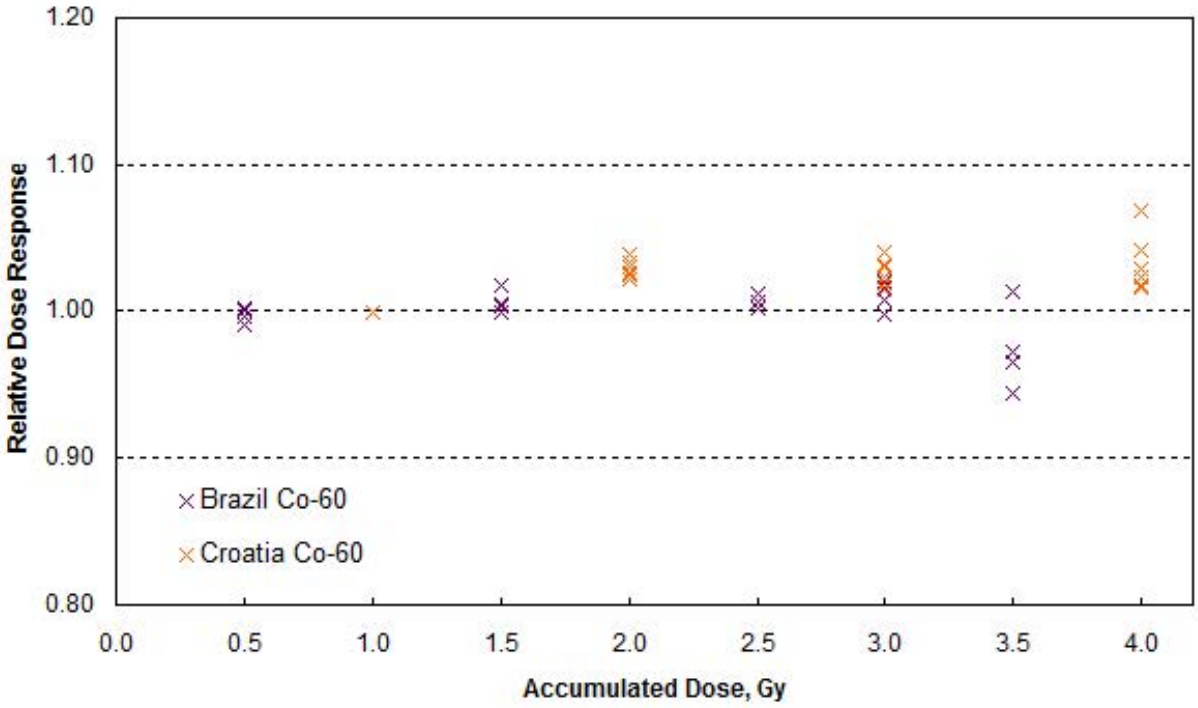

FIG. 18. Relative OSL dose response versus the accumulated dose.

6.1.5. Energy correction

Although the intrinsic sensitivity of a dosimeter may be independent of beam energy, the calibration coefficient for in vivo dosimetry on the surface of the patient is very unlikely to be energy independent because of

the effect of the buildup cap. For example, the calibration coefficients for MOSFET dosimeters at 6 MV and 15 MV differed by 18% (Annex IV). It must be emphasized that this difference is because of the effect of insufficient buildup at 15 MV. When the dosimeters are placed at depth in a phantom, the calibration coefficient of MOSFETs is only marginally affected by beam energy. Although it would in principle be possible to calibrate the dosimeters in a ^{60}Co beam, all the participants found it simpler to calibrate the dosimeters at the energy at which they were to be used.

6.1.6. Fading correction

Apart from diodes, which provide an instantaneous reading, all the dosimeters showed some degree of fading of the signal following irradiation. This made it necessary to delay readout for an appropriate interval. For MOSFETs, the manufacturer's recommendation was to wait two minutes before the readout. In principle, the MOSFET dose record is permanent, but this was not tested in this CRP.

For TLDs, the amount of fading is dependent on a number of factors, including the annealing and, more particularly, the readout cycle. TLD fading is also affected by the storage conditions, and it is recommended that the material should be kept in the dark and away from sources of heat. The measured fading correction is shown in Fig. 19. It can be seen that if the chips are read out between 2 and 50 hours after irradiation, no fading correction is needed. It may, however, be convenient for logistic reasons to insert a fixed delay, and the data in Fig. 19 provide guidance on what limits should be permitted.

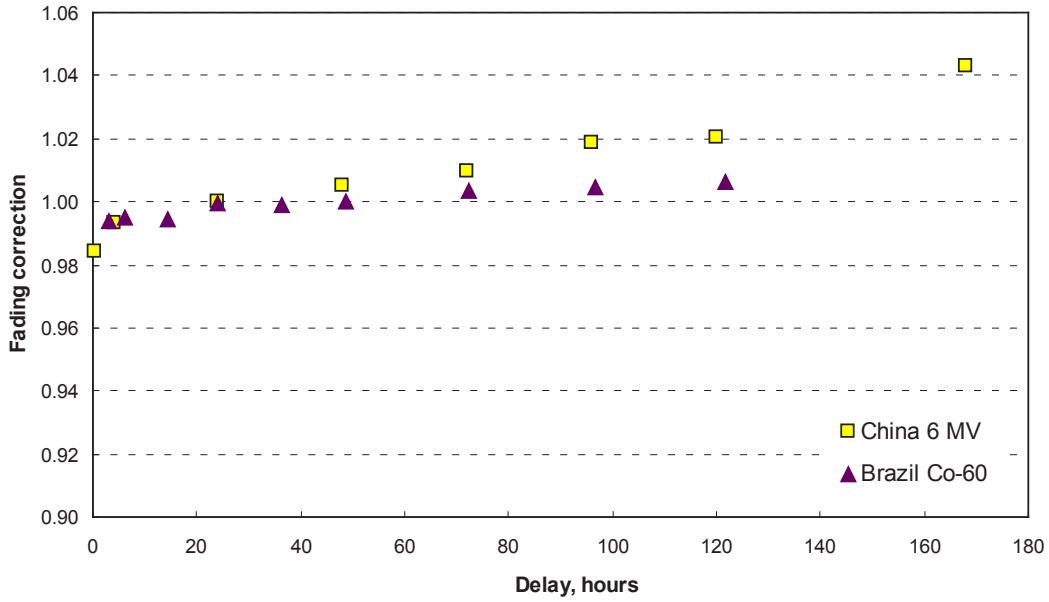

FIG. 19. Fading of the TL signal when TLDs are stored before readout. Normalization was performed at 24 hours. A lightproof container was used for storage.

For OSL dosimeters, it was found that there was a period of very rapid fading immediately following irradiation (see Section I–5.1.6, Fig. I–30, Annex III, Fig. III–9(b) and Annex VI, Fig. VI–3.1). Based on these results, it is essential to wait for a minimum period of 10 min before reading the dosimeter.

6.1.7. Angle of incidence correction

Buildup caps are generally designed for a beam incident normal to the flat base of the dosimeter. When the dosimeter is irradiated at an angle to this beam direction, the thickness of buildup between the sensitive part of the dosimeter and the surface of the assembly may be different. This effect is greater if the physical size of the sensitive volume of the dosimeter is larger. The dosimeter size is smallest for MOSFETs and largest for OSL dosimeters.

The results are shown in Fig. 20. As expected, the size of the correction is indeed larger for the larger dosimeters. For diodes, the magnitude of the effect is very dependent on the individual dosimeter and is different for different energies. It is therefore important to measure the value for every individual dosimeter (not just for each type of dosimeter) and every energy.

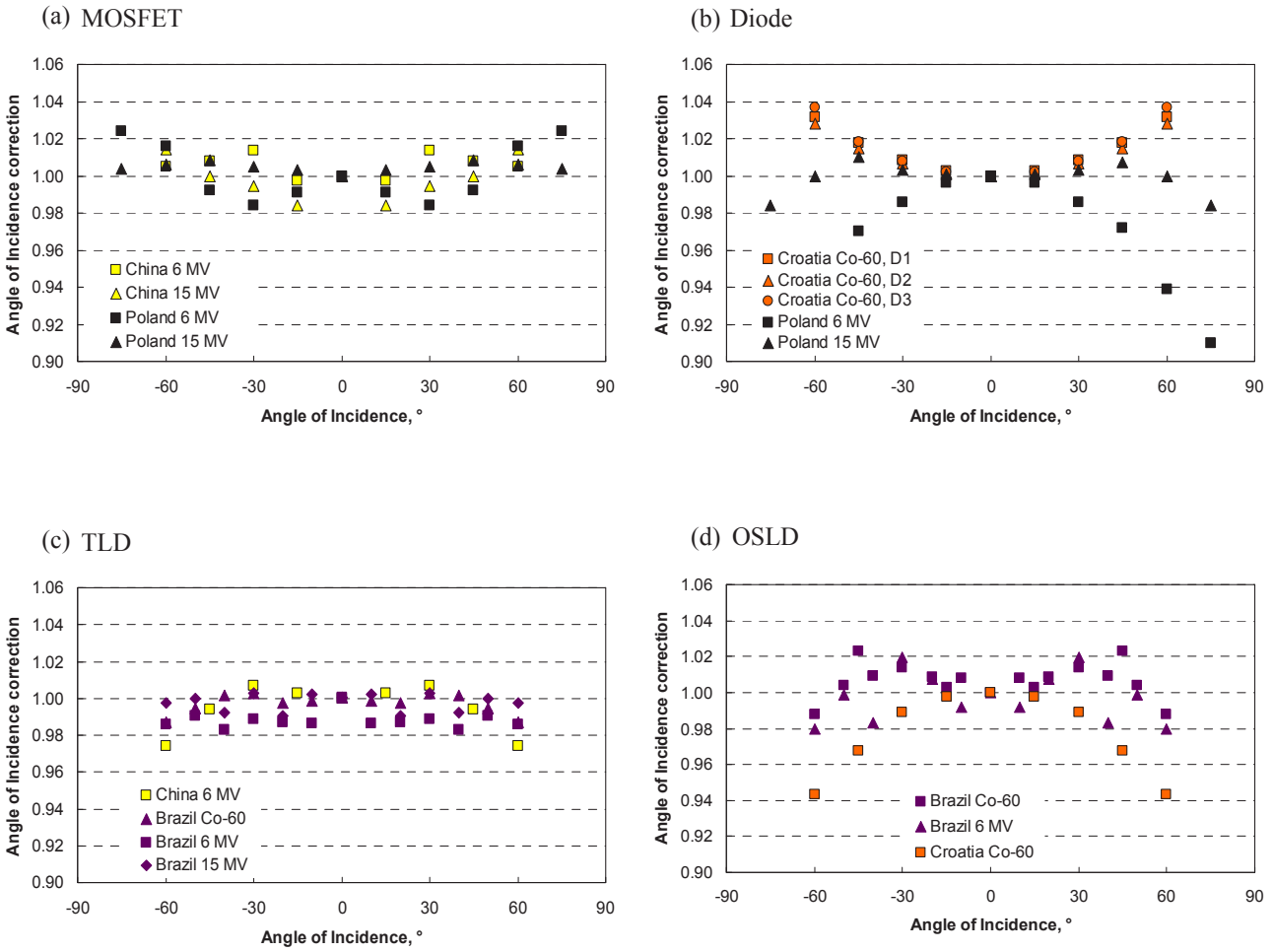

FIG. 20. Variation of angle of incidence correction for different dosimetry systems placed on the surface of a phantom. Dosimeters are shown in ascending order of the physical size of the sensitive dosimeter.

6.1.8. SSD correction

The need for SSD correction arises from the fact that close to the treatment head, there is more head scatter and electron contamination of the beam. The size of the correction depends on the adequacy of the buildup cap and the energy dependence of the dosimeter material. Results for all the dosimeters are shown in Fig. 21. It can be seen that for most dosimetry systems, no correction is needed.

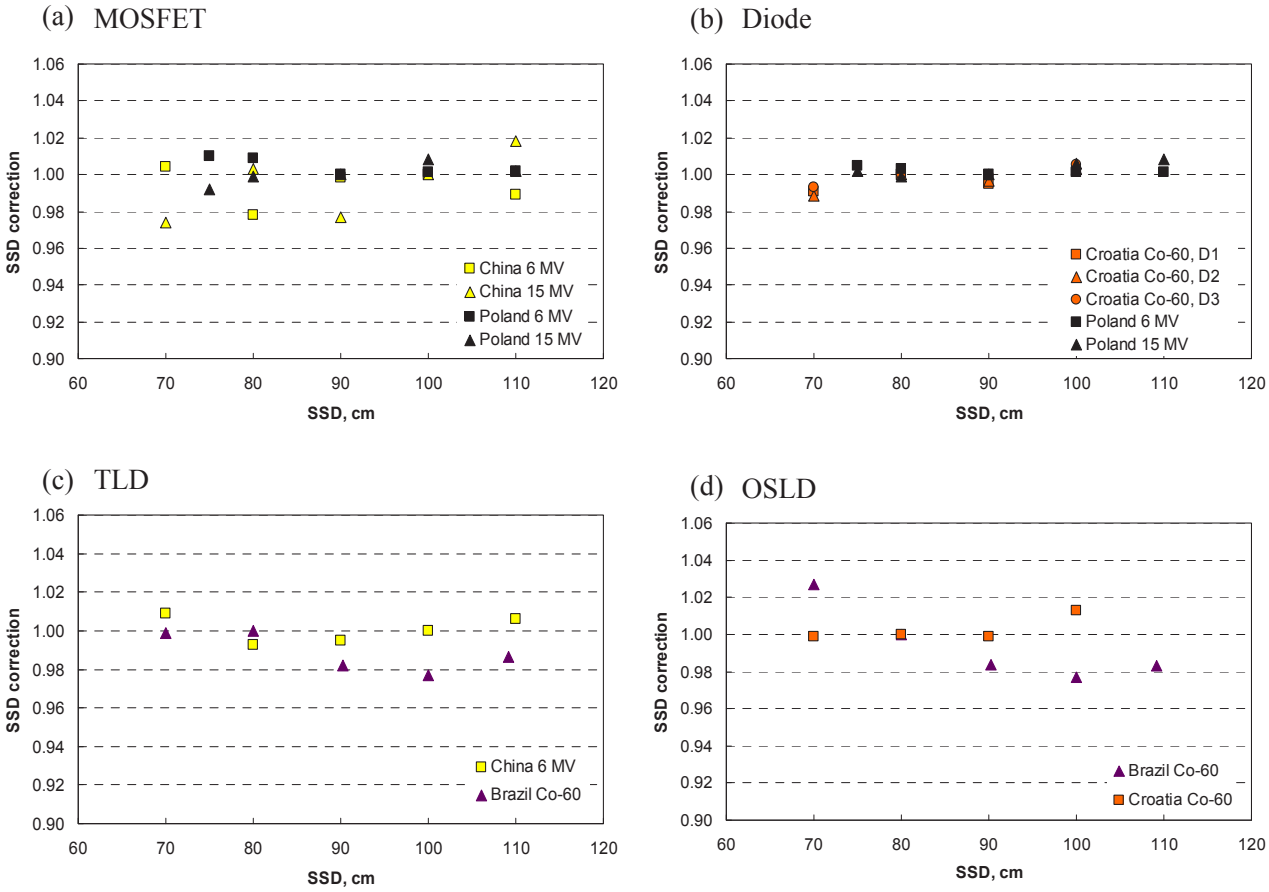

FIG. 21. Variation of SSD correction for different dosimetry systems placed on the surface of a phantom. Dosimeters are shown in order of the physical size of the sensitive dosimeter.

6.1.9. Field size correction

Field size corrections also arise from the different irradiation conditions for large fields (see Section 4.4.2.3) compared to smaller fields. It can be seen from Fig. 22 that for TLD and OSLD, there is little effect, whereas for some situations with MOSFETs and diodes, there does appear to be a significant effect. With diodes, the effect was not apparent for the Scanditronix diodes used in a ^{60}Co beam in Croatia. However, PTW diodes used in high energy X ray beams in Poland exhibited significant field size dependence. The differences between the different sets of measurements probably relate to the different diode constructions, including buildup caps.

6.1.10. Wedge correction

When a solid wedge is introduced into the beam, the spectrum of the radiation will be affected and any energy dependence there may be for a particular dosimeter will become apparent. No significant effect was observed for TLD or MOSFETs. However, for diodes and OSLD, a correction was needed for thicker wedges, as shown in Fig. 23. On the particular cobalt machine in Croatia, different wedges are used for different field sizes, and a larger correction factor was needed for the thicker wedges. The effect may therefore be particularly related to that equipment rather than being specific to the dosimeter type.

6.1.11. Block and tray correction

Measurement of the block and tray correction factor is difficult as it involves adjusting lead blocks on a shadow tray to produce a particular field size. The assumption was made that subsequently adjusting the collimators to produce the same equivalent square field produces the same output factor as the blocked field. In

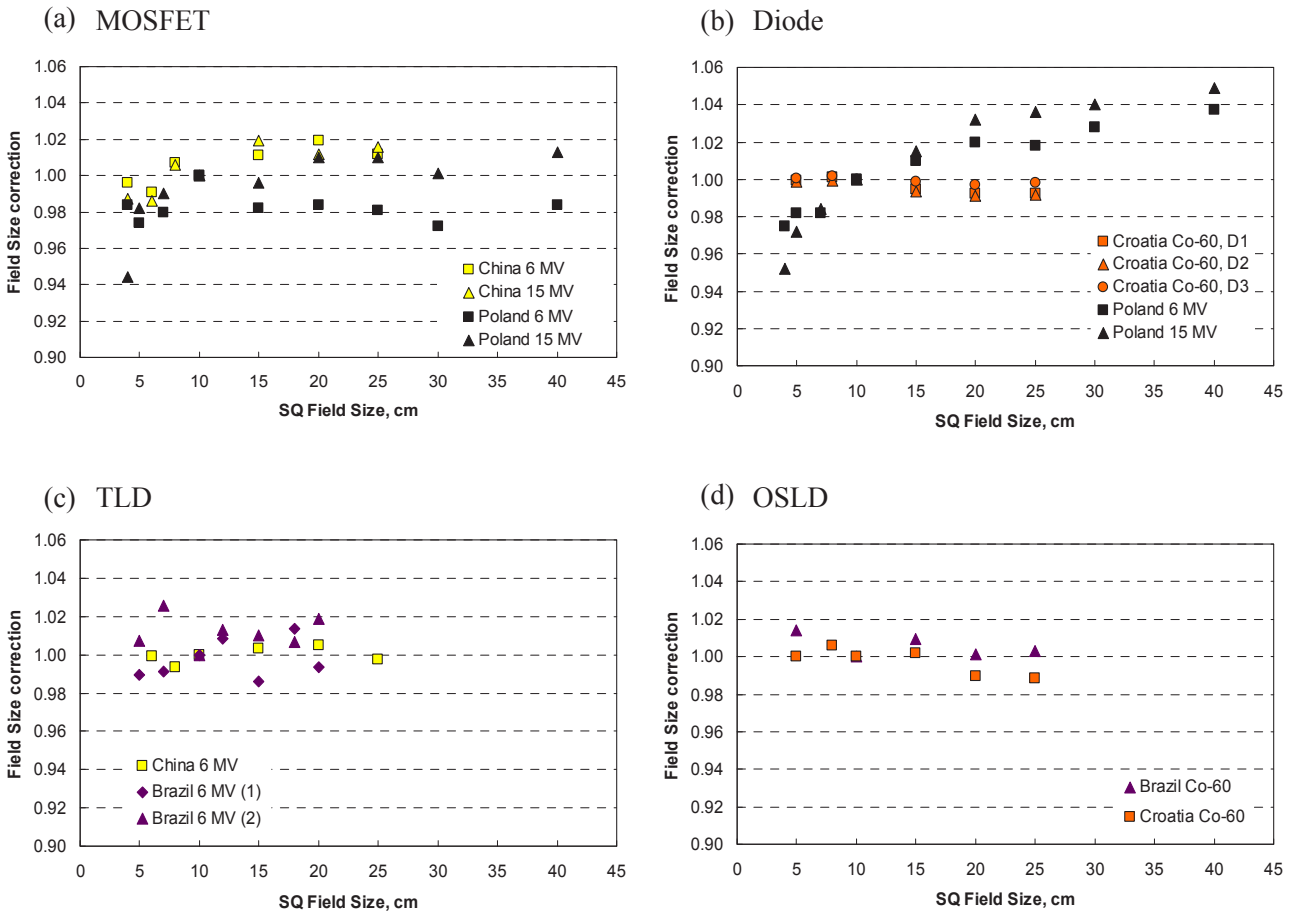

FIG. 22. Variation of correction for field size for different dosimetry systems placed on the surface of a phantom. Dosimeters are shown in ascending order of the physical size of the sensitive dosimeter.

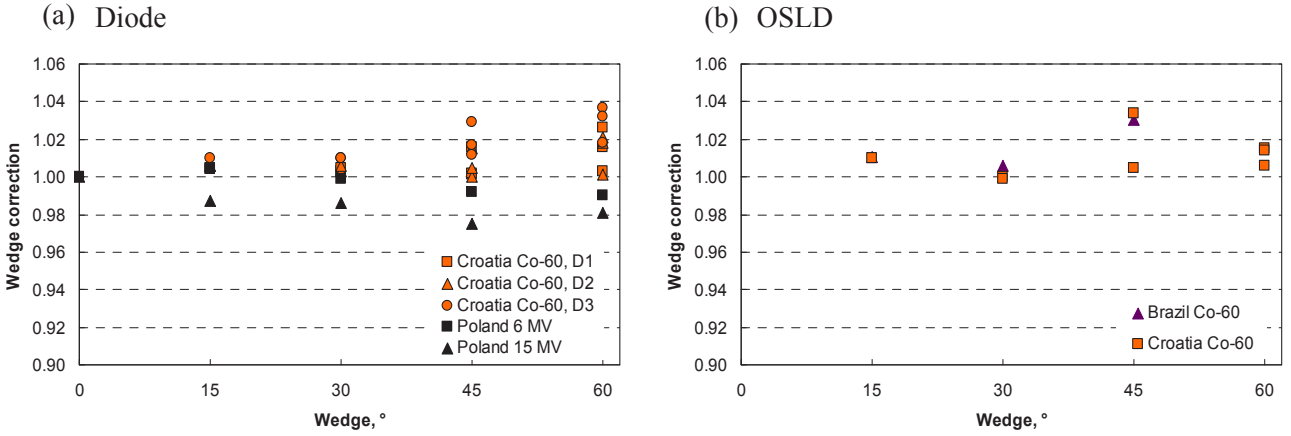

FIG. 23. Wedge correction factors for (a) Diodes and (b) OSLD. The larger deviations found for the wedges in Croatia are for thicker wedges on a ^{60}Co unit. Correction factors were measured for square fields measuring 6 cm, 8 cm and 10 cm (see Annex III).

fact, the collimator scatter factor is not affected by the block but is affected by the change in collimator size, so the methodology may not work satisfactorily for large changes in field size. It was notable, therefore, that the only situation in which a significant factor was measured was with a 15 cm × 15 cm field blocked down to an equivalent square of 10.6 cm, where the correction approached 2%. It may be concluded that no correction is needed for blocked fields provided that an appropriate calculation of the expected dose is carried out.

6.2. PHANTOM MEASUREMENTS

As a preparatory step for the measurements on patients, all centres participating in the CRP conducted the measurements using an Alderson Rando phantom for pelvis, and head and neck, as suggested in Section 4.5.3. The beams used were ^{60}Co and high energy X rays of 6 MV and 15 MV. The results of measurements are presented in the individual reports in the annexes. The measured doses were generally within 3% of the expected doses. No major difficulties were reported. The phantom measurements helped the participants to test the measurement technique and provided them with the necessary confidence regarding the acceptable level of uncertainties involved in the measurement process prior to the introduction of in vivo measurements on patients.

6.3. PATIENT MEASUREMENTS

The detailed results of in vivo measurements on patients with the dosimeters under study in this CRP are presented in the participants' reports in the annexes. A summary is given in Table 1 for TLD, diodes, MOSFET and OSLD, as well as for the different patient irradiation sites. The comparison is made for the same type of dosimeter in two different participating centres.

The values of mean ($\overline{\Delta}$) and standard deviation (σ) of the distribution of deviations between the measured and expected entrance doses are presented in Table 1 together with the percentage of measurements (%N) for which the deviation was below the 5% tolerance level. The mean of the results distribution, if significantly different from zero, may indicate a systemic problem. Standard deviation reflects the combined uncertainty of the treatment delivery and in vivo dosimetry.

A total of 482 treatment fields, mostly for pelvic and head and neck patients, were measured with TLDs in Brazil (see Table 1). Two ^{60}Co units and two linacs were used. The overall mean was $\overline{\Delta} = 0.2\%$, and the standard deviation was $\sigma = 3.3\%$. These results are quite similar to those obtained with TLDs by the Chinese participant for 445 treatment fields.

Different types of diodes and beams were used in patient measurements in Croatia and Poland (Table 1). In a study from Poland, results for pelvic and head and neck treatments (N=70) show small positive deviations, $\overline{\Delta} = +0.4\%$ and $\overline{\Delta} = +1.4\%$ with standard deviations of $\sigma = 3.2\%$ and $\sigma = 2.8\%$, respectively. They are comparable to the literature [4, 8, 11, 98] and to results from a larger number of measurements (N = 340) from Croatia, where the mean deviations were $\overline{\Delta} = +1.1\%$ and $\overline{\Delta} = +0.8\%$ for these two groups, with the respective standard deviations of $\sigma = 1.9\%$ and $\sigma = 3.1\%$.

The analysis of 1740 measurements with MOSFETs from Poland (Table 1) provided the overall mean deviation $\overline{\Delta} = -0.2\%$ and the spread of results was $\sigma = 3.5\%$. In the head and neck group of fields, a small shift of the mean was found $\overline{\Delta} = 1.4\%$ and the spread was $\sigma = 2.7\%$. A larger spread of the results of 3.6% (1σ) was observed in the pelvic and thorax field groups, while the mean deviations reported were closer to zero, $\overline{\Delta} = -0.4\%$ and $\overline{\ } = -1.0\%$, respectively. The results for 948 measurements from China show the mean $\overline{\Delta} = 0.0\%$ with a standard deviation of $\sigma = 3.8\%$. Similar to the Polish results, the head and neck measurements from China have a lower spread than the pelvic field measurements, indicating larger uncertainties for pelvic measurements (possibly reflecting that MOSFET positioning accuracy is better defined for head and neck than for pelvis).

OSL measurements (see Table 1) were conducted by the CRP participants from Brazil and Croatia. The Brazilian results from 205 measurements have a mean of $\overline{\Delta} = 0.3\%$ and standard deviation of $\sigma = 2.9\%$. They have mostly been obtained from head and neck fields. The measurements from Croatia were performed for 103 fields distributed over the various sites, including head and neck, pelvis, breast and others. The overall mean of the Croatian results was $\overline{\Delta} = 1.4\%$, and the spread was $\sigma = 3.6\%$. The measurements for head and neck, and pelvis had lower standard deviations ($\sigma = 2.4\%$) compared to other measurements; in particular, the breast fields showed quite a large spread ($\sigma = 6\%$). The participant concluded that OSLD, in conjunction with its buildup cap, was an appropriate dosimeter for the situations with normal beam incidence but not a particularly suitable one for tangential fields. The detailed analysis of these results is given in Annex III.

TABLE 1. DEVIATIONS BETWEEN THE MEASURED AND EXPECTED ENTRANCE DOSE

TLD MEASUREMENTS							
Brazil; Co-60, 6 MV and 15 MV				China; 6 MV			
Site	*N*	$\bar{\Delta} \pm \sigma$, %	%*N* (|Δ| < 5%)	Site	*N*	$\bar{\Delta} \pm \sigma$, %	%*N* (|Δ| < 5%)
Head and neck	264	0.5 ± 3.0	93.6	Head and neck	303	1.0 ± 3.1	87.1
Pelvis	178	–0.5 ± 3.7	78.7	Pelvis	120	–1.0 ± 3.6	95.0
Breast	—	—	—	Breast	—	—	—
Other	40	–1.4 ± 3.4	81.8	Other	22	–0.2 ± 2.6	100.0
All measurements	482	0.2 ± 3.3	88.4	All measurements	445	0.4 ± 3.4	90.0
DIODE MEASUREMENTS							
Croatia; Co-60				Poland; 6 MV			
Site	*N*	$\bar{\Delta} \pm \sigma$, %	%*N* (|Δ| < 5%)	Site	*N*	$\bar{\Delta} \pm \sigma$, %	%*N* (|Δ| < 5%)
Head and neck	138	0.8 ± 3.1	92.1	Head and neck	31	1.9 ± 3.2	77.4
Pelvis	202	1.1 ± 1.9	98.5	Pelvis	39	0.4 ± 2.8	92.3
Breast	118	–1.1 ± 3.9	90.5	Breast	5	—	80
Other		(see Annex III)		Other	—	—	—
All measurements	727	0.5 ± 3.2	95.1	All measurements	75	1.0 ± 3.0	85.3
MOSFET MEASUREMENTS							
China; 6 and 15 MV				Poland; 6 and 15 MV			
Site	*N*	$\bar{\Delta} \pm \sigma$, %	%*N* (|Δ| < 5%)	Site	*N*	$\bar{\Delta} \pm \sigma$, %	%*N* (|Δ| < 5%)
Head and neck	313	–0.6 ± 3.1	87.5	Head and neck	254	1.4 ± 2.7	90.9
Pelvis	404	0.8 ± 3.9	79.2	Pelvis	1331	–0.4 ± 3.6	85.4
Breast	—	—	—	Breast	—	—	—
Other	231	–0.8 ± 4.2	77.9	Other	155	–1.0 ± 3.6	87.7
All measurements	948	0.0 ± 3.8	81.6	All measurements	1740	–0.2± 3.5	86.3

TABLE 1. DEVIATIONS BETWEEN THE MEASURED AND EXPECTED ENTRANCE DOSE (cont.)

OSL MEASUREMENTS							
OSLD							
Brazil; Co-60				Croatia; Co-60			
Site	*N*	$\bar{\Delta} \pm \sigma$, %	%*N* (|Δ| < 5%)	Site	*N*	$\bar{\Delta} \pm \sigma$, %	%*N* (|Δ| < 5%)
Head and neck	160	0.0 ± 2.3	95.6	Head and neck	11	1.2 ± 2.4	90.9
Pelvis	10	2.4 ± 3.1	80.0	Pelvis	34	2.9 ± 2.4	85.3
Breast	—	—	—	Breast	21	–0.8 ± 6.0	90.5
Other	35	0.2 ± 2.1	85.3	Other	37	0.4 ± 1.7	100
All measurements	205	0.3 ± 2.9	93.2	All measurements	103	1.4 ± 3.6	91.3

Note: N denotes the number of measurements, $\bar{\Delta}$ is the percentage mean deviation, σ is the standard deviation of the distribution and %N (|Δ| < 5 %) is the percentage of measurements within the ± 5% tolerance level. The measurements are grouped according to the site: pelvis, head and neck, breast, other group and all measurements.

Based on the reported standard deviations and the means of the results' distribution in patient studies, one can conclude that it would have been appropriate to establish an action level at 7% (corresponding to two standard deviations of the results' distribution) for most centres and for major treatment sites. In some centres, the data suggest lower levels of about 5% for the selected sites measured with specific dosimeters, for example, for pelvis measurements with diodes in Croatia or head and neck measurements with OSL in Brazil. As indicated in individual reports, some centres have adopted two action levels depending on the type of field used (e.g. 7% for breast fields and 5 % for others). In Poland, a higher tolerance level of 7% was adopted for all wedged fields. If this approach is followed, it results in a lower number of measurements outside the tolerance levels (Croatia and Poland).

Overly strict tolerance may have the undesirable effect of an increased number of repeated measurements and an extra workload that is not completely justified. At the same time, it also introduces mistrust and anxiety to the working environment.

The percentage of acceptable results, defined as those measurements for which the deviation was less than ±5%, exhibits some differences between different participating centres, anatomical sites and dosimeters (see Table 1). On average, approximately 90% of total measurements were within the 5% tolerance levels. The best results have been achieved with diodes, 95% (Croatia) and then with OSL, 94 % (Brazil). If one accepts a higher tolerance level of 7% for all wedged fields, as is routinely accepted in Poland, the percentage of acceptable results for their MOSFET measurements approaches 100%. Comparable results of roughly 90%–92% within the tolerance level were achieved in two centres: one in Brasil with TLDs and the other in Croatia with OSLDs.

Major deviations were observed in some diode measurements (Croatia), for example, when the wedge was not inserted into the beam, and in a few cases when SSD set-up was wrongly handled as an isocentric treatment. OSLD measurement discovered a wrong fractionation scheme that was not properly accounted for during the computer treatment planning, effectively delivering a lower dose per fraction than planned to the patient. Some of these human errors, however, would have been avoided if an RV system had been in place. In a large number of patient measurements with MOSFETs (Poland), six errors were detected when the treatment data were entered into the RV system manually rather than being transferred electronically from planning to delivery. In other participants' reports, major deviations were not listed or explained.

Practical problems experienced with the dosimeters include fixation problems, usually caused by poor quality tape, and problems with posterior fields when the dosimeter was fixed to a 'tennis racket' (a mylar sheet reinforced with a nylon net) when it was difficult to achieve accurate positioning in relation to the radiation field. Precise positioning of the dosimeter turned out to be most important in combined wedged and oblique fields (as in breast treatments). The inability to precisely position the dosimeter combined with an uncertainty in determining the

actual angle of beam incidence that is used for the correction factor largely influence the accuracy and precision of in vivo dosimetry in these type of treatments.

7. SUMMARY AND CONCLUSION

This CRP provided a very useful experience for all participants, which started with the development of in vivo dosimetry protocols for measurements with various dosimeters, continued with the understanding of the operation principles of each dosimetry system used in the project and concluded with patient data measurements and analysis. The importance of following a common procedure when comparing the data from various centres deserves to be particularly stressed.

All the dosimeters used for in vivo measurements in this project belong to the class of solid state dosimetry systems, which do not require a correction for atmospheric pressure. The dosimeters were TLD chips (which are long established and well understood), diodes, MOSFETs and OSL dosimeters, which have been recently introduced to medical applications. Each participant used two different dosimetry systems: one well established system (such as TLD or diodes) with which the participant had considerable experience, and another that was relatively new in radiotherapy as compared with TLDs and diodes. Below is the assignment list of the dosimeters:

— Brazil: TLD and OSLD;
— China: TLD and MOSFET;
— Croatia: Diodes and OSLD;
— Poland: Diodes and MOSFET.

This dosimeter assignment allowed for comparison of the data obtained for each type of dosimeter from two independent laboratories, which increased the overall level of confidence in the results.

It is believed that this report will be useful not only for the participants of this project but also for any radiotherapy physicist who plans to introduce an in vivo dosimetry programme in a cancer centre.

This CRP developed a methodology and resulted in comprehensive sets of dosimeter characteristics and comprehensive documentation of tests that may serve as reference data for other centres. The summary of in vivo dosimeter characteristics measured by the CRP participants is given in Table 2.

All the dosimeters showed some level of energy dependence in the energy range ^{60}Co–15 MV (MOSFET: ^{192}Ir–15 MV). Therefore, it is recommended that each dosimeter is calibrated for the energy at which it is going to be used.

Based on the experience gained during this project, the CRP participants were able to identify advantages and disadvantages of each type of dosimeter and their suitability for particular clinical circumstances.

For TLDs, which are widely available and well understood in the literature, the participants identified the following advantages: small size, no cables and a possibility of reuse after annealing. Very few corrections were required, so the dosimetry system characterization is rather simple. However, to achieve good measurement reproducibility of 2% or less, careful annealing and handling of TLDs is required with individual dosimeter calibration and the need to keep track of individual dosimeters, which is labour intensive. TLDs are not waterproof and can be sensitive to temperature and humidity. The participants found the best results with a delay of several hours between the irradiation and readout, which may be considered a disadvantage in the clinical environment. The overall standard deviation of the TLD results of in vivo dosimetry on patients was 3.4% for both of the participants from Brazil and China.

Both institutions using diodes for in vivo dosimetry (i.e. the participants from Croatia and Poland) emphasized a number of advantages of diodes in routine clinical application such as their stability and excellent reproducibility of the signal, ease of calibration and use, and rather straightforward although cumbersome measurement of correction factors. Other advantages are related to immediate on-line readout and the long lifespan of diodes. Diode based in vivo dosimetry systems offer a possibility of handing over the responsibility of patient measurements to radiation therapists owing to their ease of use. Special attention needs to be given to the temperature dependence of the diode signal, which has to be properly accounted for (this can be circumvented by using a thin Styrofoam base

TABLE 2. SUMMARY OF CHARACTERISTICS OF IN VIVO DOSIMETERS TESTED WITHIN THE PROJECT

Parameter	Dosimeter characteristics or correction factor			
	Diode	MOSFET	TLD	OSLD
Reproducibility (1 SD)	<1%	<2%	<2%	<2%
Dose rate dependence	Negligible[a]	Negligible	Negligible	Negligible
Dose response non-linearity (1 Gy–4 Gy)	Negligible	Negligible	~8%	4%–8%
Fading (3 days)	n/a	Negligible	<2%	<2%
Angle of incidence[b] (at 60°)	Up to 10%	<2%	~2%	8%–10%
SSD	<1%	<2%	Negligible	<2%
Field size 5 cm × 5 cm to 40 cm × 40 cm	±4%	±2%	Negligible	Negligible
Wedge	<5%	Negligible	Negligible	Negligible
Tray	<2%	Negligible	Negligible	Negligible
Special precautions	Temperature dependence	Recalibration at 2/3 lifetime	Careful annealing and handling required	Early fading (<10 min)
Main advantages	Good reproducibility, on-line reading	Immediate reading, little fading	No cables, can be reused after annealing, few corrections required	No cables, can be reused after bleaching
Main disadvantages	Cumbersome calibration with many corrections; cables present	Limited lifetime; high price	Labour consuming; expensive TLD equipment	Short lifetime; dependence on accumulated dose

[a] Within the uncertainty of the measurement.
[b] Tests performed for detectors equipped with buildup caps placed at the surface of a solid phantom.

to isolate them from the patient's skin). Their slight disadvantage is reflected in the fact that for different energies, a different set of diodes must be used, and therefore they have to be completely characterized and tested prior to any clinical application. For higher energies, diodes require additional buildup material. Another disadvantage is related to cumbersome cables present during the measurements. The overall standard deviation of the results of diode based in vivo dosimetry on patients was 3.0% for the Polish participant and 3.2% for the Croatian participant.

The participants using MOSFET dosimeters, i.e. China and Poland, saw an advantage in their small size with no correction factors larger than 2%. MOSFET dosimeters offer fast reading with a short delay after irradiation for best results. The MOSFETs used in this project exhibited little fading and were temperature independent. MOSFETs are waterproof and can be used in brachytherapy. There are some cables present during measurements as MOSFETs have to be connected to a bias box. They can be reused several times but they require a new calibration at about 2/3 of their lifetime. For a busy in vivo dosimetry programme, the limited lifetime of MOSFETs needs to be considered in budgetary planning as it involves moderate ongoing expenses for dosimeter replacements as they reach the end of their lives. The overall standard deviation of the results of MOSFET based in vivo dosimetry on patients was 3.5% for the Polish participant and 3.8% for the Chinese participant.

The OSLD system provided for this project had recently been introduced to radiation therapy, and it had not yet been optimized for routine in vivo dosimetry use. This sort of OSL dosimetry system has been previously used for radiation protection dosimetry, where wider levels of dose tolerances are acceptable than in radiation therapy. Several problems with the OSL readers were encountered during the early stage of the project, which caused some delay with the data collection in the centres involved. However, this early experience enabled the group not only to understand how the system works but also to identify its shortcomings and the methods to work around them. The participants have provided the manufacturer with detailed feedback that was considered useful to optimize the system for radiation therapy applications. In addition, experience with the OSL system clearly confirms the existence of a learning curve for a new technology. When measuring any characteristics of an unknown dosimeter, one of the basic principles is to perform the readings in such an order that systemic problems with the reader are avoided.

The participants testing OSLDs (Brazil, Canada, Croatia, UK) considered that OSLD presents several advantages such as good readout reproducibility, temperature independence and little long term fading. Special attention needs to be paid to the significant rapid fading of the signal during the first few minutes after the dosimeter irradiation. After having received a dose of the order of a few grays, OSLD sensitivity exhibits strong dependence on the accumulated dose and, consequently, the dosimeter response changes significantly. Thus OSLDs have a rather short useful lifetime, and they need to be replaced frequently. However, if bleaching is carefully carried out, the OSLDs can be reused several times. No cables are required for OSLDs in a passive mode as used in this CRP.

The overall standard deviation of the results of OSLD based in vivo dosimetry on patients was 2.8% for the Brazilian participant and 3.6% for the Croatian participant.

It was felt by the participants that for standard QA of teletherapy treatments, diodes would be the most logical choice. They have a high reproducibility and provide immediate feedback on the dose delivered to the patient. They also can be used for a long time before any radiation damage occurs. Similar to diodes, MOSFETs are easy to handle and also provide almost immediate readout. However, they have larger readout uncertainties than diodes and a finite lifetime in relation to accumulated dose. Nevertheless, due to a very small size combined with waterproof encapsulation, it is the dosimeter of choice for in vivo dosimetry in brachytherapy (see Annexes II and V). As discussed above, TLDs may be more difficult to handle. Although they are the best established technology for in vivo dosimetry, they are quite cumbersome to use in the standard clinical set-up. In developing countries with tropical climates where the clinical environment may be hard to control at all times, TLD dosimetry may encounter special difficulties related to the ambient temperature and humidity. The OSL system tested during this CRP promises to be easier to use than TLDs once the hardware is optimized for radiation therapy dosimetry.

The considerations above gathered by this CRP may be useful for a radiotherapy physicist who wishes to choose an appropriate dosimetry system and to test the measurement methodology properly. The results will provide assurance that the uncertainties involved in the measurement process are within the expected levels.

At the same time, the CRP has developed and tested a step by step methodology for introducing in vivo dosimetry into radiotherapy clinics. Following the characterization of a dosimetry system of choice and prior to beginning routine measurements on patients, an initial set of in vivo measurements need to be conducted using an anthropomorphic phantom to properly test the measurement methodology and provide assurance that the uncertainties involved in the measurement process are within the expected levels. This CRP suggests that simple treatment beam arrangements such as those used for irradiation of the pelvis and of the head and neck would be a suitable choice for testing on phantoms. The next test suggested would be a breast irradiation with tangential fields, which is more difficult to measure due to higher uncertainties in the dosimeter positioning and the correction factors involved. The CRP participants believe that in vivo measurements using an anthropomorphic phantom constitute a necessary preparatory step before measurements on patients are initiated.

For measurements on patients, firstly, a pilot study needs to be carried out including a limited number of patients irradiated with simple techniques. In vivo dosimetry is easier to implement in sites with regular body contours not involving high dose gradients, such as the pelvis. For this reason, it is recommended that implementation should begin with such sites and techniques. Once the system has been established and validated for these sites, more complex areas need to be considered. After completion of the pilot study, the routine in vivo dosimetry programme should be incorporated in the quality management system of the radiotherapy department.

Overall scientific supervision of an in vivo dosimetry programme resides with a qualified radiotherapy physicist. Obviously, the treatment staff need to be fully involved in the routine implementation of in vivo dosimetry, and they should play an active role in managing the logistics of the programme. It is important that the radiotherapy

staff understand the philosophy and rationale for in vivo dosimetry. The roles and responsibilities for different staff groups need to be defined and instructions written for the use of the equipment available along with measurement and reporting documentation. Commitment from the treatment staff is essential to the success of in vivo dosimetry, and demonstration of improvements resulting from the programme will help this commitment. Team work and appropriate communication between staff groups are essential for the integrity of the in vivo dosimetry programme in a hospital. The results of in vivo dosimetry need to be routinely reported both to the medical staff and to the staff who perform the treatments. Any errors should be analysed and rectified in order to limit the possibility of escalating the dose misadministration to many treatments or many patients. Lessons leant from the errors detected should provide feedback to improve the quality management system of the radiotherapy centre.

Until recently, the routine clinical implementation of in vivo dosimetry has been quite limited in many radiotherapy centres. However, there is growing interest in establishing in vivo dosimetry programmes. This has been partially triggered by a recent series of radiotherapy accidents in industrialized countries [20] that would have been avoided if such programmes were in place. It is believed that the present publication provides suitable guidance for the preparation and implementation of in vivo dosimetry programmes for stationary techniques in radiotherapy. Once established, in vivo dosimetry constitutes a QA tool that may help to reduce the number of misadministrations of dose to radiotherapy patients. To conclude, in vivo dosimetry is a suitable tool to detect errors in radiotherapy, to assess clinically relevant differences between the prescribed and delivered doses, to document doses received by individual patients and to fulfil requirements set forth by some national regulations.

REFERENCES

[1] WORLD HEALTH ORGANIZATION, Radiotherapy Risk Profile, WHO Press, Geneva (2008).

[2] INTERNATIONAL ATOMIC ENERGY AGENCY, Investigation of an Accidental Exposure of Radiotherapy Patients in Panama: Report of a team of experts, IAEA, Vienna (2001).

[3] INTERNATIONAL COMMISSION ON RADIOLOGICAL PROTECTION, Prevention of Accidents to Patients Undergoing Radiation Therapy, ICRP Publication 86, ICRP, Bethesda, MD (2000).

[4] EUROPEAN SOCIETY FOR THERAPEUTIC RADIOLOGY AND ONCOLOGY, Practical Guidelines for the Implementation of In Vivo Dosimetry with Diodes in External Radiotherapy with Photon Beams (Entrance Dose), Physics for Clinical Radiotherapy, Booklet No. 5, ESTRO, Brussels (2004).

[5] AMERICAN ASSOCIATION OF PHYSICISTS IN MEDICINE, Diode In Vivo Dosimetry for Patients Receiving External Beam Radiation Therapy, AAPM Task Group 62, Report No. 87, M.P. Publishing, Madison, WI (2005).

[6] EUROPEAN SOCIETY FOR THERAPEUTIC RADIOLOGY AND ONCOLOGY, Methods for In Vivo Dosimetry in External Radiotherapy, 2 ed, Physics for Clinical Radiotherapy, Booklet No. 1, ESTRO, Brussels (2006).

[7] LEUNENS, G., et al., Quality assurance in radiotherapy by in vivo dosimetry. 2. Determination of the target absorbed dose, Radiother. Oncol. **19** (1990) 73–87.

[8] ESSERS, M., MIJNHEER, B.J., In vivo dosimetry during external photon beam radiotherapy, Int. J. Radiat. Oncol. Biol. Phys. **43** (1999) 245–259.

[9] CALANDRINO, R., et al., Detection of systematic errors in external radiotherapy before treatment delivery, Radiother. Oncol. **45** (1997) 271–274.

[10] MILLWATER, C.J., et al., In vivo semiconductor dosimetry as part of routine quality assurance, Br. J. Radiol. **71** (1998) 661–668.

[11] LEUNENS, G., et al., Quality assurance in radiotherapy by in vivo dosimetry. 1. Entrance dose measurements, a reliable procedure, Radiother. Oncol. **17** (1990) 141–151.

[12] VAN ELMPT, W., MCDERMOTT, L.N., NIJSTEN, S., WENDLING, M., LAMBIN, P., MIJNHEER, B.J., Electronic portal imaging for radiotherapy dosimetry: review of current practice, Radioth. Oncol. **88** (2008) 289–309.

[13] EUROPEAN SOCIETY FOR THERAPEUTIC RADIOLOGY AND ONCOLOGY, Monitor Unit Calculation for High Energy Photon Beams, Physics for Clinical Radiotherapy, Booklet No. 3, ESTRO, Brussels (1997).

[14] EUROPEAN SOCIETY FOR THERAPEUTIC RADIOLOGY AND ONCOLOGY, Monitor Unit Calculation for High Energy Photon Beams - Practical Examples, Physics for Clinical Radiotherapy, Booklet No. 6, ESTRO, Brussels (2001).

[15] GEORG, D., Monitor unit calculation on the beam axis of open and wedged asymmetric high-energy photon beams, Phys. Med. Biol. **44** (1999) 2987–3007.

[16] GEORG, D., et al., Formalisms for MU calculations, ESTRO booklet 3 versus NCS report 12, Radiother. Oncol. **60** (2001) 319–328.

[17] GEORG, D., et al., Patient-specific IMRT verification using independent fluence-based dose calculation software: experimental benchmarking and initial clinical experience, Phys. Med. Biol. **52** (2007) 4981–4992.

[18] BRIDIER, A., DUTREIX, A., A method for dose calculation for high energy photon beams based on measurements performed at reference depth, Acta Oncol. **32** (1993) 425–433.

[19] DERREUMAUX, S., et al., Lessons from recent accidents in radiation therapy in France, Radiat. Prot. Dosim. **131** (2008) 130–135.

[20] INTERNATIONAL COMMISSION ON RADIOLOGICAL PROTECTION, Preventing accidental exposures from new external beam radiation therapy technologies, ICRP Report 112, ICRP, Elsevier, Maryland Heights, MD (2009).

[21] AGUIRRE, J.F., et al., Thermoluminescence dosimetry as a tool for the remote verification of output for radiotherapy beams: 25 years of experience, Standards and Codes of practice in Medical Radiation Dosimetry (Proc. Int. Symp. Vienna 2004), Vienna, IAEA (2004) 191–199.

[22] IZEWSKA, J., et al., IAEA/WHO TLD postal dose audit service and high precision measurements for radiotherapy level dosimetry, Radiat. Prot. Dosim. **101** (2002) 387–392.

[23] FERREIRA, I.H., et al., The ESTRO-Quality assurance network (EQUAL), Radiother. Oncol. **55** (2000) 273–284.

[24] IZEWSKA, J., ANDREO, P., The IAEA/WHO TLD postal programme for radiotherapy hospitals, Radiother. Oncol. **54** (2000) 65–72.

[25] YUKIHARA, E.G., MCKEEVER, S.W., Optically stimulated luminescence (OSL) dosimetry in medicine, Phys. Med. Biol. **53** (2008) 351–379.

[26] REFT, C.S., The energy dependence and dose response of a commercial optically stimulated luminescent detector for kilovoltage photon, megavoltage photon, and electron, proton, and carbon beams, Med. Phys. **36** (2009) 1690–1699.

[27] HU, B., et al., Performance of Al_2O_3:C optically stimulated luminescence dosimeters for clinical radiation therapy applications, Australas. Phys. Eng. Sci. Med. **32** (2009) 226–232.

[28] YUKIHARA, E.G., et al., Evaluation of Al_2O_3:C optically stimulated luminescence (OSL) dosimeters for passive dosimetry of high-energy photon and electron beams in radiotherapy, Med. Phys. **35** (2008) 260–269.

[29] JURSINIC, P.A., Changes in optical stimulated luminescent dosimeter (OSLD) dosimetric characteristics with accumulated dose, Med. Phys. **37** (2010) 132–140.
[30] HEUKELOM, S., et al., In vivo dosimetry during pelvic treatment, Radiother. Oncol. **25** (1992) 111–120.
[31] ADEYEMI, A., LORD, J., An audit of radiotherapy patient doses measured with in vivo semiconductor detectors, Br. J. Radiol. **70** (1997) 399–408.
[32] MAYLES, W.P.M., et al., "Treatment Verification and In Vivo Dosimetry", in Radiotherapy Physics in Practice, Oxford University Press, Oxford (2000) 220–246.
[33] MAYLES, P., et al., Handbook of Radiotherapy Physics: Theory and Practice, Taylor & Francis (2007).
[34] HOROWITZ, Y.S., LiF:Mg,Ti Versus LiF:Mg,Cu,P: The Competition Heats Up, Radiat. Prot. Dosim. **47** (1993) 135–141.
[35] FURETTA, C., et al., A precise investigation on the TL behavior of LiF: Mg, Cu, P (GR-200A), Med. Phys. **21** (1994) 1605–1609.
[36] EISENLOHR, H.H., JAYARAMAN, S., IAEA-WHO cobalt-60 teletherapy dosimetry service using mailed LiF dosemeters. A survey of results obtained during 1970–75, Phys. Med. Biol. **22** (1977) 18–28.
[37] BOYD, A.W., EISENLOHR, H.H., IAEA/WHO ^{60}Co teletherapy dosimetry service using mailed LiF dosimeters. A survey of results obtained during 1975-–1982, Med. Phys. **10** (1983) 491–492.
[38] IZEWSKA, J., et al., Analysis of uncertainties in the IAEA/WHO TLD postal dose audit system, Radiat. Meas. **43** (2008) 959–963.
[39] BARTOLOTTA, A., et al., The response behaviour of LiF:Mg,Cu,P thermoluminescence dosimeters to high-energy electron beams used in radiotherapy, Phys. Med. Biol. **40** (1995) 211–220.
[40] HOROWITZ, Y.S., The theoretical and microdosimetric basis of thermoluminescence and applications to dosimetry, Phys. Med. Biol. **26** (1981) 765–824.
[41] MA, C.M., NAHUM, A.E., Bragg-Gray theory and ion chamber dosimetry for photon beams, Phys. Med. Biol. **36** (1991) 413–428.
[42] NAHUM, A.E., Perturbation effects in dosimetry: Part I. Kilovoltage x-rays and electrons, Phys. Med. Biol. **41** (1996) 1531–1580.
[43] MOBIT, P.N., et al., The quality dependence of LiF TLD in megavoltage photon beams: Monte Carlo simulation and experiments, Phys. Med. Biol. **41** (1996) 387–398.
[44] MOBIT, P.N., et al., The energy correction factor of LiF thermoluminescent dosemeters in megavoltage electron beams: Monte Carlo simulations and experiments, Phys. Med. Biol. **41** (1996) 979–993.
[45] ROBAR, V., et al., Thermoluminescent dosimetry in electron beams: energy dependence, Med. Phys. **23** (1996) 667–673.
[46] DRISCOLL, C.M., MCKINLAY, A.F., Particle size effects in thermoluminescent lithium fluoride, Phys. Med. Biol. **26** (1981) 321–327.
[47] ARIB, M., et al., Optimum parameters of TLD100 powder used for radiotherapy beams calibration check, Med. Dosim. **31** (2006) 184–189.
[48] KROUTILKOVA, D., et al., Thermoluminescent dosimeters (TLD) quality assurance network in the Czech Republic, Radiother. Oncol. **66** (2003) 235–244.
[49] SWINNEN, A., et al., Feasibility study of entrance in vivo dose measurements with mailed thermoluminescence detectors, Radiother. Oncol. **73** (2004) 89–96.
[50] DERREUMAUX, S., et al., A European quality assurance network for radiotherapy: dose measurement procedure, Phys. Med. Biol. **40** (1995) 1191–1208.
[51] WOOD, J.J., MAYLES, W.P., Factors affecting the precision of TLD dose measurements using an automatic TLD reader, Phys. Med. Biol. **40** (1995) 309–313.
[52] JORNET, N., et al., In vivo dosimetry: intercomparison between p-type based and n-type based diodes for the 16–25 MV energy range, Med. Phys. **27** (2000) 1287–1293.
[53] RIKNER, G., GRUSELL, E., General specifications for silicon semiconductors for use in radiation dosimetry, Phys. Med. Biol. **32** (1987) 1109–1117.
[54] DIXON, R.L., EKSTRAND, K.E., Silicon Diode Dosimetry, Int. J. Appl. Radiat. Isotop. **33** (1982) 1171–1176.
[55] GEORG, D., et al., Build-up modification of commercial diodes for entrance dose measurements in 'higher energy' photon beams, Radiother. Oncol. **51** (1999) 249–256.
[56] GRUSELL, E., RIKNER, G., Evaluation of temperature effects in p-type silicon detectors, Phys. Med. Biol. **31** (1986) 527–534.
[57] THOMSON, I., et al., Radiation dosimetry with MOS sensors, Radiat. Prot. Dosim. **6** (1983) 121–124.
[58] SOUBRA, M., et al., Evaluation of a dual bias dual metal oxide-silicon semiconductor field effect transistor detector as radiation dosimeter, Med. Phys. **21** (1994) 567–572.
[59] BUTSON, M.J., et al., A new radiotherapy surface dose detector: the MOSFET, Med Phys **23** (1996) 655–658.
[60] RAMASESHAN, R., et al., Performance characteristics of a microMOSFET as an in vivo dosimeter in radiation therapy, Phys. Med. Biol. **49** (2004) 4031–4048.
[61] SCALCHI, P., FRANCESCON, P., Calibration of a MOSFET detection system for 6-MV in vivo dosimetry, Int. J. Radiat. Oncol. Biol. Phys. **40** (1998) 987–993.

[62] SCALCHI, P., et al., Characterization of a new MOSFET detector configuration for in vivo skin dosimetry, Med. Phys. **32** (2005) 1571–1578.
[63] JORNET, N., et al., Comparison study of MOSFET detectors and diodes for entrance in vivo dosimetry in 18 MV x-ray beams, Med. Phys. **31** (2004) 2534–2542.
[64] SZE, S.M., "MOSFET" , Physics of Semiconductor Devices, Wiley & Sons, New York, NY (1981) 431–496, Ch. 8.
[65] SCARANTINO, C.W., et al., An implantable radiation dosimeter for use in external beam radiation therapy, Med. Phys. **31** (2004) 2658–2671.
[66] CHEUNG, T., et al., Effects of temperature variation on MOSFET dosimetry, Phys. Med. Biol. **49** (2004) N191–196.
[67] KINHIKAR, R.A., et al., Dosimetric evaluation of a new OneDose MOSFET for Ir-192 energy, Phys. Med. Biol. **51** (2006) 1261–1268.
[68] RAMANI, R., et al., Clinical dosimetry using MOSFETs, Int. J. Radiat. Oncol. Biol. Phys. **37** (1997) 959–964.
[69] EDWARDS, C.R., et al., The response of a MOSFET, p-type semiconductor and LiF TLD to quasi-monoenergetic x-rays, Phys. Med. Biol. **42** (1997) 2383–2391.
[70] CHUANG, C.F., et al., Investigation of the use of MOSFET for clinical IMRT dosimetric verification, Med. Phys. **29** (2002) 1109–1115.
[71] ROWBOTTOM, C.G., JAFFRAY, D.A., Characteristics and performance of a micro-MOSFET: an "imageable" dosimeter for image-guided radiotherapy, Med. Phys. **31** (2004) 609–615.
[72] CYGLER, J.E., et al., Feasibility study of using MOSFET detectors for in vivo dosimetry during permanent low-dose-rate prostate implants, Radiother. Oncol. **80** (2006) 296–301.
[73] AKSELROD, M.S., et al., Highly sensitive thermoluminescent anion-defect a-Al_2O_3:C single crystal detectors, Rad. Prot. Dosim. **33** (1990) 119–122.
[74] AKSELROD, M.S., McKEEVER, S.W.S., A radiation dosimetry method using pulsed optically stimulated luminescence, Rad. Prot. Dosim. **81** (1999) 167–176.
[75] McKEEVER, S.W., MOSCOVITCH, M., On the advantages and disadvantages of optically stimulated luminescence dosimetry and thermoluminescence dosimetry, Radiat. Prot. Dosim. **104** (2003) 263–270.
[76] AKSELROD, M.S., et al., A procedure for the distinction between static and dynamic radiation exposures of personal radiation badges using pulsed optically stimulated luminescence, Rad. Meas. **32** (2000) 215–225.
[77] AZNAR, M.C., et al., Real-time optical-fibre luminescence dosimetry for radiotherapy: physical characteristics and applications in photon beams, Phys. Med. Biol. **49** (2004) 1655–1669.
[78] McKEEVER, S.W.S., Optically stimulated luminescence dosimetry, N. Instr. Meth. Phys. Res. Sec. B **184** (2001) 29–54.
[79] BØTTER-JENSEN, L., et al., Optically Stimulated Luminescence Dosimetry, Elsevier, Amsterdam (2003).
[80] SCHEMBRI, V., HEIJMEN, B.J., Optically stimulated luminescence (OSL) of carbon-doped aluminum oxide (Al2O3:C) for film dosimetry in radiotherapy, Med. Phys. **34** (2007) 2113–2118.
[81] JURSINIC, P.A., Characterization of optically stimulated luminescent dosimeters, OSLDs, for clinical dosimetric measurements, Med. Phys. **34** (2007) 4594–4604.
[82] YUKIHARA, E.G., et al., Evaluation of Al_2O_3:C Optically stimulated luminescence (OSL) dosimeters for passive dosimetry of high-energy photon and electron beams in radiotherapy, Med. Phys. **35** (2007) 260–269.
[83] VIAMONTE, A., et al., Radiotherapy dosimetry using a commercial OSL system, Med. Phys. **35** (2008) 1261–1266.
[84] AKSELROD, M.S., et al., Optically stimulated luminescence and its use in medical dosimetry, Rad. Meas. **41** (2007) S78–S99.
[85] McKEEVER, S.W.S., Optically stimulated luminescence dosimetry, Nucl. Instrum. Meth. B **184** (2001) 29–54.
[86] BØTTER-JENSEN, L., Luminescence techniques: instrumentation and methods, Rad. Meas. **27** (1997) 749–768.
[87] PERKS, C.A., et al., Introduction of the InLight monitoring service, Radiat. Prot. Dosim. **125** (2007) 220–223.
[88] GOOSSENS, O., et al., Radiation dosimetry for microbial experiments in the International Space Station using different track-etch and luminescent detectors, Rad. Prot. Dosim. **120** (2006) 433–437.
[89] YUKIHARA, E.G., et al., Effect of high-dose irradiation on the optically stimulated luminescence of Al_2O_3:C, Radiat. Meas. **38** (2004) 317–330.
[90] YUKIHARA, E.G., McKEEVER, S.W.S., Spectroscopy and optically stimulated luminescence of Al_2O_3:C using time-resolved measurements, J. Appl. Phys. **100** (2006) 083512–083519.
[91] YUKIHARA, E.G., et al., High-precision dosimetry for radiotherapy using the optically stimulated luminescence technique and thin Al_2O_3:C dosimeters, Phys. Med. Biol. **50** (2005) 5619–5628.
[92] SOMMER, M., HENNIGER, J., Investigation of a BeO-based optically stimulated luminescence dosimeter, Radiat. Prot. Dosim. **119** (2006) 394–397.
[93] SOMMER, M., et al., New aspects of a BeO-based optically stimulated luminescence dosimeter, Rad. Meas. **42** (2007) 617–620.
[94] KNIGHT, R.T., MAYLES, W.P., An application of a computer spreadsheet to checking dose plans in radiotherapy planning, Phys. Med. Biol. **36** (1991) 655–658.
[95] INTERNATIONAL ATOMIC ENERGY AGENCY, Absorbed Dose Determination in External Beam Radiotherapy: An International Code of Practice for Dosimetry Based on Standards of Absorbed Dose to Water, Technical Reports Series No. 398, IAEA, Vienna (2000).

[96] NATH, R., et al., Dosimetry of interstitial brachytherapy sources: recommendations of the AAPM Radiation Therapy Committee Task Group No. 43. American Association of Physicists in Medicine, Med. Phys. **22** (1995) 209–234.
[97] GOLDSTEIN, N., Dose-rate dependence of lithium fluoride for exposures above 15,000 R per pulse, Health Phys. **22** (1972) 90–91.
[98] LONCOL, T., et al., Entrance and exit dose measurements with semiconductors and thermoluminescent dosemeters: a comparison of methods and in vivo results, Radiother. Oncol. **41** (1996) 179–187.

Annex I

BRAZIL — DEVELOPMENT OF PROCEDURES FOR IN VIVO DOSIMETRY IN RADIOTHERAPY: IN VIVO DOSIMETRY WITH THERMOLUMINESCENT AND OPTICALLY STIMULATED LUMINESCENT DOSIMETERS FOR PHOTON BEAMS

A.M. CAMPOS DE ARAUJO, A. VIAMONTE, C.C.B. VIEGAS
Radiotherapy Quality Control Program
Quality Assurance on Ionizing Radiation Service
National Cancer Institute
Rio de Janeiro, Brazil

Abstract

This paper is the product of extensive work performed by the Radiotherapy Quality Control Programme (PQRT) at the Brazilian National Cancer Institute (INCA) from 2005 to 2008. It describes the studies of both TLD and OSL dosimetry systems, commissioning, the physical characterization involving studies of dose response non-linearity, energy dependence, source surface distance and other relevant effects due to the various accessories used in planning for radiotherapy (wedge, tray). After that, three treatment plans for two sites were prepared and irradiations were carried out using an Alderson Rando anthropomorphic phantom in order to verify the accuracy of the in vivo dosimetry systems under study. Following this, in vivo measurements were carried out. In total, 315 patients were monitored with in vivo measurements that were performed during at least one irradiation fraction. This includes 482 TLD measurements on 216 patients, mostly for pelvis and for head and neck treatments with ^{60}Co, 6 MV and 15 MV beams, and 205 OSLD measurements on 99 patients, mostly for head and neck, in a ^{60}Co beam.

I–1. INTRODUCTION

The Brazilian National Cancer Institute (INCA) is the branch of the Ministry of Health responsible for developing and coordinating policies for prevention, epidemiological surveillance, treatment, information, education and research on cancer in Brazil.

With its headquarters in Rio de Janeiro, INCA is composed of five care units and seven other scientific and administrative departments, and currently has 4027 employees. Every year, there are about 10 000 new admissions, more than 220 000 consultations and approximately 15 000 inpatients. The radiotherapy service at INCA is responsible for a yearly average of approximately 5100 new patients and in the last four years it was responsible for 13 000 irradiated fields.

The staff consists of 13 medical doctors specialized in radiotherapy, 11 medical physicists, 52 radiotherapy technicians, trained nurses and a social worker.

The infrastructure comprises the following equipment:

— Two cobalt therapy units (Theratron 780C);
— One linear accelerator (Varian, Clinac 2300CD) with photon energies of 6 MV and 15 MV, electron energies from 6 MeV to 20 MeV, and MLC and IMRT capabilities;
— One accelerator (Varian, Clinac 600C) with photon energy of 6 MV;
— One accelerator (Siemens, Primus) with photon energies of 6 MV and 10 MV and electron energies from 6 MeV to 18 MeV;
— One linear accelerator (Varian, Trilogy) with cone beam CT, and energies of 6 and 10 MV (in installation);
— Six treatment planning workstations (4 Varian Eclipse and 2 AcQsim);
— Two high dose rate brachytherapy units (Varian GammaMed and Nucletron).

The Quality Control Programme in Radiotherapy (PQRT) is carried out by an independent team of five physicists, one TLD technician, one office clerk and one secretary.

The PQRT has the following objectives:

(a) To assist Brazilian radiotherapy services with scientific and technical support in order to treat their patients with quality and efficacy;
(b) To promote the training of various radiotherapy staff.

Its main activities are:

— Performing on-site and TLD postal audits (photon and electron beams) in regard to physical dosimetry and quality assurance (QA) in teletherapy and brachytherapy practices;
— Local and distance assisted courses;
— Development of new postal evaluation systems;
— Patient dose evaluations;
— Specific research programmes.

Participation in the IAEA CRP E2.40.14 had the approval of the INCA director and has been carried out by the PQRT staff in the radiotherapy service at Hospital Centre I. Although the radiotherapy service has their own QA programme, they were very interested in the results of this study to implement in vivo measurements as part of the routine quality control programme.

This report presents the results of measurements, calculations and data analyses performed in the radiotherapy service and the PQRT of INCA in the period 2005–2008.

The aim of this study was not only to develop in vivo dosimetry procedures but also to test a new technology for radiotherapy dosimetry, Optically Stimulated Luminescence (OSL), and compare it with a well-known technology, Thermoluminescence Dosimetry (TLD).

I–2. EQUIPMENT AND MATERIAL

The dosimetry systems used were 445 thermoluminescent chip dosimeters from a single unsorted batch (TLD-100 LiF:Mg;Ti 3.2 mm × 3.2 mm × 0.9 mm, Harshaw, Fig. I–1(a)) and 400 dots of optically stimulated luminescent dosimeters (OSLD Al_2O_3:C, 7 mm diameter and 0.2 mm thick, Landauer, Fig. I–1(b)), encased in a plastic cover (the total thickness of the casing and dosimeter is approximately 2 mm).

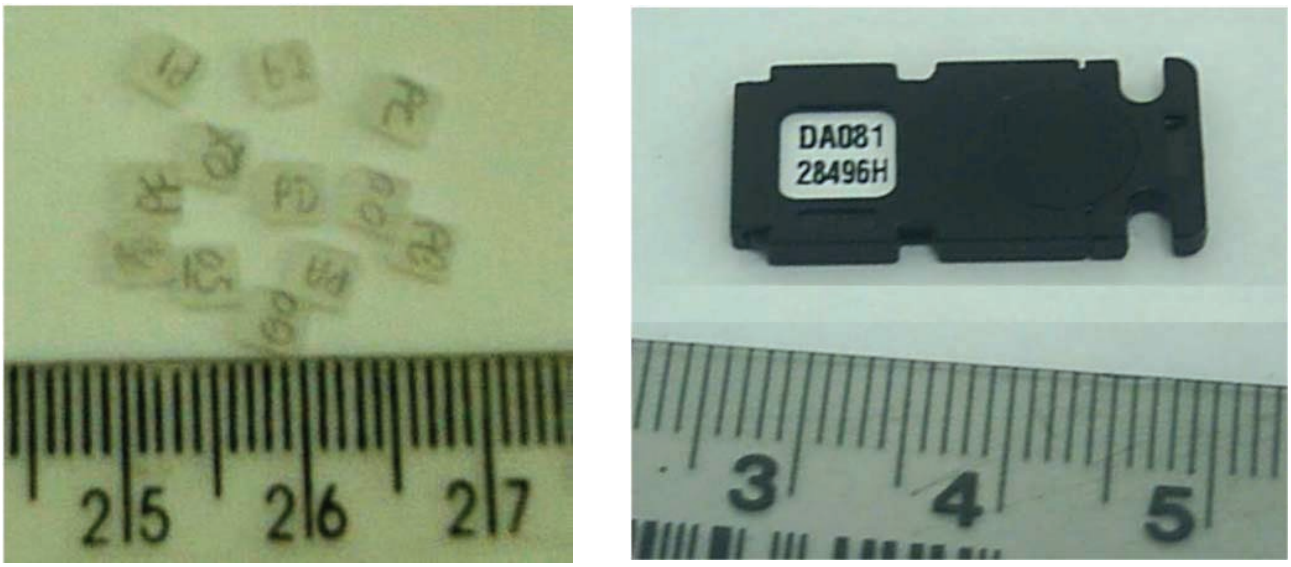

(a) (b)

FIG. I–1. (a) TLD chips and (b) an encased OSL dot.

The reading systems were a PCL3 TLD reader (Fimel, Fig. I–2(a)), an automatic reader which can read up to 93 TLD chips in one load with an ETT Oven (Fimel) and an InLight MicroStar OSL reader (Landauer, Fig. I–2(b)).

(a) (b)

FIG. I–2. (a) Fimel PCL3 TL reader and (b) Landauer InLight MicroStar OSL reader.

The reference dosimetric system was a TN30013 Farmer ionization chamber 0.6 cm^3, serial number 491, and an UNIDOS-E electrometer serial number T10010–00279 (PTW). The corrections for temperature and pressure were taken by a thermometer (Minipa) and a DB-898 barometric station. The dosimetry system was calibrated by the SSDL at the Institute of Nuclear and Energy Research (IPEN, São Paulo, Brazil).

For the calibration, dosimeter studies and simulations, the following phantoms were used: an open top water phantom 40 cm × 40 cm × 35 cm (CNMC), a virtual water G211 plastic phantom 40 cm × 40 cm slabs of 3 cm and 5 cm thickness (Standard Imaging) and a female Alderson Rando anthropomorphic phantom (Alderson, Fig. I–3).

FIG. I–3. The female Alderson Rando anthropomorphic phantom used in the project.

For treatment planning, the Eclipse 7.3.10 (Varian) was used. Beams from two Theratron 780C ^{60}Co units (Theratronics AECL), 6 MV from Clinac 600C (Varian) as well as 6 MV and 15 MV from Clinac 2300CD (Varian) available at INCA were used for dosimeter irradiation for the determination of dosimeter properties, studies on an anthropomorphic pantom and on patients.

I–3. MEASUREMENT METHODOLOGY

In general, the common measurements methodology developed under the CRP and described in Section 4 was followed for both TL and OSL dosimeters.

The TLD procedures were the following:

(a) Thermoluminescent dosimeter annealing — irradiation without reading cycles;
(b) TLD checks to select the batch through repeatability and chip factor determination;
(c) Calibration in a plastic phantom;
(d) Measurement of correction factors;
(e) Alderson Rando phantom measurements;
(f) In vivo measurements on patients.

The OSL procedures were similar to those for TLDs:

(a) Reader reproducibility study;
(b) Initial calibration and sensitivity of OSLDs;
(c) Determination of repeatability and OSLD individual calibration;
(d) Determination of correction factors;
(e) Alderson Rando phantom measurements;
(f) In vivo measurements on patients.

Prior to starting the dosimeter characterization, the symmetry and flatness of beams which were used for dosimeter irradiations were checked at 5 cm depth in water for both in-plane and cross-plane directions with an ionization chamber, as described in Section 4. The results were calculated following IAEA TECDOC 1151 [I–1]. They show good uniformity of the beam over the area of the dosimeters' positions (i.e. less than 0.5% symmetry and flatness, which is within the limit stated in the CRP procedures).

Slabs of G211 virtual water phantom of 5 cm thickness, one specially drilled for the PTW 30013 ion chamber and one for OSLDs, were used for calibration and all measurements necessary to determine the various correction factors. As described in the CRP procedure (Section 4), for measurements in a virtual water phantom, it was necessary to determine the water to plastic correction using ionization chamber measurements in water and in a solid phantom. The plastic to water correction factors, determined within this study, were 1.005 for ^{60}Co, 1.014 for 6 MV, and 1.013 for 15 MV beams.

The characterization of both TLD and OSL systems for in vivo dosimetry was performed. The calibration of both systems as well as a complete set of correction factors as defined in Section 4 were determined, and the results are described below in Sections I–4 and I–5 for TLDs and OSLDs, respectively.

As mentioned above, the next step involved Rando phantom measurements for selected sites and simple beam arrangements to test the methodology. A female Alderson Rando anthropomorphic phantom was used for pelvis and for head and neck treatments. The expected dose was compared to the TPS dose and the independent manual calculations.

Pelvis. Entrance dose measurements were made for a three field beam arrangement as per the CRP procedure (see Section 4.5.3), i.e. one anterior and two opposing lateral fields. Measurements were performed for one beam at a time. Two treatment plans were prepared: one with three open fields and the other with an open anterior field and two lateral wedged fields. Doses were calculated by the TPS to deliver 50 cGy to the isocentre positioned at the centre of one of the phantom slices. TPS and manually calculated doses agreed within ±3%.

Head and neck. Two parallel opposed 6 cm × 6 cm fields without wedges were used in these irradiations (see Section 4.5.3). The centre of the field was positioned at the centre of a slice in the region of the junction of the neck and the chin slices. A dose of 100 cGy was delivered at the isocentre from each field without the immobilization mask (Fig. I–4(a)). The same set-up was used with the mask (Fig. I–4(b)).

(a) (b)

FIG. I–4. Irradiation geometry for head and neck measurements: (a) without immobilization mask, and (b) with mask.

After validation of the in vivo dosimetry procedure with the irradiations on the Rando phantom, patient measurements started. Most measurements were performed for pelvis and for head and neck patient treatments with ^{60}Co, 6 MV and 15 MV linac beams. A total of 216 patients and 482 fields were measured with TLDs. A summary of TLD measurements on patients is given in Table I–1.

TABLE I–1. TOTAL NUMBER OF PATIENTS AND FIELDS FOR WHICH TLD MEASUREMENTS WERE PERFORMED

Beam	Number of patients	Number of fields
Co-60, Unit C	26	52
Co-60, Unit X	74	189
Subtotal, Co-60	*100*	*241*
6 MV (2300CD)	4	6
6 MV (600C)	60	109
Subtotal, 6 MV	*64*	*115*
15 MV	52	126
Total	*216*	*482*

The in vivo measurements with OSLD were performed with 99 patients and 205 fields from a ^{60}Co unit. Most OSLD patient measurements were performed for head and neck treatments. A summary of OSLD measurements is given in Table I–2.

TABLE I–2. THE TOTAL NUMBER OF PATIENTS AND FIELDS FOR WHICH OSLD MEASUREMENTS WERE PERFORMED

Co-60 beam	Patients	Fields
Unit C	52	87
Unit X	47	118
Total	99	205

Figure I–5 shows in vivo measurements on patients treated for pelvic (Fig. I–5(a)) and head and neck cancers (Fig. I–5(b)).

The results of these measurements are given below in Section I–4 for TLDs and I–5 for OSLDs.

(a) (b)

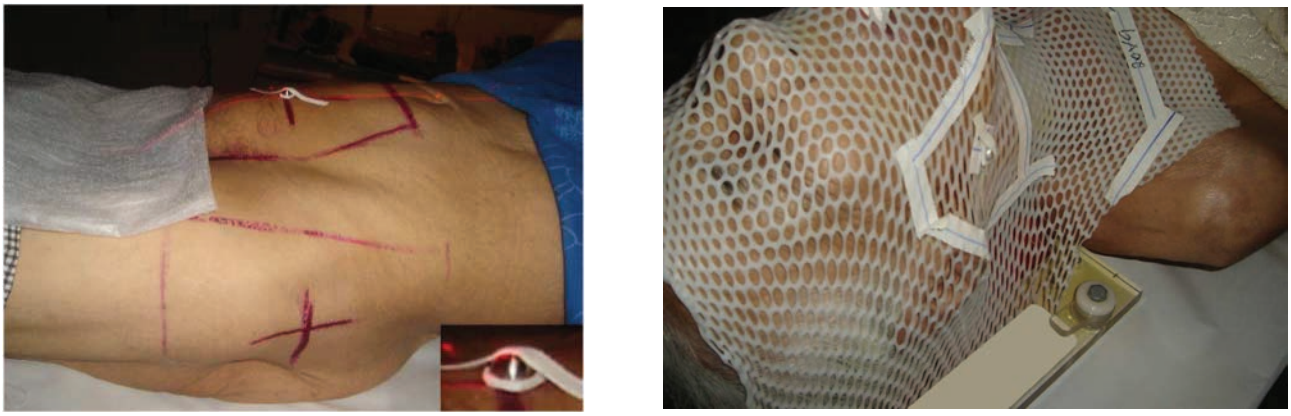

FIG. I–5. In vivo measurement using TLD with a buildup cap (detail) for (a) pelvis and (b) head and neck sites.

I–4. TLD RESULTS

I–4.1. TLD characterization

I–4.1.1. TLD chip factor

Following the CRP procedure (Section 4.1 and 4.3.3), all new TLDs were cycled five times without reading their results (i.e. they were irradiated with 100 cGy and then annealed). Following this, three irradiation annealing cycles with TLD measurements in between were made to determine individual chip factors. The factor used for all subsequent measurements was the average of these three measurements. From a batch of 500 new TLDs, 445 TLDs were analysed, and 226 (51%) dosimeters were within the ±3% limit criterion as described in Section 4.3.3. From the TLDs selected in this way, 113 chip pairs of TLDs were formed.

Figure I–6 shows the scatter of chip factors for the TLDs under testing with the relevant standard deviations.

I–4.1.2. TLD batch calibration

The calibration coefficient N_{cal} of the batch was determined in the ^{60}Co beam. For this purpose, for each subsequent series of measurements, five pairs of 'calibration chips' were randomly chosen from the TLD batch and irradiated with aluminium buildup caps (see Fig. I–5) placed on the top of the virtual water phantom. The calibration coefficient for the associated group of measurement chips is the average of the calibration coefficients of the five 'calibration chip' pairs. The average calibration result for ^{60}Co was: $(4.03 \pm 0.04)\ 10^{-5}$Gy/TL signal.

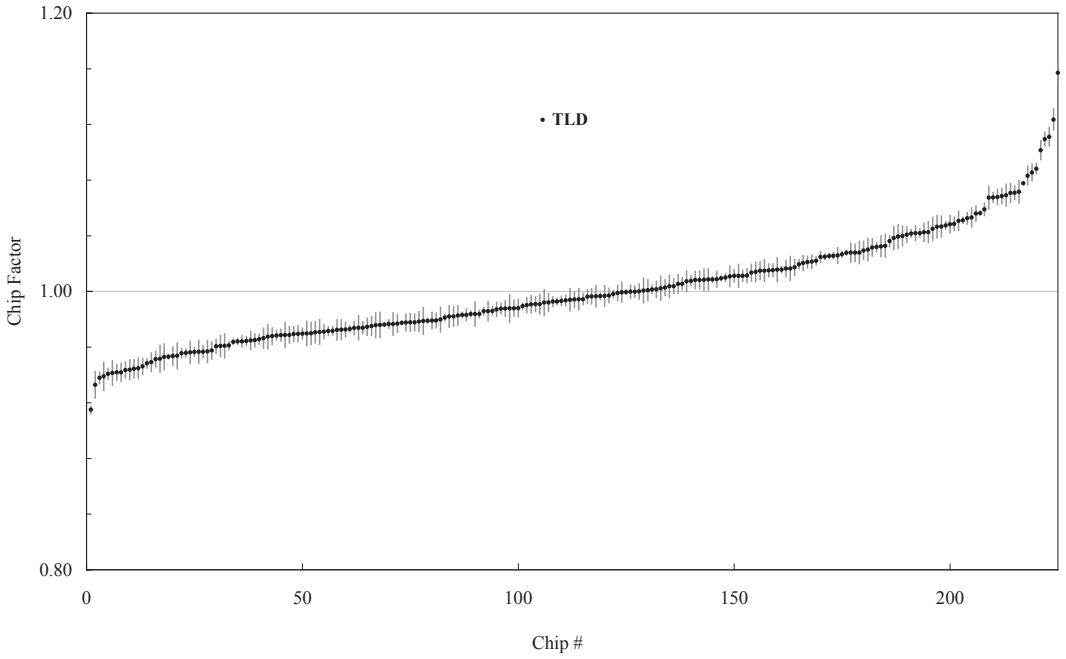

FIG. I–6. Individual chip factors for TLD dosimeters under testing.

I–4.1.3. TLD non-linearity dose response correction

TLD chips with buildup caps were placed on the surface of the virtual water phantom for calibration with the ionization chamber in the reference position. They were irradiated with the following doses: 20, 50, 100, 150, 200, 300 and 400 cGy. The resulting correction factor was normalized to the reading at 1 Gy. For doses below 2 Gy, the correction fluctuates within ± 2 %. However, above 2 Gy, it becomes more pronounced and exceeds 8% for a dose of 4 Gy. Figure I–7 shows the variation of the correction factor with dose.

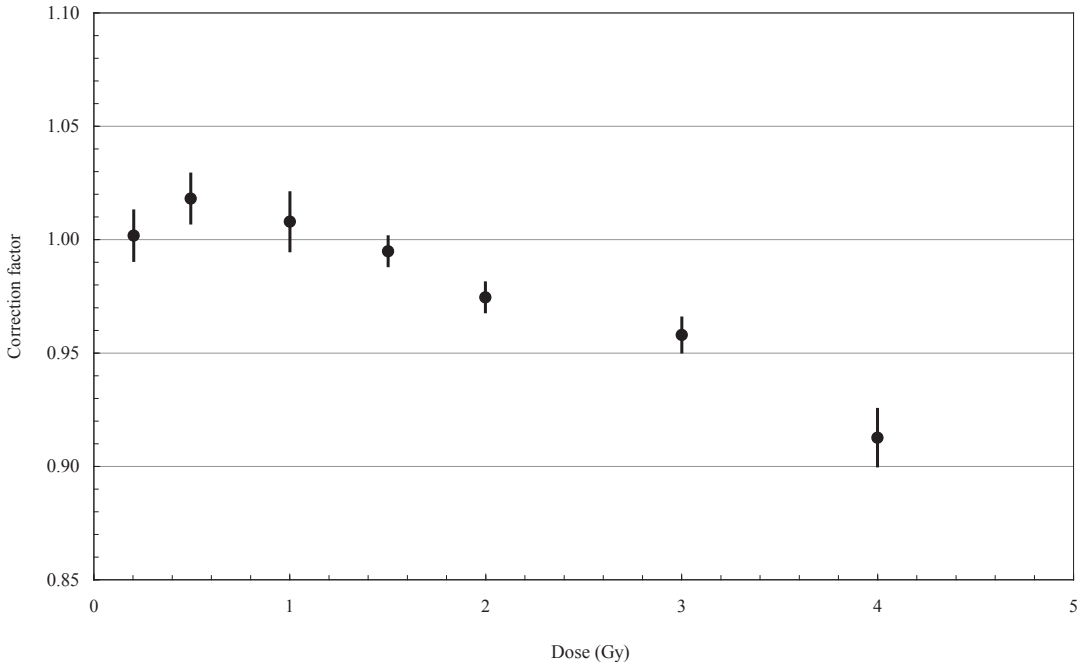

FIG. I– 7. Non-linearity dose response correction for TLDs determined in a ^{60}Co beam with associated standard error.

I–4.1.4. TLD energy correction

The reference calibration N_{cal} is based on measurements in the ^{60}Co beam. The energy correction factors were determined for 6 and 15 MV beams as defined in Section 4. The results are shown in Table I–3 together with the beam qualities D_{20}/D_{10}.

TABLE I–3. TLD ENERGY CORRECTION FACTOR

Beam	D_{20}/D_{10}	k_{engy}
^{60}Co	0.502	1.000
6 MV, 600C	0.569	0.971
6 MV, 2300CD	0.579	0.967
15 MV, 2300CD	0.648	0.937

I–4.1.5. TLD fading

The fading correction factor is the ratio of the dosimeter reading taken for the reference time delay Δt_{ref} for which no fading is assumed to the dosimeter readout taken for the time delay Δt (see Section 4.4.1.3).

The fading test was carried out over a one week period. The results are presented in Fig. I–8. One can see that this TLD batch has good stability 24 h post-irradiation. However, the experience of this group shows that the time from irradiation to readout should be at least 48 h as after such a period the readings have smaller average standard deviations. However, the fading correction is not necessary if the calibration TLDs are irradiated and read out at the same time as the TLDs used for patient measurements.

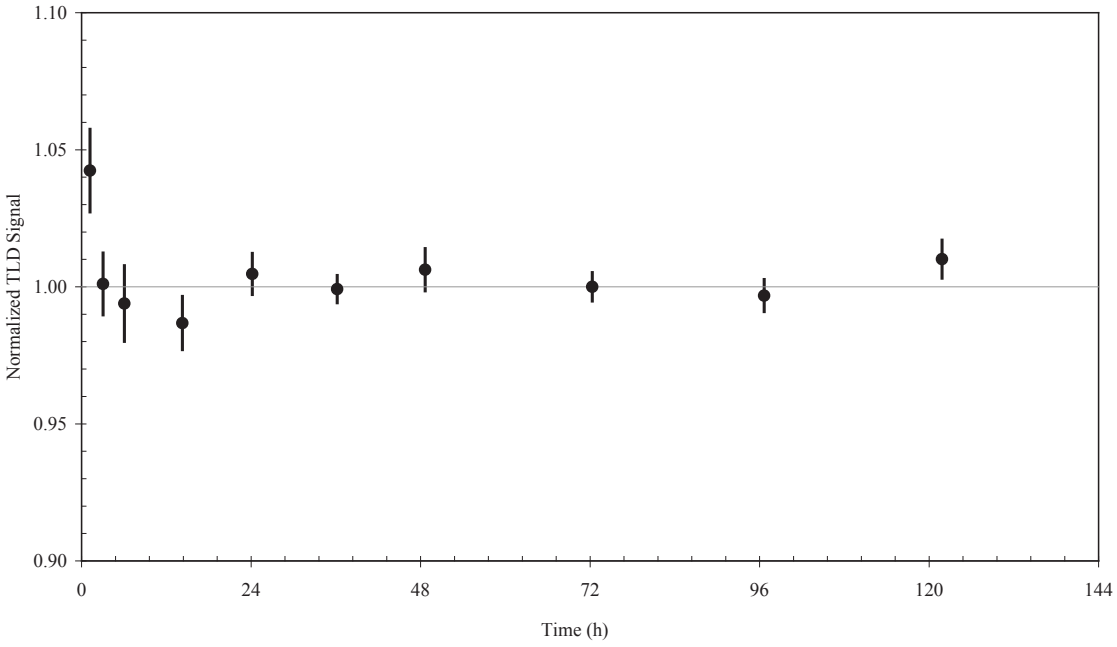

FIG. I–8. TLD fading normalized to the reading taken 48 h after the chip irradiation with associated standard error.

I–4.1.6. TLD angle of incidence correction

To study angular dependence, TLDs with buildup caps (aluminium for a ^{60}Co beam and stainless steel for 6 MV and 15 MV) were irradiated in the same set-up with each energy as shown in Fig. I–9. The chips were placed on the surface of the virtual water phantom with buildup caps and acrylic bases. They were irradiated with the gantry at 0º, 10º, 20º, 30º, 50º and 60º. The correction factor k_{ang} was calculated using Eq. 9 (Section 4.4.2.1). The results of the TLD angular dependence study are presented in Fig. I–10.

FIG. I–9. Angular dependence study with TLD in ^{60}Co beam.

I–4.1.7. Source surface distance

The source surface distance (SSD) correction measurements were performed with dosimeters on the surface of the phantom as for the calibration set-up at different SSDs: 70.0, 80.0, 90.2, 100.0 and 109.2 cm and for the reference field size (10 cm × 10 cm). The time of irradiation was calculated to deliver the same dose D =100 cGy at d_{max} for each SSD. Figure I–11 shows the results of this study. For the linac beams, the factors were re-normalized to 100 cm.

I–4.1.8. Field size

Since the radiation beam spectrum changes with field size, one needed to evaluate the possible effect of field size on the dosimeter response. Field size correction factors account for the effect of the irradiation field size on the dosimeter response. Table I–4 shows the correction factors determined for each square field size (FS) in this study. No significant field size corrections were found. Corrections for ^{60}Co and 6 MV are within the measurement uncertainty, whereas for 15 MV, a correction of 2% to 3% is required for very large fields.

I–4.1.9. TLD wedge and tray corrections

The wedge and tray correction factors were determined to check whether the change in the energy spectrum has a significant effect on TLD readings. The TLDs with their buildup caps were placed on the surface of the virtual water phantom with a TLD dosimeter placed on the central axis of the beam. TLDs were irradiated with an open field, and the exercise was repeated for wedged fields and with an accessory tray in place.

Table I–5 shows the wedge correction factors for ^{60}Co and 6 MV beams. As can be seen from Table I–6, the effect of the wedge is negligible (within the measurement uncertainty) and therefore the wedge correction is not required.

There are two types of trays in use in INCA: one is solid acrylic and another is perforated and has elongated milled holes specially made for fixing blocks used for different gantry angles (Fig. I–12). The measurements of a tray factor were made for both the solid and the perforated trays. Table I–7 presents the resulting tray correction factors.

(a)

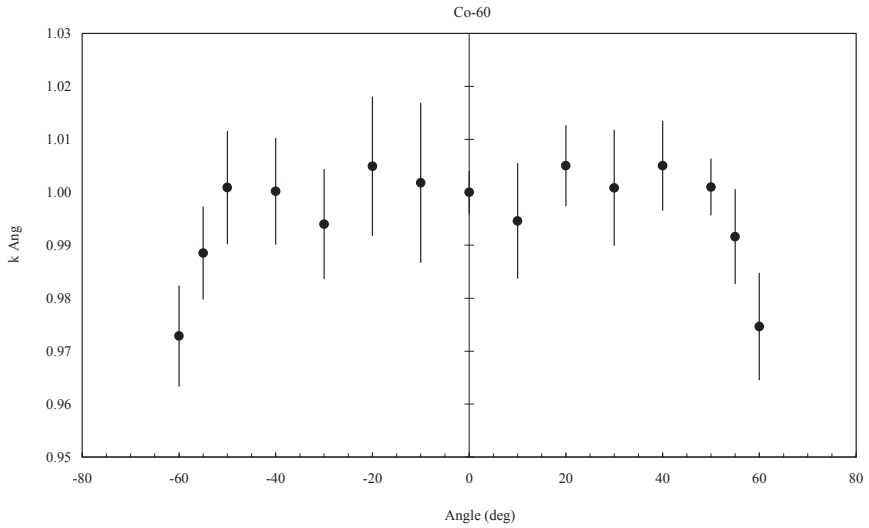

(b)

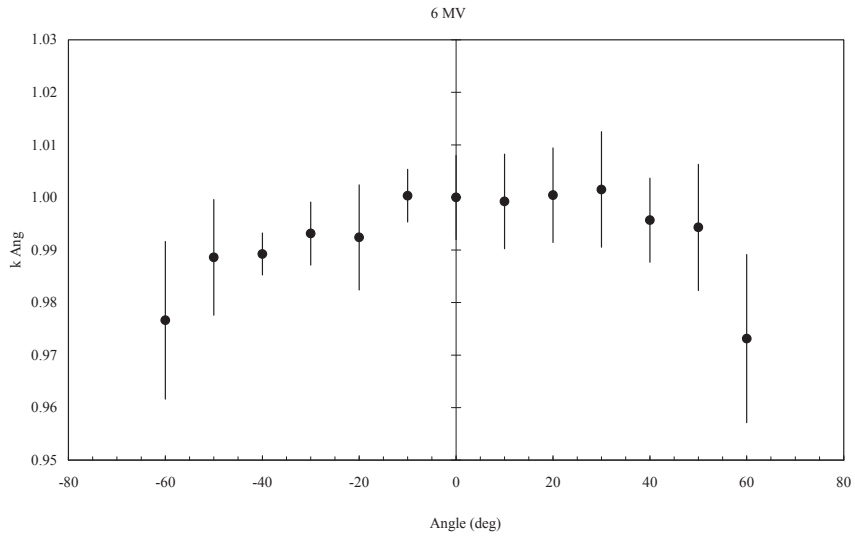

(c)

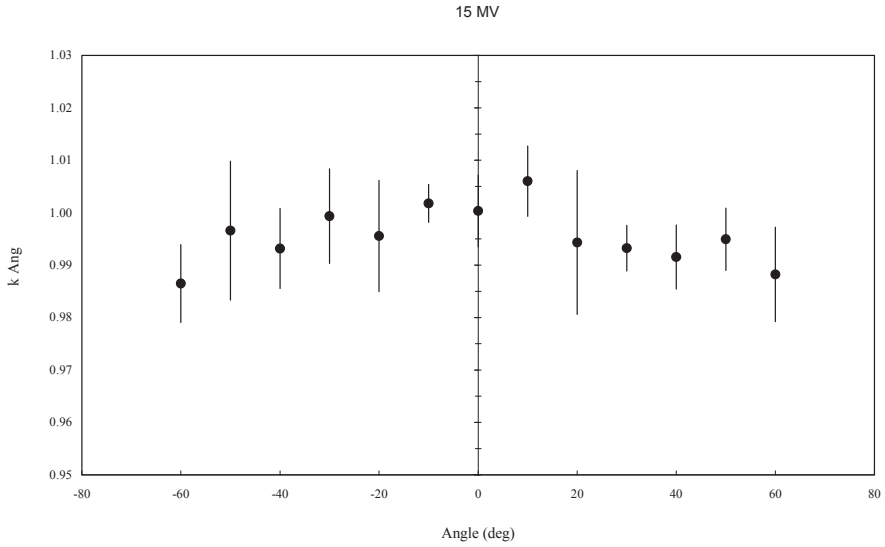

FIG. I–10. TLD angle of incidence correction factor shown with associated standard error for (a) ^{60}Co beam, (b) 6 MV beam and (c) 15 MV beam.

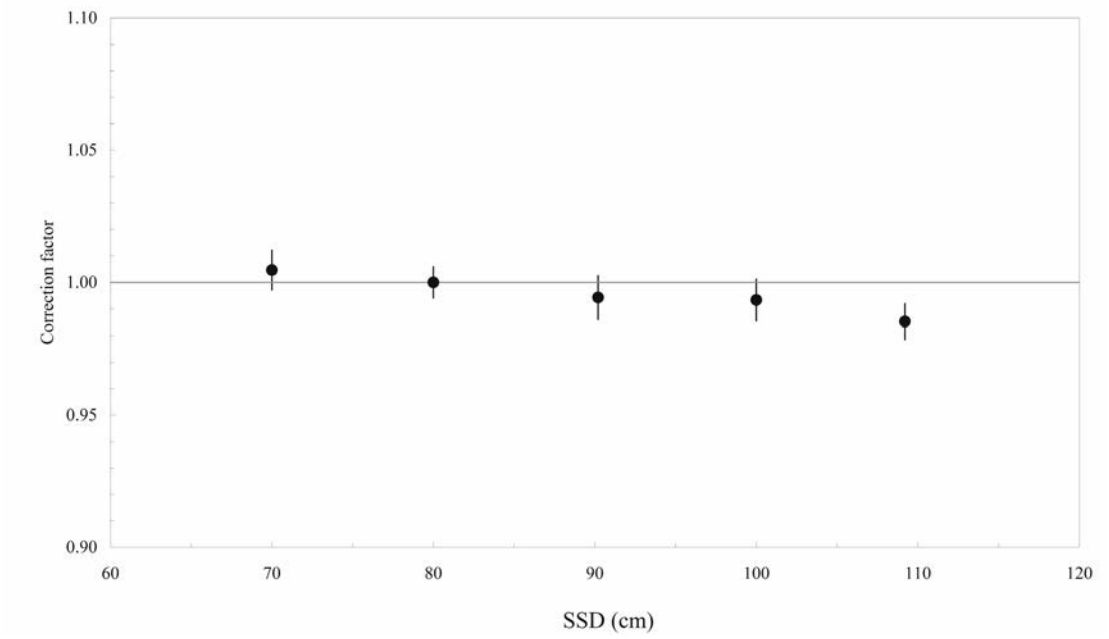

FIG. I–11. TLD correction factors for SSD for a ^{60}Co beam with associated standard error.

TABLE I–4. FIELD SIZE CORRECTION FACTORS FOR ^{60}CO, 6 MV AND 15 MV BEAMS

FS (cm)	^{60}Co		6 MV		15 MV
	Unit C	Unit X	600C	2300CD	2300CD
5	1.007	0.987	0.989	1.007	1.000
7	1.016	0.993	0.991	1.026	—
10	1.000	1.000	1.000	1.000	1.000
12	1.014	0.998	1.008	1.013	—
15	1.013	0.985	0.986	1.010	0.984
18	1.010	1.008	1.013	1.007	—
20	1.029	1.004	0.994	1.018	0.971
25	—	—	—	—	0.977
30	—	—	—	—	0.966

TABLE I–5. WEDGE FILTER CORRECTION FACTORS FOR TLDs AND RELATED UNCERTAINTIES

Wedge	^{60}Co				6 MV	
	Unit C	s_M*	Unit X	s_M*	600C*	s_M*
15°	1.008	0.012	1.008	0.015	0.996	0.009
30°	1.007	0.011	1.006	0.014	0.998	0.008
45°	1.000	0.011	1.008	0.014	1.008	0.007
60°	—	—	—	—	1.008	0.007

* Experimental standard deviation of the mean.

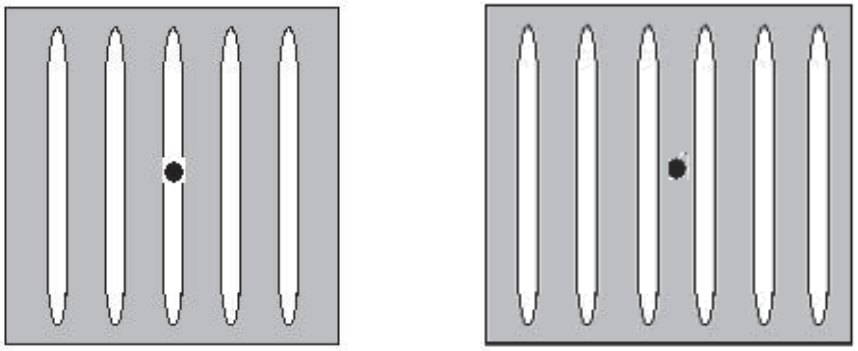

FIG. I–12. (a) TLD in the centre of the gap and (b) TLD under solid acrylic.

TABLE I–6. TRAY CORRECTION FACTORS AND RELATED UNCERTAINTIES

Tray type	^{60}Co	s_M	6 MV	s_M
Plain tray	1.004	0.005	1.002	0.005
Perforated tray:				
Under acrylic	0.998	0.003	0.993	0.009
Under gap	1.001	0.004	0.989	0.007

As can be seen from Table I–6, there is no need to correct TLD readings due to the presence of a tray.

I–4.2. Rando phantom measurements with TLDs

The expected dose for Rando phantom measurements was calculated using the Eclipse treatment planning system by placing a calculation point at the isocentre. In this case, the programme also calculates the dose at the depth of d_{max}. The dose determined from in vivo measurments was compared to the TPS dose and the independent manual dose calculations, both for pelvis and for head and neck treatments.

I–4.2.1. Pelvis: Rando phantom measurements with TLDs

Figure I–13 shows the ratio of TLD measurements compared with the expected dose obtained from TPS and manual calculations for pelvic irradiation with a ^{60}Co beam using three 20 cm × 20 cm open fields (one anterior and two opposing lateral fields); 50 cGy was delivered to the isocentre positioned at the centre of one of the Rando phantom slices. In the graph, ratios of the TLD measured dose, D_m, to the dose calculated with the TPS, D_{TPS}, are shown as well as similar ratios of the TLD measured dose and the manually calculated dose, D_{calc}. All but two results are within the ±3% limit.

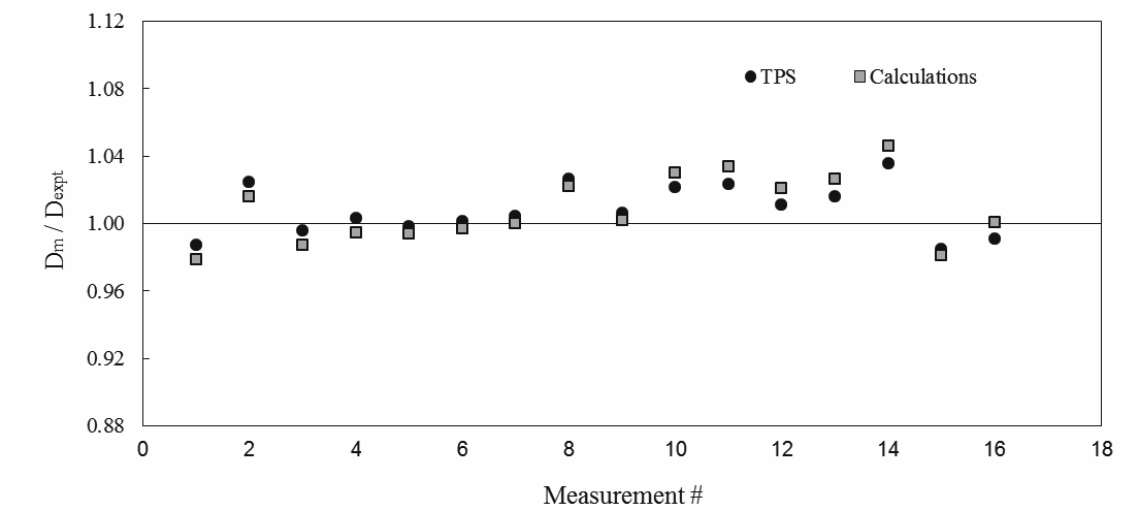

FIG. I–13. TLD Rando measurements for irradiation of the pelvis with a 20 cm × 20 cm field. D_{expt} refers to the TPS or manually calculated doses as appropriate.

The second pelvic treatment plan under testing used 10 cm × 10 cm field sizes with 30º wedges on the two lateral wedged fields. Figure I–14 summarizes the results of the TLD measurements for the second plan. Similar to the first plan, the ratios of the TLD measured doses to the expected doses are given. The results are generally within ±3% limits.

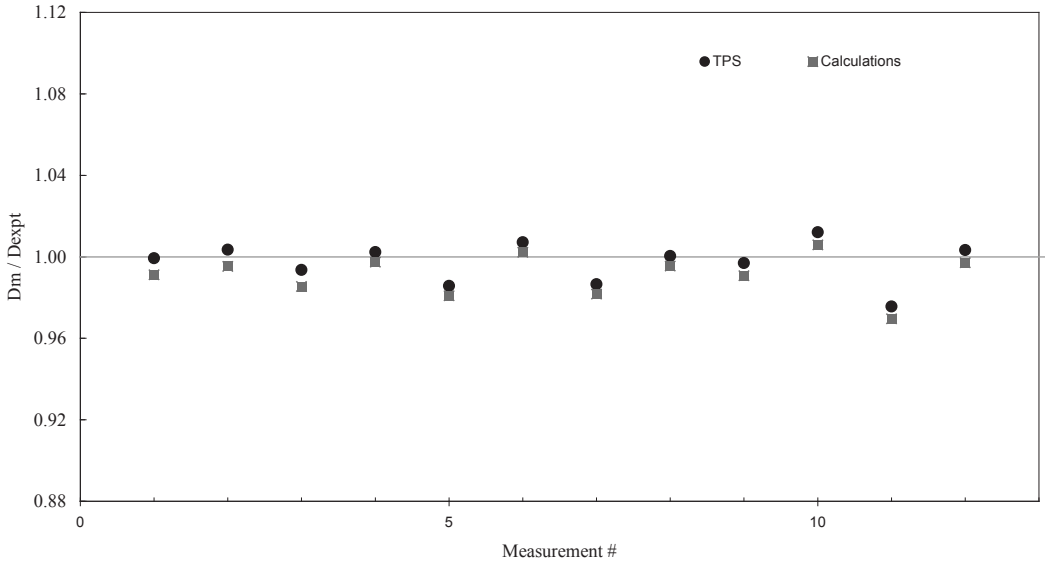

FIG. I–14. TLD Rando measurements for irradiation of the pelvis with a 10 cm × 10 cm wedged field.

I–4.2.2. Head and neck: Rando phantom measurements with TLDs

For the head and neck site, two parallel opposed 6 cm × 6 cm fields without wedges were used. A dose of 100 cGy was delivered to the isocentre from each field. The exercise was repeated twice with and without the immobilization mask. Figure I–15 presents the TLD results compared with the TPS calculations. All but two values are within the ±3% limits. Differences between the manual and TPS calculations may be explained by the inhomogeneity correction used by the TPS for the throat air cavity, which is not considered with manual calculations.

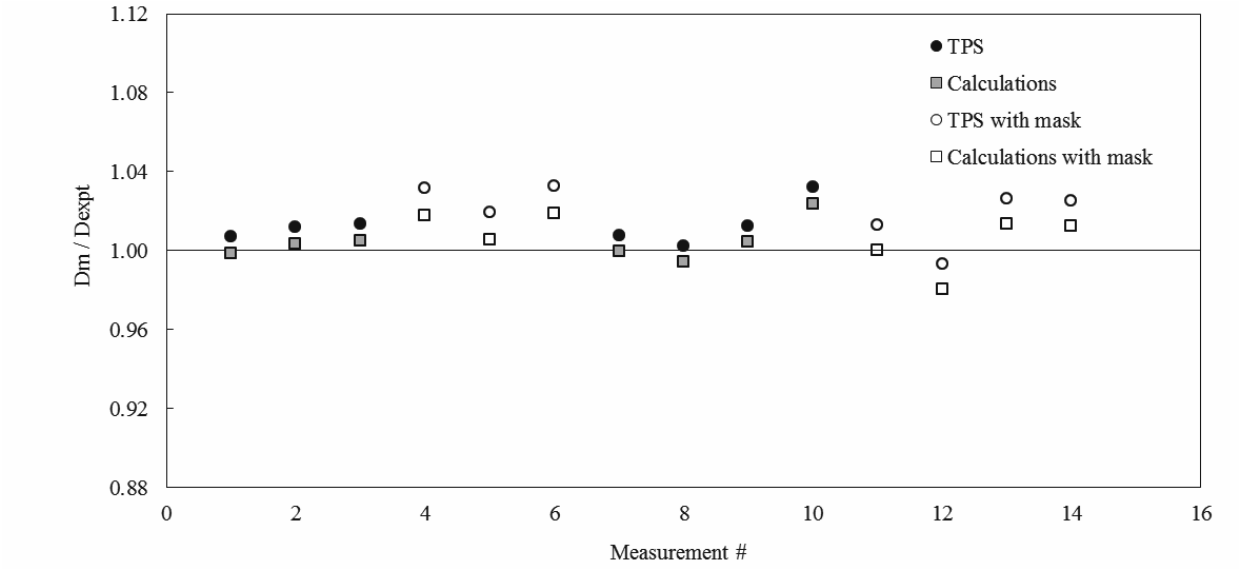

FIG. I–15. TLD Rando measurements for neck irradiation with a 6 cm × 6 cm field.

I–4.3. TLD in vivo measurements on patients

After the validation of the in vivo dosimetry process with irradiations on the Rando anthropomorphic phantom, the patient measurements were started. Most patient measurements were performed for pelvis and for head and neck treatments with the ^{60}Co units C and X, and with the 6 MV (Clinac 600C) and 15 MV (Clinac 2300C/D) photon beams available at Hospital Centre I.

A total of 482 fields were measured for 216 patients. 241 fields for 100 patients were treated with a ^{60}Co beam, 115 fields for 64 patients were treated with a 6 MV beam and 126 fields for 52 patients were treated with a 15 MV beam. The results are shown in Table I–7 and in the figures below (Figs I–16 to I–19) for each radiotherapy machine separately. Figure I–20 is a histogram of the results distribution summarizing all in vivo measurements on patients; 88% of all measurements were within ± 5%.

TABLE I–7. THE TOTAL NUMBER OF PATIENTS, FIELDS AND THE FRACTION OF TREATMENTS WITHIN THE TOLERANCE LEVEL

Beam	Patients	Fields	Fields within ±5%	% within tolerance
15 MV	52	126	112	88.9%
6 MV	4	6	6	100.0%
6 MV	60	109	83	76.1%
Subtotal, 6 MV	64	115	89	77.4%
Unit C	26	52	52	100.0%
Unit X	74	189	173	91.5%
Subtotal, Co-60	100	241	225	93.4%
Total	216	482	426	88.4%

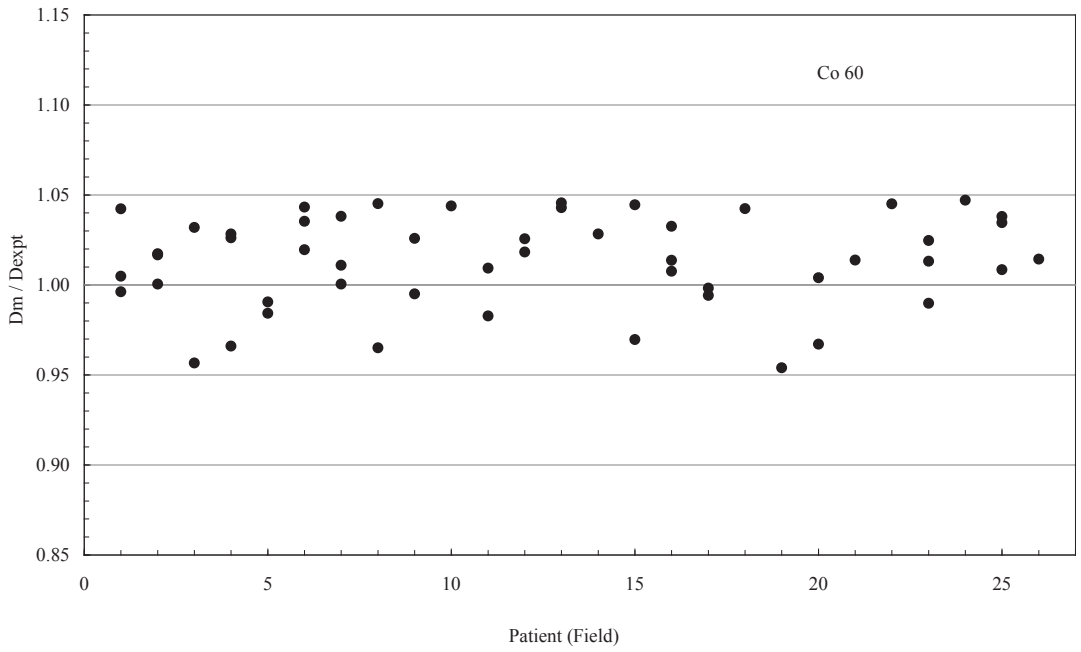

FIG. I–16. In vivo measurements of patients treated with a ^{60}Co beam, unit C.

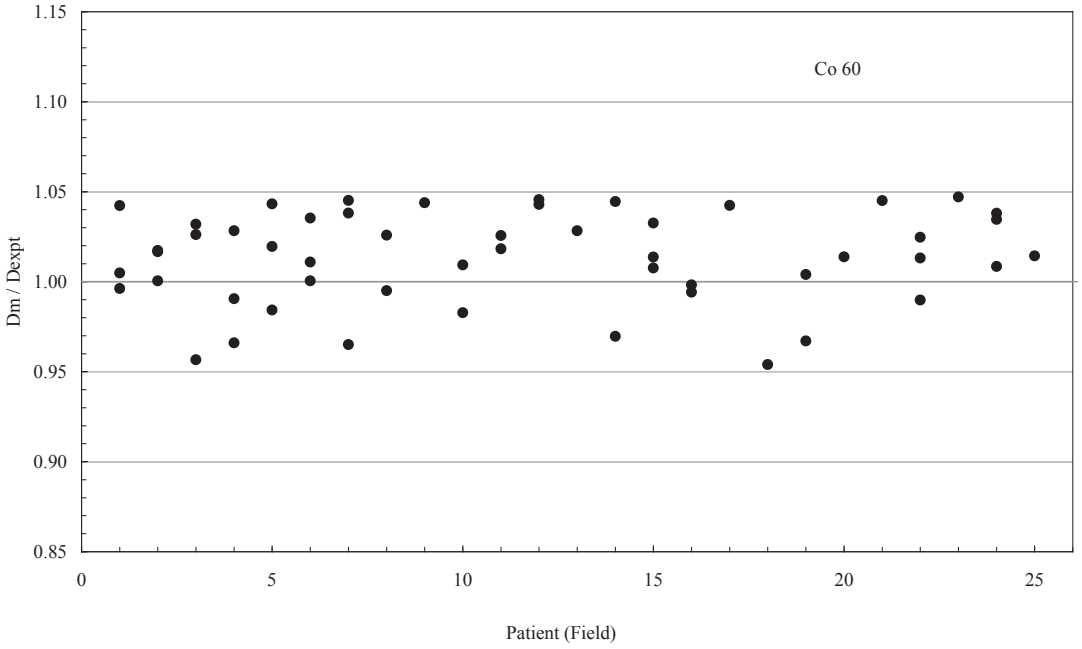

FIG. I–17. In vivo measurements of patients treated with a ^{60}Co beam, unit X.

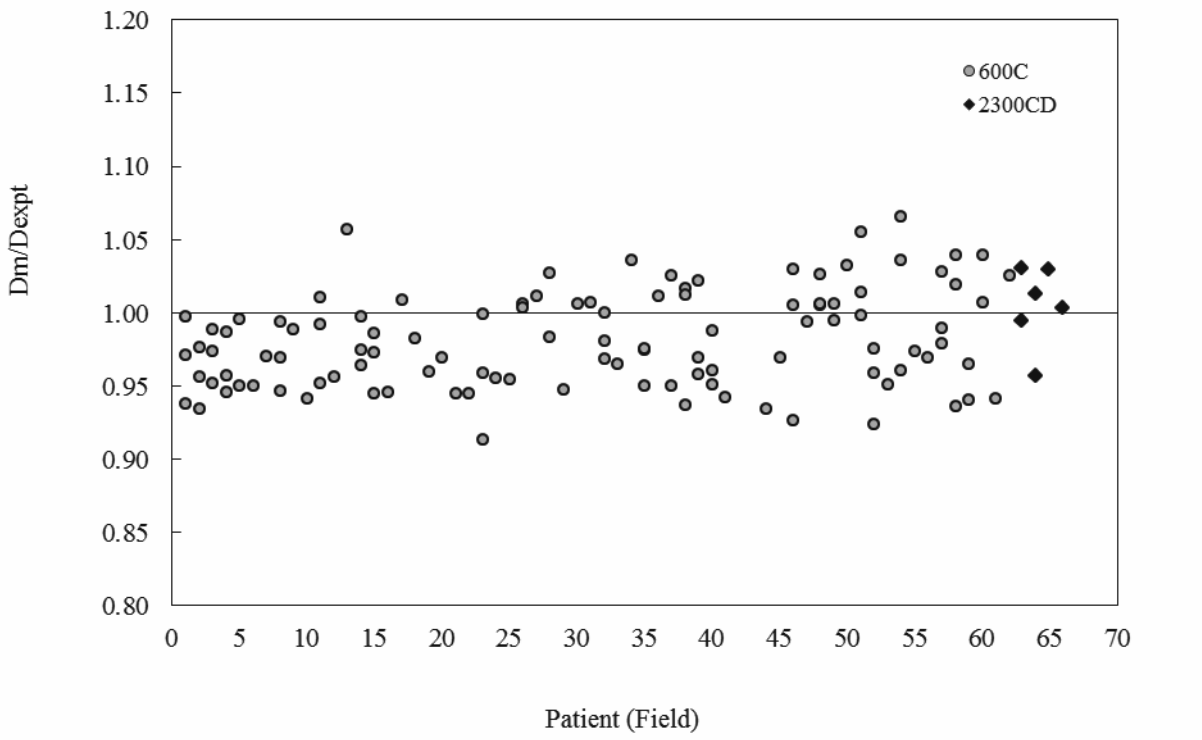

FIG. I–18. In vivo measurements of patients treated with a 6 MV beam (Clinac 600C and 2300C/D).

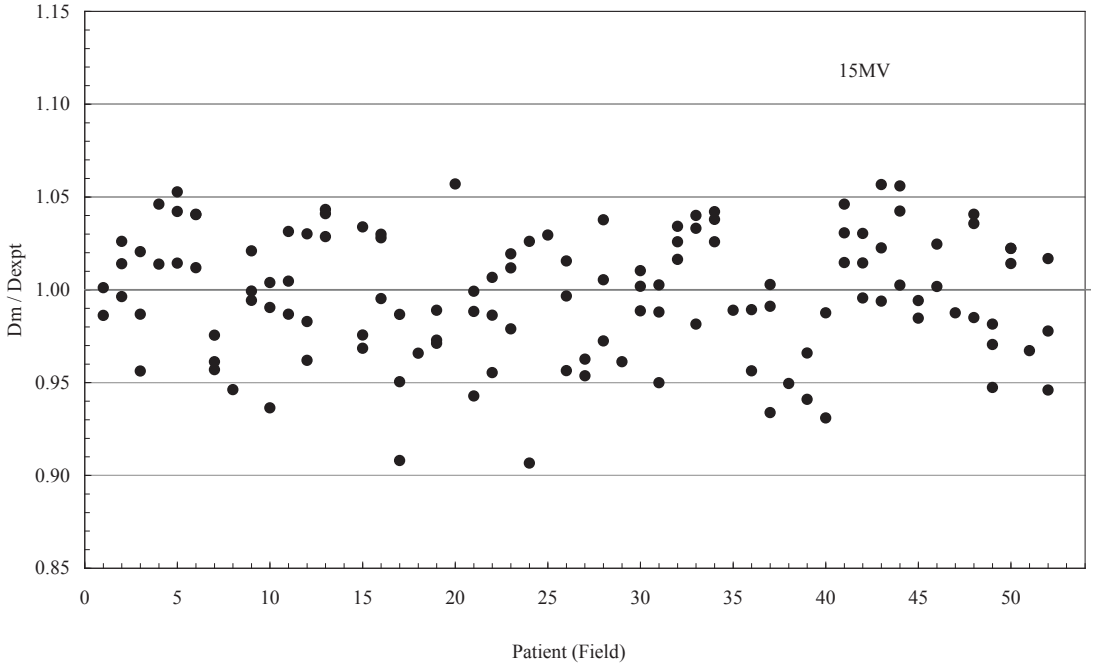

FIG. I–19. In vivo measurements of patients treated with 15 MV beam (Clinac 2300C/D).

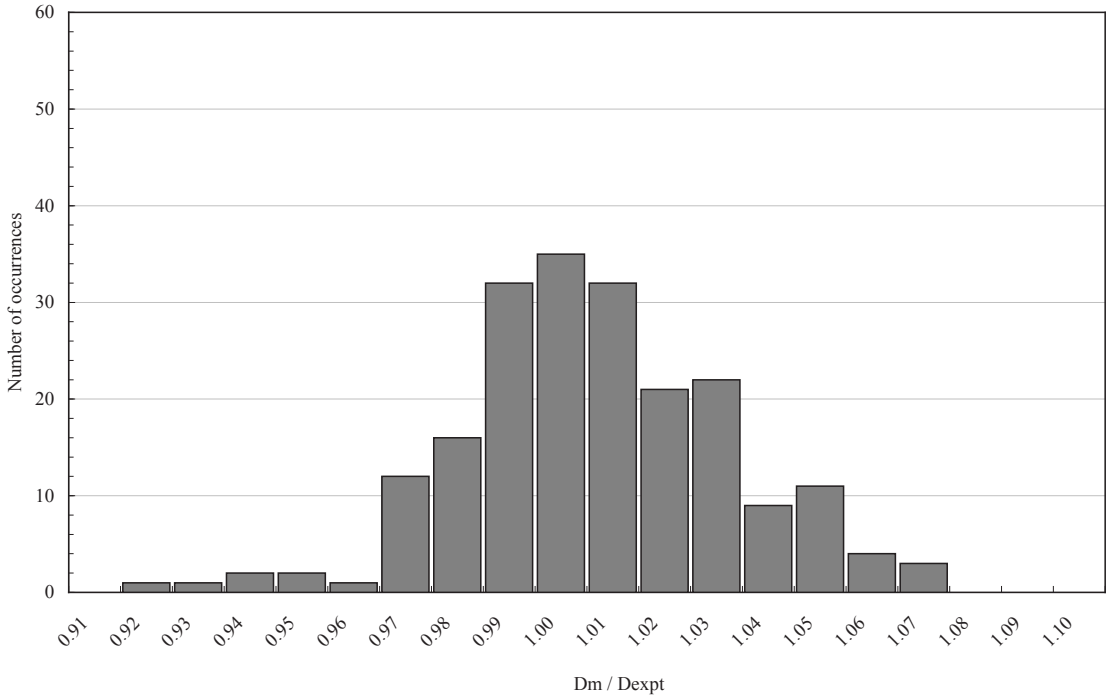

FIG. I–20. Histogram of frequency for all measurements.

I–5. OSL MEASUREMENTS

I–5.1. OSL dosimeter characterization

I–5.1.1. OSL reader stability

The first step in the OSL procedure was the verification of the OSL reader's performance (i.e. its stability needs to be within the limits of tolerance stated by the manufacturer). There were three tests made without OSLDs: a test for the calibration (CAL), a test for the laser performance (LED) and a test of reading without the laser (DRK). For CAL and LED tests, the tolerance levels are ±10% and for the DRK test, the counts should be below 30.

The results of the reader stability tests are shown in Fig. I–21.

The calibration curve, generated automatically by the software, was based on 12 OSLDs irradiated with doses between 50 cGy and 300 cGy, and this gave an internal non-linearity correction factor of 0.96. The average standard deviations (sample mean) were less than 1%. The reader was controlled by the MicroStar software version 1.1.1. It was possible to calibrate the reader for non-linearity and for sensitivity. To investigate the stability of the OSL signal, a set of OSLDs was irradiated with 50 cGy and then read 40 times. The measured loss of signal per readout was approximately 0.03%.

I–5.1.2. OSLD factor and batch calibration

To perform the study of the distribution of OSL readings within a batch of dosimeters, OSLDs were irradiated in a virtual water slab phantom (40 cm × 40 cm slabs of 3 cm and 5 cm thicknesses). One slab had four slots milled in order to accommodate four OSL dots neatly centred and aligned. The same set-up was used to determine the individual dot factors.

To calculate the individual factors, the average reading for all dots was calculated and divided by the reading for each dot to determine the 'dot factor'. Three measurements were made for each dot factor following the initial manufacturer instructions (i.e. the irradiation readout cycles without bleaching).

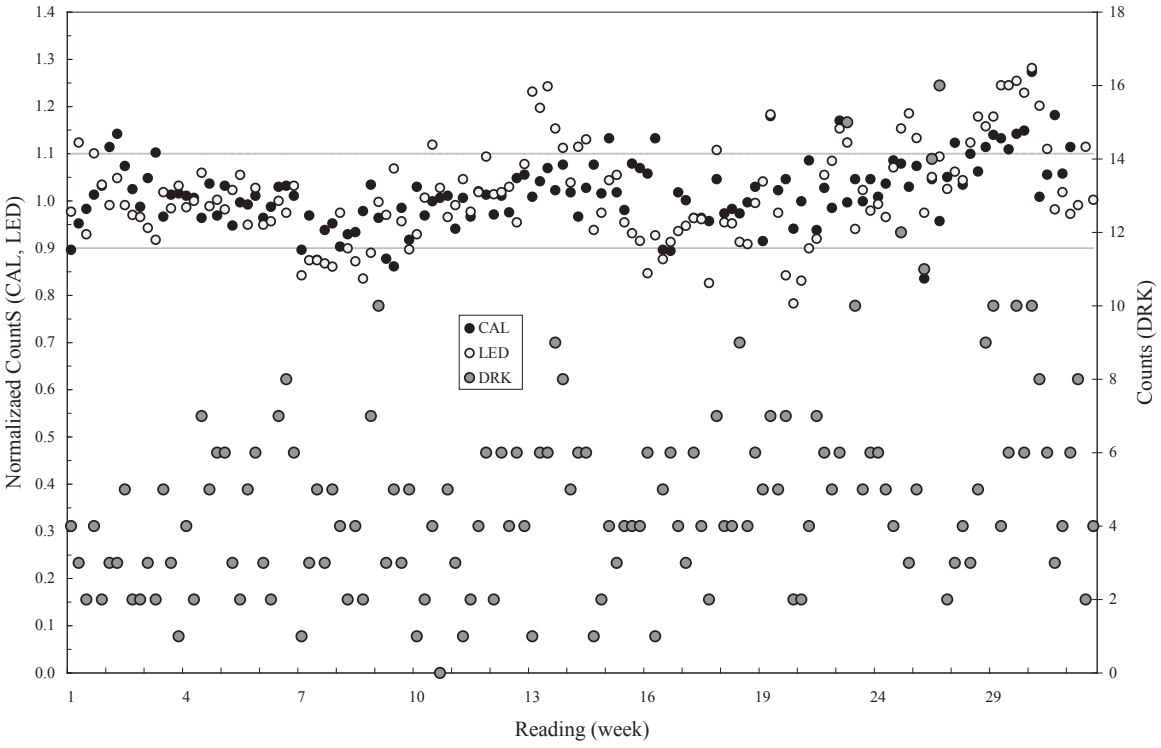

FIG. I–21. Reader fluctuation tested over 30 weeks.

The study started with 192 dots from a single batch (labelled 0.81). These dosimeters were not pre-selected by the manufacturer, and the results showed a large scatter of individual dosimeter sensitivities with only a small fraction of dosimeters having sensitivities within ±3%. This approach appeared to be impractical and was abandoned for further measurements. Subsequently, selected dots were irradiated with 50 cGy and read in several sessions performing five readings of each dot per session. With this methodology, it was observed that the sensitivities with the batch were more homogeneous, but the sensitivity measured was only relevant for a single irradiation. The average sensitivity for the single irradiation of 50 cGy was $(8.03 \pm 0.02) \times 10^{-6}$ Gy/rdg (0.3% of average standard deviation). However, after several irradiation reading cycles, the dots' sensitivity changed dramatically.

I–5.1.3. OSL bleaching

Based on the OSL results and TLD experience with annealing, it was decided to bleach the OSL dots. Bleaching is the process in which the irradiated dosimeter releases all the energy trapped in Al_2O_3:C crystals when exposed to light.

To perform this process, the dots were illuminated for three hours with a halogen light of 500 W at a distance of 60 cm from the light source. This time was sufficient for doses of about 100 cGy. To avoid damage to the dosimeter and any structural changes to the Al_2O_3:C crystals due to excessive heat coming from the light source, a water phantom was positioned between the dots and the light source, providing a thickness of 10 cm of water, which was sufficient to absorb the heat (Fig. I–22). In addition, the flux of light, when in the presence of the water phantom, increases by 20%. After two hours, the water was replaced in order to decrease the temperature near the dots. This way, the air temperature was always less than 40°C near the dots.

To monitor the amount of light arriving at the dots, a luximeter Icel LD550 was used to scan the surface. The result can be seen in Fig. I–23. The average exposure measured around 55% of the area was 40 000 ±10% lx.

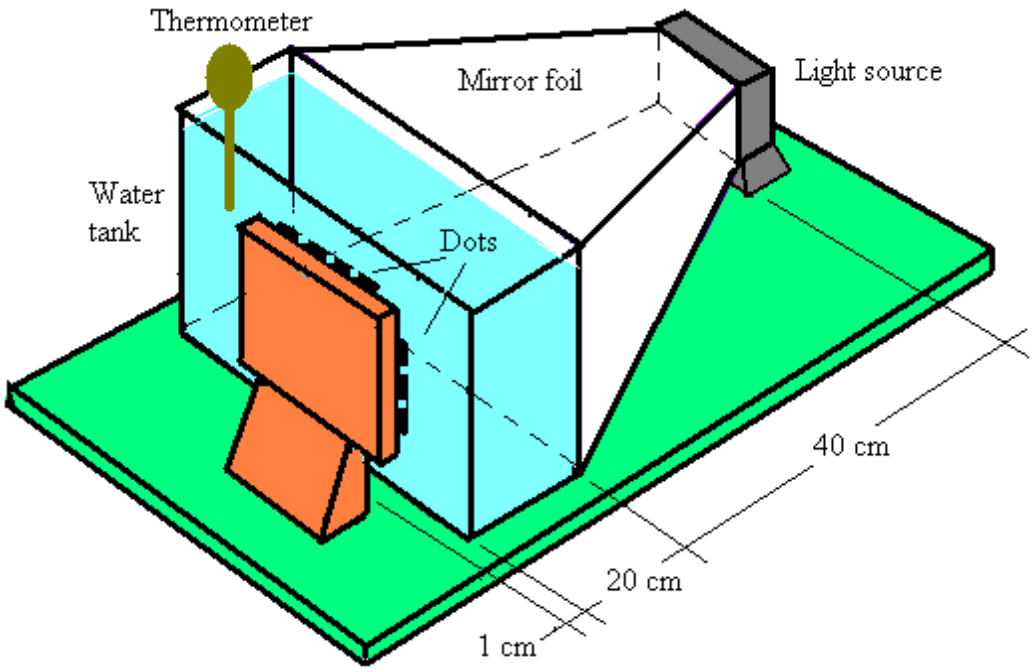

FIG. I–22. Set-up for OSL dot bleaching.

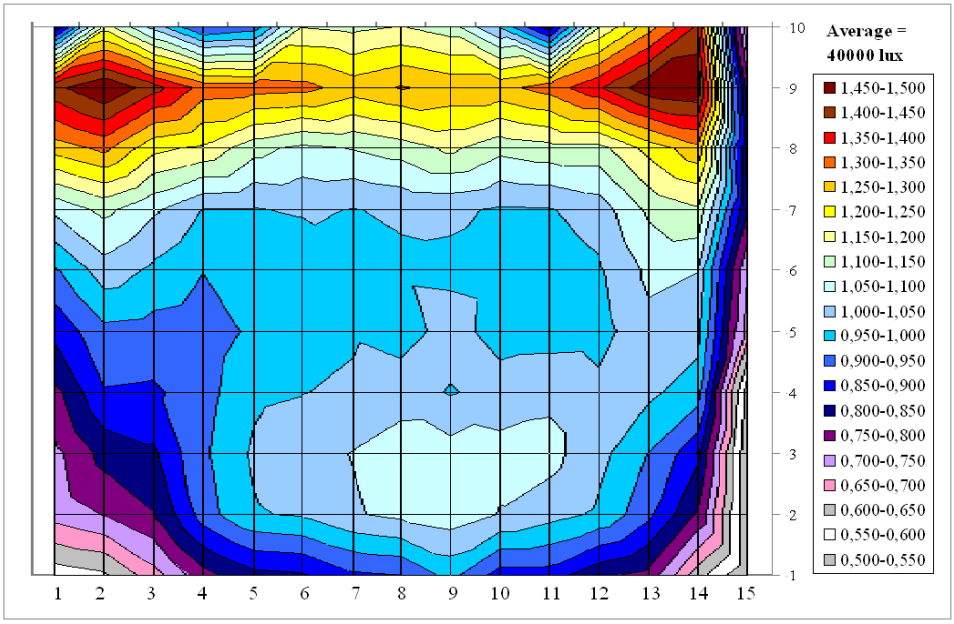

FIG. I–23. Light distribution on the surface behind the water phantom, where the dots were placed for bleaching.

Figure I–24 shows the removal of the OSL signal in the bleaching process as a function of the bleaching time. OSL dots were irradiated to 50 cGy (^{60}Co). The following bleaching conditions were used: 45 000 lx provided by a 500 W halogen bulb with the dots placed 60 cm away from the light source, behind a water tank.

In the following steps of OSLD characterization, five cycles of bleaching, irradiation and readout were performed on a group of dots for the reproducibility study. For this, OSLDs were irradiated with 50 cGy (^{60}Co, SSD = 80 cm, 5 cm depth, 10 cm ×10 cm field size). The results were satisfactory (Fig. I–25), with almost 70% of dosimeter factors within ±3% of the average for the group.

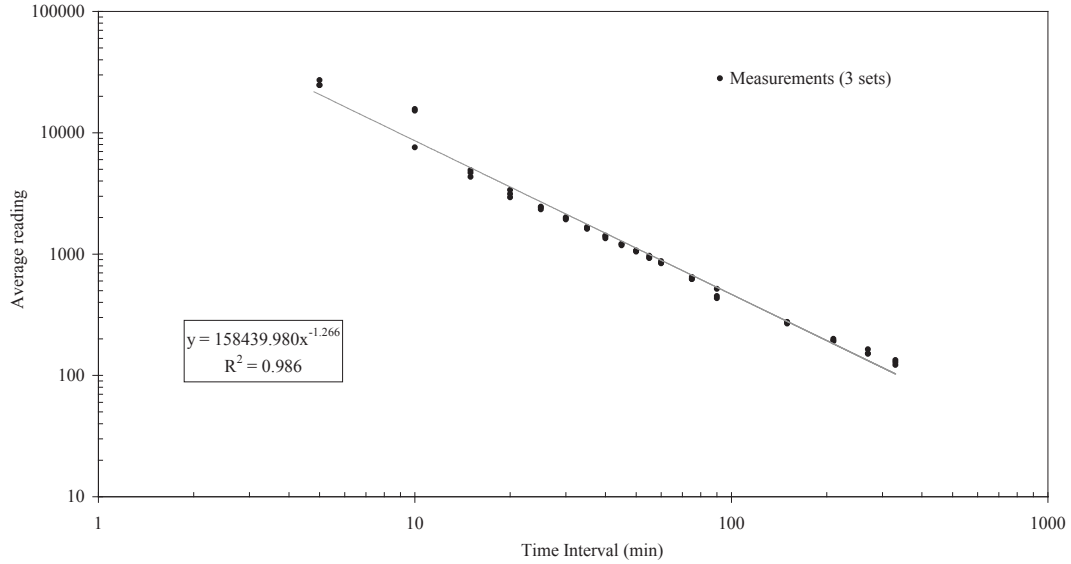

FIG. I–24. Removal of an OSL signal in the bleaching process.

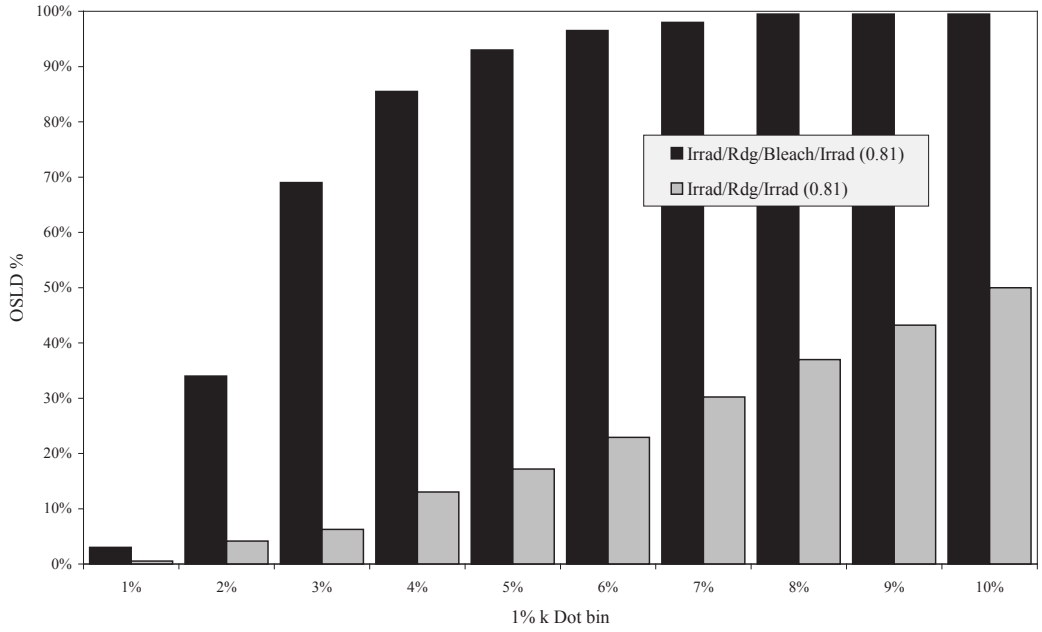

FIG. I–25. Cumulative histogram comparing the dosimeter factor distribution with and without bleaching.

New experience acquired as the result of the various repeatability tests carried out using OSL dots provided useful information on handling OSLDs and processing them for the optimum use for in vivo dosimetry. After extensive studies, it was decided to take the individual calibration dot coefficients derived after a single irradiation with a dose of 50 cGy in a ^{60}Co beam in the reference conditions (i.e. 5 cm depth, 10 cm × 10 cm field size and SSD = 80 cm). The dot response was derived from an average of five readings. The resulting calibration coefficients are shown in Fig. I–26.

After choosing this method, another non-linearity test was performed. Four dots from the selected group were chosen, and they were irradiated with 20, 50, 100, 150, 200, 300 and 400 cGy (10 cm × 10 cm field size and SSD = 80 cm in a ^{60}Co beam).

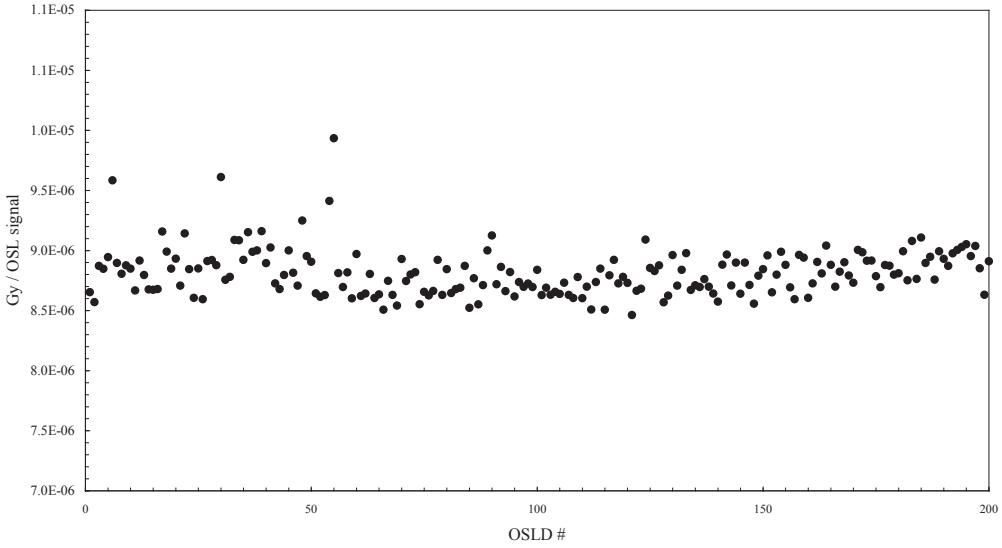

FIG. I–26. Individual calibration coefficients for 200 OSLDs. Dosimeters were irradiated with 50 cGy.

I–5.1.4. OSLD non-linearity dose response

The dots with the buildup caps were placed on the surface of a virtual water phantom for calibration with the ionization chamber at the reference depth (Section 4, Fig. 8). They were irradiated with the following doses: 50, 100, 150, 200, 300 and 400 cGy. The non-linearity dose response correction factor was defined in Section 4.4.1.

Three different studies were carried out for three dosimeter groups of the same batch. The first group was given the calibration dose of 50 cGy before the doses for the non-linearity test (50 cGy + *D*). For the second group, the 'non-linearity' dose *D* was given without the calibration dose of 50 cGy. After this, the dots were irradiated again with the calibration dose of 50 cGy, resulting in the dose *D* + 50 cGy (third group). The results are shown in Fig. I–27. After bleaching OSL dots, the non-linearity becomes similar to when they were irradiated for the first time, as shown in Fig. I–28.

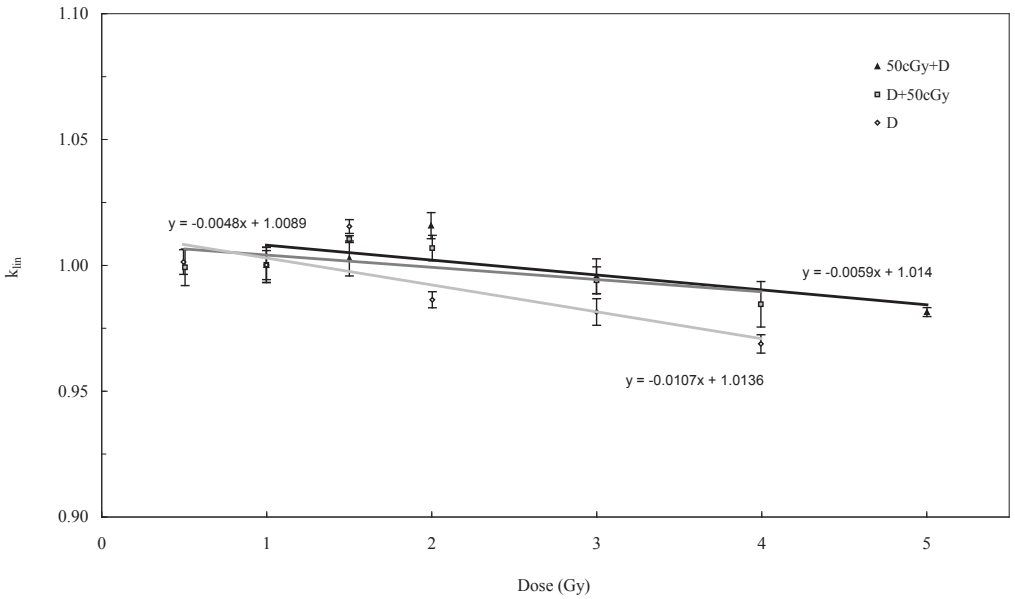

FIG. I–27. Non-linearity dose response correction.

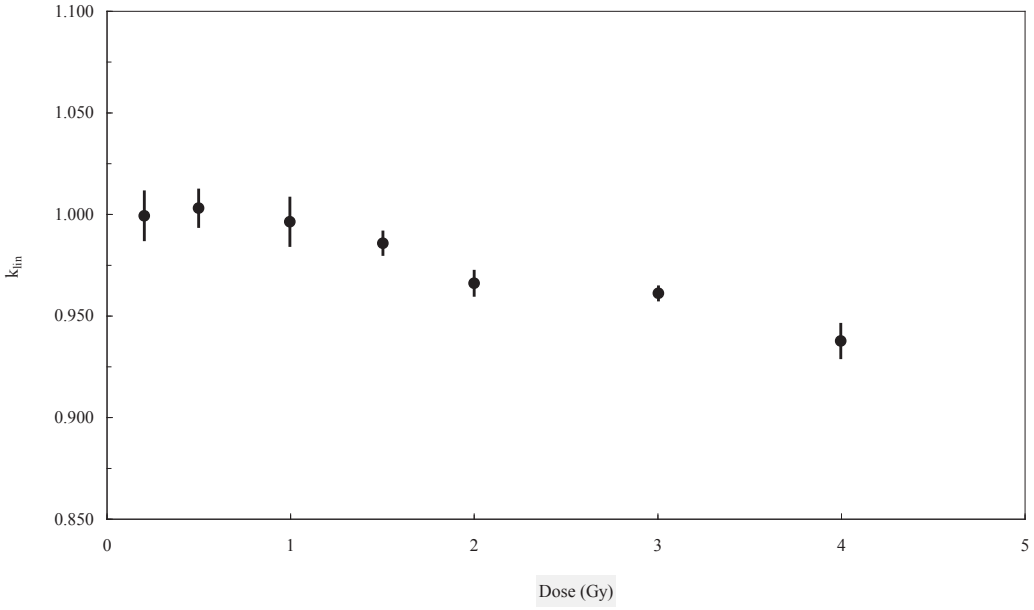

FIG. I– 28. Non-linearity of the dose response correction after bleaching.

I–5.1.5. OSLD energy correction

No energy dependence study was performed as part of this project. In earlier work [I–2], no energy dependence for the photon energy 6 MV–18 MV was found. However, for ^{60}Co, dot sensitivity increased by approximately 4%.

I–5.1.6. OSLD fading

A fading test was made for a single dot irradiated with 50 cGy in the reference conditions with a ^{60}Co beam. The readings were taken during a one hour period. Figure I–29 shows the results; individual readings were normalized to the reading taken one hour after the OSLD irradiation. It can be seen that although early fading is strong, after about 8–10 minutes, the signal stabilizes.

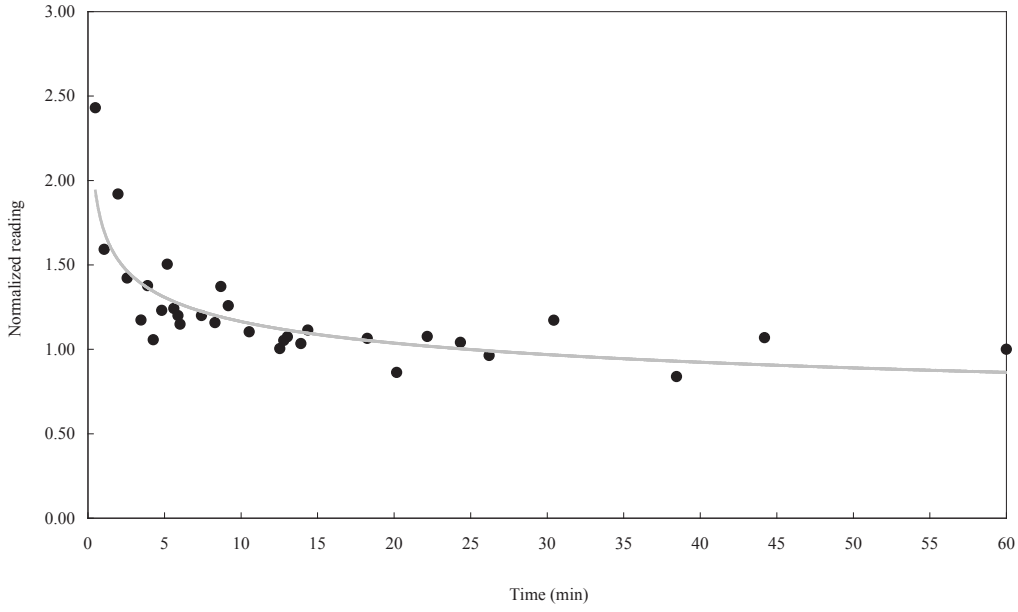

FIG. I–29. Early fading during a one-hour period.

For time delays longer than one hour after the irradiation, the OSLDs show a slow signal loss (about 3% after 72 h), as can be seen in Fig. I–30. Considering that the entire process of in vivo dosimetry using OSLD takes less than two hours, it is concluded that the fading correction can be omitted in the calculation of the dose from OSL readings. For practical reasons, OSLD readings were made between one hour and two hours after the dosimeter irradiation.

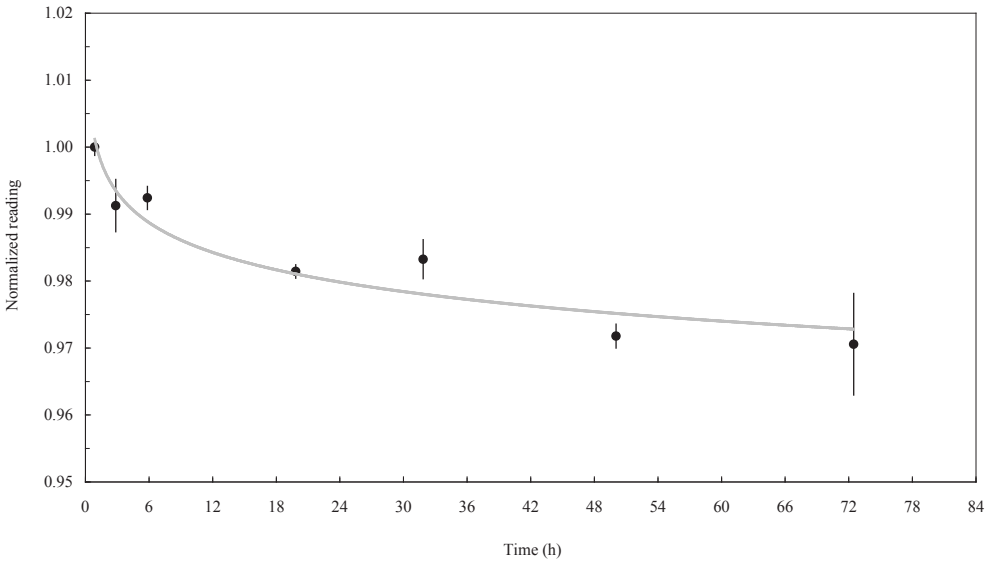

FIG. I–30. OSLD fading for up to 72 hours after irradiation.

I–5.1.7. OSLD angle of incidence correction

To study angular dependence, OSLDs with buildup caps (aluminium for the ^{60}Co beam and stainless steel for 6 MV and 15 MV) were placed on the surface of the virtual water phantom. They were irradiated with 50 cGy at d_{max} (10 cm ×10 cm field size and SSD = 80 cm) with the gantry at 0º and the same time for: ±10º, ±20º, ±30º, ±40º, ±50º and ±60º (and ±55º only for the ^{60}Co beam).

The angular dependence study for OSLDs was performed with dots in two different positions. First, the dosimeter with the buildup cap was positioned ‘in plane’ (i.e. with its long axis parallel to the gantry rotation axis) on the surface of the virtual water phantom and irradiated with 50 cGy in the ^{60}Co beam with the gantry at 0º, ±15º, ±30º, ±45º and ±60º (Fig. I–31).

In the second position, the dot was aligned longitudinally in the ‘cross-plane’ for the irradiations with its long axis perpendicular to the gantry rotation axis (Fig. I–32). Then the dots were irradiated as in the first case with doses of 50 cGy and the gantry at the same angles as before.

I–5.1.8. OSLD source to surface distance correction

The SSD correction measurements were performed with dosimeters on the surface of the phantom with the calibration set-up (^{60}Co beam) at different SSDs: 70, 80, 90.2, 100, 109.2 and 110 cm and with a fixed collimator opening for the reference conditions. The time of irradiation was calculated such that the same dose D = 100 cGy was delivered to a point at d_{max} for each SSD. Four OSLDs were used for each SSD in this exercise. The resulting correction factor, k_{SSD}, is shown in Fig. I–33. Each point in the graph represents the average OSL response for four dots, five readings per dot.

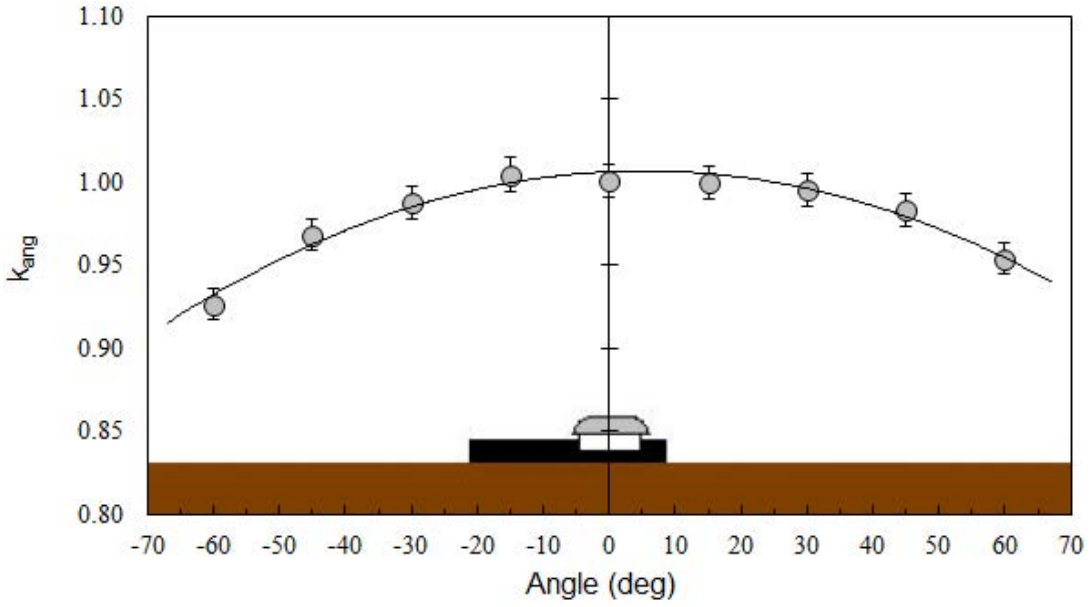

FIG. I–31. Angular dependence of OSLD for in-plane position with associated standard error.

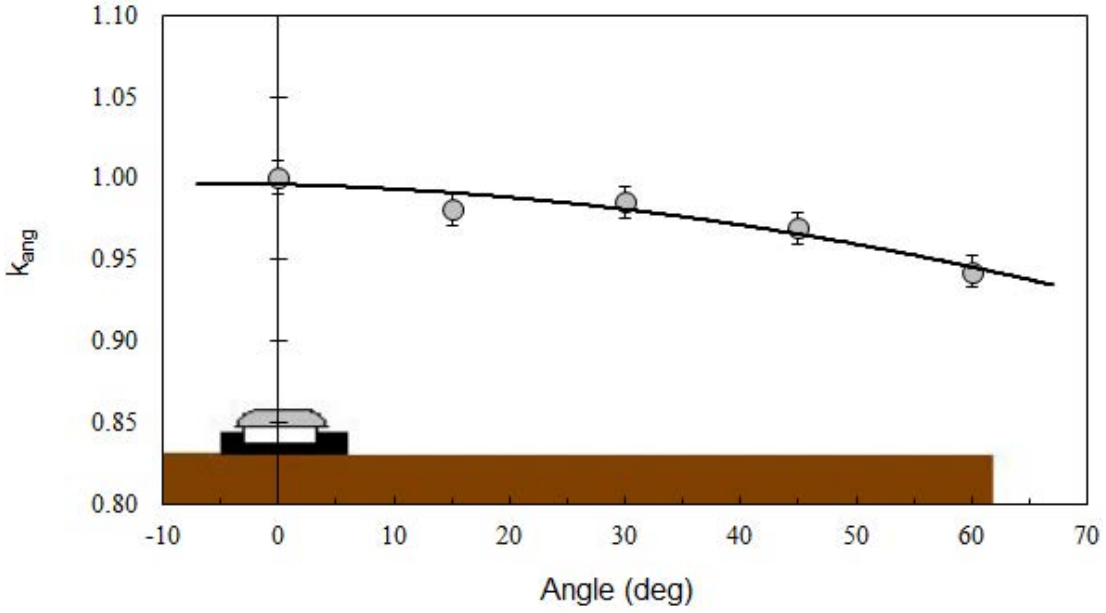

FIG. I–32. Angular dependence of OSLD for cross-plane position with associated standard error.

I–5.1.9. OSLD field size correction

Just as for TLDs, field size correction factors were measured. OSLD measurements were performed on the surface of the solid water phantom in a ^{60}Co beam. Figure I–34 shows the results of these measurements. It can be seen that the field size correction factor may be omitted from the calculation of the dose from OSL readings.

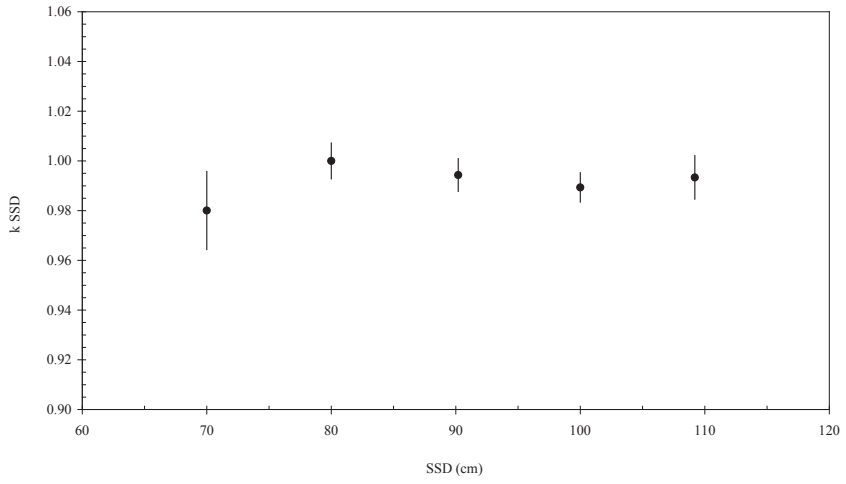

FIG. I–33. SSD correction factor for OSLD in a ^{60}Co beam shown with associated standard error.

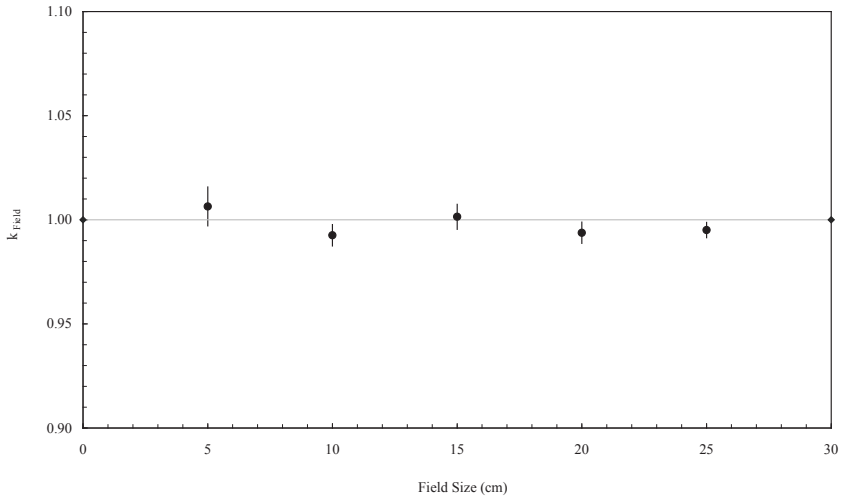

FIG. I–34. OSLD field size correction factors for ^{60}Co shown with associated standard error.

I–5.1.10. OSLD wedge and tray correction

The wedge filter correction factor was derived from the ratio between the wedge transmission factor for a 10 cm × 10 cm open field measured with an ionization chamber at the reference depth and converted to d_{max} and the wedge transmission factor for the same field size measured with the OSL dosimeter (with a buildup cap) placed on the surface of the virtual water phantom. For these measurements, OSLD was placed on the central axis of the beam. Table I–8 shows the resulting wedge correction factors for a ^{60}Co beam.

TABLE I–8. WEDGE FILTER CORRECTION FACTORS FOR OSLD

Wedge	k_{wedge}	s_M
15°	1.010	0.010
30°	1.006	0.008
45°	1.017	0.007

With the same irradiation set-up, a tray correction factor was investigated for OSLDs. As in the case of TLDs, the tray correction factor was determined from the measurements with and without the tray. The results are presented in Table I–9. Dots were irradiated directly for the tray factor with the dose D, without the prior irradiation to 50 cGy. It can be seen that no tray correction is required.

TABLE I–9. TRAY CORRECTION FACTORS FOR OSLD

Tray	k_{tray}	s_M
No tray	1.000	0.010
Plain tray	1.007	0.013
OSLD under acrylic	1.007	0.004
OSLD under gap	1.011	0.006

I–5.2. Rando phantom measurements with OSLDs

A female Alderson Rando anthropomorphic phantom was used for measurements simulating the planning and treatment of a head and neck tumour. As per the CRP procedure, the measurements were performed with and without an immobilization mask. Two parallel opposed 6 cm × 6 cm fields without wedges were used in this exercise. For each field, a dose of 100 cGy was delivered at the isocentre, as for the TLD study.

The expected dose was calculated using the TPS and, in parallel, an independent manual method. Figure I–35 shows the ratios between the measured doses, D_m, and the doses calculated by the TPS, D_{TPS}, and manually, D_{calc}. Results are shown with and without a mask. Differences between the manual and TPS calculations may be due to the inhomogeneity correction used by the TPS for the throat air cavity, which is not considered in manual calculations.

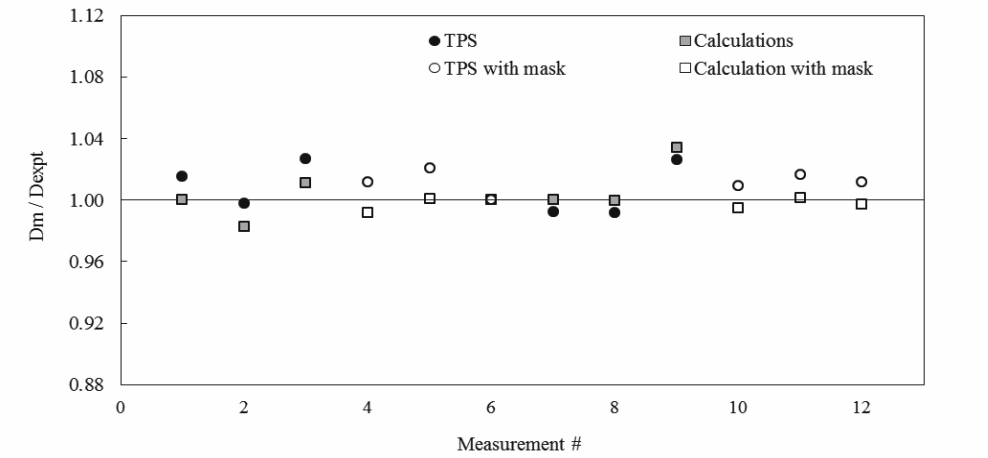

FIG. I–35. Rando phantom measurements for head and neck, with and without an immobilization mask.

I–5.3. Patient in vivo measurements with OSLDs

The in vivo measurements with OSLD were carried out for 99 patients and 205 fields treated with a ^{60}Co beam. The results are shown in Figs I–36 and I–37. A histogram of the results distribution is shown in Fig. I–38. In total, 191 out of 205 measurements (93.2%) were within the ±5% acceptance limit.

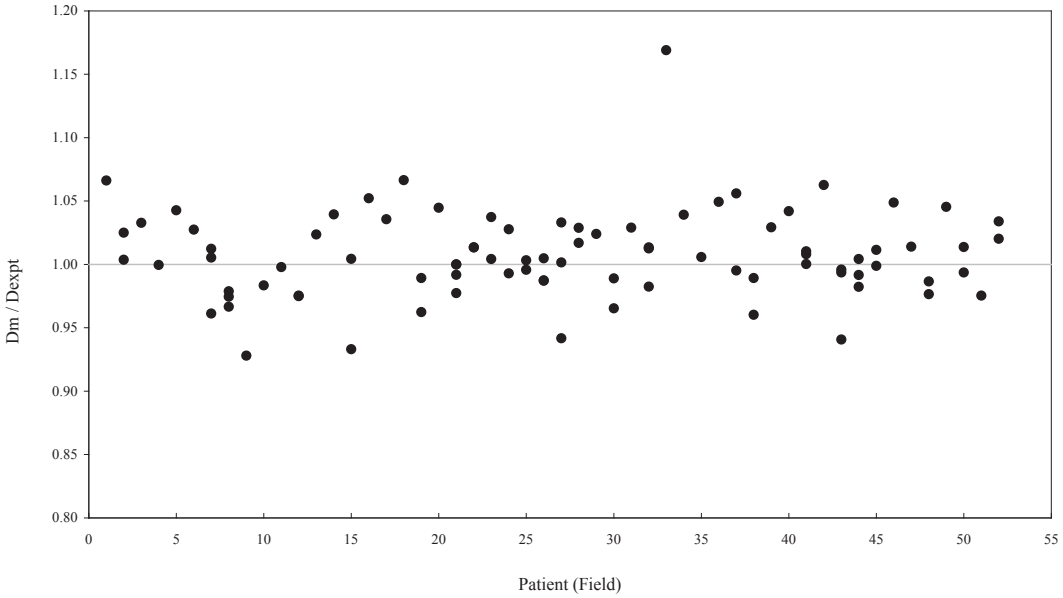

FIG. I–36. OSLD in vivo measurements on patients treated in a ^{60}Co beam, unit C.

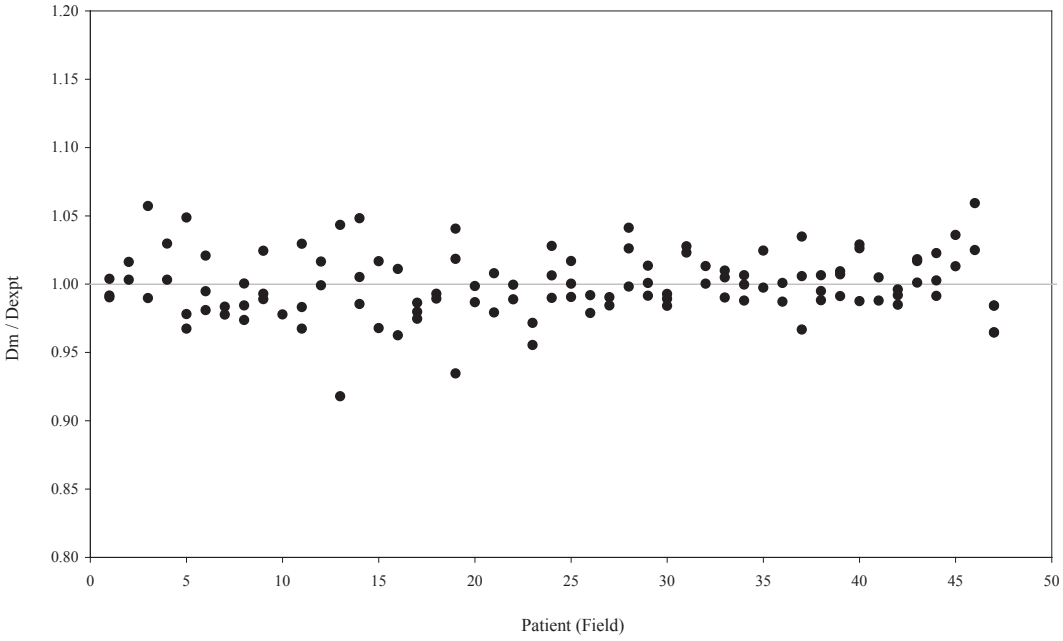

FIG. I–37. OSLD in vivo measurements on patients treated in a ^{60}Co beam, unit X.

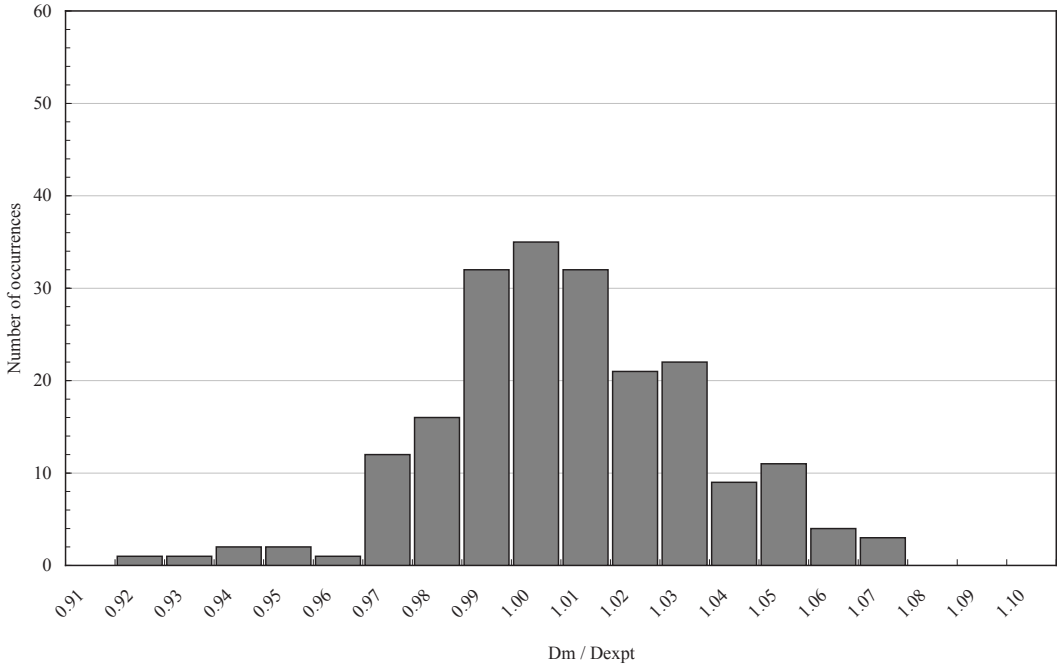

FIG. I–38. Histogram of the patient result distribution for OSLD measurements performed using a ^{60}Co beam.

I–6. SUMMARY AND CONCLUSION

The physical characteristics of TLDs and OSLDs have been analysed and investigated in this project, and present several considerable advantages:

(a) They are very simple to handle since they are free of any cables or wire connections, which makes the set-up easy; this also increases the patient's comfort.
(b) They are temperature independent since they do not use electronic components.
(c) They can be reused after a simple process is carried out (thermal annealing for TLDs and optical bleaching for OSLDs).
(d) These properties have been the reason to study and to compare the routine application of both systems for in vivo dosimetry as a part of a QA programme in a radiotherapy department.
(e) The TLD system stability and reproducibility were investigated and the calibration of the TLD batch performed. Intrinsic characteristics such as non-linearity, energy and angular dependence as well as other correction factors (i.e. SSD dependence and wedge, tray and field size factors) were determined.

Alderson Rando phantom studies for head and neck and pelvis irradiation with TLD were performed. All differences found between the calculated (TPS and manual) and measured doses for different sites and set-ups were within ±3%. This demonstrates that after phantom measurements with the proper use of all the correction factors, in vivo clinical studies for selected treatment sites could be performed without problems.

There were differences between the TPS and manual calculations for the analysed head and neck fields. It is believed that these differences are due to the inhomogeneity correction method used by the TPS for the throat air cavity, which is not considered with manual calculations.

In the second part of the project, an OSL dosimetry technology was extensively studied. The reader calibration, stability and reproducibility were investigated. The same intrinsic characteristics determined for TLD were also determined for OSLD.

Alderson Rando phantom studies for head and neck irradiation with OSLD were also performed. Even though the measurements remained within the ±3% tolerance level, it was concluded that the uncertainties were higher because individual dot sensitivity factors were not used.

During the previous irradiation with various doses, in steps of 50 cGy (by cumulative irradiations, without bleaching), it could be seen that in many cases the dot sensitivities vary by more than 1% after each irradiation.

For all the reasons mentioned above, it was decided not to proceed with patient measurements using consecutive measurements on the same dot without bleaching. Instead a process in which the dots were bleached between measurements was evaluated, and better stability of the signal to dose ratio (0.8% 1SD) was obtained. This was comparable to the performance of TLD (1.0%, 1 SD).

After an extensive study with this methodology, the optimum way to deal with OSLD for in vivo dosimetry was decided on. Having established the methodology for clinical in vivo dosimetry, the in vivo measurements on patients were started.

During the project, absorbed doses for 315 patients were recorded. 199 patients were measured in ^{60}Co beams (100 with TLD and 99 with OSLD), and 116 patients were measured with TLD in linac X ray beams (64 with a 6 MV beam and 52 with a 15 MV beam). These data comprise 687 measurements (fields): 424 head and neck (264 with TLD and 160 with OSLD), 188 pelvis (178 with TLD and 10 with OSLD), and 78 other sites (44 with TLD and 34 with OSLD). In total, 617 (89.8%) measurements were within the ±5% acceptance limit: 426 (88.4%) measurements performed with TLD and 191 (93.2%) with OSLD.

For most of the entrance dose measurements deviating by more than 5% from the expected dose, a review of the measurement was performed, including all factors involving the measured and the calculated doses.

The results of two in vivo systems may be compared by analysing histograms of the result distribution, where 100 patients (241 measurements) with TLD and 99 patients (205 measurements) with OSLD taken in a ^{60}Co beam are presented. For TLDs, 241 measurements performed in the ^{60}Co beam had an average D_m/D_{expt} of 1.005 (3.0%, 1 SD), and 205 measurements with OSLD performed in the ^{60}Co beam had an average of 1.003 (2.9%, 1 SD).

It has been decided to continue in vivo dosimetry as a routine activity for randomly chosen patients and to follow up the data analysis as an additional tool for the QA programme.

In deciding which dosimetry system to use, the first consideration is whether an appropriately economical system is available in the country. If there is no established system, the choice should be made bearing in mind what is practicable in the local environment.

For unselected TLDs, the variation in the calibration coefficient between dosimeters was ±10%, while for OSLD the variation was ±20%. Because of the variability of OSLD, we suggest the use of individual calibration factors because in vivo results using individual calibration factors were much better than using a single batch calibration coefficient, but this is still subject to further investigations.

Before starting any in vivo measurements, all the treatment techniques should be simulated and evaluated using an Alderson Rando phantom.

ACKNOWLEDGEMENTS

The authors acknowledge the IAEA for its support of this project. We are grateful to Landauer Inc. and Sapra-Landauer for the loan of OSL dosimetric systems, and we would like to thank the following collaborators for their assistance in performing the studies:

— Paul Clivland de Oliveira, Techician (pcoliveira@inca.gov.br);
— Luiz Carlos Albuquerque da Silva, M.Sc, Physicist (lcasrad@gmail.com);
— Marcela Andrade Leal, Engineer and D.Sc. student (nem-be@uol.com.br);
— Lucas Oliva de Sousa, Medical Physicist and M.Sc. student (lucaonb@yahoo.com.br);
— Kenji Vianna Notsu, B.Sc. student (k.notsu@yahoo.com.br).

REFERENCES TO ANNEX I

[I–1] INTERNATIONAL ATOMIC ENERGY AGENCY, Aspectos Físicos de la Garantía de Calidad en Radioterapia: Protocolo de Control de Calidad, IAEA-TECDOC-1151, IAEA, Vienna (2000).

[I–2] VIAMONTE, A., et al., Radiotherapy dosimetry using a commercial OSL system, Med. Phys. **35** (2008) 1261–1266.

Annex II

CANADA — USE OF MOSFET DOSIMETERS IN QUALITY ASSURANCE OF LOW DOSE RATE PROSTATE RADIOTHERAPY

J.E. CYGLER, A. SAOUDI, G. PERRY, C. MORASH, E.C.
Department of Medical Physics
The Ottawa Hospital Cancer Centre
Ottawa, Ontario, Canada

Abstract

The commercial MOSFET system was investigated for its possible application in the in vivo dosimetry of LDR permanent prostate implants. The study involved measurements for several patients who have undergone the implant procedure with iodine-125 seeds. New micro-MOSFET dosimeters were used as a tool for in vivo measurement of the initial dose rate within the urethra. MOSFETs were calibrated using a single special order calibration seed. The angular response was investigated in a 100 kVp X ray beam. MOSFET measurements allowed us to evaluate the overall quality of the implant by analysing the maximum dose received by the urethra, the prostate base coverage, the length of the prostatic urethra that is irradiated and the apex coverage.

II–1. INTRODUCTION

The Ottawa Hospital Cancer Centre (TOHCC) is a university teaching facility. The radiation oncology programme has at its disposal eight linear accelerators, two tomotherapy units and an orthovoltage unit. Until recently, there were also two ^{60}Co units. In addition to external beam capabilities, the centre has an active brachytherapy programme with both high dose rate (HDR), low dose rate (LDR) and permanent prostate implant capabilities.

TOHCC holds an IAEA research agreement on in vivo dosimetry. In vivo dosimetry has been used in Ottawa for many years as QA for patient treatments. The methods included TLDs, diodes, MOSFETs and OSL. Medical physicists have been involved in the development of MOSFET dosimeters with Thomson-Nielsen (now Best Medical) and most recently in the development of a 4-D dosimetry system which allows for simultaneous measurement of dose and a spatial position of the dose point as well as for the continuous monitoring of the patient movement, including the breathing pattern.

The in vivo dosimetry programme is the responsibility of the Medical Physics and Radiotherapy Departments involving physicists, physics technologists and therapists. In vivo dosimetry (both TLDs and MOSFETs) is routinely used for QA of total body irradiation. In vivo dosimetry with TLD and MOSFET dosimeters has also been used in the brachytherapy programme (both HDR and LDR) for selected cases. A new method of using micro-MOSFETs for QA of permanent prostate implants has been developed in recent years [II–1] and some results are described below.

II–2. MATERIALS AND METHODS

The dosimeters used for the in vivo measurements of prostate implants were specially designed high sensitivity dual-MOSFETs [II–2], model TN1002RDM (micro-MOSFETS) from Thomson & Nielsen Electronics Ltd., Ottawa, Canada. The high setting of the bias supply was used. The external dimensions of the dosimeters were 1 mm in diameter and 0.5 mm in thickness. The silicon oxide thickness was about 1 μm. The dosimeters fit inside one branch of the Foley catheter, which was inserted inside the patient's urethra. Metal leads of the dosimeters had special 1 cm graduated marks to allow for easy measurement of the dosimeter position inside the urethra during the in vivo dosimetry procedure.

Three different dosimeters were used in this study. They were calibrated in a solid water phantom using a special calibrated high activity ^{125}I seed (type 6702, Nycomed Amersham) and TG-43 formalism. These seeds were

of higher activity than the 6711 type used for prostate implants in our clinic. Higher activity seeds allowed for shorter calibration times. The air kerma strength of the calibration seed was verified to be 45.2 U (where U = cGy cm^2 h^{-1}) using a Capintec well chamber, the calibration coefficient of which was traceable to the Accredited Dosimetry Calibration Laboratory (ADCL).

The ^{125}I source and each dosimeter were embedded in a solid water phantom separated by 1 cm of material. There was a 6 cm thick solid water slab under the source as well as above the MOSFET to provide full scatter conditions. Each MOSFET was positioned on the transverse axis of the source at a distance of 1 cm from the source. The dose rate constant for the 6702 seed applied in the calibration procedure was 1.04 cGyh^{-1} U^{-1} [II–3].

According to TG-43 for any cylindrical symmetrical sources, the dose, $\dot{D}(r,\theta)$, at point (r,θ) can be written as:

$$\dot{D}(r,\theta) = S_K \Lambda \left[G(r,\theta) / G(r_0,\theta_0) \right] g(r) F(r,\theta) \tag{II–1}$$

where r is the distance from the origin at the source centre to the point of interest, θ is the angle with respect to the long axis of the source, S_K is the air kerma strength of the source, Λ is the dose rate constant, $G(r,\theta)$ is the geometry factor, $g(r)$ is the radial dose function, and $F(r,\theta)$ is the anisotropy function. The reference point, (r_0,θ_0), is defined at r_0 = 1 cm and $\theta_0 = 90^\circ$. At the reference point, the Eq. II–1 simplifies to:

$$\dot{D}(r,\theta) = S_K \Lambda \tag{II–2}$$

Using Eq. (II–2) and applying the dose rate constant of 1.04 cGy/hU for this type of seed [II–3], the dose rate at the reference point, where the MOSFET was positioned for the calibration, was 47.0 cGy/h.

Each MOSFET dosimeter was left in the calibration geometry for 10 minutes. The total dose accumulated by each dosimeter was therefore 7.83 cGy. This allowed us to derive the calibration coefficients for each MOSFET subsequently used in the in vivo experiments.

The MOSFET calibration coefficients ranged from 29.87 to 32.87 mV/cGy, with an average SD of ±2.5% over at least three measurements per dosimeter. The angular dependence of each MOSFET response was measured in a 100 kVp orthovoltage beam (Pantak) in a polystyrene phantom (25 cm × 25 cm × 3 cm). The dosimeter was positioned at a depth of 1.5 cm inside a special rotating insert, Fig. II–1. The MOSFET response was found to be isotropic within ±2.4% (1SD), which is within the dosimeter response reproducibility.

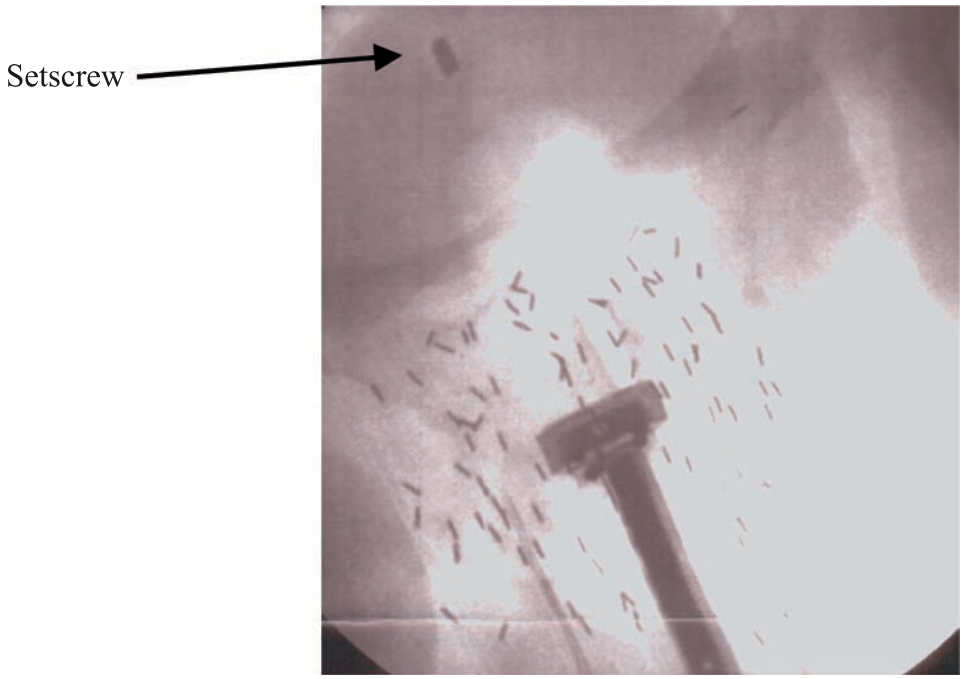

FIG. II–1. Fluoroscopy image of the prostate after implant.

Trans-perineal permanent prostate implants were performed under ultrasound guidance (Leopard, B&K). The iodine seeds used in the procedure were 6711 type (Nycomed Amersham).

Before the in vivo measurements, all the MOSFETs were sterilized in a Cidex solution (Johnson & Johnson) for a prescribed period of time (approximately 10 min). The dosimeter was inserted into one branch of a Bardex threeway sterile catheter (C.R. Bard Inc.). The catheter was subsequently inserted into the urethra. A small stainless steel setscrew was fixed to the tip of the catheter to act as a radio-opaque marker to help visualize, under fluoroscopy, the initial MOSFET position in the bladder. Later, new MOSFET dosimeters were designed, equipped with their own radio-opaque markers.

For each measurement point, the distance between the MOSFET and the internal bladder wall, coinciding with the lower edge of the Foley balloon, was recorded. Figure II–1 shows a fluoroscopy image of the prostate implant with the modified Foley catheter in place.

II–3. RESULTS AND DISCUSSION

II–3.1. MOSFET calibration

The results of the calibration for the individual dosimeters are listed in Table II–1 and show 10% variation for this batch of dosimeters. This level of variation in MOSFET responses warrants an individual calibration coefficient for each dosimeter used for patient measurements.

TABLE II–1. CALIBRATION COEFFICIENTS FOR MOSFET DOSIMETERS MEASURED WITH A 6702 ^{125}I SEED

Dosimeter	Average reading (mV/h)	Calibration coefficient (cGy/mV)	1SD %
MOSFET#1	1354	33.48 E-3	2.19
MOSFET#2	1410	32.14 E-3	2.95
MOSFET#3	1490	30.42 E-3	1.63

Figure II–2 shows the angular dependence of the micro-MOSFET response measured in a 100 kVp beam. This beam energy was chosen because it has an effective energy of about 30 keV, similar to that of a ^{125}I source. The data on the graph are normalized to the dosimeter response at 0°. It can be seen that these dosimeters have a practically isotropic response. The largest deviation from isotropy is about 2.5%. This makes them ideal for in vivo dosimetry in a low energy radiation field such as is present inside the ^{125}I implanted prostate gland.

II–3.2. Patient dose measurements

Table II–2 summarizes patient information and shows that all patients had a prostate volume of about 50 cm^3 or less and an average number of seeds per unit volume of 2.1 seeds/cm^3. The patient who received a greater number of seeds per unit volume had a small prostate (patient #3). In this patient, the smaller prostate volume resulted in a higher proportion of seeds close to the urethra, causing a higher urethral dose. The maximum initial dose rate (IDR_{max}) to the urethra was 15.6 cGy/h for this patient, which corresponds to a maximum total dose to the urethra of 320.7 Gy (Fig. II–3, top left). This value is greater than the recommended urethra dose limit, which is 1.5–2 times *mPD* [II–4, II–5].

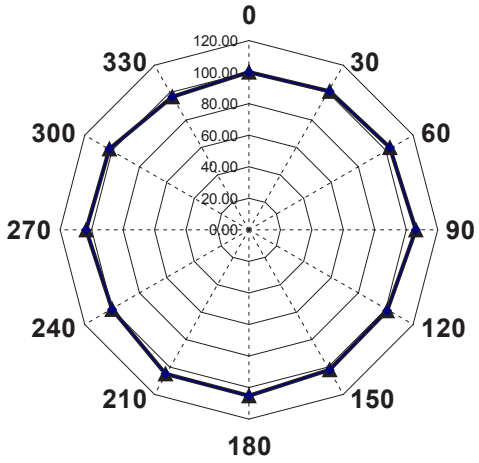

FIG. II–2. Angular dependence of the micro-MOSFET response measured in a 100 kVp beam.

TABLE II–2. PATIENT INFORMATION PRE- AND POST-IMPLANTATION

Patient	PUL^{*} (mm)	Prostate volume US (cm^3)	Prostate volume CT (cm^3)	Number of seeds implanted	Number of seeds per cm^3	IDR_{max} cGy/h	$L_{CT}^{mPD}{}^{**}$/PUL[b]	(MPL[***]+ Base-mPD[§])$_{mPD}$/PUL	Base-mPD)$_{mPD}$ (mm)
#1	35	49.2	55.38	93	1.9	12.2	1.07	1.34	0.00
#2	50	50.9	69	108	2.1	11.1	0.96	1.09	5.43
#3	25	16.1	32	51	3.2	15.6	1.06	1.26	8.57
#4	40	42.5	37	89	2.1	10.8	0.65	0.86	8.23
#5	35	38.5	60	93	2.4	10.4	0.85	1.23	2.23

* PUL: Prostatic Urethra Length before implantation measured by ultrasound.

** L_{CT}^{mPD} : CT based post-plan prostate sup-inf length covered by *mPD*.

*** MPL: Measured (at the end of the implantation procedure) Prostatic urethra Length covered by mPD.

§ *mPD*: minimal peripheral dose.

After the implant, there is no practical way to reduce this urethral dose, but in vivo measurements might suggest that such a patient be followed closely and considered to be at increased risk for urethral complications. Our in vivo procedure follows the general recommendations of AAPM TG-64 [II–6], which state that in order to create an acceptable treatment plan, one should adequately identify the entire length of the prostatic urethra and calculate the dose profile along the urethra. The same recommendation applies to the CT-based post-plan created one month after the implantation procedure in order to aid in evaluation of treatment outcomes. The in vivo measurements of the dose in the urethra were carried out by moving the MOSFET dosimeter along the urethra in 1 cm steps. The dosimeter was left at each position for 10 minutes to accumulate dose, long enough to provide a reasonable measurement signal. We have measured the initial dose rate along the urethras of several patients. An example of the measured and calculated initial dose rate for the urethra as a function of the distance from the bladder wall is shown in Fig. II–3. The dose rate increases for the parts of the urethra surrounded by the prostate implant. For this patient, the maximum initial dose rate to the urethra was 12 cGy/h.

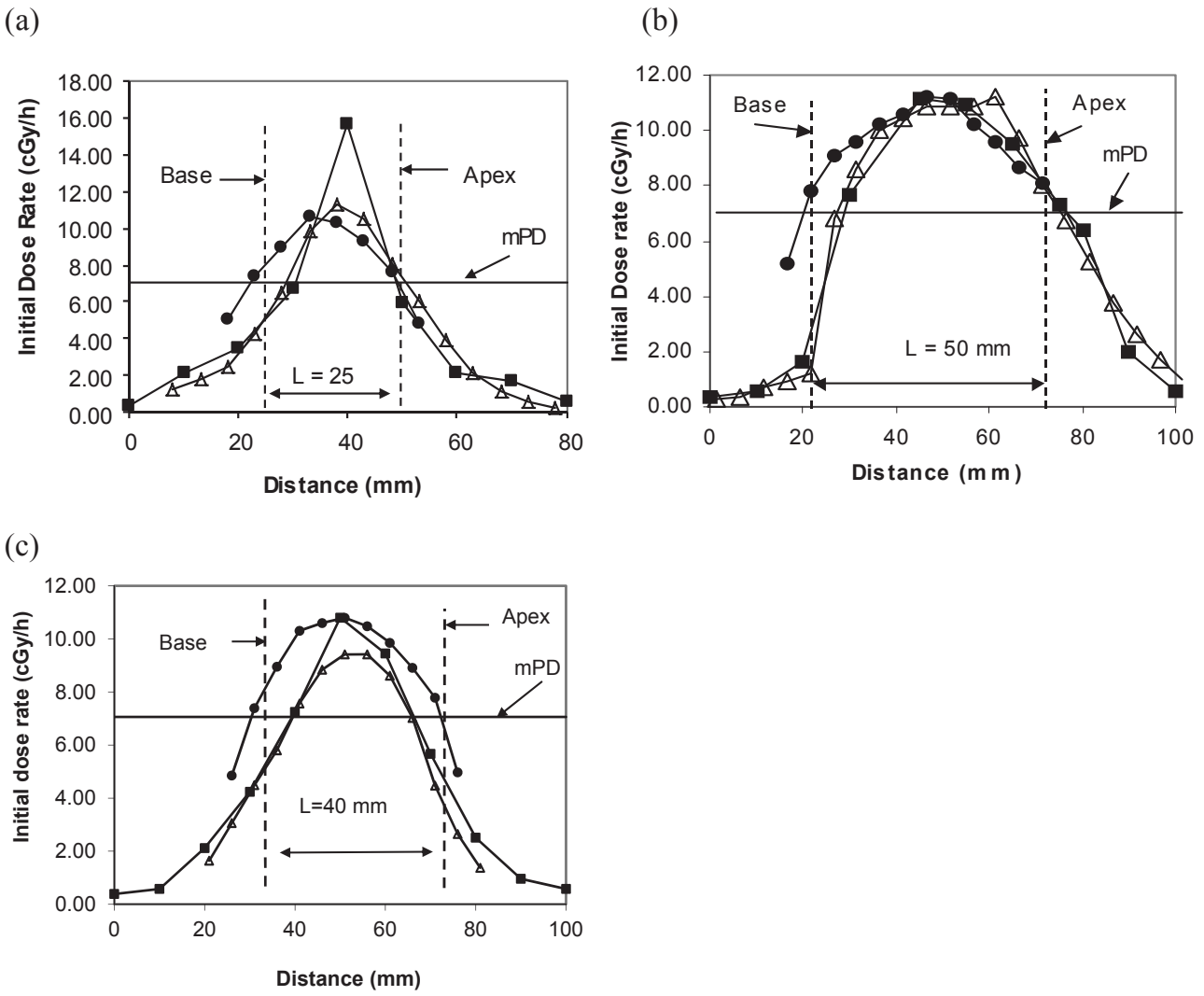

FIG. II–3. Examples of measured initial dose rate along urethra. (a) Patient #3; (b) Patient #2; (c) Patient #4. • *Pre-plan,* ■ *Measurement,* Δ *Post-plan*

Applying the following equation for the total integral dose,

$$Dose = \dot{D}_0 \times 1.44 \times T_{1/2} \qquad \text{(II–3)}$$

where $\dot{D}_0$ is the initial dose rate, $T_{1/2}$=59.4 days is the half-life of ^{125}I, the maximum dose to the urethra is 246.3 Gy. This is 1.7 times larger than the minimum peripheral dose (mPD) of 145 Gy prescribed to the prostate gland. For this patient, the full width at half maximum of the dose versus distance curves for the urethra is 5.2 cm. This means that 5.2 cm of the urethra receives a dose larger than 123 Gy and less than 246.3 Gy.

The value of the maximum urethral dose rates for different patients in this study ranged from 10 to 16 cGy/hr, corresponding to a total absorbed dose of 205 to 328 Gy. The shape of the dose rate vs. distance curve can help to evaluate the overall implant quality.

Patient data are summarized in Table II–2. All patients in this study had a prostate volume of about 50 cm^3 or less and an average number of seeds per unit volume of 2.1 seeds/cm^3.

The analysis of the measured data for all patients has been performed in terms of the following parameters, shown in Table II–2:

UL	Pre-implant prostatic urethra length in mm (based on US imaging);
N	Number of implanted seeds;
IDR_{max}	Maximum initial dose rate along the urethra (cGy/h) based on MOSFET measurement;
PUL(mPD)	Post-implant prostatic urethra length (mm) covered by dose = *mPD* (based on MOSFET measurement);
PUL(150% *mPD*)	Post-implant prostatic urethra length (mm) covered by dose = 150% *mPD* (based on MOSFET measurement);
$L(P_B - P_{mPD})$	Post-implant distance along the prostatic urethra from the bladder/base interface, P_B, to the point P_{mPD}, at which the urethral dose reaches the mPD value. It corresponds to the length of the prostate not covered by mPD and indicates 'cold' or underdosed regions of the gland.

Based on these data, the clinical evaluation of the quality of the prostate implant can be extracted as discussed below.

II–3.3. Discussion

II–3.3.1. Quality of the prostate implant in terms of the target coverage

Minimum peripheral dose, *mPD*, is the dose that encompasses the target volume (prostate with appropriate margin) [II–6]. The goal of the permanent prostate implant with ^{125}I seeds is to deliver an *mPD* equal to 145 Gy. However, *mPD* describes the dose to the prostate surface only. Actual doses to the central portions of the gland and tumour may be considerably higher. Since the urethra is positioned centrally inside the implanted volume, it usually receives doses equal to or higher than *mPD*. The dose to the urethra can vary significantly, depending on the strength of the sources and the implant technique. During generation of the pre-implant treatment plans, the utmost care is taken to minimize the dose to the urethra without compromising the tumour coverage.

The measured dose versus distance curve along the prostatic urethra also contains information about two distinct parameters related to the quality of the implant: the dose rate at the base of the prostate, and the length of the urethra that receives the minimum peripheral dose, *PUL* (*mPD*), compared to the ultrasound based preplanned length of the urethra to receive the *mPD*, *UL*. A properly implanted base of the gland will result in a steep dose gradient at the superior end of the prostatic urethra. The value of *mPD* will be reached very rapidly within millimetres from the prostate wall as is the case for patients #1 and #5 where this distance is 0–2.2 mm. This rapid increase is expected especially when the base is preplanned to receive *mPD* at the external wall of the prostate (the bladder–prostate interface), see Fig. II–3. In the case of patients #3 and #4, the distance over which the prostatic urethra reaches *mPD* is greater than 8 mm. This clearly demonstrates a deficiency of the dose delivered to the base. It also underscores the potential value of real time dosimetry using MOSFETs since a measurement made immediately post-implant could allow correction of the underdose of the base of the prostate.

For patient #2, it is difficult to conclude that the base is underdosed, especially with a 10 mm measurement step, which is too crude in this case. In this case, the dose sampling should have been done with a maximum 5 mm step in the base region.

The length of the prostatic urethra before implant, *UL*, is the same or smaller than the length of the prostate covered by the *mPD*, *PUL* (*mPD*), in the superior–inferior direction immediately post-implant. This is expected due to the prostate swelling during the implant procedure.

In Table II–2, the last column indicates that for patients 1, 2, 3 and 5, the apex of the prostate is well covered by the *mPD*. However for patient 4, about 14% of the initial length of the prostate appears to be underdosed. The reason why the base and/or the apex are often not well covered is probably related to prostate movement with needle

insertion and retraction and the frequent change of the relative base position during the implant procedure due to oedema caused by the trauma of needle insertion [II–7, II–8]. In order to minimize the potential of underdosing the base and/or apex of the gland, one has to ensure that the length of the prostate covered by *mPD* in the superior–inferior direction is greater than or equal to the length of the prostatic urethra before implant, *UL*. This can be done during pre-planning by adding an appropriate superior–inferior margin.

II–3.3.2. Percentage of the urethra receiving a dose higher than 150% of mPD

The urethra is the main organ at risk in transperineal interstitial permanent prostate brachytherapy (TIPPB). Urethral irritation is the main cause of symptoms following prostate brachytherapy. It has been recommended that the urethra should receive a dose no higher than 200% of *mPD* [II–4, II–5]. Table II–2 shows that for patients #1–#3, the length of the prostatic urethra receiving more than 150% of *mPD* varies between 13 and 27 mm. For patient #3, the initial dose rate in the central part of the urethra was 15.62 cGy/h, which corresponds to a total dose of 320.7 Gy. This is greater than the recommended dose limit, which is 1.5 to 2 times *mPD*. For this patient, the smaller prostate volume resulted in a higher proportion of seeds close to the urethra, causing a higher urethral dose. After the implant, there is no practical way to reduce this urethral dose, but in vivo measurements might suggest that such patients be followed closely and considered to be at increased risk for urethral complications. It also underscores the potential value of real time dosimetry using MOSFETs.

II–4. CONCLUSIONS

Specially designed MOSFET dosimeters are very useful for in vivo dosimetry of permanent prostate implants. When inserted into the urethra, they can measure the initial dose rate received by this organ in real time. This can serve not only as an indicator of possible treatment complications due to excessive dose to the urethra but also as a measure of the overall quality of the implant.

The drawback of using one MOSFET dosimeter to measure the dose along the entire length of the prostate is that it takes about one hour (approximately 10 minutes per position). This is excessively long if the measured data are to be used as the basis for adjusting the implant. However, the data are still useful for evaluation of the overall quality of the implant. In order to decrease the measurement time to a practical limit, a special linear array of MOSFET dosimeters was proposed and designed to enable the simultaneous reading of the initial dose rate at several positions inside the urethra [II–9–II–11].

ACKNOWLEDGMENTS

We gratefully acknowledge Thomson-Nielsen for providing us with special MOSFET dosimeters and Nycomed Amersham for donating a high-activity ^{125}I seed.

REFERENCES TO ANNEX II

[II–1] CYGLER, J.E., SAOUDI, A., PERRY, G., MORASH, C., EC, Feasibility study of using MOSFET detectors for in vivo dosimetry during permanent low-dose-rate prostate implants, Radiother. Oncol. **80** (2006) 296–301.

[II–2] SOUBRA, M., CYGLER, J.E., MACKAY, G., Evaluation of dual bias dual metal oxide-silicon semiconductor field effect transistor detector as radiation dosimeter, Med. Phys. **21** (1994) 567–572.

[II–3] RIVARD, M., et al., Update of AAPM Task Group No. 43 Report: A revised AAPM protocol for brachytherapy dose calculations, Med. Phys. **31** (2004) 633–74.

[II–4] NAG, S., et al., The American Brachytherapy Society recommendations for permanent prostate brachytherapy postimplant dosimetric analysis, Int. J. Rad. Onc. Biol. Phys. **46** (2000) 221–230.

[II–5] NAG, S., BEYER, D., FRIEDLAND, J., GRIMM, P., NATH, R., American Brachytherapy Society (ABS) recommendations for transperineal permanent brachytherapy of prostate cancer, Int. J. Rad. Onc. Biol. Phys. **44** (1999) 789–799.

[II–6] YU, Y., et al., Permanent prostate seed implant brachytherapy: Report of the American Association of Physicists in Medicine Task Group, No. 64, Med. Phys. **26** (1999) 2054–2076.

[II–7] WATERMAN, F.M., YU, N., CORN, B.W., DICKER, A.P., Edema associated with I-125 or Pd-103 prostate brachytherapy and its impact on post-implant dosimetry: an analysis based on serial CT acquisition, Int. J. Rad. Onc. Biol. Phys. **41** (1998) 1069–1077.

[II–8] YU, N., DICKER, A.P., NATH, R., WATERMAN, F.M., The impact of edema on planning ^{125}I and ^{103}Pd prostate implants, Med. Phys. **26** (1999) 763–767.

[II–9] CYGLER, J.E., et al., Measurement of urethral dose profiles in prostate brachytherapy using a linear MOSFET array dosimeter, Proc. of GEC-ESTRO-ABS-GLAC Joint Brachytherapy Mtg, Barcelona, Spain, 2004, Radioth. Oncol. **71**, Supl 2 (2004) 592–593.

[II–10] HALLIL, A., et al., "Radiation response of a new linear MOSFET array dosimeter", AAPM 46th Ann. Mtg, Pittsburgh, USA, 2004, Med. Phys. **31 (**2004) 1912.

[II–11] BLOEMEN-VAN GURP, E. et al., Real time dosimetry with a linear MOSFET array to evaluate the urethra dose during permanent implant brachytherapy using iodine-125, Int. J. Radiat. Onc. Biol. Phys. **73** (2009) 314–321.

Annex III

CROATIA — IN VIVO DOSIMETRY WITH DIODES AND OPTICALLY STIMULATED LUMINESCENCE DOSIMETERS: CHARACTERIZATION AND PHANTOM AND PATIENT STUDIES

T. BOKULIĆ, I. MRČELA, M. BUDANEC, A. FROBE, Ž. SOLDIĆ, Z. KUSIĆ
Department of Oncology and Nuclear Medicine
Sestre Milosrdnice University Hospital
Zagreb, Croatia

Abstract

This work provides the results of complete dosimeter characterization and phantom as well as patient measurements obtained with silicon diode dosimeters as an already established system and OSLDs as an emerging dosimetry system to implement an in vivo dosimetry programme in radiotherapy. The measurement procedures developed during the course of the CRP were followed to calibrate the dosimeters for entrance dose measurements and to determine their physical properties such as reproducibility, stability, fading and dose perturbation as well as intrinsic and beam related correction factors. The Alderson phantom studies conducted demonstrated that the mean deviation between the measured and expected entrance dose was below 3% in almost all cases. Patient studies revealed results comparable to the published results for the most frequently measured sites, e.g. pelvis, head and neck, and breast. A mean deviation of +0.5% (3.2%, 1σ) was observed in the diode measurements (N=727) and +1.4% (3.6%, 1σ) in the OSLD measurements (N=103).

III–1. INTRODUCTION

In vivo dosimetry measures the radiation dose delivered to a patient during external beam (EB) radiotherapy or brachytherapy (BT). Most established in vivo dosimetry systems are based either on a single point diode [III–1, III–2], an array of silicon diodes or TLDs [III–3, III–4]. New systems such as MOSFET dosimeters [III–5, III–6] and OSL dosimeters [III–7, III–8] are rapidly being tested and introduced into clinical practice.

National and international organizations have published guidelines [III–9, III–10] and reports [III–11] dealing with in vivo dosimetry, characterizing and clinically testing different dosimetry systems and promoting their use for an ultimate check of treatment in radiotherapy.

This report describes the results of dosimeter characterizations as well as phantom and patient measurements obtained with an already established system, silicon diode dosimeters, and with an emerging dosimetry system, OSLDs, to implement an in vivo dosimetry programme in patients subjected to external beam radiation therapy.

The Department of Oncology and Nuclear Medicine at the University of Zagreb Medical School and School of Dentistry, where this investigation was carried out, provides a comprehensive oncology service to patients. It encompasses radiotherapy, chemotherapy and nuclear medicine diagnostic procedures. More than one thousand oncological patients are admitted yearly and about the same number of patients are treated as outpatients. Approximately 600 patients receive radiation treatments with a ^{60}Co radiotherapy machine and an HDR brachytherapy unit. Current intracavitary and intraluminal brachytherapy practices are based on the state of the art HDR brachytherapy remote afterloading unit.

During this project, the overall responsibility for in vivo dosimetry, including acceptance testing, the development of QA procedures, the establishment of action/tolerance levels and the creation of spreadsheet forms and solutions, was held by medical physicists. The radiotherapy technicians' work consisted of the actual field set-up as well as patient and dosimeter positioning. Radiation oncologists reviewed the dosimetry records and discussed practical problems encountered during routine work with the physicists.

Although quality control (QC) tests defined for radiotherapy exist in Croatian legislation, with specified frequencies and precise tolerance levels for ^{60}Co units and accelerators, there is no strict demand that every patient treated with radiation therapy should undergo in vivo dosimetry.

The objective of this research project was twofold: (a) To investigate the feasibility and usefulness of performing the in vivo programme with an established dosimetry system (diodes) in a small radiotherapy department, aiming at improved clinical procedures; and (b) To characterize a new dosimetry system based on OSLD and to carry out a clinical pilot study by applying a methodology for the determination of the calibration and correction factors similar to those used for the diodes, and to investigate their potential use in a clinical setting.

III–2. MATERIALS AND METHODS

For both in vivo dosimetry systems, diodes and OSLDs, a common approach was applied: Dosimeters were firstly checked for their important physical characteristics, and then a full set of correction factors was determined. In the next step, the dosimeters were tested on an Alderson Rando phantom for typical field arrangements, and the investigation was completed with patient studies that included a large number of measurements with diodes (more than 700) and a pilot study of approximately 100 measurements with OSLDs.

All phantom and patient entrance dose measurements were performed using the Cirus ^{60}Co teletherapy unit (CIS Bio International, France). Solid phantoms employed for these tasks were the white polystyrene phantom (RW3, PTW Freiburg) and the Alderson Rando phantom. The dose rate at 5 cm depth was approximately 60 cGy/min for a 10 cm × 10 cm field size. The ^{60}Co treatment unit does not possess an automatic record and verify system to check either treatment or mechanical set-up parameters.

The procedure used to determine the entrance doses for both dosimeter systems is based on the calibration and measurement of correction factors as described in Section 4 of this report, where the CRP methodology is described in detail. The entrance dose derived from the diode or OSLD measurements (D_m) is compared to the expected doses (D_{TPS}) that are calculated from the prescribed dose using an algorithm of the treatment planning system (Theraplan Plus 1000 Ver. 3.8, Varian). Throughout this paper, the percentage difference Δ between D_m and D_{TPS} is defined below:

$$\Delta(\%) = \frac{D_m - D_{TPS}}{D_{TPS}} \cdot 100 \qquad \text{(III–1)}$$

The standard deviation (σ) of Δ is also expressed where applicable.

III–2.1. Diodes

Diode dosimeters used in the project were EDE-5 (Scanditronix, Sweden), high doped p type silicon chips, 0.5 mm thick with a 1.5 mm radius. The diode's hemispherical buildup cap is made of 2 mm polystyrene and 3 mm epoxy plastic, which is equivalent to 5 mm water. Three diodes connect to a DPD-3 (Scanditronix, Sweden) electrometer. The dosimeters were preirradiated to 8 kGy with 10 MeV electron beams by the manufacturer.

To avoid problems with diode cables, in-house lightweight metal rails with a slider for diodes (Fig. III–1(a)) were mounted on the ceiling. They extend from one wall towards the head of the treatment unit (Fig. III–1(b)). The end of this hanging construction was positioned close to the unit, but in such a way that it dose not interfere with the ^{60}Co head rotation.

Initial testing or pre-calibration checks of the diodes included checks on the reproducibility of the system, the stability of the signal after irradiation, leakage and perturbation of the field underneath the diode.

Signal stability and leakage were measured as indicated in the published guidelines [III–10], and for reproducibility and field perturbation, the procedures and tolerances defined in this report were followed. The perturbation effect of the diode was explored using film in a solid phantom. The dosimeters were attached to the surface of the phantom on the central axis of the beam. The film was exposed at 0.5, 5 and 10 cm depths in a RW3 phantom with 10 cm × 10 cm fields and later scanned with a point optical densitometer DensiX (PTW, Freiburg). The optical density was determined either in the circular region, where the shadow of the diode was visualized, and in a nearby flat field region, or along a straight line crossing the diode spot. This enabled the optical density profile to be compared with an ionization chamber measurement in a water phantom. The average values of optical densities in a circular region were calculated, and the perturbation, P, was expressed as:

(a) (b)

FIG. III–1. (a) Diode holder on the rails; (b) ^{60}Co unit with a water phantom.

$$P = 100 \cdot (R_f - R_d)/R_f \quad \text{(III–2)}$$

where R_f is the average readout in a flat field region, and R_d is the average readout in a region of the diode spot.

III–2.2. Optically stimulated luminescence dosimeters (OSLDs)

III–2.2.1. OSLD reader system

A commercial OSL reader, InLight Microstar (Landauer Inc.), was used for the in vivo dosimetry study (Fig. III–2(a)). The dosimeters are small discs made of Al_2O_3:C powder held between two thin plastic films (Fig. III–2(a)). OSL discs are 7 mm in diameter, 0.2 mm thick and encased in a 2 mm thick light-tight plastic carrier measuring 12 mm × 24 mm. Buildup caps, 2 mm thick aluminium studs of 9 mm in diameter prepared by the IAEA for this study, were used for irradiations on each phantom and for measurements on patients. A plastic carrier bearing a serial number and a bar code that uniquely identifies the dosimeter was used. It can be inserted into and pulled out of the plastic adapter.

Prior to the reading process, the carrier is clipped into the plastic adapter, which is then inserted into the sliding drawer of the reader (Fig. III–2(b)). The adapter holds the dosimeter in the narrow metal groove, which enables the opening of the carrier once it is situated in a position where it can be illuminated by a bank of light emitting diodes (LED) stimulating the light emission. The reader operates in a continuous wave (CW) illumination mode, and two modes of stimulation, high or low, are available depending on the amount of dose the dosimeter received.

(a) (b)

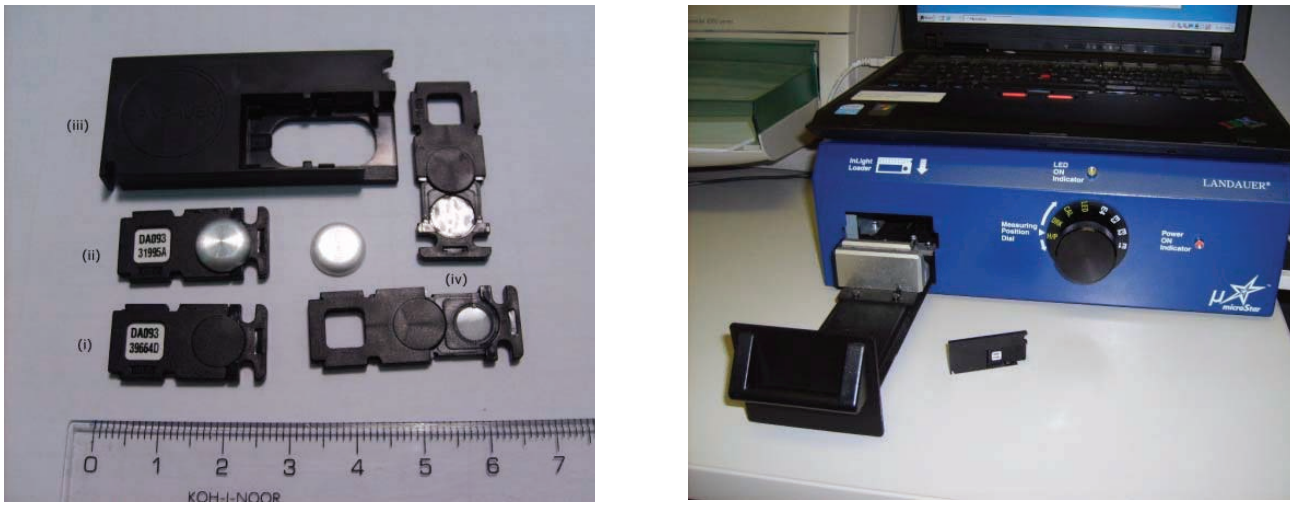

FIG. III–2. (a) OSLDs: (i) closed with serial number indicated; (ii) with aluminium buildup cap positioned on a plastic carrier containing the dosimeters; (iii) adapter to accommodate the carrier; (iv) opened carrier showing a dot dosimeter on both sides. (b) Reader: MicroStar reader ready for the insertion of an adapter.

III–2.2.2. Reuse of OSLDs

The OSLD's radiation induced signal can be easily reset (bleached) by exposing the active element to light. We used a 75 W halogen lamp (Halopar, OSRAM) with a UV filter at a distance of 0.5 m from the dosimeters. It is important to avoid overheating the dosimeters to prevent deformation of the plastic housing.

The zero dose signal, an insignificant residual signal left after the bleaching, was always read prior to the calibration of the dosimeter and subtracted from the signal obtained after the measurement.

III–2.2.3. OSLDs: preliminary investigations

Pre-calibration investigations of OSLDs consisted of a reproducibility check, short and long term fading measurements and the determination of the signal depletion correction for the readings of multiple dosimeters.

The reproducibility of the OSLDs was investigated in various ways. One method was by taking two sets of dosimeters and irradiating them multiple times with 100 cGy at the phantom surface. One set was bleached after each irradiation, and the other was left to accumulate the dose. The net reading after each new irradiation in the second set was obtained by subtracting the previous readout from the current one.

To estimate fading, five new OSLDs were irradiated and read out as quickly as possible, but no later than 2 minutes after irradiation. The first readout was taken 40 seconds after irradiation. The dosimeters were read repeatedly based on the following scheme: after 2, 3, 5, 6 minutes and then every 10 minutes during the first hour; every 30 minutes in the next two hours, and, finally, a few readings were taken every day for one week. The results were normalized to the mean of five readings taken one hour after irradiation. Verification of the manufacturer's data on the depletion of the signal due to a readout process was performed by reading 100 times several OSLDs that were irradiated with three different doses.

III–2.2.4. Calibration of OSLDs

All irradiations of the OSLDs were performed in the same way as the diode measurements using a Cirus ^{60}Co treatment unit. The OSLDs with buildup caps were positioned on the surface of the RW3 slab phantom that was 10 cm thick (or more, as appropriate) in such a way that they did not shadow the ionization chamber inserted into the adapter hole at a depth of 5 cm.

The reader connected to a laptop computer was kept in the same place during the calibrations, the measurements of the correction factors, measurements with the Alderson Rando phantom and other phantom

measurements. However, for the fading study, the reader was taken to the ^{60}Co control console to facilitate early readouts following irradiations.

Each day, when the dosimeters were read, the stability of the system was checked by the standard system checks available in the reader, i.e. the measurement of the dark current values (DRK), the readout from the irradiation with a built-in small ^{14}C calibration (CAL) source and the readout with the LED on to indicate the stability of the beam intensity.

For all measurements, the OSLDs were read five times, and each time the loader was opened and the dosimeters repositioned. An average of these readings was taken as the dosimeter's signal. In the standard operating mode, the system readings are in mGy.

III–2.2.5. OSLD correction factors

The correction factors were determined in a similar way to the diodes. All correction factors were measured with dosimeters that had been previously calibrated. For calibrations, field size, SSD and non-linearity dose response correction, two dosimeters were irradiated on the phantom surface. The ionization chamber was in place whenever necessary to record the dose at a depth of 5 cm. To determine the angle, wedge, and block and tray correction factors, one dosimeter at a time was placed at the field centre without an ionization chamber in place.

The non-linearity dose response factor was determined in the following ways: (a) After individual calibration factors had been determined and taken into account (no signal reset); (b) Before individual OSLD calibration and with the calibration performed afterwards; (c) Without the calibration of individual OSLDs but applying the manufacturer's batch calibration; (d) After individual calibration followed by annealing of the OSLDs. In this way, we were able to observe differences in sensitivity changes originating from different dose histories of dosimeters.

III–2.3. Alderson Rando phantom measurements

Measurements with the Alderson Rando phantom consisted of three steps: (1) CT scanning of the phantom; (2) Field simulation and manual contouring; (3) Computerized treatment planning based on both the CT slices and manual contours. The CT scanning of the phantom was performed with a multi-slice CT scanner (Somatom Sensation 16, Siemens). The reconstructed slice thickness was 5 mm, and the slice separation for the head and neck region and for the thorax/pelvic region was 4.6 and 5.6 mm, respectively. These two regions were separately reconstructed and both image sets were imported into the anatomy modelling module of the TPS. The simulation was performed with a Simview 3000 (Siemens) simulator. The radiation oncologist set up the fields for all localizations.

Entrance dose measurements for pelvic irradiations were made for a three field beam arrangement (AP, RL and LL fields), one beam at a time (Fig. III–3(a)– III–3(c)). The first plan used three non-wedged fields of 20 cm × 20 cm in a fixed SSD set-up. Single field dose calculation routinely used as an independent check of the TPS was also performed. Different plans were made based on: (a) Manual contour through the central slice of the phantom; (b) CT, excluding inhomogeneities; and (iii) CT with inhomogeneity correction. Doses of 50 cGy were delivered to a dose normalization point at the intersection of the field's central axes. The measurement was performed three times for each diode/field combination and with two OSLDs per field. These readouts were inserted into a spreadsheet to calculate the average relative percentage difference between the measured and entrance doses, taking into account all correction factors.

The second pelvic plan was similar to the previous one, but with 10 cm × 10 cm lateral fields (Fig. III–3(a)) with 30º/10 cm wedges orientated with the thin end of the wedge posteriorly. Again, the AP open field was 20 × 20 cm. The plane containing the beam axes was always precisely positioned at the midthickness of the phantom slice (Fig. III–3(c)).

The head and neck fields were simulated with and without a thermoplastic mask. Two parallel opposed 6 cm × 6 cm fields without wedges were utilized (Fig. III–3(d)). The centre of the field was at the centre of a slice in the neck region. A 100 cGy dose calculated according to the TPS was delivered to the isocentre for each field. These measurements were made with and without a mask (Fig. III–3(f)). The CT scan of the phantom was available only without a mask, so the measured doses for the phantom with a mask were compared to the manual contour plan of a homogenous phantom (Fig. III–3(e)).

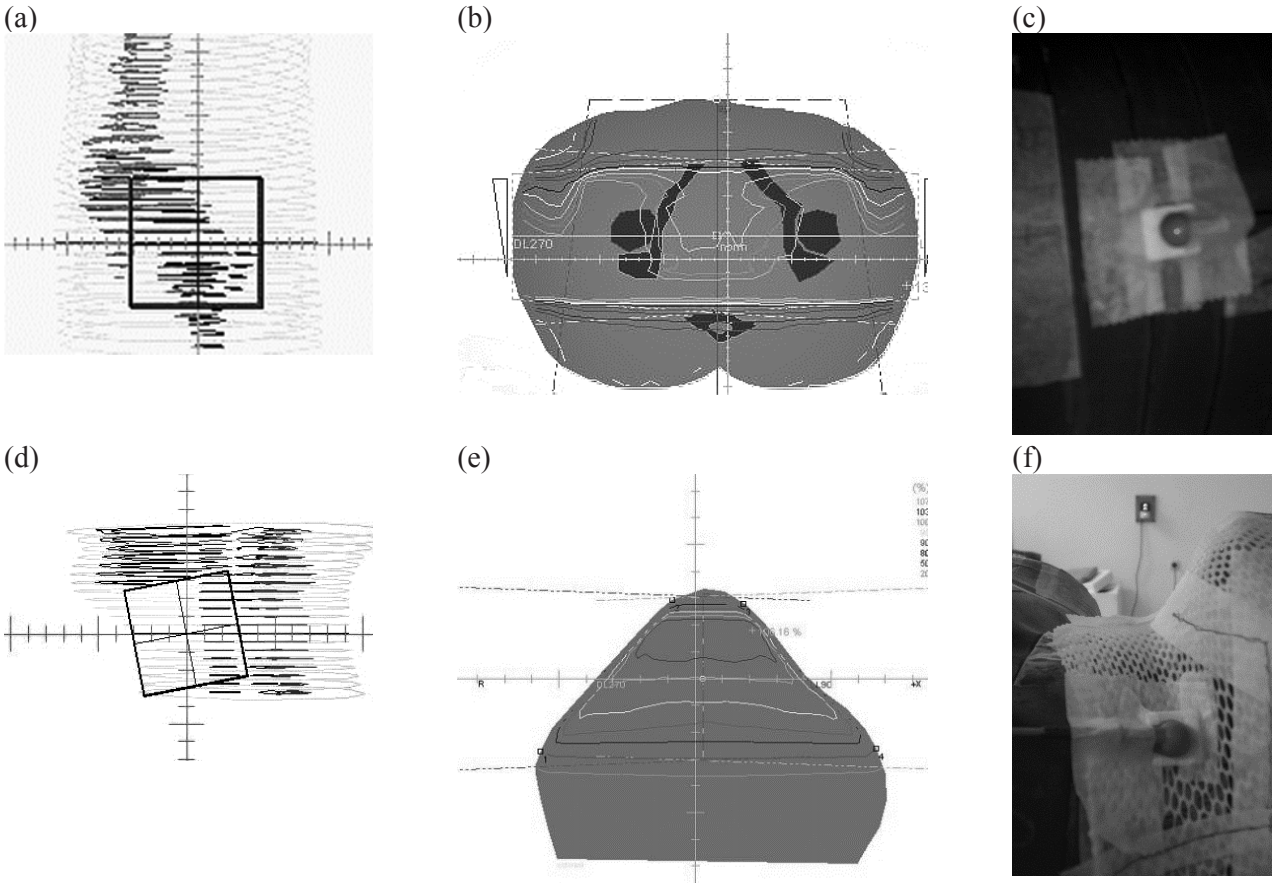

FIG. III–3. Alderson phantom planning and irradiation details. Upper row: (a) Beam's eye view of a lateral 10 cm × 10 cm pelvic field; (b) Isodose distribution for a pelvic central slice; (c) Diode positioned at a central axis of the lateral pelvic field. Lower row: (d) Beam's eye view of a lateral 6 cm × 6 cm head and neck field; (e) Isodose distribution for a manual contour; (f) Diode attached to a thermoplastic mask.

A breast irradiation was tested by measuring opposed 30° wedged tangential fields (6 cm × 18 cm). A fixed SSD technique with symmetrical jaws was used to deliver 100 cGy to the point of beam intersection.

III–2.4. Description of patient studies

At the beginning of the study, an introductory lecture explaining the aims and particularly the methodology of the study was provided to radiation therapy technicians. During the initial period of about three months, the positioning of the dosimeters and the readouts were carried out exclusively by a physicist, and later by RTTs, but with the presence of a physicist during measurements. After the patient set-up for the treatment, the diode was positioned at the centre of the field. Diodes with a styrofoam plate underneath and OSLDs were fixed directly on the patient's skin, except for the posterior fields, where they were fixed on Mylar foil supported by a nylon racket, and the head and neck fields, where they were fixed on a thermoplastic mask. Readouts were noted on a hardcopy form that enabled a quick check of the calculation of the corrected entrance dose from the readout. This calculation was immediately noted on the patient's chart. In a pilot patient study, the OSLDs were read approximately 24 hours after the irradiation.

According to the initial estimate, a deviation of 5% between the measured and expected dose was considered acceptable. If the deviation was greater, possible causes were immediately investigated (e.g. diode positioning, field size, SSD or SAD technique, wedge and block). If this quick screening did not reveal any obvious mistakes, the measurement was repeated the next day.

Head and neck treatments: The primary tumour and lymph nodes were irradiated with two laterally opposed fields isocentrically. The lower cervical and supraclavicular nodes were irradiated with an anterior field at a fixed SSD = 80 cm. In a limited number of cases, two extended lateral fields were used for patients with short necks. The

treatment couch was therefore rotated to avoid the uncessary irradiation of the ipsilateral shoulder and to include the lower cervical and supraclavicular nodes. In this report, owing to the small number of patients, these two techniques are not analysed separately. The patients were immobilized either with a baseplate, headrest and plastic arch, or a thermoplastic mask.

Pelvic treatments: The large blocked three or four field (box) techniques were used for these sites. Patients were not immobilized except for the use of rest pillows.

Breast treatment: Patients were positioned on an inclined PMMA board with a handle above the head. CT based planning was used in a limited number of cases, but the majority of plans were based on a conventional simulation process with manual contours. In the case of CT based planning, the tissue inhomogeneity correction was employed.

Remainder: Measurements in the 'remainder' group were conducted for irradiation of the abdomen and thorax in AP/PA fields as well as for the irradiation of the brain, arms, limbs and vertebrae, in addition to some specific AP/PA fields for thyroid and parotid cancer treatments and supraclavicular anteroposterior fields.

III–2.5. Statistical analysis

The mean per cent deviation (Δ) between the measured and calculated (TPS) entrance dose, the standard deviation (1σ), the median, and the percentage of the results where the deviation was between 5% and 10% and over 10% were expressed for various anatomical locations and treatment fields. The latter were grouped by field type, irradiation technique and the use of accessories such as wedges and blocks.

III–2.6. QA/QC of in vivo dosimetry systems

The diode QC schedule accepted for the project implementation is shown in Table III–1. For an OSLD system the manufacturer's recommendations to check the reader's inherent parameters daily should be followed, and, in addition, the reader should always be kept in the same place if feasible, and the control dots should be read frequently. More details on calibration are provided in the results and discussion sections of this report.

TABLE III–1. QC SCHEDULE OF THE DIODE IN VIVO DOSIMETRY SYSTEM

Frequency	Procedure	Tolerance	Personnel
Daily[a]	Visual inspection, cabling, mechanical damage, integrity of the diode, display stability	Functional	RTT/Physicist
Monthly	Calibrate diodes according to the protocol	New calibration coefficients are introduced	Physicist
Annually	Check diodes for field size, SSD, linearity, wedge, tray dependence	Confirm that correction factors change less than 2%	Physicist

[a] On days where measurements are being made.

III–3. RESULTS

III–3.1. Diodes

III–3.1.1. Pre-calibration checks for diodes

Before calibration, the reproducibility of the diodes was checked by positioning the diodes on top of the white polystyrene phantom (RW3) and irradiating with a ^{60}Co beam (10 times with a 10 cm × 10 cm field at SSD = 80 cm). Measurements were repeated several times over two weeks. The signal stability after irradiation was determined by recording the signal immediately after irradiation and approximately five minutes later. Leakage was estimated

by measuring the leakage current for a period that was five times longer than the typical clinical times. Repeated measurements demonstrated that the group per cent standard deviation (σ) of the diode readouts was below 0.5% and overall that σ was also less than 1%. The signal stability five minutes after irradiation was less than 0.5%, and the leakage was negligible.

The beam profile at 5 cm depth was obtained from the measurements with the automatic water Blue Phantom (Scanditronics) equipped with an IC 15 ionization chamber. The average diode perturbation value obtained from the measurements was 2.7% for a depth of 5 cm. Similarly, the values from the film profiles in repeated measurements were about 2.1% for depths of 0.5 cm, 5 cm and 10 cm in the phantom.

III–3.1.2. Calibration

The diode calibration coefficients were determined once a month after the initial period of about two months when measurements had been performed weekly. The delivered dose *D* was determined based on an ionization chamber (30002 PTW, Freiburg) measurement. The chamber was positioned at the reference depth (5 cm) in the phantom (Fig. III–4). The dose was determined according to the IAEA TRS 398 Code of Practice [III–12].

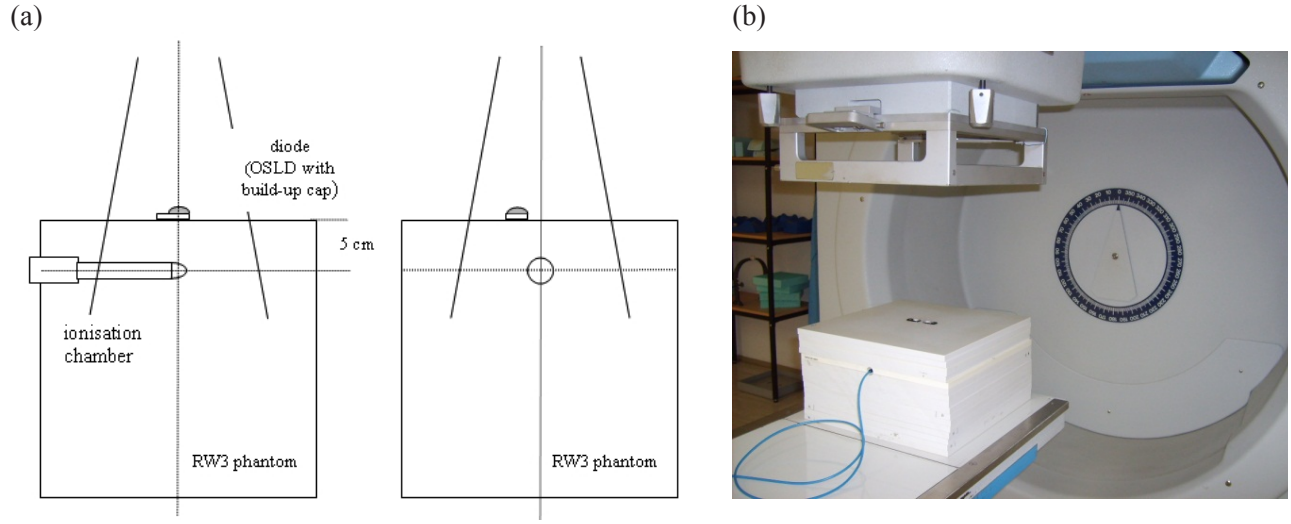

FIG. III–4 (a) Schematic representation of a calibration set-up; (b) Experimental set-up with a ^{60}Co unit.

To follow the proposed protocol, a small 2 mm thick styrofoam plate was placed under the diode during the calibration. The plastic to water correction factor necessary for calibrations was determined from the measurements as $k_{pl} = 1.008$.

The dose rate dependence was checked by measuring the calibration coefficient at the standard SSD (80 cm), and at an extended SSD, i.e. SSD + 25 cm = 105 cm. The percentage depth dose at the extended SSD was calculated according to the expression that relates the tissue air ratio and PDD [III–13]. The percentage differences between the calibration coefficient at the standard SSD and at the extended SSD were 1.0%, 1.0% and 0.7% for the three diodes, respectively.

III–3.1.3. Correction factors for diodes

Figure III–5 illustrates the correction factors determined according to the procedures described in Section 4 of this report. Each datapoint represents the three readings that were taken for each diode.

The correction factors were also determined for a set of nine physical wedges available in the department. A set-up was designed to determine a combined block and tray correction factor. Explicitly, the 10 cm × 10 cm and 15 cm × 15 cm fields were blocked with triangular blocks positioned in the corners of a field (Fig. III–6), and the correction factor was determined for increasingly blocked fields. The equivalent square fields were calculated by

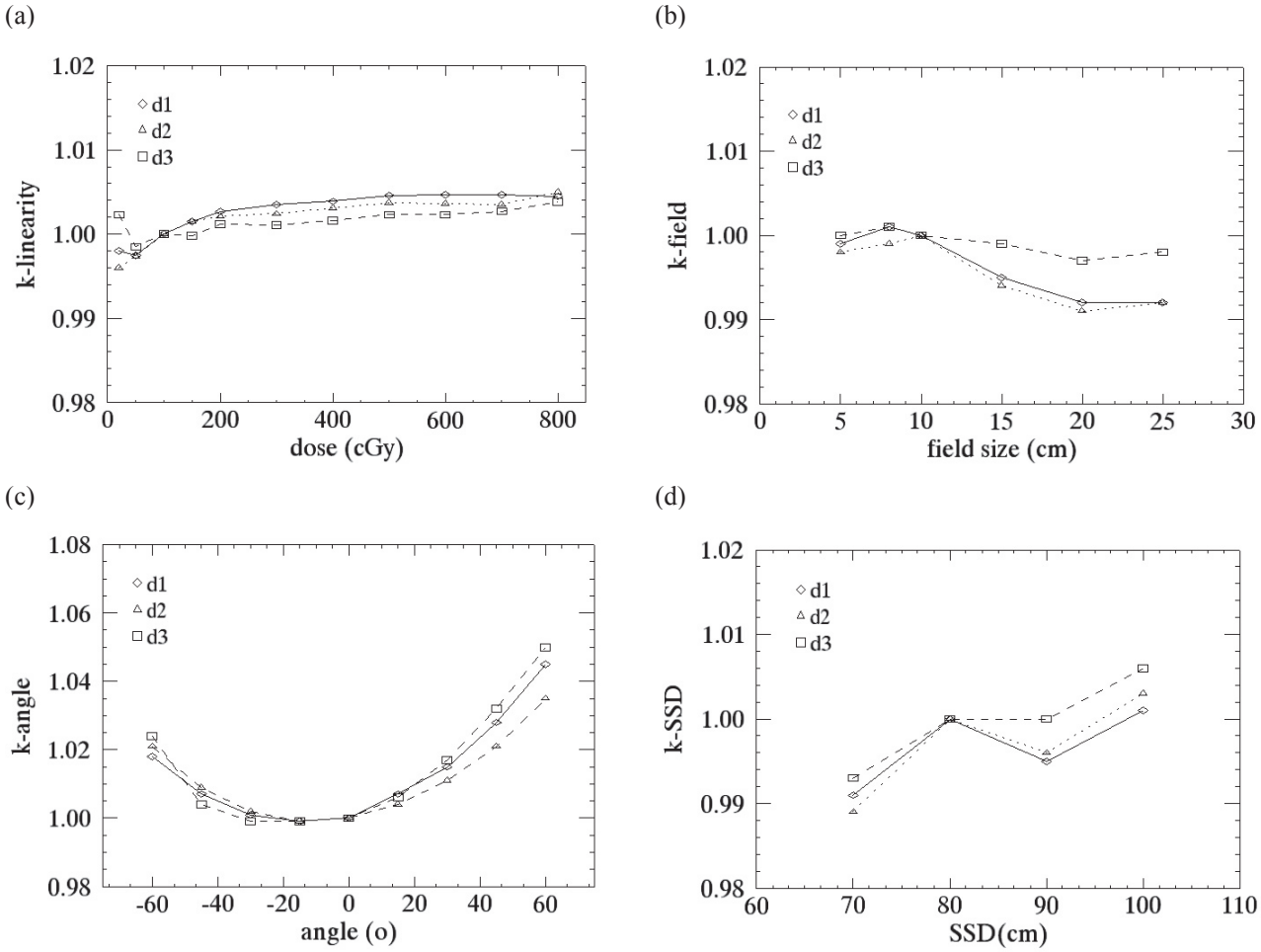

FIG. III–5. Correction factors (diodes). (a) Non-linearity correction factor versus the dose in the range of 20 –800 cGy; (b) Field size correction factor in the square field size range 5–25 cm; (c) Angular correction factor (i.e. directional dependence of the diode); (d) SSD correction factor for different SSDs from 70 cm to 100 cm. (Lines are drawn to visualize the trend rather than to represent any functional form).

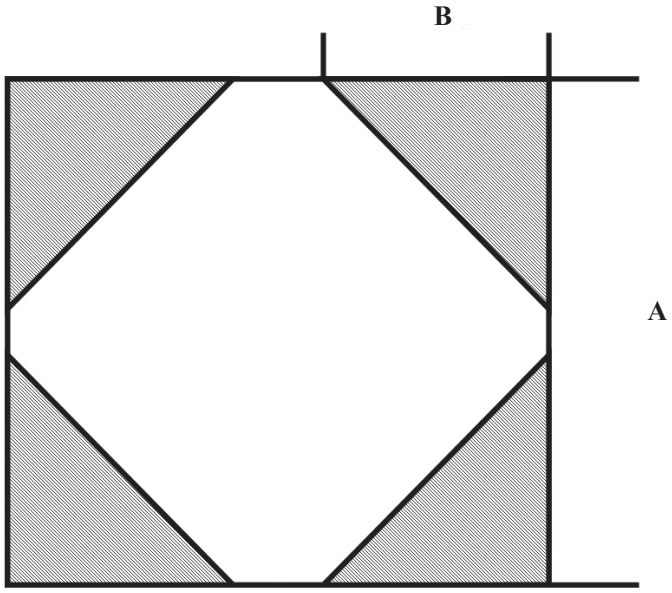

FIG. III–6. Cross-section of the blocked field used to determine the block and tray correction factor.

the Clarkson method. In both cases, a dose of 100 cGy was delivered at d_{max}. In Tables III–2 and III–3, the results for wedge correction factors and combined block and tray correction factors are given.

TABLE III–2. MEASURED WEDGE CORRECTION FACTORS (k_{wedge}) FOR AVAILABLE PHYSICAL WEDGES (DIODES)

Field/wedge	6 cm			8 cm			10 cm		
	30^0	45^0	60^0	15^0	45^0	60^0	30^0	45^0	60^0
d1	1.003	1.001	1.003	1.005	1.016	1.026	1.005	1.002	1.016
d2	1.003	1.000	1.001	1.006	1.015	1.021	1.006	1.005	1.018
d3	1.010	1.017	1.018	1.010	1.029	1.037	1.010	1.012	1.032

TABLE III–3. BLOCK AND TRAY (k_{block}) CORRECTION FACTORS (DIODES)

Field (A)	15 cm			10 cm	
Block (B)	7.5 cm	5 cm	2.5 cm	5 cm	2.5 cm
EQS field size	10.6 cm	13.2 cm	14.5 cm	7.1 cm	9.3 cm
d1	0.984	0.990	1.000	1.002	1.002
d2	0.982	0.991	0.999	1.006	1.001
d3	0.984	0.992	1.000	0.999	1.004

III–3.1.4. Alderson Rando phantom results for diodes

Tables III–4, III–5 and III–6 include the columns from the Excel spreadsheets where the calibration and correction factors are used to calculate the measured and corrected entrance doses, and to compare them to the TPS calculated doses. All percentage differences between the measured and TPS calculated doses, except for one breast measurement, were below 3% as requested for commencing the patient measurements.

TABLE III–4. MEAN PERCENTAGE DIFFERENCES BETWEEN THE MEASURED AND EXPECTED ENTRANCE DOSE FOR THREE 20 cm × 20 cm FIELDS (AP, RL AND LL) AND TWO (RL-W AND LL-W) 10 cm × 10 cm WEDGED FIELDS (DIODES)

Field type	Field size (cm)	%Δ (± σ)
AP	20 × 20	0.2 ± 0.4
RL	20 × 20	1.4 ± 0.4
LL	20 × 20	1.3 ± 0.3
RL-w	10 × 10	−0.1 ± 0.9
LL-w	10 × 10	−0.6 ± 0.7

The correction factors were determined for a set of nine physical wedges available in the department. We also designed a set-up to determine a combined block and tray correction factor. Explicitly, the 10 cm × 10 cm and 15 cm × 15 cm fields were blocked with triangular blocks positioned in the corners of a field (Fig. III–6), and the correction factor was determined for increasingly blocked fields. The equivalent square fields were calculated by the Clarkson method. In both cases, a dose of 100 cGy was delivered at d_{max}. In Tables III–5 and III–6, the results for wedge correction factors and combined block and tray correction factors are given.

TABLE III–5. MEAN PERCENTAGE DIFFERENCES BETWEEN MEASURED AND CALCULATED (TPS) ENTRANCE DOSE FOR TWO 6 × 6 cm FIELDS (RL AND LL) AND TWO 6 × 6 cm FIELDS (RL-M AND LL-M) FOR THE PHANTOM WITH A MASK (DIODES)

Field type	Field size (cm)	%Δ (± σ)
RL	6 × 6	0.1 ± 0.9
LL	6 × 6	−0.4 ± 0.9
RL-m	6 × 6	1.4 ± 0.5
LL-m	6 × 6	0.3 ±0.5

TABLE III–6. PERCENTAGE DIFFERENCES BETWEEN THE MEASURED AND CALCULATED (TPS) ENTRANCE DOSE FOR TWO (MED AND LAT) WEDGED 6 × 20 cm FIELDS (DIODES)

Field type	Field size (cm)	%Δ (± σ)
MED	6 × 20	−4.5 ± 0.4
LAT	6 × 20	−2.2 ± 2.1

III–3.1.5. Patient measurements with diodes

In total, 740 measurements were collected, out of which 13 were eliminated mainly because the diode became detached during the irradiation.

The summary of the main accuracy descriptors for all the measurements and of the measurements grouped according to anatomical site are shown in Table III–7. An additional summary used in statistical analysis is provided in Table III–8. The analysis of all available measurements gave a mean per cent deviation Δ of 0.5% and standard deviation (σ) of 3.2%. The smallest spread of results was obtained for the pelvic fields (Δ=1.1 ±1.9 %), and the largest deviation of 2.3% with a standard deviation of 4.6% was obtained for the small ‘remainder’ group that mostly included irradiations with very elongated fields.

Thirty-six measurements were obtained with Δ >5%. Of these, seven measurements were measurements of breast treatment fields which were actually considered acceptable due to a higher tolerance level of Δ > 7%. The frequency distributions of deviations between the measured and expected entrance doses are depicted in Fig. III–7 for three major sites and groups with similar techniques and/or with the use of additional accessories. Another summary of frequency and different causes of error is presented in Table III–9.

TABLE III–7. DEVIATIONS BETWEEN THE MEASURED AND EXPECTED ENTRANCE DOSE Δ CATEGORIZED INTO DIFFERENT GROUPS ACCORDING TO THE ANATOMICAL SITE

	N	Median Δ%	Mean Δ%	σ (%)	(5% < |Δ|< 10%) %	(|Δ| ≥ 10%) %
All data	727	0.7	0.5	3.2	4.1	0.8
Abdomen	48	0.9	1.8	5.6	2.1	2.1
Brain	26	−0.3	−0.1	1.8	0.0	0.0
Breast	118	−1.5	−1.1	3.9	9.3	0.8
Head/neck	138	0.7	0.8	3.1	7.2	0.7
Pelvis	202	1.1	1.1	1.9	1.5	0.0
Spine/palliation	30	1.6	1.4	1.5	0.0	0.0
Supraclavicular	64	0.5	0.1	2.3	1.6	0.0
Thorax (anteroposterior-posteroanterior)	86	0.9	0.4	3.2	2.3	2.3
Remainder	15	1.5	2.3	4.6	13.3	6.7

TABLE III–8. DEVIATIONS Δ BETWEEN THE MEASURED AND EXPECTED ENTRANCE DOSE CATEGORIZED INTO DIFFERENT GROUPS AND ANALYSED STATISTICALLY

		N	Median Δ%	Mean Δ %	σ (Δ%)	(5% < |Δ| < 10%) %	(|Δ| ≥ ±10%) %
Wedges	With	125	−1.1	−0.5	5.5	11.2	2.4
	Without	602	0.9	0.8	2.4	2.7	0.5
Blocks	With	383	1.0	1.1	3.1	3.9	0.5
	Without	344	0.3	0.0	3.2	4.4	1.2
Mask brain & head/neck	With	52	0.3	0.4	3.8	9.6	1.9
	Without	112	1.0	0.8	2.5	4.5	0.0
Technique	Isocentric	149	0.7	1.0	3.2	6.7	1.3
	Fixed SSD	578	0.7	0.4	3.2	3.5	0.7
Angle of incidence	0°	548	1.0	1.0	3.0	3.1	0.9
	Other	179	−1.0	−0.9	3.5	7.3	0.6
Field type	AP	167	0.3	0.4	3.9	1.8	1.2
	PA	167	1.4	1.2	2.1	1.8	0.6
	RL	132	1.1	1.0	2.6	6.1	0.0
	LL	129	0.9	0.9	2.6	3.1	0.8
Breast fields	Medial	60	−2.0	−1.9	2.8	11.7	0.0
	Lateral	58	−0.2	−0.2	4.6	6.9	1.7

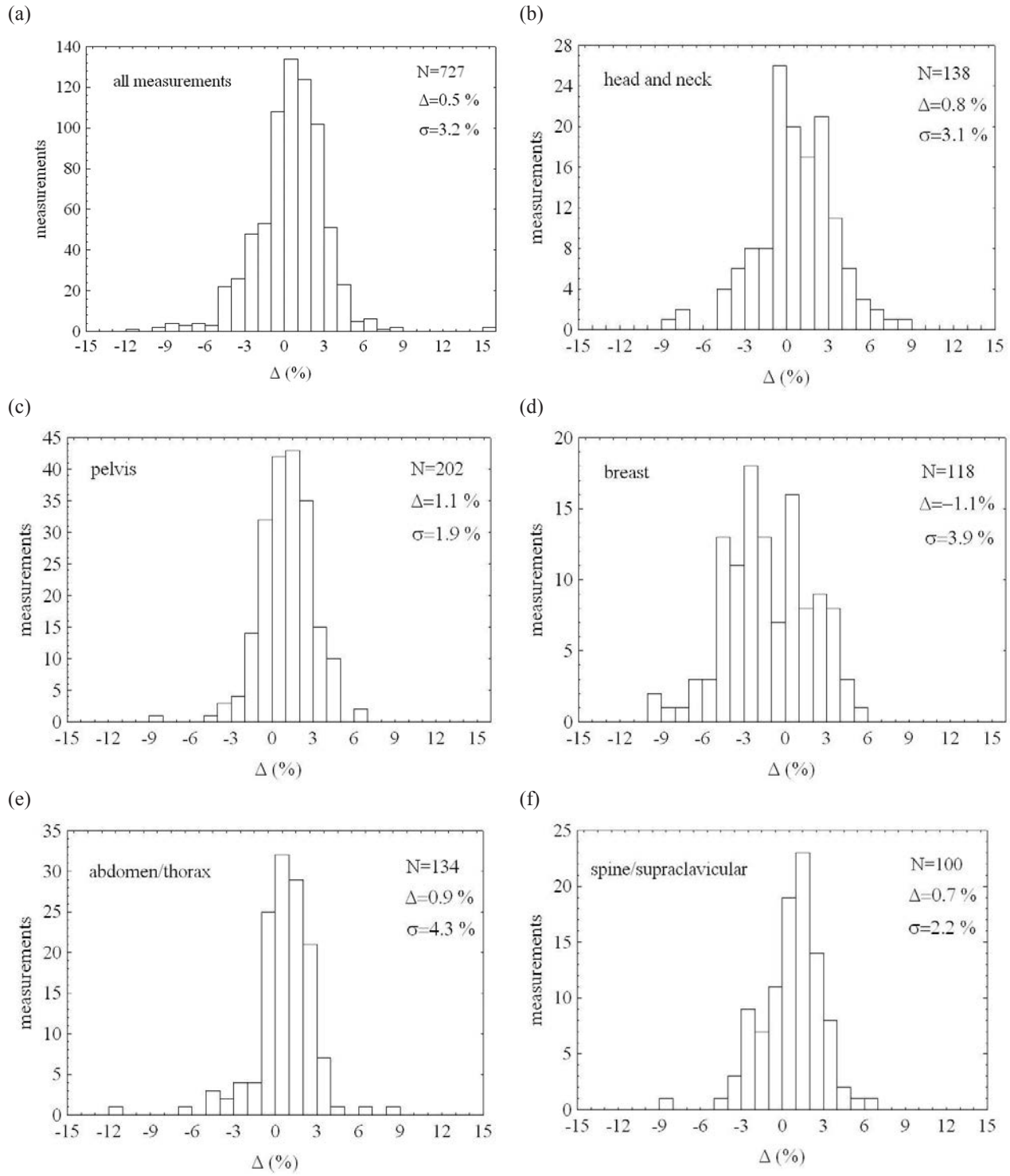

FIG. III–7. Frequency distributions of Δ for all measurements and for the major treatment groups: head and neck, pelvis, breast, abdomen/thorax and spine/supraclavicular fields.

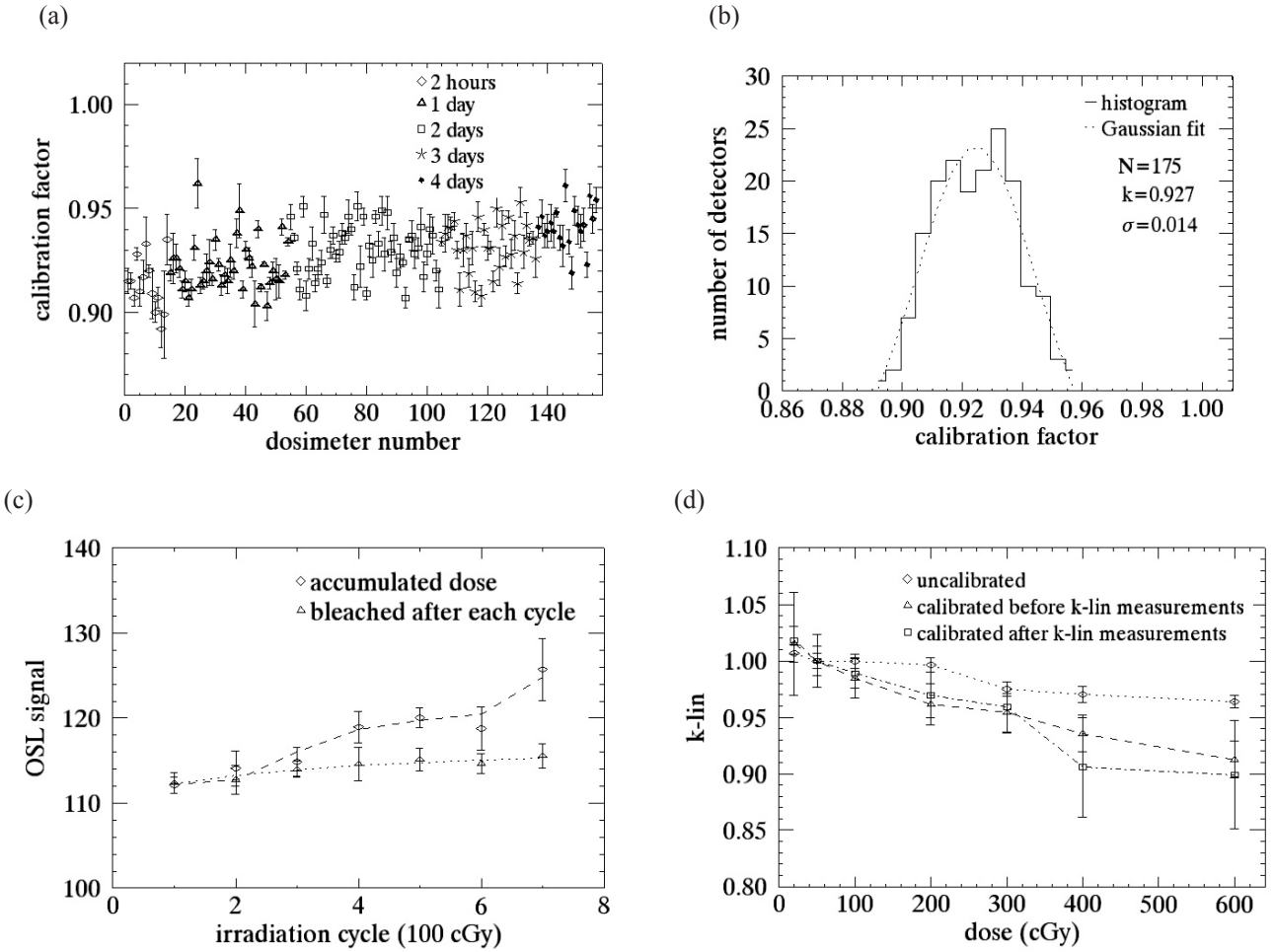

FIG. III–8. Upper row: (a) Calibration coefficients and experimental standard deviations for a set of OSLDs read at different times after irradiation; (b) Histogram of calibration coefficients (N = 175) read after the same time interval post-irradiation. Lower row: (c) OSL signal measured after seven bleaching cycles (700 cGy) and signal read without bleaching OSLDs; (d) OSLD sensitivity change observed during non-linearity measurement.

III–3.2. OSLDs

III–3.2.1. Initial checks for OSLDs

The analysis of repeated raw readouts from different irradiation cycles showed that the reproducibility of an individual dosimeter was 1.5% (1σ). The reproducibility of a batch (N = 175) response was 1.6% (1σ). Likewise, when the OSLDs were located in the RW3 phantom and irradiated with 50 cGy at a depth of 0.5 cm to check the in-phantom reproducibility, a comparable level of response reproducibility (1.7%, 1σ) was found.

III–3.2.2. Calibration coefficient for OSLDs

The calibration coefficients, determined by irradiating the OSLDs with 50 cGy (N = 175 dosimeters) and a test calibration with 100 cGy (N=10), gave average calibration coefficients of 0.927 ± 0.014 cGy/rdg and 0.924 ± 0.014 cGy/rdg, respectively. The potential influence of the time of a reading of the OSLDs on the spread of calibration coefficients was investigated. The dosimeters were distributed into five unequal groups according to the time of reading after irradiation. OSLDs from the first group were read after two hours, those in the second after one day, and in the third, fourth and fifth groups after two, four and five days following irradiation (Fig. III–8(a)). The standard deviations (range 1.2 to 1.6%) of calibration coefficients in different groups were comparable to the results obtained in the batch of 175 measurements (Fig. III–8(b)).

TABLE III–9. DEVIATIONS DETECTED BY IN VIVO DOSIMETRY AND THEIR RESPECTIVE CAUSES

Deviation	Number	Cause of error
5–10%	4	Wrong SSD
	1	Wrong irradiation time entered at the control console
	1	Block drawn on patient but not planned
	2	Mask not fitted to skin — air gap beneath the diode
	12	Unknown — possible patient movement
	2	Problem with TPS calculation for very elongated fields
	1	Angle of incidence greater than 70°
	23	Total
5–7%	7	Breast treatments – within tolerance levels
>10%	1	Missing wedge
	3	Wrong SSD
	2	Unknown, the next measured fraction was within tolerance levels
	6	Total
	36	Total

The results of investigations into the effects of bleaching on the calibration of OSLDs are shown in Fig. III–8(c) and III–8(d). In the former, the effect of repeat measurements using the OSLD without bleaching (the dose being obtained by subtraction of the two successive readings) is compared with the results of bleaching between irradiations. With bleaching, the calibration coefficient is more stable. In Fig. III–8(d), the effect of a calibration exposure before or after the measurement is compared with using the manufacturer's calibration (see Section III–3.2.3).

III–3.2.3. Field perturbation in OSLDs

The procedure for determining a field perturbation by an OSLD was repeated in a way analogous to the case of diode perturbation. The values calculated from the profiles in repeated measurements were 2.6% and 2.8% at 5 and 10 cm depths of a film in the phantom.

III–3.2.4. Depletion of signal due to readout in OSLDs

As specified by the manufacturer, each reading of a dosimeter depletes the charge and reduces the signal by a small increment. We checked this behaviour on a very large sample (N=100) of readouts for the three dosimeters that were exposed to different doses (100, 350 and 400 cGy) and read. If we denote the signal on the n-th readout by s (n), the signal at the first readout by s (1), and the fraction by which the signal is depleted on each readout by f, then the following equation holds:

$$s(n) = s(1) \cdot f^{n-1} \tag{III–3}$$

It can be linearized by noting that:

$$a = 1 - f \qquad f^{n-1} \approx 1 - (n-1) \cdot a \qquad s(n) = s(1) - s(1) \cdot a \cdot n \tag{III–4}$$

A linear regression (Fig. III–9(b)) on these two datasets gave the parameters of a linear fit (Table III–10). From these data, it appears that each reading decreases the OSLD signal by approximately 0.04%.

TABLE III–10. DEPLETION ANALYSIS FOR OSLDS IRRADIATED WITH DIFFERENT DOSES: 100, 350, 400 cGy

Parameter	Dosimeter 1	Dosimeter 2	Dosimeter 3
($a \pm \sigma$) Slope	−0.00037 ± 0.00002	−0.00029 ± 0.00002	−0.00036 ± 0.00001
($b \pm \sigma$) Intercept	0.9923 ± 0.0009	0.9882 ± 0.0009	1.0023 ± 0.0009
R^2	0.850	0.768	0.854
f	0.99963	0.99971	0.99964

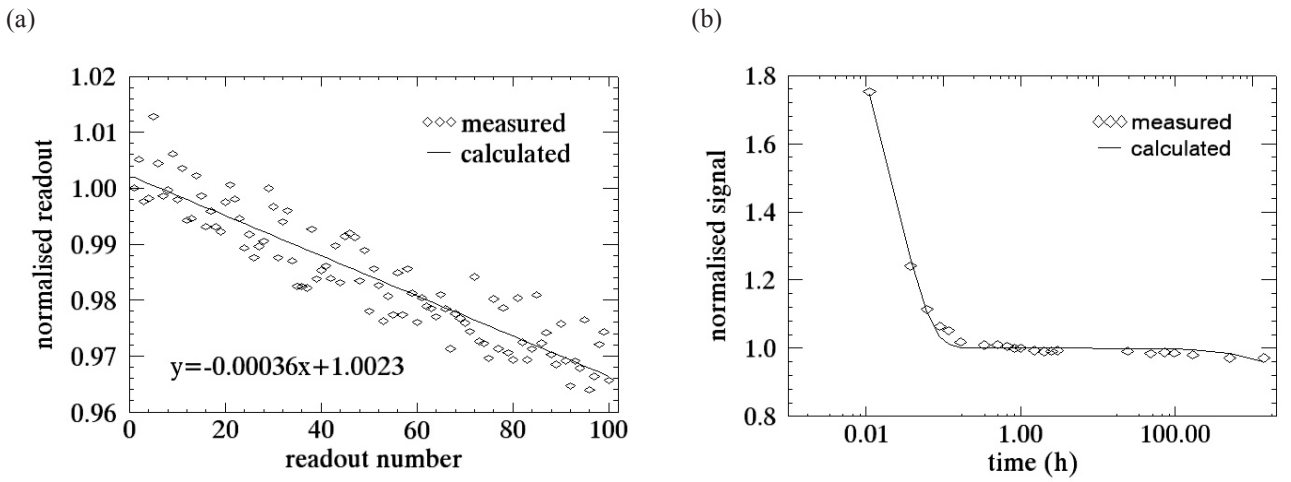

FIG. III–9. (a) Sequential readouts (N = 100) of an OSLD after irradiation with 100 cGy. Each readout depletes the signal by a small amount, calculated to be approximately 0.04%; (b) Measured early fading data and fitted exponential curve.

III–3.2.5. Fading of OSLD dose signal

The measured signal in the fading experiment for representative OSLDs is depicted in Fig. III–9(a). There is an obvious transient signal that decays with time and fades out after a few minutes. To extract the parameters of this decaying curve, an exponential plus linear model was fitted to the data:

$$y(t) = A + Bx + C \cdot e^{-\frac{\ln(2)\cdot t}{T_{1/2}}} \quad \text{(III–5)}$$

where $y(t)$ stands for the OSLD signal at time t after irradiation, and A, B, C and $T_{1/2}$ are fit parameters determined by the non-linear least square Levenberg-Marquart algorithm. This approach was applied for four dosimeters; the fifth was withdrawn since its first readout was taken late. The experimental points were corrected for a fractional signal decrease due to the readout procedure. The weighted average result of $T_{1/2}$ for these four dosimeters was 1.18 ± 0.03 minutes.

III–3.2.6. Correction factors for OSLDs

After all the correction factors were evaluated, only those larger than 1% were taken into account. Although some of the wedge (Table III–12) and block tray factors (Table III–13) were slightly higher than that value, we decided to neglect them because of the relatively high standard deviations.

TABLE III–11. EARLY FADING CURVE PARAMETERS

Dosimeter	A	B	C	$T_{1/2}$(min)	R
1	1.000 ± 0.004	–0.00003 ± 0.00001	1.15 ± 0.04	1.06 ± 0.04	0.993
2	0.993 ± 0.004	–0.00003 ± 0.00001	0.86 ± 0.04	1.25 ± 0.04	0.987
3	1.000 ± 0.004	–0.00003 ± 0.00001	0.79 ± 0.04	1.29 ± 0.08	0.989
4	0.976 ± 0.004	–0.00003 ± 0.00001	0.79 ± 0.07	1.33 ± 0.12	0.975

Note: OSLDs were read starting 40 s after the end of irradiation.

TABLE III–12. MEASURED WEDGE CORRECTION FACTORS (k_{wedge}) FOR AVAILABLE PHYSICAL WEDGES (OSLDs)

Wedge	6 cm			8 cm			10 cm		
	30^0	45^0	60^0	15^0	45^0	60^0	30^0	45^0	60^0
	1.000	1.034	1.015	1.010	1.005	1.006	0.999	1.001	1.014

Note: Experimental uncertainties are at the level of 1.5%.

TABLE III–13. COMBINED BLOCK AND TRAY FACTOR MEASURED WITH OSLDs

Field (A)	15 cm			10 cm	
Block (B)	7.5 cm	5 cm	2.5 cm	5 cm	2.5 cm
EQS field size	10.6 cm	13.2 cm	14.5 cm	7.1 cm	9.3 cm
Factor	0.982	1.005	0.997	0.990	0.975

III–3.2.7. Alderson Rando phantom results for OSLDs

A small RW3 phantom test (N = 8 fields) was conducted prior to the Alderson phantom measurements to verify the accuracy and reproducibility of the proposed calibration cycle and correction factors employed for calculating the entrance dose. Irradiations were performed with different field sizes, SSDs, wedged or non-wedged fields and with an angle of incidence either equal to or different from 0°. The mean deviation and respective standard deviation were −0.8 ± 1.0 % for these eight measurements.

Two OSLDs were irradiated per field and per site in the Alderson phantom study. The average of five readouts was multiplied by a calibration coefficient and relevant correction factors. Tables III–14, III–15 and III–16 list the mean percentage differences between the measured entrance dose and the TPS calculated dose. All percentage differences except one were below 3%, which was the threshold for permitting the pilot patient study to begin.

III–3.2.8. Patient measurements — OSLDs

Over a hundred entrance dose measurements with OSLDs for different treatment set-ups were done. The patient frequency distribution for Δ is shown for all measurements in Fig. III–11. Table III–17 shows the tabulated results. A major deviation was discovered in a patient treated with tangential breast fields. Deviations from the expected dose were −18.3% and 16.6% for two fields. Later inspection of a treatment plan showed the wrong fractionation of the total prescribed dose (45 Gy in 25 fractions instead of in 20), which resulted in a lower dose per fraction.

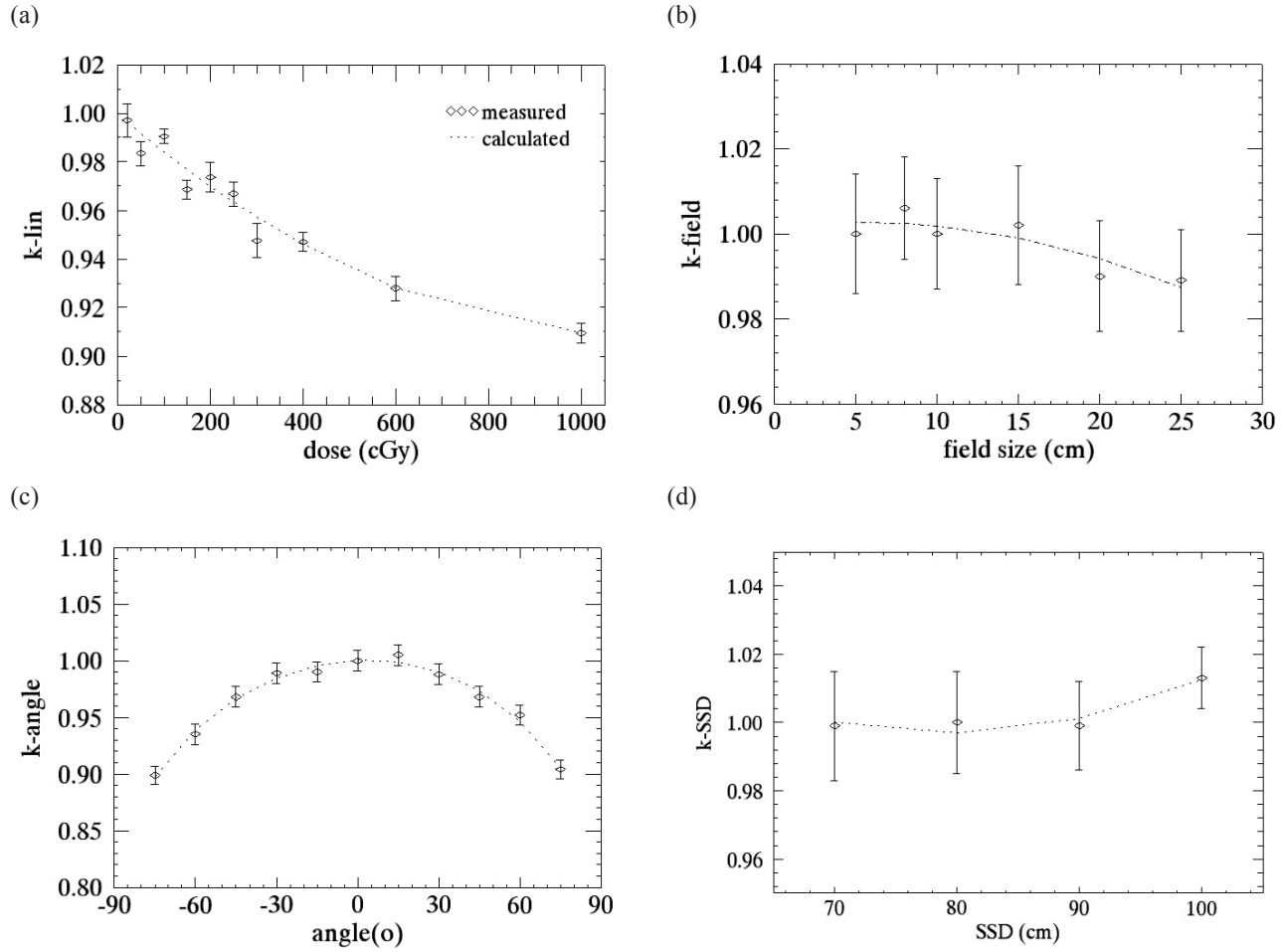

FIG. III–10. Correction factors — upper row: (a) Non-linearity correction factor versus dose in the range 20 cGy to 1000 cGy (bleached dosimeters); (b) Field size correction factor in the square field size range 5 cm to 25 cm; (c) Angular correction factor — directional dependence of the diode; (d) SSD correction factor for different SSDs from 70 cm to 100 cm (lines are drawn to visualize the trend only).

TABLE III–14. MEAN PERCENTAGE DIFFERENCES BETWEEN MEASURED AND EXPECTED ENTRANCE DOSE FOR THREE 20 × 20 cm PELVIC FIELDS (AP, RL AND LL) AND TWO 10 × 10 cm WEDGED FIELDS (RL-W AND LL-W)

Field type	Field size (cm)	Δ (%)	
AP	20 × 20	−2.0	−2.7
RL	20 × 20	0.3	0.7
LL	20 × 20	0.0	−0.6
RL-w	10 × 10	0.1	−0.6
LL-w	10 × 10	1.3	−0.2

Note: Results are shown for two OSLDs.

TABLE III–15. MEAN PERCENTAGE DIFFERENCES BETWEEN MEASURED AND EXPECTED ENTRANCE DOSE FOR TWO 6 × 6 cm FIELDS (RL AND LL) AND TWO 6 × 6 cm FIELDS FOR THE PHANTOM WITH A MASK (RL-M AND LL-M)

Field type	Field size (cm)	Δ% (± σ)
RL	6 × 6	0.2 ± 1.2
LL	6 × 6	1.4 ± 1.2
RL-m	6 × 6	2.0 ± 0.1
LL-m	6 × 6	4.7 ± 0.9

Note: The measurements were repeated three times.

TABLE III–16. PERCENTAGE DIFFERENCES BETWEEN MEASURED AND EXPECTED ENTRANCE DOSE FOR TWO WEDGED 6 × 20 cm FIELDS (MED AND LAT)

Field type	Field size (cm)	Δ%	
MED	6 × 20	−2.9	−2.4
LAT	6 × 20	0.4	−0.7

TABLE III–17. DEVIATIONS BETWEEN MEASURED (OSLD) AND EXPECTED ENTRANCE DOSE Δ AND OTHER ACCURACY DESCRIPTORS CATEGORIZED INTO MAJOR GROUPS ACCORDING TO THE ANATOMICAL SITE

	N	Median Δ%	Mean Δ%	σ (%)	(5% < |Δ| < 10%) %	(|Δ| ≥ 10%) %
All data	103	1.8	1.4	3.6	7.8	1.9
Pelvis	34	3.2	2.9	2.4	14.7	0.0
Head/neck	11	1.2	1.2	2.4	9.1	0.0
Breast	21	0.7	−0.8	6.0	9.5	0.0
Thorax	15	0.7	0.9	1.7	0.0	0.0

Discrepancies in a range of 5% to 10% were found in eight patients (7.8%), and they were all positive. For two of them, it was found that the SSD was incorrect, and in one case, it was very difficult to measure a real angle of incidence; there was also a small empty space between the patient's skin and the dosimeter.

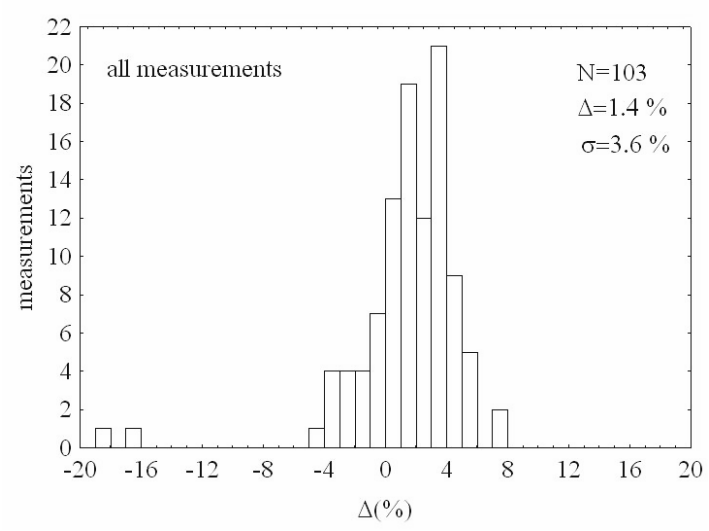

FIG. III–11. Frequency distribution of Δ for all OSLD patient measurements.

III–4. DISCUSSION

III–4.1. Characteristics of dosimeters

The silicon diodes used in this investigation provided a highly reproducible, sensitive and simple means of measuring the entrance dose in ^{60}Co radiotherapy beams. Their small size, robustness, immediate readout and effortless maintenance position them at the top of the list of preferred in vivo dosimetry systems, particularly for small departments with limited staff and without a RV system available on-site.

One of the most important advantages of diodes is the immediate readout, which significantly speeds up the process of entrance dose estimation. The approximate agreement of the measured and expected entrance dose can be verified immediately after irradiation. By having a spreadsheet form readily available on a nearby computer, it is possible to calculate the corrected entrance dose within a minute. In contrast, OSLDs, although sensitive, small and lightweight, can be read only after the 10–12 minutes necessary to deplete the short lifetime shallow traps that would otherwise overestimate the dose.

One of the advantages of OSLDs over diodes lies in the possibility of using the same dosimeters and one reader in a department with a number of different machines, provided the correction factors have been measured. Furthermore, the OSLDs and the reader can be used in other applications in the hospital environment such as the estimation of doses in mammography and other diagnostic radiology procedures. The demonstrated power of this technique in personal radiation dosimetry needs no additional advocacy.

For OSLDs to become more reliable and practical dosimeters, a small thin frame would need to be constructed with an affixed buildup cap that could slide over the sensitive portion of the dosimeter to accurately and reproducibly cover it. During our measurements, the buildup cap was individually positioned over the dot and taped each time the measurement was carried out. Thus, an additional uncertainty was introduced. Having OSLDs with attached buildup caps, fixation on the patient's skin and removal of the plastic carriers could be completed more quickly and easily than in the case of the diodes, which are connected by cables.

In general, better reproducibility (<1%) was obtained for diodes than for OSLDs (1.5%). The result for diodes is similar to other results in the literature [III–10], and the figure for OSLDs is within the range of the results obtained in recent studies [III–7, III–14–III–16]. The lower limits were obtained using a different type of reader and methodology.

The perturbation of the field is similar for diodes and OSLDs, at below 3%. Correction factors (>1%) that were effectively used for diode measurements were those for wedges and angle of beam incidence, while non-linearity and angular correction factors were applied in the case of OSLDs.

The dependence of the OSL signal on the delivered dose was assessed by irradiating OSLDs to doses from 20 cGy up to 10 Gy at the surface of the RW3 slab phantom as indicated in the protocol. Figure III–8(d) shows that the OSL response is linear for doses lower than 200 cGy if the OSLDs were not calibrated or irradiated to any dose at all before the actual non-linearity measurement. The calibration of the dots either before or after the linearity test changes this behaviour, and nonlinearity of a few percentage points is observed for doses even lower than 200 cGy. Since we performed our Alderson Rando phantom and clinical pilot study once the calibration had been completed, a polynomial curve that takes into account supra-linearity was fitted to the experimental data and later applied as a correction factor.

The above mentioned non-linearity results agree with data published by Yukihara et al. [III–17]. They studied the dose response of Al_2O_3: C to beta radiation in a range from approximately 0.7 Gy to 1000 Gy and observed that the OSL dose response shows linear-supralinear-saturation behaviour.

The OSL response was linear for doses from 0.7 Gy to approximately 2 Gy, and a supra-linear region accompanied by an increase in sensitivity was observed before the signal saturation. The dose response behaviour and sensitivity changes are similar to those observed in TL of Al_2O_3:C.

To allow for variation in the sensitivity between different OSLDs and to avoid difficulties with the individual calibration and non-linearity factor determination, a calibration curve could be constructed using a separate set of OSLDs from the same batch. The data would be presented as the ratio of the reading for the dose of interest to that obtained for a chosen reference dose. The measurement procedure would be to irradiate the dosimeter with the dose to be measured and subsequently with the reference dose. This technique [III–15] has recently been described.

The field size dependence, determined in a 6 MV photon beam and expressed as OSL responses per delivered dose (2 Gy) relative to the overall mean for three different field sizes and five depths, gave deviations within ±2.5% [III–7]. Other authors [III–18] did not obtain any observable field size effect. Their measurements with 6 MV photon beams were also made in a phantom at d_{max}, and the angular correction factor measurements in a cylindrical phantom did not find any angular dependence of OSLDs for 6 MV and 18 MV beams.

III–4.2. Results on the Alderson Rando phantom

The diode results for large AP, RL and LL pelvic fields revealed a small deviation of less than 2% between the measured and expected entrance dose and a small uncertainty of less than 0.5%. For wedged fields, a small negative deviation was observed. Head and neck field measurements showed an even smaller deviation with no significant difference between fields with and without the mask. Slightly worse results were obtained with OSLDs, where standard deviations in repeated measurements were somewhat higher. This seems to be related to the larger inherent uncertainties of the calibration, readout and bleaching cycle.

A practical difficulty experienced with OSLDs during the Alderson Rando phantom measurements was the rigidity of the plastic carrier, particularly when the dosimeter was positioned on the neck of the phantom.

III–4.3. Results of measurements on patients

The diode measurements of lateral opposed head and neck fields (N=138) gave a mean deviation equal to 0.8% with a σ equal to 3.1%. A deviation larger than 5% and 10% was observed in 7.2% and 0.7% measurements, respectively.

Here we measured blocked and unblocked fields with the exception of very small blocked fields where it was not possible to position the diode far enough from the edge of the block.

Several papers have addressed treatment accuracy for head and neck sites. An early study [III–1] reported a mean deviation of about 0% with a σ equal to 2.3% (N = 364). Other authors obtained results comparable to the results presented here (Table III–18).

The largest number of measurements (N = 202) was made for pelvic fields. They resulted in a mean deviation of 1.1% with a σ equal to 1.9%. A moderately high positive deviation probably correlates with the use of blocks and the inclusion of PA fields for which a statistical analysis also indicated a significant difference from unblocked fields and fields with another direction of beams (RL, LL, AP).

TABLE III–18. SOME RESULTS OF HEAD AND NECK IN VIVO MEASUREMENTS WITH DIODES

Reference	*N*	Δ% (± σ)
Mitine et al. [III–19]	176	0.9 ± 1.9
Loncol et al. [III–20]	217	1.2 ± 2.6
Millwater et al. [III–21]	284	1.2 ± 2.7
Leunens et al. [III–1]	364	0.0 ± 2.3
This work	138	0.8 ± 3.1

As anticipated, breast treatments demonstrated a negative mean deviation of −1.1%, with a σ equal to 3.9%, between the expected and measured dose. The precise positioning of the dosimeter turns out to be most important in combined wedged and oblique fields. Even when the diode is precisely positioned, another uncertainty arises from the determination of the angle of incidence for correction factors. Our approach was to estimate it from the central slice isodose distribution containing the patient anatomy and beam directions.

There are few published results for actual clinical in vivo measurements with OSL dosimeters. Aznar et al. [III–22] tested a real time OSL fibre dosimeter for the direct measurement of the delivered dose at the normalization point. Two typical pelvic treatments were simulated on an Alderson phantom, and the dose was within 1%. In the actual IMRT treatment of the head and neck in one patient, the measured OSL dose was 5% below the TPS expected dose. A recent study by Danzer et al. [III–18] investigated Landauer's InLight OSL system with dot dosimeters for entrance dose measurements. The study included 22 patients treated with photons (16), electrons (4) and IMRT (2) techniques. The agreement between the dosimeters and the calculation was 3.7 ± 2.5%. Luxel (Landauer) film OSL dosimeters were used by Meeks et al. [III–23] for the in vivo measurements of extra target doses in tomotherapy. Their in-phantom testing, perfomed prior to patient dosimetry, showed results within 5% of the known delivered doses, accompanied by a minor systematic trend toward dose overestimation by the dosimeters.

III–4.4. Workload

The workload involved in checks of dosimetric accuracy during the development of a dosimetric QA protocol based on a pilot patient study may require a few weeks of intensive measurements and analyses. An exact calculation of the workload cannot be performed easily, but in our case a retrospective estimate shows that regular calibrations, once properly rehearsed, can be performed in 15–20 minutes for three diodes. Correction factors for the same set of diodes can be determined, depending on the machine, in about 10–12 hours, and the Alderson Rando phantom study to verify the calibration and correction factors can be completed in 4–5 hours. Here we did not take into account the transfer of the measured data, the preparation of suitable spreadsheet forms to calculate the entrance dose or additional analyses of the acquired records. Moreover, these estimates are based on the assumption that a person involved in performing measurements has a clear concept of how to proceed with each step of a measurement, i.e. has previous experience with measurements.

About 15 minutes is needed to irradiate ten OSLDs in the calibration process. Five readouts and the transfer of data to a worksheet in which the operator carefully keeps track of the records may take another 20 minutes. To derive correction factors for OSLDs, about the same time is needed as for the diodes, although a more careful manual introduction of the measured data into the spreadsheet is required. The automatic recording of readouts employed for personal dosimetry could be adapted for the in vivo RT dosimetry system, thereby avoiding potential mistakes in identifying the dosimeters.

III–5. CONCLUSION

In this work, the essential characteristics of diodes and OSLDs for dosimetry in ^{60}Co beams were investigated. Based on the protocol developed, the response dependencies on the delivered dose, field size, SSD, wedges and block or tray were measured and verified in phantom studies.

Diodes can easily be used in a small RT department with limited resources to enhance the QA programme. The mean deviation $\Delta = 0.5\%$ and standard deviation of 3.2% obtained in a patient study is comparable to most published results. Depending on the department's goal, different tolerance levels can be set for different techniques and localizations, e.g. lower for large pelvic fields (4%) and higher for breast fields (7–8%).

OSLDs demonstrate good accuracy and precision in measuring entrance doses and have the potential to replace TLDs or diodes, or to complement them in certain radiotherapy applications. A slight positive bias observed for the mean deviation $\Delta = 1.6\%$ in the pilot study can probably be attributed to the way the non-linearity effect was accounted for in the calculation.

Further research with an enhanced version of the reader, to avoid the random mechanical problems during the reading process (knob turning) experienced at the beginning of the study, together with better modelled buildup caps, is needed to explore further the potential of Al_2O_3: C dot OSLDs in radiotherapy dosimetry.

In a department without an in vivo dosimetry programme, a higher incidence of errors might occur owing to undetected systematic errors. If a decision is made to introduce in vivo dosimetry, many requirements have to be fulfilled for the programme to reach a certain quality: a stable, reproducible and accurate measurement system, regular calibrations and frequent checks of correction factors, as well as personnel devoted to continuous quality improvement. At the beginning of the programme, a clear explanation of objectives and methodology should be provided to the staff and, later, proper feedback on the results of in vivo measurements is crucial to maintain the staff's confidence and motivation.

ACKNOWLEDGMENTS

This research project was supported by IAEA Research Contract 13115 RBF within the CRP E2.40.14 "Development of procedures for in vivo dosimetry in radiotherapy". The authors acknowledge Landauer Inc. for providing the OSL Microstar reader and supplying the dosimeters during the project's implementation. Several practical suggestions from Dr. Cliff Yahnke are appreciated.

REFERENCES TO ANNEX III

[III–1] LEUNENS, G., VAN DAM, J., DUTREIX, A., VAN DER SCHUEREN, E., Quality assurance in radiotherapy by in vivo dosimetry. 1. Entrance dose measurements, a reliable procedure, Radiother. Oncol. **17** (1990) 141–151.

[III–2] LEUNENS, G., VAN DAM, J., DUTREIX, A., VAN DER SCHUEREN, E., Quality assurance in radiotherapy by in vivo dosimetry. 2. Determination of the target absorbed dose, Radiother. Oncol. **19** (1990) 73–87.

[III–3] KRON, T., Applications of thermoluminescence dosimetry in medicine, Radiat. Prot. Dosim. **85** (1999) 341–344.

[III–4] SWINNEN, A., VERSTRAETE, J., HUYSKENS, D.P., Feasibility study of entrance in vivo dose measurements with mailed thermoluminescence dosimeters, Radiother. Oncol. **73** (2004) 89–96.

[III–5] SOUBRA, M., CYGLER, J., MACKAY, G., Evaluation of a dual bias dual metal-oxide-silicon semiconductor field effect transistor detector as radiation dosimeter, Med. Phys. **21** (1994) 567–572.

[III–6] RAMASESHAN, R., et al., Performance characteristics of a microMOSFET as an in vivo dosimeter in radiation therapy, Phys. Med. Biol. 49 (2004) 4031–4048.

[III–7] SCHEMBRI, V., HEIJMEN, B.J.M., Optically stimulated luminescence (OSL) of carbon-doped aluminum oxide (Al2O3: C) for film dosimetry in radiotherapy, Med. Phys. **34** (2007) 2113–2118.

[III–8] YUKIHARA, E.G., et al., High-precision dosimetry for radiotherapy using the optically stimulated luminescence technique and thin Al2O3:C dosimeters, Phys. Med. Biol. **50** (2005) 5619–5628.

[III–9] EUROPEAN SOCIETY FOR THERAPEUTIC RADIOLOGY AND ONCOLOGY, Methods for In Vivo Dosimetry in External Radiotherapy, Booklet No. 1, Garant, Brussels (1994).

[III–10] EUROPEAN SOCIETY FOR THERAPEUTIC RADIOLOGY AND ONCOLOGY, Practical Guidelines for the Implementation of In Vivo Dosimetry with Diodes in External Radiotherapy with Photon Beams (Entrance Dose), Physics for Clinical Radiotherapy, Booklet No. 5, Brussels (2001).
[III–11] AMERICAN ASSOCIATION OF PHYSICISTS IN MEDICINE, Diode in vivo dosimetry for patients receiving external beam radiation therapy, Report of Task Group 62 (Wisconsin, Med. Phys. Pub.), Report Nr. 87, College Park (2005).
[III–12] INTERNATIONAL ATOMIC ENERGY AGENCY, Absorbed Dose Determination in External Beam Radiotherapy: An International Code of Practice for Dosimetry Based on Standards of Absorbed Dose to Water, Technical Reports Series No. 398, IAEA, Vienna (2001).
[III–13] INTERNATIONAL ATOMIC ENERGY AGENCY, Radiation Oncology Physics: A Handbook for Teachers and Students, IAEA, Vienna (2005).
[III–14] JURSINIC, P.A., Optically stimulated luminescent dosimeters for clinical dosimetric measurements, Med. Phys. **34** (2007) 4594–4604.
[III–15] YUKIHARA, E.G., MARDIROSSIAN, G., MIRZASADEGHI, M., GUDURU, S., AHMAD, S., Evaluation of Al_2O_3:C optically stimulated luminescence (OSL) dosimeters for passive dosimetry of high-energy photon and electron beams in radiotherapy, Med. Phys. **35** (2008) 260–269.
[III–16] VIAMONTE A., DA ROSA, L.A.R., BUCKLEY, L.A., CHERPAK, A., CYGLER, J.E., Radiotherapy dosimetry using a commercial OSL system, Med. Phys. **35** (2008) 1261–1266.
[III–17] YUKIHARA, E.G., WHITLEY, V.H., MCKEEVER, S.W.S., AKSELROD, A.E., AKSELROD, M.S., Effect of high-dose irradiation on the optically stimulated luminescence of Al_2O_3:C, Radiat. Meas. **38** (2004) 317–330.
[III–18] DANZER, J., et al., Optically stimulated luminescence of aluminum oxide detectors for radiation therapy quality assurance, TH-C-M100–02, Med. Phys. **34** (2007) 2628–2629.
[III–19] MITINE, C., et al., Is it necessary to repeat quality control procedures for head and neck patients? Radiother. Oncol. **21** (1991) 201–210.
[III–20] LONCOL, T.H., GREFFE, J.L., VYNCKIER, S., SCALLIET, P., Entrance and exit dose measurements with semiconductors and thermoluminescent dosimeters: a comparison of methods and in vivo results, Radiother. Oncol. **41** (1996) 179–187.
[III–21] MILLWATER, C.J., MacLEOD, A.S., THWAITES, D.I., In vivo semiconductor dosimetry as part of routine quality assurance, Brit. J. Radiol. **71** (1998) 661–668.
[III–22] AZNAR, M.C., et al., Real time optical fibre luminescence dosimetry for radiotherapy: physical characteristics and application in photon beams, Phys. Med. Biol. **49** (2004) 1655–1669.
[III–23] MEEKS, S.L., et al., J.M., In vivo determination of extra target dose received from serial tomotherapy, Radiother. Oncol. **63** (2002) 217–222.

Annex IV

CHINA — DEVELOPMENT OF PROCEDURES WITH THERMOLUMINESCENT AND MOSFET DOSIMETERS FOR IN VIVO DOSIMETY IN RADIOTHERAPY

Suming LUO*, Jie QIU**, Weiguo ZHU*, Zhijiang HE*, Bo YANG**, Tingtian PANG**
* Chinese Centre for Disease Control and Prevention
National Institute for Radiological Protection and Nuclear Safety
** Peking Union Medical College Hospital
Department of Radiotherapy
Beijing, China

Abstract

As part of the IAEA collaborative research programme on in vivo dosimetry, a comparison was carried out between TLD and MOSFET dosimeters. After characterization of the dosimeters following the agreed protocols, in vivo dosimetry was carried out on pelvic and on head and neck patients using 6 MV and 15 MV photon beams. The Alderson Rando phantom is a useful tool to validate the system for in vivo measurements. For both dosimeter types, the measurements obtained were closely aligned with the calculations. Patient measurements with TLDs and MOSFETs were conducted for the pelvic site. The number of results within 5% for the TLD measurements and for the MOSFETs were similar.

IV–1. INTRODUCTION

At the Peking Union Medical College Hospital, there are three linear accelerators (Varian Trilogy, Siemens Primus M and Varian 2300CD). These machines offer 6 MV and 15 MV photons. The 2300CD and Primus machines were the machines used for this project. There are also two high dose rate brachytherapy units (Nucletron HDR and Tianjing Rongli HDR); 1200 patients are treated each year.

Three in vivo dosimetry systems are available: TLD, diode and MOSFET, although at the start of the CRP, the MOSFET system had not been commissioned. TLD had been used for in vivo dosimetry on five patients, but the results had been unsatisfactory. Diodes were only used for the dosimetry of total body irradiation.

Physicists are responsible for the calibration and QA of the radiation treatment unit, including both mechanical and radiation aspects of the equipment. They are also responsible for the preparation of the treatment plan, its associated set-up parameters and the calculation of the dose.

IV–2. CALIBRATION AND CHARACTERIZATION OF DOSIMETERS

IV–2.1. TLD Procedures

IV–2.1.1. Handling of TLD material

The TLD material used was TLD-1000S, which is lithium fluoride doped with magnesium and titanium (LiF:Mg,Ti) and is made in China. The chip size is 3.0 mm × 3.0 mm × 0.89 mm. The annealing cycle used was 400°C for one hour followed by 100°C for two hours. After this annealing, the chips were placed at room temperature for 12 hours before use. The chips were kept in a plastic tray supplied by the manufacturers. The glow curve obtained from the reader is shown in Fig. IV–1.

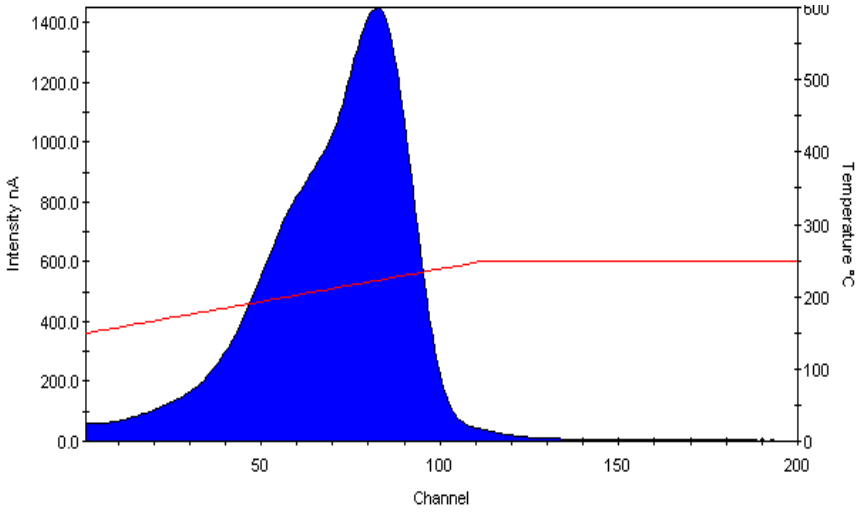

FIG. IV–1. TLD glow curve.

IV–2.1.2. Pre-calibration irradiation

The chips were irradiated to 100 cGy and then read out and annealed. This process was repeated five times.

IV–2.1.3. Measurement of individual chip factors

The chips were laid side by side on a plastic tray as shown in Fig. IV–2. A dose of 100 cGy was delivered with ^{60}Co gamma rays using a 20 cm × 20 cm field size at 80 cm SSD. This provided a margin of at least 3 cm around the chips. Beam uniformity over the area of the chips was within 0.5%. This process was repeated three times, and the results were used to calculate individual chip calibration factors (k_{chip}). The variation of these is shown in Fig. IV–3. Out of 140 chips, 5 were found to be outside a range of ±3%, and these chips were not used for further measurements.

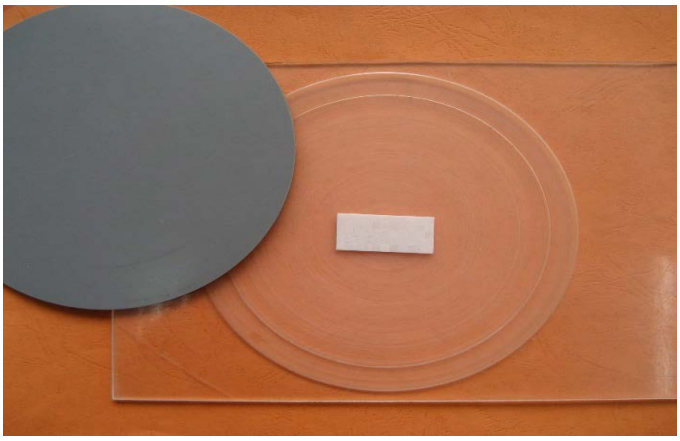

FIG. IV–2. Set-up for uniform irradiation of whole batch of chips.

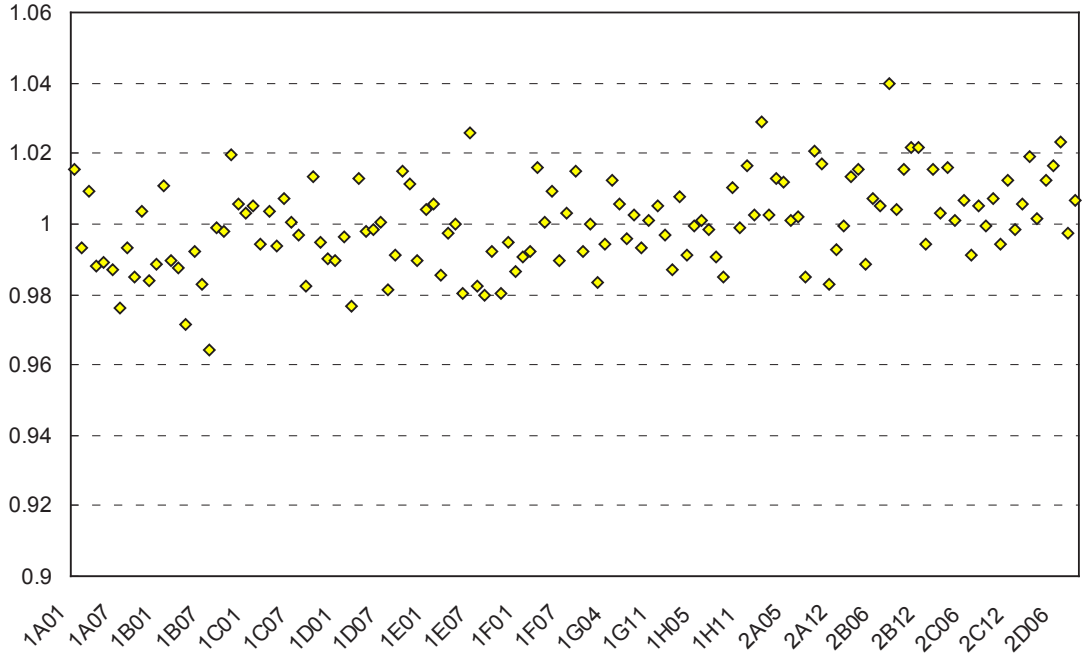

FIG. IV–3. Variation of individual chip factors.

IV–2.1.4. Measurement of batch calibration

After each annealing, 10 chips were selected at random from the batch in order to measure a batch calibration coefficient. For this purpose, chips covered by a 2 mm thick buildup cap (supplied by the IAEA) were irradiated with 6 MV X rays on the surface of a plastic phantom with an ionization chamber at 5 cm depth. The dose at d_{max} was calculated from the ionization chamber measurements following Ref. [IV–1]. The number of monitor units necessary to deliver 100 cGy at d_{max} was calculated, and this number of monitor units was used to deliver 100 cGy to each of the 10 chips. Because measurements were made in a plastic phantom, a factor was used to convert the dose measured in the phantom to the dose that would be measured in water for the same number of monitor units. The measured value of this factor, k_{pl}, was 1.0085. Measured calibration coefficients for different annealing cycles are shown in Table IV–1.

TABLE IV–1. CALIBRATION COEFFICIENTS, N_{cal}, MEASURED ON DIFFERENT DATES

Calibration date	N_{cal} (cGy/nC)
June, 2006	0.01212
September, 2006	0.01188
October, 2006	0.01181
November, 2006	0.01232
December, 2006	0.01230

IV–2.1.5. Non-linearity correction

The linearity of the TLD response with dose was measured. Chips were placed on the surface of the plastic phantom and given doses of 20, 50, 100, 150, 200, 300 and 400 cGy. The non-linearity correction factor was defined as in Section 4.4.1.1. The results are given in Table IV–2. Each point was the average of the readings from four chips and two irradiations per chip. No correction was needed for measurements below 100 cGy.

TABLE IV–2. k_{lin} LINEARITY CORRECTION FACTORS FOR DIFFERENT DOSES FOR TLD

Dose (cGy)	Chamber values (cGy)	TLD values (cGy)	k_{lin}
20	19.97	19.85	1.006
50	49.60	49.46	1.003
100	99.84	99.84	1.000
150	149.54	153.80	0.972
200	199.25	205.72	0.969
300	299.19	315.52	0.948
400	397.14	431.87	0.920

IV–2.1.6. Fading correction

All the chips were laid out side by side in a plastic box (see Fig. IV–4), and a dose of 100 cGy was delivered. Groups of chips were read out at various intervals following irradiation. These results are shown in Table IV–3.

FIG. IV–4. Plastic box used to house TLDs.

IV–2.1.7. Angle of incidence correction

Chips were placed inside the buildup cap on the surface of the plastic phantom. The centre of the chip was placed at the isocentre of the machine. 100 cGy were delivered with the gantry at different angles. Four chips were irradiated at each gantry angle. The results are shown in Table IV–4.

TABLE IV–3. FADING CORRECTION FOR TLD

Hours after irradiation	Chip values (cGy)	k_{fading}
0.5	100.1	1.000
4	99.21	1.009
24	98.55	1.016
48	98.00	1.021
72	97.57	1.026
96	96.71	1.035
120	96.52	1.037
168	94.44	1.060

TABLE IV–4. EFFECT OF ANGLE OF INCIDENCE ON TLD READING

Angle (°)	Chip reading (*nC*)	k_{ang}
0	9048.129	1.000
15	9016.974	1.003
30	8997.641	1.006
45	9103.444	0.994
60	9295.799	0.973
−15	9017.938	1.003
−30	8977.617	1.008
−45	9105.808	0.994
−60	9283.460	0.975

IV–2.1.8. SSD correction

Measurements were performed with chips placed on the surface of the plastic phantom. The phantom surface was placed successively 70, 80, 90, 100 and 110 cm from the source. A fixed collimator opening of 10 cm × 10 cm defined that an SSD of 100 cm was used. The monitor units were calculated using the Burns formula to give 100 cGy at d_{max} for each SSD. The dose at 5 cm deep was also measured with the ionization chamber. The results of these measurements are given in Table IV–5.

IV–2.1.9. Field size correction

The dose at d_{max} for different field sizes was calculated from measurements made at the reference depth of 5 cm. Results are shown in Table IV–6.

TABLE IV–5. SSD CORRECTION FOR TLD

SSD (cm)	Chamber values (cGy)	TLD values (cGy)	k_{SSD}
70	100.77	99.85	1.009
80	104.50	106.12	0.992
90	110.90	114.49	0.995
100	101.87	101.87	1.000
110	101.30	100.72	1.006

TABLE IV–6. FIELD SIZE CORRECTION FACTORS FOR TLD

Field size (cm × cm)	Chamber values (cGy)	TLD readings (*nC*)	k_{field}
10 × 10	100.0	8496.5	1.000
6 × 6	100.0	8503.1	0.999
8 × 8	100.9	8628.0	0.994
15 × 15	100.5	8512.7	1.003
20 × 20	100.1	8459.9	1.005
25 × 25	99.3	8459.1	0.997

IV–2.1.10. Wedge correction

Readings of TLDs on the surface of the phantom were measured with and without wedges using a field size of 10 cm × 10 cm. 100 MU were delivered with an open field. For the wedged fields, the monitor units were 100/WF, where W is the wedge factor, which should give the same dose. The results are shown in Table IV–7, from which it will be seen that no correction is necessary.

TABLE IV–7. CORRECTION FACTORS FOR USE WITH WEDGES

Field size	6 cm × 6 cm			8 cm × 8 cm			10 cm × 10 cm		
Wedge angle	30°	45°	60°	30°	45°	60°	30°	45°	60°
k_{wedge}	0.999	0.999	1.000	1.000	1.000	1.000	1.000	1.000	1.000

IV–2.1.11. Block and tray correction

TLDs were placed on the phantom surface at 100 cm SSD. An 8.3 cm thick lead block was placed on the block tray to reduce the field size to an equivalent smaller field. The TLD reading with 100 MU to the blocked field was compared to the TLD reading with an open field with the same equivalent square size. It was concluded that it would be impractical to include a block and tray correction factor as the correction factors do not change with the equivalent square in a systematic way.

TABLE IV–8. CORRECTION FACTORS FOR BLOCKED FIELDS

Bounding open field (cm)	4.2 × 6		10 × 10	15 × 15		25 × 25
Equivalent square cm	4.35	6.0	8.0	8.4	11.7	18.2	23.1
k_{block}	1.014	0.996	0.991	1.000	1.010	1.012	1.012

IV–2.1.12. Energy correction

All patient measurements were carried out using 6 MV photons, and calibrations were carried out at this energy. It was not therefore necessary to include an energy correction.

IV–2.2. MOSFET procedures

IV–2.2.1. Handling of MOSFETs

The MOSFET used was type TN-502RD in high sensitivity mode. All readings were made more than two minutes after irradiation.

IV–2.2.2. Dose rate dependence of MOSFETs

MOSFETs were placed on the surface of the calibration phantom with an ionization chamber at the reference depth (5 cm for 6 MV and 10 cm for 15 MV). Monitor units were calculated in order to deliver 100 cGy at d_{max} and the dose recorded by the MOSFET was noted. Each reading was repeated three times, and the experiment was carried out with five different MOSFETs. The results are given in Table IV–9.

TABLE IV–9. DOSE RATE DEPENDENCE OF MOSFETs

MOSFET	100 cm SSD			130 cm SSD			Mean 100 cm	Mean 130 cm
15 MV								
M1	100.9	101.2	101.7	101.6	101.6	101.9	101.3	101.7
M2	101.7	100.9	101.2	101.4	101.4	102.0	101.3	101.6
M3	101.1	101.3	101.6	101.1	101.7	102.3	101.3	101.7
M4	100.9	101.2	101.8	101.3	101.6	102.2	101.3	101.7
M5	101.1	101.3	101.5	101.4	101.7	102.0	101.3	101.7
6 MV								
M1	100.1	101.8	101.2	99.6	99.6	100.0	101.0	99.7
M2	99.6	99.6	100.0	99.9	99.9	100.3	99.7	100.0
M3	100.7	100.7	100.3	99.9	99.9	100.3	100.6	100.0
M4	101.2	101.2	102.6	99.5	99.1	98.7	101.7	99.1
M5	100.8	100.8	100.4	98.7	99.4	99.4	100.7	99.2

Note: MOSFET readings were repeated three times, and five MOSFETS were used.

IV–2.2.3. Reproducibility at different dose levels

Each of the five MOSFETs was placed with a buildup cap on the surface of the solid phantom and was irradiated five times at both 6 MV and 15 MV with doses of 50 cGy and 100 cGy. The dose delivered was monitored with an ionization chamber at 5 cm deep in the case of 6 MV and 10 cm deep at 15 MV. The standard deviation of the five readings was calculated. The standard deviations obtained are shown in Table IV–10. It can be seen that the absolute standard deviation is not dependent on the dose delivered, so the percentage standard deviation is less the higher the dose.

TABLE IV–10. STANDARD DEVIATIONS OF REPEATED MOSFET READINGS

MOSFET number	Standard deviation of reading			
	6 MV		15 MV	
	50 cGy	100 cGy	50 cGy	100 cGy
M1	2.6	3.6	3.1	2.3
M2	1.8	1.6	3.1	2.4
M3	2.4	2.4	2.3	3.0
M4	2.7	2.4	1.8	3.0
M5	1.6	3.4	3.3	3.4

IV–2.2.4. Calibration of MOSFETs

Each MOSFET was calibrated following the procedure described in Section 4.3. The MOSFET was placed with a buildup cap on the surface of the solid phantom. Micropore tape was used to ensure that the MOSFET was held securely on the phantom. An appropriate number of monitor units to give a dose at d_{max} of 50 cGy was delivered. The actual dose delivered was measured with an ionization chamber placed at the reference depth. The dose delivered to the ionization chamber was determined using Ref. [IV–1]. This calibration exposure was repeated three times for each MOSFET, and the mean calibration coefficient, N, as defined in Eq. (IV–1), was calculated. k_{pl}, the phantom factor, was measured as 1.013 for 15 MV.

$$N = \frac{D_0}{M} \cdot \left(\frac{SSD - d_s}{SSD + d_{\max}} \right)^2 \cdot k_{pl} \qquad \text{(IV–1)}$$

where $D_0 = D/(PDD/100)$, and d_s is the effective distance of the MOSFET centre to the surface of the solid phantom. The ionization chamber reading was corrected for temperature and pressure. The measured calibration coefficients are given in Table IV–11. It will be noted that the calibration coefficients are different for the two energies. Rather than apply an energy correction, it was decided to calibrate the dosimeters at the specific energy at which they were to be used.

IV–2.2.5. Non-linearity of dose response

A MOSFET with a buildup cap was placed on the surface of the solid phantom, such as for calibration, with the ionization chamber in position. 20, 50, 100, 200, 300 and 400 cGy were delivered to the MOSFET. The non-linearity dose response correction factor k_{lin} is expressed as the ratio of MOSFET response M per unit dose

measured at the dose D_o to the ionization chamber response per unit dose measured at the dose D. The results are given in Table IV–12, from which it will be seen that the response was linear.

TABLE IV–11. CALIBRATION COEFFICIENTS FOR THE FIVE MOSFETs AT 6 MV AND 15 MV

MOSFET number	Calibration coefficient (cGy/MOSFET reading)	
	6 MV	15 MV
M1	0.3567	0.2890
M2	0.3603	0.2921
M3	0.3612	0.2923
M4	0.3637	0.2945
M5	0.3597	0.2899

TABLE IV–12. MEASUREMENT OF NON-LINEARITY WITH DOSE FOR MOSFETs

Ionization chamber measured dose cGy	MOSFET measured dose			k_{lin}
	M1	M2	M3	Mean value
20.4	20.6	20.3	20.4	1.01
50.6	51.2	51.1	51.3	0.99
101.2	102.5	102.7	101.8	0.99
151.8	153.1	153.4	152.9	0.99
202.8	204.1	203.2	202.9	1.01
304.3	308.4	305.9	307.3	0.99
406.1	409.4	410.4	405.4	0.99

IV–2.2.6. Angle of incidence

Each MOSFET was placed with a buildup cap on the surface of the solid phantom with its sensitive volume at the isocentre. Readings were taken for 50 MU with the gantry at ±60°, ±45°, ±30°, ±15°, 0°. The measurements were repeated three times for each MOSFET. The results are shown in Table IV–13 and in Fig. IV–5.

TABLE IV–13. CORRECTION FACTORS FOR OBLIQUE INCIDENCE MEASURED FOR MOSFETs

Angle (degrees)	MOSFET readings		k_{ang}		
	M1	M2	M1	M2	Mean
6 MV					
0	145.5	140.67	1.000	1.000	1.000
15	146.5	142.0	0.993	0.991	0.992
30	143.0	140.0	1.017	1.004	1.010
45	144.5	144.0	1.007	0.977	0.992
60	143.0	144.5	1.017	0.973	0.995
−15	144.5	141.0	1.007	0.998	1.003
−30	146.5	139.0	1.021	1.012	1.017
−45	142.0	137.5	1.025	1.023	1.024
−60	142.0	140.0	1.025	1.005	1.015
15 MV					
0	185.3	183.0	1.000	1.000	1.000
15	184.7	188.5	1.003	0.971	0.987
30	185.5	185.5	0.999	0.987	0.993
45	185.5	184.5	0.999	0.992	0.996
60	181.5	183.5	1.021	0.997	1.009
−15	188.0	187.5	0.986	0.976	0.981
−30	185.5	184.5	0.999	0.992	0.996
−45	182.0	185.0	1.018	0.989	1.004
−60	178.0	183.5	1.041	0.997	1.019

IV–2.2.7. SSD correction

The MOSFETs were placed on the surface of the solid phantom and irradiated at SSDs 70, 80, 90, 100 and 110 cm with a fixed collimator opening of 10 cm × 10 cm. The monitor units for each SSD were calculated to give 50 cGy at d_{max}. The correction factor is given by:

$$K_{SSD} = \left[\frac{M_0}{D_0}\left(\frac{SSD_0 - d_s}{SSD_0 + d_{max}}\right)^2\right] \Big/ \left[\frac{M_{SSD}}{D_{SSD}}\left(\frac{SSD - d_s}{SSD + d_{max}}\right)^2\right] \quad \text{(IV–2)}$$

Where M_0, D_0 and SSD_0 correspond to the standard distance of 100 cm and M, D and SSD are related to the SSD of interest. The results are shown in Table IV–14.

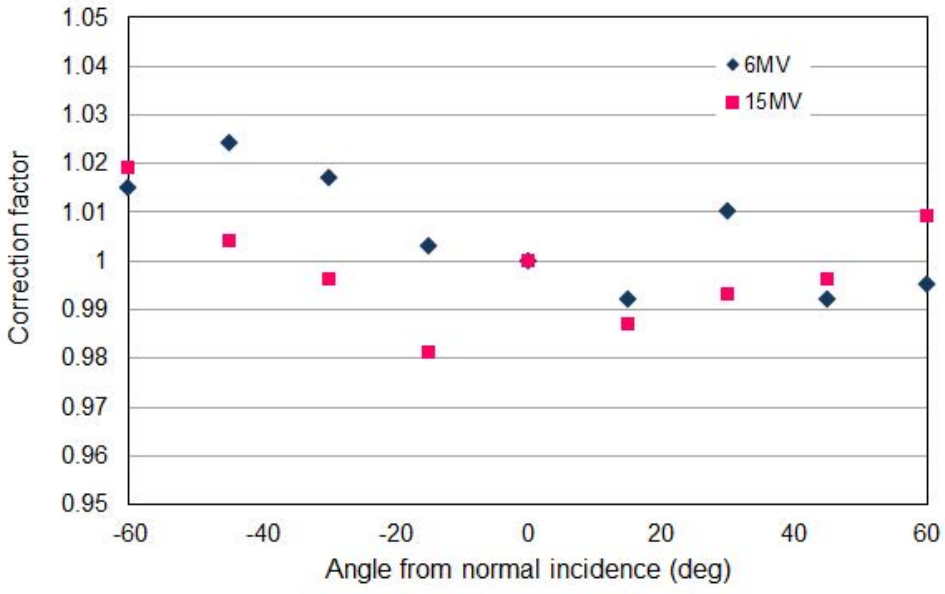

FIG. IV–5. Variation of angle of incidence correction factor for MOSFETs at 6 MV and 15 MV.

TABLE IV–14. SSD CORRECTION FACTORS FROM 70 CM TO 110 CM FOR 6 MV AND 15 MV BEAMS

SSD (cm)	Measured dose cGy	MOSFET reading		k_{SSD}
		M1	M2	Mean
6 MV				
70	50.8	143.5	146.5	1.004
80	49.41	148.0	150.5	0.978
90	50.5	143.5	143.5	0.999
100	50.3	143.67	140.67	1.000
110	51.2	142.0	143.5	0.989
15 MV				
70	50.30	188.0	187.0	0.974
80	51.01	182.0	186.0	1.003
90	50.68	189.0	187.0	0.977
100	50.30	181.0	186.0	1.000
110	50.35	181.0	187.0	0.993

IV–2.2.8. Field size correction

The field size correction was measured for field sizes from 4 cm × 4 cm to 25 cm × 25 cm giving doses calculated to deliver 100 cGy for 6 MV and 50 cGy for 15 MV. The results are shown in Table IV–15 and Table IV–16.

TABLE IV–15. FIELD SIZE CORRECTION FACTORS FOR MOSFETs AT 6 MV

Field size (cm)	Dose to d_{max} (cGy)	MOSFET readings			k_{field}
		M1	M2	M3	mean
4 × 4	102.5	296.0	291.0	292.0	0.996
6 × 6	101.4	288.0	292.0	294.0	0.991
8 × 8	101.9	291.0	289.0	285.0	1.007
10 × 10	101.2	288.0	289.3	287.0.	1.000
15 × 15	99.75	281.0	278.0	284.0	1.011
20 × 20	99.38	272.0	277.0	284.0	1.019
25 × 25	98.39	277.0	276.0	277.0	1.012

TABLE IV–16. FIELD SIZE CORRECTION FACTORS FOR MOSFETs AT 15 MV

Field size (cm)	Dose to d_{max} (cGy)	MOSFET readings		k_{field}
		M1	M2	Mean
4 × 4	50.2	187.5	185.0	0.987
6 × 6	50.4	184.5	190.0	0.986
8 × 8	50.2	185.0	180.5	1.006
10 × 10	50.3	185.3	183.0	1.000
15 × 15	49.9	181.5	178.5	1.019
20 × 20	49.5	178.5	181.0	1.012
25 × 25	48.9	176.0	177.5	1.016

IV–2.2.9. Wedge correction

The correction factor for wedges was measured for three different field sizes at both 6 MV and 15 MV. In order to give the same dose at d_{max}, 50 MU were delivered without a wedge and 50/WF MU (WF = wedge factor) were delivered with the wedge. The results for 6 MV are shown in Table IV–17. For each measurement, two exposures were carried out. It will be seen that no correction is necessary. Similar results were obtained for 15 MV.

IV–2.2.10. Block and tray correction

The block and tray correction was measured in the same way as for TLDs (see Section IV–2.1.11). Each measurement was the result of two irradiations of the MOSFET. This was not an easy measurement to make, and the variability between the two dosimeters suggests that there is no sufficient evidence to justify the application of a correction.

TABLE IV–17. WEDGE CORRECTION FACTORS MEASURED FOR MOSFETs AT 6 MV

Field size	6 cm × 6 cm			8 cm × 8 cm			10 cm × 10 cm		
Wedge angle	30º	45º	60º	30º	45º	60º	30º	45º	60º
M1	0.997	1.019	1.000	0.994	1.000	0.983	0.998	1.001	0.997
M2	1.005	0.981	0.984	1.018	0.997	1.036	0.991	1.000	0.997
Mean	1.001	1.000	0.992	1.006	0.999	1.010	0.995	1.001	0.997

TABLE IV–18. BLOCK AND TRAY CORRECTION FOR MOSFETS

Bounding open field (cm)		4 × 4	8 × 8	10 × 10	15 × 15	20 × 20	25 × 25
Equivalent square (cm)		3.5	7.5	8.9	12.8	15.7	18.5
				6 MV			
k_{block}	M1	1.005	1.042	1.021	0.994	0.974	1.011
	M2	1.008	1.010	0.972	1.016	1.013	1.015
				15 MV			
k_{block}	M1	1.027	1.022	1.023	0.992	0.976	0.989
	M2	0.981	0.976	0.991	0.990	1.010	0.976

IV–3. ALDERSON RANDO PHANTOM MEASUREMENTS

Prior to carrying out patient measurements, the in vivo dosimetry system was tested with an Alderson phantom. CT scans of both the pelvis and the head and neck region of the phantom were first obtained using a 3 mm slice width at 3 mm slice spacing. Field simulation was then carried out under the supervision of the radiation oncologist, and manual contours of the phantom were taken. For the head and neck region, the simulation was carried out both with and without a thermoplastic mask. Computerized treatment plans were then created based on both the CT data and the manual contour using a Hewlett Packard 715/100xc treatment planning system. A manual calculation to provide an independent check of the TPS calculation was carried out using a programme implemented in an Excel spreadsheet.

IV–3.1. Pelvis phantom measurements

Entrance dose measurements were made for a three field beam arrangement with anterior–posterior and right and left lateral fields. Measurements were made for each individual beam. Field sizes were 20 cm × 20 cm, and wedges were not used. Three plans were created: using the manual contour through the central slice of the phantom, using the CT data with no inhomogeneity correction and using the CT data with an inhomogeneity correction. The plans were designed to give 50 cGy to the intersection of the beams from each field. Four TLD chips were irradiated at the entrance of each beam, and the irradiation was carried out twice. The relative percentage difference was calculated between the measured doses and the entrance doses calculated by the TPS for the CT based plan with an inhomogeneity correction.

A second set of plans were carried out with the beam arrangement shown in Fig. IV–7. The anterior–posterior field was again 20 cm × 20 cm. The lateral fields were 10 cm × 10 cm, and a wedge filter was used with its toe

pointing posteriorly. For the TLD measurements, 45º wedges were used, and for the MOSFET measurements, 30º wedges were used. The phantom is shown in Fig. IV–6 and the treatment plan in Fig. IV–7.

FIG. IV–6. Alderson phantom set-up for pelvic measurements.

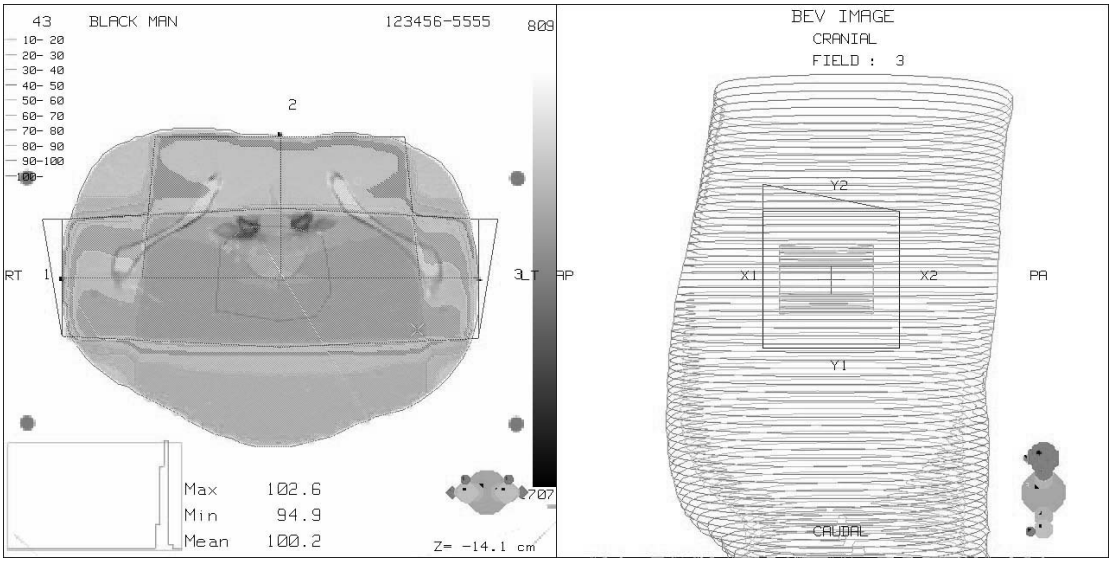

FIG. IV–7 Treatment plan for pelvic Alderson phantom measurements.

The results of the measurements for TLD are shown in Table IV–19 and for MOSFETs in Table IV–20.

TABLE IV–19. PERCENTAGE DIFFERENCE BETWEEN TPS CALCULATED ENTRANCE DOSES FOR THE PELVIC REGION OF THE ALDERSON PHANTOM AND TLD MEASURED ENTRANCE DOSES

Beam direction	Field size (cm)	D_{TLD} (cGy)	D_{TPS} (cGy)	$(100)\times\frac{D_{TLD}-D_{TPS}}{D_{TPS}}$
Left lateral	20 × 20	96.8	98.2	−1.4
Right lateral	20 × 20	91.0	90.8	+0.2
Anterior–posterior	20 × 20	72.1	72.6	−0.5
Right lateral	10 × 10 wedged	93.4	94.3	−0.9
Left lateral	10 × 10 wedged	105.8	101.8	+3.8

Note: 6 MV beams were used. Wedged fields had a wedge angle of 45°.

TABLE IV–20. PERCENTAGE DIFFERENCE BETWEEN TPS CALCULATED ENTRANCE DOSES FOR THE PELVIC REGION OF THE ALDERSON PHANTOM AND MOSFET MEASURED ENTRANCE DOSES

Beam direction	Field size (cm)	D_{MOSFET} (cGy)		D_{TPS} (cGy)		$(100)\times\frac{D_{MOSFET}-D_{TPS}}{D_{TPS}}$	
		6 MV	15 MV	6 MV	15 MV	6 MV	15 MV
Left lateral	20 × 20	97.2	83.7	98.8	83.7	−1.7	0.0
Right lateral	20 × 20	92.1	78.0	90.61	78.46	1.6	−0.5
Anterior−posterior	20 × 20	72.7	64.6	72.25	65.27	0.7	−1.0
Right lateral	10 × 10 wedged	104.2	86.0	104.55	85.52	−0.3	0.6
Left lateral	10 × 10 wedged	96.3	81.2	95.21	79.66	1.1	1.9

Note: Measurements were made with both 6 MV and 15 MV. Wedged fields had a wedge angle of 30º.

IV–3.2. Head and neck phantom measurements

For the head and neck section of the phantom, the beam arrangement was as shown in Fig. IV–9. Two parallel opposed 6 cm × 6 cm fields were used without wedges. The centre of the field was on the slice at the junction of the neck and the chin. The treatment plan was designed to give 100 cGy to the isocentre for each field. These measurements were done both with and without the immobilization mask. CT scans of the phantom were only available without the mask, so measurements made with the mask were compared to calculations based on the manual outline. Measurements were again compared to the TPS calculated entrance doses. The phantom is shown in Fig. IV–8 and the treatment plan in Fig. IV–9.

The results of the phantom measurements for the head and neck area using TLD are shown in Table IV–21, and those obtained with MOSFETs are shown in Table IV–22.

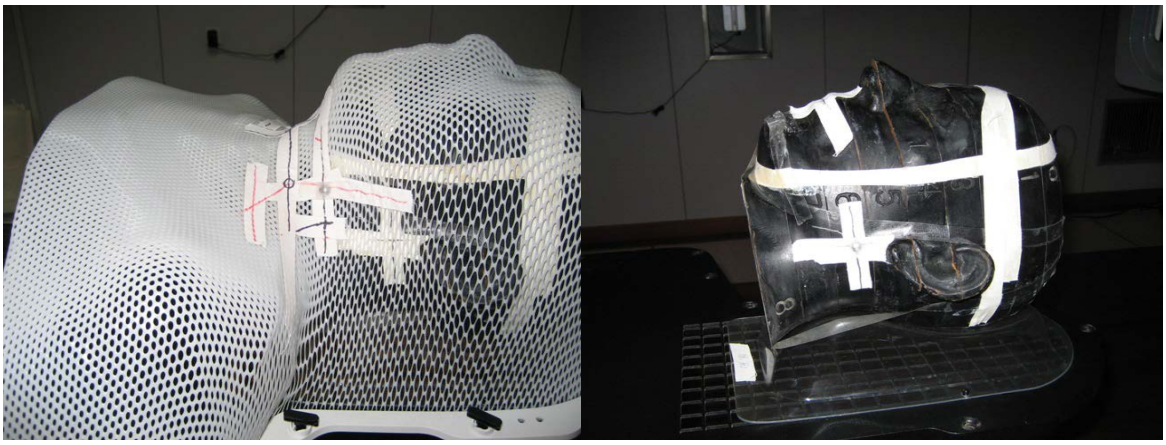

FIG. IV–8. Alderson Rando phantom set-up for head and neck measurements.

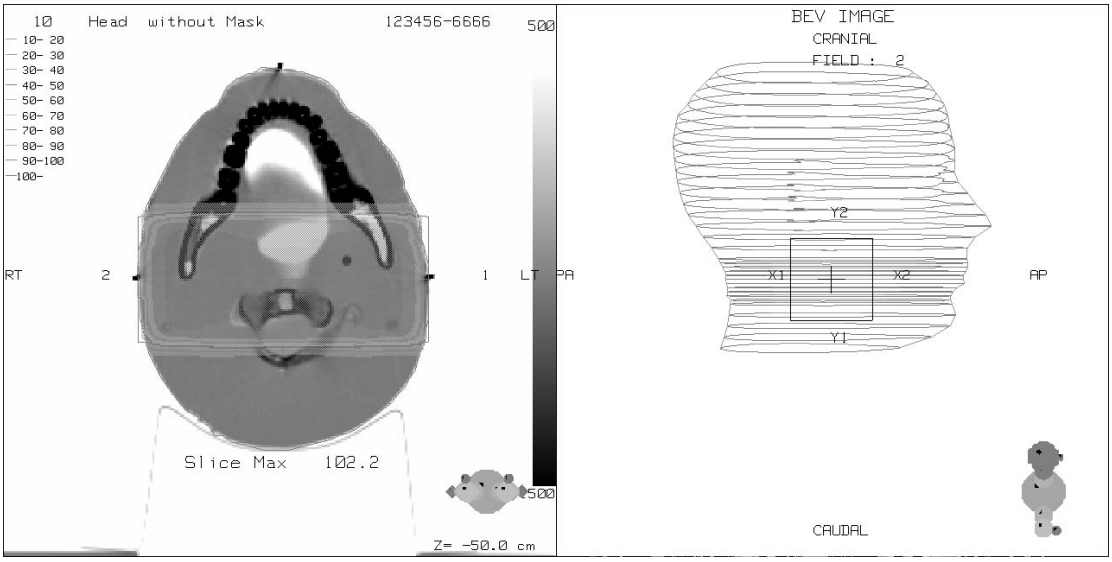

FIG. IV–9. Treatment plan for head and neck Alderson phantom measurements.

TABLE IV–21. PERCENTAGE DIFFERENCE BETWEEN TPS CALCULATED ENTRANCE DOSES FOR THE HEAD AND NECK REGION OF THE ALDERSON PHANTOM AND TLD MEASURED ENTRANCE DOSES

Beam direction	D_{TLD} (cGy)	D_{TPS} (cGy)	$(100)\times\frac{D_{TLD}-D_{TPS}}{D_{TPS}}$
Left lateral	128.0	127.6	+0.3
Right lateral	127.2	127.6	−0.4
Left lateral with mask	128.5	127.6	+0.7
Right lateral with mask	126.6	127.6	−0.8

Note: 6 cm × 6 cm beams with 6 MV beam energy were used. Data are presented with and without the immobilization mask.

TABLE IV–22. PERCENTAGE DIFFERENCE BETWEEN TPS CALCULATED ENTRANCE DOSES FOR THE HEAD AND NECK REGION OF THE ALDERSON PHANTOM AND MOSFET MEASURED ENTRANCE DOSES

Beam direction	D_{MOSFET} (cGy)		D_{TPS} (cGy)		$(100)\times\frac{D_{MOSFET}-D_{TPS}}{D_{TPS}}$	
	6 MV	15 MV	6 MV	15 MV	6 MV	15 MV
Left lateral	129.0	113.7	129.14	111.89	−0.1	1.6
Right lateral	126.2	111.4	127.47	112.12	−1.0	−0.7
Left lateral with mask	125.8	111.7	128.57	112.41	−2.2	−0.7
Right lateral with mask	126.4	114.2	127.0	112.1	−0.5	1.8

Note: Measurements were made with both 6 MV and 15 MV. 6 cm × 6 cm beams were used. Data are presented with and without the immobilization mask.

IV–4. PATIENT MEASUREMENTS

Patient measurements were carried out with both TLD and MOSFETs. For the TLD measurements, the chips were annealed in the dosimetry laboratory and then carried to the hospital. Two physicists in the hospital were responsible for both the batch calibration of the TLD and for the patient measurements. Each week, the irradiated TLDs were taken back to the dosimetry laboratory to be read out with the 3500 TLD readers. The data were put into an Excel spreadsheet. Figure IV–10 shows the measurements being made. A total of 445 field measurements with TLD have been made. Of this number, 131 measurements were for pelvic patients and 303 for head and neck patients. All of these were using 6 MV beams.

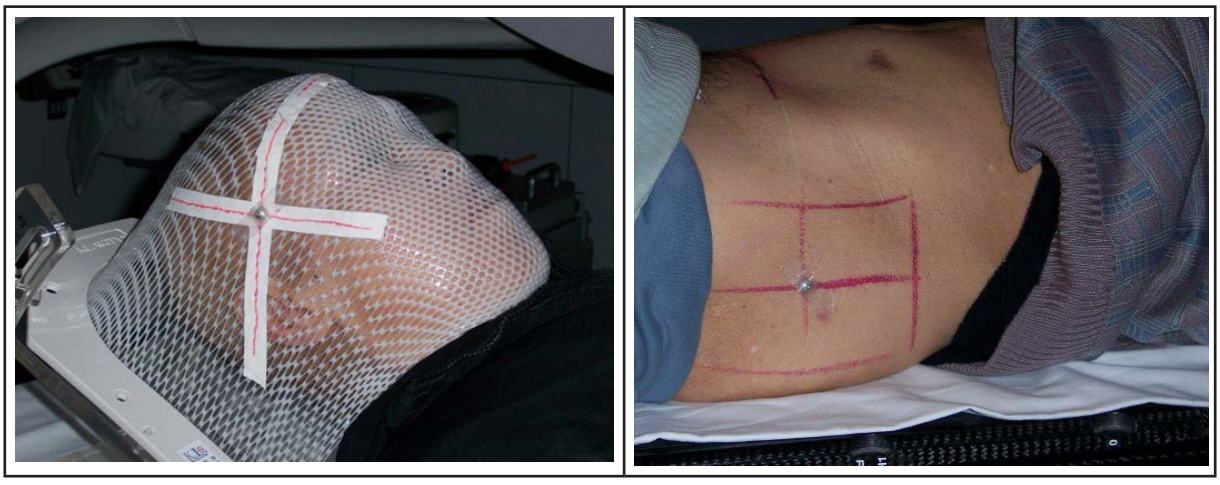

FIG. IV–10. Measurements being made on patients with TLD (head and neck on left and pelvis on right).

The two physicists were also responsible for the calibration of the MOSFETs and the patient measurements. The measurements made were entered into a spreadsheet and sent to the dosimetry laboratory weekly. In total, 948 measurements with MOSFETs have been made: 374 for pelvic patients using 6 MV and 245 using 15 MV. 233 measurements for head and neck patients were made, all at 6 MV. In addition, 231 measurements were made for other sites. The patient measurement results are shown in Tables IV–23 and IV–24.

TABLE IV–23. TLD MEASUREMENTS: RESULT STATISTICS OF PATIENT MEASUREMENTS COMPARED TO TREATMENT PLANNING SYSTEM CALCULATION OF ENTRANCE DOSE, 6 MV BEAM

Site	Number of fields measured	Mean ±SD %	Percentage of measurements within ±5% of TPS calculation
Head and neck	303	1.1 ± 3.1	87.1
Pelvis	120	−1.0 ± 3.6	95.0
Other	22	−0.2 ± 2.6	100.0
All TLD measurements	445	0.4 ± 3.4	90

TABLE IV–24. MOSFET MEASUREMENTS: RESULT STATISTICS OF PATIENT MEASUREMENTS COMPARED TO TREATMENT PLANNING SYSTEM CALCULATION OF ENTRANCE DOSE, 6 MV AND 15 MV BEAMS

Site	Number of fields measured	Mean ±SD %	Percentage of measurements within ±5% of TPS calculation
Head and neck	313	−0.6 ± 3.1	87.5
Pelvis	404	0.8 ± 3.9	79.2
Other	231	−0.8 ± 4.2	77.9
All MOSFET measurements	948	0.0 ± 3.8	81.6

Examples of the result distributions for patient measurements are shown in Figs IV–11 and IV–12.

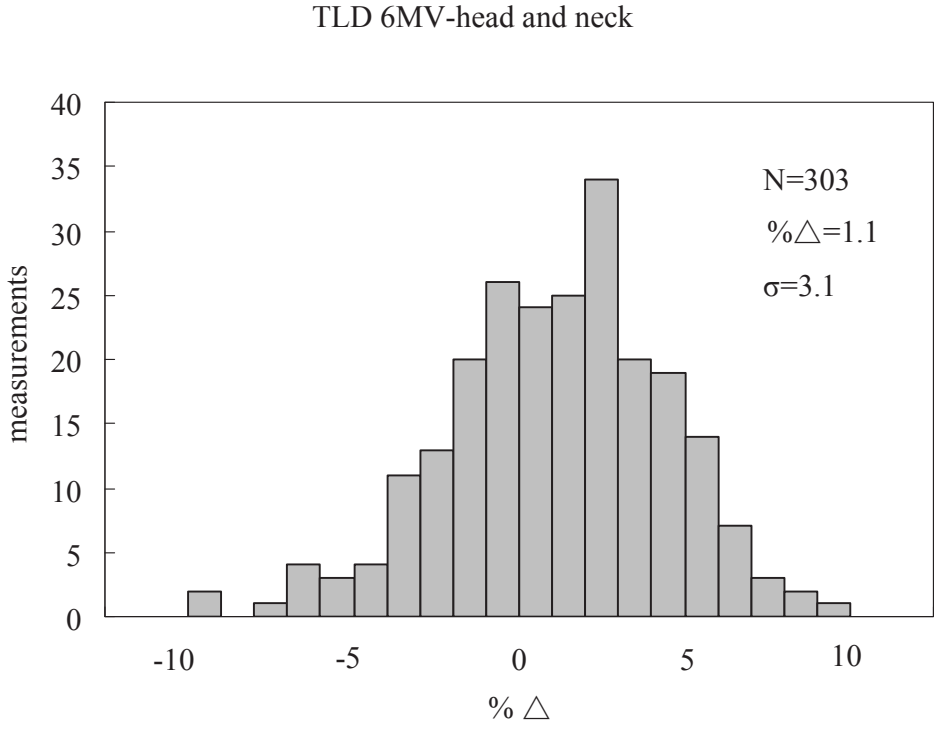

FIG. IV–11. Patient results from TLD measurements in the head and neck region for a 6 MV beam.

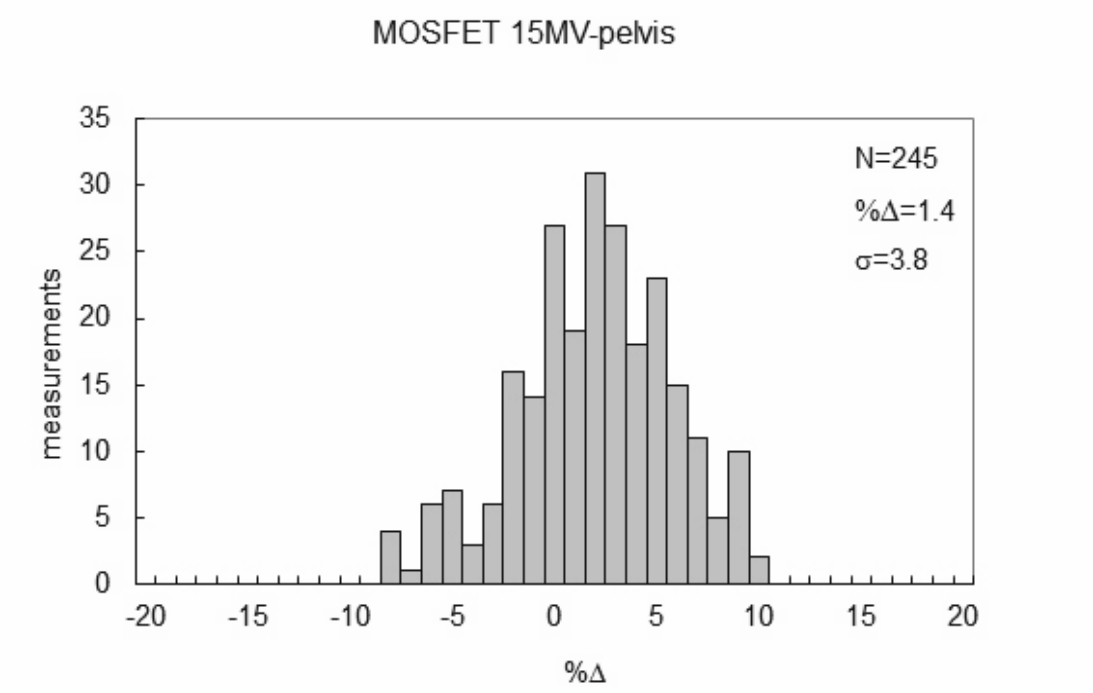

FIG. IV–12. Patient results from MOSFET measurements in the pelvic region for a 15 MV beam.

IV–5. DISCUSSION

IV–5.1. Dosimeter characteristics

TLD is a stable and economic method to use for clinical measurements. Unless they are damaged, the TLD chips can be reused indefinitely. However, care needs to be taken to ensure that the chips are correctly identified and that irradiated chips are not muddled with those that have not been irradiated. MOSFETs have the benefit of providing an immediate measurement, but they are more expensive than TLD and their life is limited.

The Alderson Rando phantom is a useful tool to validate the system for in vivo measurements. For both dosimeter types, the measurements on phantoms were in close alignment with the calculations.

IV–5.2. Patient measurements

TLDs and MOSFETs were used for similar measurements in the pelvis. More of the results were within 5% for the TLD measurements than for the MOSFETs. The key problem was the way in which the calibrations were carried out at the reference point compared to the positioning of the MOSFET detector on a patient. The measurement conditions were not the same because fixing MOSFETs on a patient slightly changes the positioning geometry and a correction factor of 1.046 proved to be necessary. When this factor was applied, the MOSFET results became similar to the TLD results.

IV–6. CONCLUSION

In this work, a set of TLD and MOSFET parameters for in vivo dosimetry using 6 MV and 15 MV photon beams were investigated. The dose response characteristics, angular dependence, field size, SSD, wedges and block/tray corrections were measured. Prior to use on patients, the dosimeters were used on an Alderson Rando phantom that allowed the in vivo dosimetry protocol developed within this CRP to be verified.

Both dosimetry systems tested in this study demonstrate adequate accuracy and precision in measuring entrance doses for a range of stationary techniques as used in radiotherapy. In general, the results obtained from in vivo measurements for head and neck, and pelvis patients are similar, although the result distribution shows slightly higher standard deviation for MOSFETs than for TLDs.

REFERENCE TO ANNEX IV

[IV–1] INTERNATIONAL ATOMIC ENERGY AGENCY, Absorbed Dose Determination in Photon and Electron Beams: An International Code of Practice, Technical Reports Series No. 277, IAEA, Vienna (1987).

Annex V

POLAND — DEVELOPMENT OF PROCEDURES FOR IN VIVO DOSIMETRY IN RADIOTHERAPY

P. KUKOLOWICZ, J. MIEDZINSKA, J. WITTYCH, K. BULINSKI, P. WOLOWIEC, A. WACHOWICZ
Holycross Cancer Center
Kielce, Poland

Abstract

At the Holycross Cancer Centre (HCC), procedures for in vivo dose measurement for teletherapy and brachytherapy were tested as part of the IAEA CRP. The dosimetric characteristics of MOSFETs (TN-RD 502, Thomson and Nielsen) and diodes (T60010M and T60010H PTW-Freiburg) as dosimeters for in vivo measurements were investigated in photon beams of 6 MV and 15 MV. In addition, MOSFET characteristics were also investigated in ^{192}Ir HDR brachytherapy treatments. In the case of teletherapy, excellent agreement between calculations made with the TPS and in vivo measurements using the Rando phantom was obtained. MOSFET dosimeters were routinely used for in vivo dose measurements for patients treated with external beams. In more than 6000 measurements, 6 errors were discovered. In 5 cases, the wrong photon beam energy was applied, and in one case, the wrong MU was used due to a typing error. In the case of brachytherapy, differences between calculated (Abacus Varian) and measured doses in simple phantom geometry were smaller than 12%. Differences obtained for measurements of dose to the rectum were in the range ±40% (in 97 of 121 measurements, the differences were in the range ±20%). Diodes had not been used in the HCC for routine in vivo dosimetry before. Full characterization of diodes for teletherapy was carried out, followed by Alderson Rando phantom and patient measurements.

V–1. INTRODUCTION

The Holycross Cancer Center is a comprehensive cancer hospital mostly serving the Świętokrzyskie Province. The population of the province is 1.2 million. In 2007, nearly 3000 new patients were treated with teletherapy (2100) and brachytherapy (800). About 50% of patients are treated with curative intent. The external beam treatments are performed with three linear accelerators and a cobalt unit. In December 2007, the cobalt unit was replaced with a new accelerator, the Siemens Artiste. For brachytherapy, the HDR Microselectron and LDR Selectron machines are used. The staff consists of 13 specialists in radiation oncology, 11 specialists in medical physics and 24 radiation technologists. The Radiotherapy, Brachytherapy and Medical Physics Departments have all the equipment needed for highly specialized treatment protocols, i.e. IMRT and IGRT. A Quality Management system based on the ISO standard has been implemented in the HCC.

For over four years, in vivo dosimetry has routinely been performed on all teletherapy patients treated with curative intent. In brachytherapy, in vivo dosimetry is mostly performed for prostate cancer patients to measure rectal doses. MOSFETs (four sets of MOSFET systems) are used for in vivo dosimetry. QA and QC tests are performed according to well established written protocols. Most tasks related to QA/QC are performed by medical physicists and radiation technologists.

The advantages of participating in the project “Development of Procedures for In Vivo Dosimetry in Radiotherapy” are primarily the opportunity to compare local experience with those of the other participants, and to obtain an experienced medical physicist’s advice based on the review of the measured data, and ultimately to improve in vivo dosimetry procedures.

In Poland, in vivo dosimetry is compulsory for so-called ‘specialized procedures’ in radiotherapy. The HCC treats patients with these types of procedures and so in vivo dosimetry has to be performed for all patients. Medical physicists are responsible for in vivo dosimetry. The actual measurements are made by radiation technologists who were specifically trained for this purpose.

V–2. MATERIALS AND METHODS

V–2.1. MOSFET system

In vivo measurements with MOSFETs were introduced to the HCC in 2003. The Thomson and Nielsen MOSFET dosimeter system was used. Figure V–1 shows the system used in the HCC hospital.

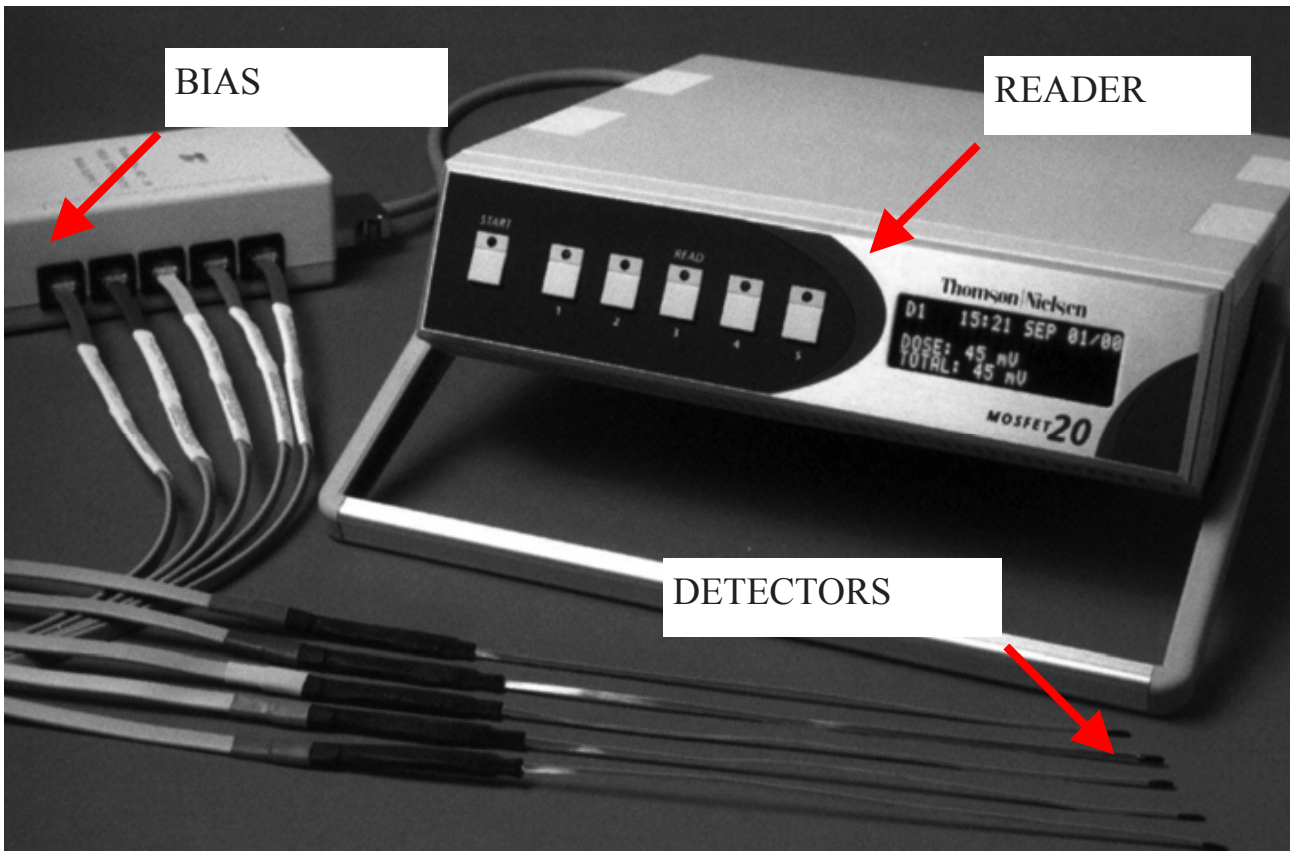

FIG. V–1. The MOSFET system (MOSFET 20 Dose Verification System, Thomson & Nielsen) used in the Holycross Cancer Centre for in vivo dosimetry.

Two years later, the same system was implemented for in vivo measurements in brachytherapy.

V–2.1.1. MOSFET measurements for teletherapy

All MOSFET measurements for external beams were performed with homemade buildup caps. The buildup caps are shown in Fig. V–2.

For ^{60}Co and 6 MV X rays, the buildup caps were made of aluminium of thickness measuring 0.54 g/cm^2 and 1.62 g/cm^2, respectively. For 15 MV X rays, the buildup cap was made of brass of thickness measuring 2.55 g/cm^2.

Before the MOSFET system was used in the clinic for in vivo dosimetry on patients, the dosimeters had to be characterized in the radiation field of interest. Some measurements were also performed on the Alderson Rando anthropomorphic phantom. During more than four years of using the MOSFET system, 65 dosimeters were used, and more than 6000 measurements were made. Initially, all measurements were made by medical physicists and after about two years, radiation technologists were trained and participated in making measurements. Once some experience had been collected, the written procedure for in vivo dosimetry was prepared.

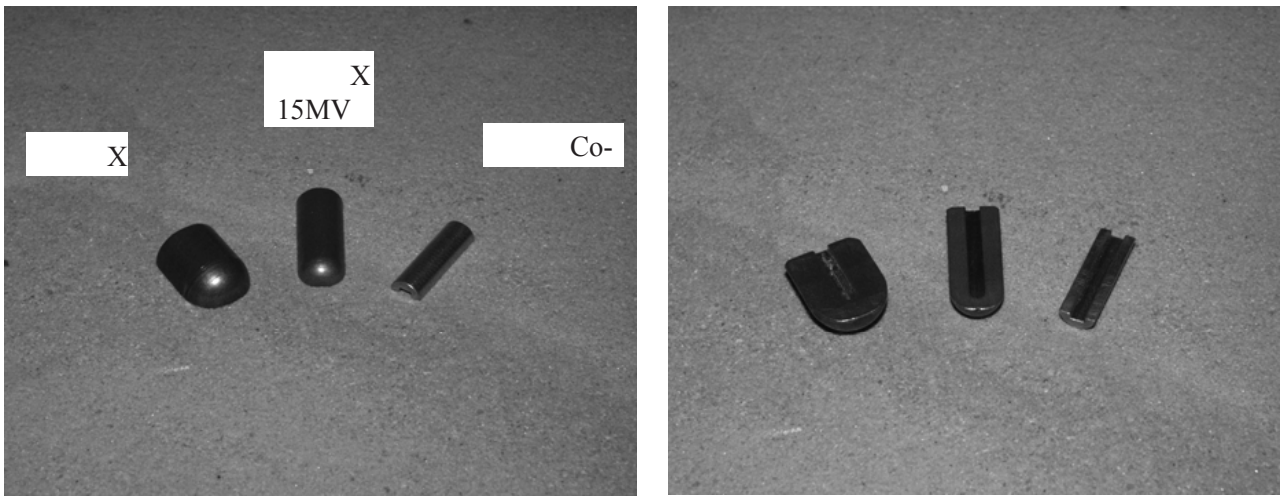

FIG. V–2. Buildup caps for in vivo dosimetry for 6 MV, 15 MV and ^{60}Co radiation.

The procedure for in vivo dosimetry in the HCC is as follows:

— *Step 1.* The in vivo measurement is made during the third or fourth treatment session for all patients treated curatively with stationary techniques such as 3-D conformal radiotherapy. All new treatment plans are checked except for IMRT.
— *Step 2.* The absolute value of the difference DIF_{abs} between the measured and calculated dose at d_{max} is compared with the appropriate action level. Action levels (ACT_{lev}) are:
  - For open photon fields 5%;
  - For wedged photon fields 7%.
— *Step 3.* If:
  (a) The $DIF_{abs} < ACT_{lev}$, then it is assumed that the treatment has been performed within specifications, and the in vivo procedure is complete;
  (b) The $DIF_{abs} > ACT_{lev}$, then the measurement is repeated during the next session.
— *Step 4.* Following the repeat measurement, if:
  (a) The $DIF_{abs} < ACT_{lev}$, then it is assumed that the treatment has been performed within specifications and the in vivo procedure is complete.
  (b) The $DIF_{abs} > ACT_{lev}$, action is initiated to explain the difference. The action starts with a manual check of all data used for treatment, e.g. to check whether the number of actual MU is equal to that calculated with the treatment planning system, etc.:
  If:
    (i) The error is found, an appropriate corrective action is taken;
    (ii) The error is not found; a measurement with the solid water phantom is made.
  Then if:
    (iii) *DIFabs* < ACTlev, it is assumed that the treatment has been performed correctly; the follow-up procedure is concluded;
    (iv) $DIF_{abs} > ACT_{lev}$, an individual decision is made; the head of the Medical Physics Department is responsible for this decision.
— *Step 5.* Before the sixth treatment session, all data are checked by the head of the Medical Physics Department, who approves the results.

When the HCC initially introduced the in vivo dosimetry programme, a slightly different procedure of measurements of dosimeter characteristics was followed. Therefore, all measurements were repeated according to the procedure proposed in this report. The results are presented later in this annex together with the clinical results of the in vivo measurements.

V–2.1.2. Brachytherapy

For in vivo measurements in brachytherapy, the Thomson & Nielsen MOSFET system (the same as for teletherapy) was used. Two different types of MOSFET dosimeters were used: model TN-502 RD and TN-502 RDM. A special rectal probe composed of three MOSFET dosimeters was designed. The rectal probe is shown in Fig. V–3.

In order to identify the position of MOSFETs on the radiographic films, three lead markers are placed inside the probe at a known distance from the dosimeters.

Before using the MOSFET system for in vivo dosimetry on patients, the dosimeters were characterized in the ^{192}Ir radiation field, starting with their careful calibration. The brachytherapy group measured the same characteristics as the teletherapy group. The only difference was that the calibration coefficient was measured with

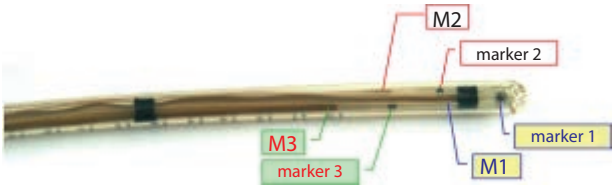

FIG. V–3. Rectal probe composed of three MOSFET dosimeters.

^{60}Co radiation and with ^{192}Ir, as described in Section V–4. The system was tested using phantom measurements. Measurements with the rectal probe were performed in a homemade wax phantom. A treatment plan based on AP and LT radiographs taken with an X ray mobile C-arm was prepared with the Abacus TPS. The irradiation was carried out with the ^{192}Ir source of the HDR Gammamed Plus unit. Measured doses were compared with the TPS calculations.

During more than two years of clinical use of the MOSFET system measurements, 43 applications in brachytherapy took place. The system was used for patients treated with HDR brachytherapy for prostate cancer. All the measurements were made by medical physicists. The treatment was considered acceptable if all three doses measured with MOSFETs were smaller than the maximum calculated dose delivered to the rectum (the maximum dose to the rectum was calculated with the TPS). Additionally, the doses at the MOSFET dosimeter positions calculated with the TPS were compared with the measured ones.

V–2.2. Diode system

The following equipment was used for the measurements with diodes: a linear accelerator (SIEMENS ONCOR, 6 and 15 MV photon beams) and in vivo dosimetry equipment, including an electrometer: VIVODOS E (PTW-Freiburg), and diodes T60010M for 6 MV and T60010H for 15 MV (PTW-Freiburg). All measurements were performed using high sensitivity mode.

All measurement points were repeated several times. In this paper, the measured values are always represented by the mean value. The uncertainty is always presented in terms of 1 SD.

In Fig. V–4, the diode system is shown.

The diode system was tested in order to compare it with the MOSFET system.

FIG. V–4. PTW VIVODOS E diode system.

V–3. RESULTS FOR IN VIVO DOSIMETRY WITH DIODES

The calibration coefficient and all correction factors were defined as recommended in the procedure for in vivo dosimetry with solid state dosimeters, Section 4.

In all situations when the ratio of doses at d_{max} is needed for the calculation of a correction factor, the doses at d_{max} were calculated with the computer program REF used in the HCC for MU calculations.

V–3.1. Reproducibility of diode readings

The reproducibility of readings was obtained by repeating the measurement performed under the reference conditions ten times. The measurements were made for 10 MU, 25 MU and 100 MU. The reproducibility was calculated as the standard deviation of the readings (Table V–1).

TABLE V–1. REPRODUCIBILITY FOR DIODES — DEPENDENCE ON THE DOSE

Beam; MU	M (*nC*)	SD (*nC*)	Reproducibility (%)
X6; 10	−24.43	0.04	0.16
X15; 10	−31.28	0.13	0.40
X6; 25	−60.25	0.06	0.10
X15; 25	−76.46	0.12	0.16
X6; 100	−241.00	0.08	0.03
X15; 100	−305.84	0.06	0.02

V–3.2. Diode calibration (entrance dose)

In all measurements, 100 MU was delivered to the point at d_{max}. The measurement set-up is shown in Section 4. The set-up shown in Section 4 will be referred to as the ‘reference conditions’.

Measurements of D_0 were made with a PTW 30003 ion chamber and a UNIDOS electrometer traceable to the Polish SSDL. All measurements were repeated three times. The D_0 dose was recalculated to a depth of

maximum dose using the per cent depth dose. Diode calibration coefficients for 6 and 15 MV X rays were $(-5567 \pm 1) \times 10^3$ Gy/C and $(-4225 \pm 1) \times 10^3$ Gy/C, respectively.

V–3.3. Intrinsic correction factors

V–3.3.1. Non-linearity dose response correction factor for diodes

The measurements of k_{lin} were performed in the reference conditions. The diode signal was measured for monitor units in the range of 25 MU to 200 MU in steps of 25 MU (the dose at d_{max} was in the range 40–300 cGy for 6 MV, and in the range 30–240 cGy for 15 MV). The results are shown in Table V–2.

TABLE V–2. THE NON-LINEARITY CORRECTION FACTOR

MU	25	50	75	100	125	150	175	200
k_{lin} (6 MV)	0.993	0.995	1.000	1.000	1.001	1.001	1.003	1.003
k_{lin} (15 MV)	1.001	0.998	1.000	1.000	1.002	1.003	1.004	1.005

V–3.3.2. Energy correction factor for diodes

The energy correction factor was not measured. For each beam energy, a separate calibration coefficient was measured.

V–3.4. Beam dependent correction factors for diodes

V–3.4.1. Angle of incidence correction

A square beam size of 30 cm was used. The signal was measured for 100 MU with gantry –45° (315°), 0°, 15°, 30°, 45°, 60° and 75°. For each angle, three measurements were made. M_0 and M_{ang} are the diode signals for 0° and the angle under test, respectively. The results are given in Fig. V–5.

V–3.4.2. SSD correction factor

Measurements were carried out for a 10 cm square field. 100 MU was delivered for each measurement. The dosimeters were placed on the solid water phantom. Measurements were made for six different source–surface distances: 75, 80, 90, 95, 100 and 110 cm.

For each SSD, measurements were repeated three times. Doses D_0 and D_{SSD} were calculated with the program, which is used in our hospital for MU calculations. The results are given in Table V–3.

V–3.4.3. Field size correction factor for diodes

At first, the measurements were made under the reference conditions. The dosimeters were placed on the surface of the solid phantom. Next, the measurements were repeated for several square fields of 4, 5, 7, 10, 15, 20, 25, 30, 35 and 40 cm. 100 MU were delivered for each measurement. Three measurements were made for each field size. The results are given in Fig. V–6.

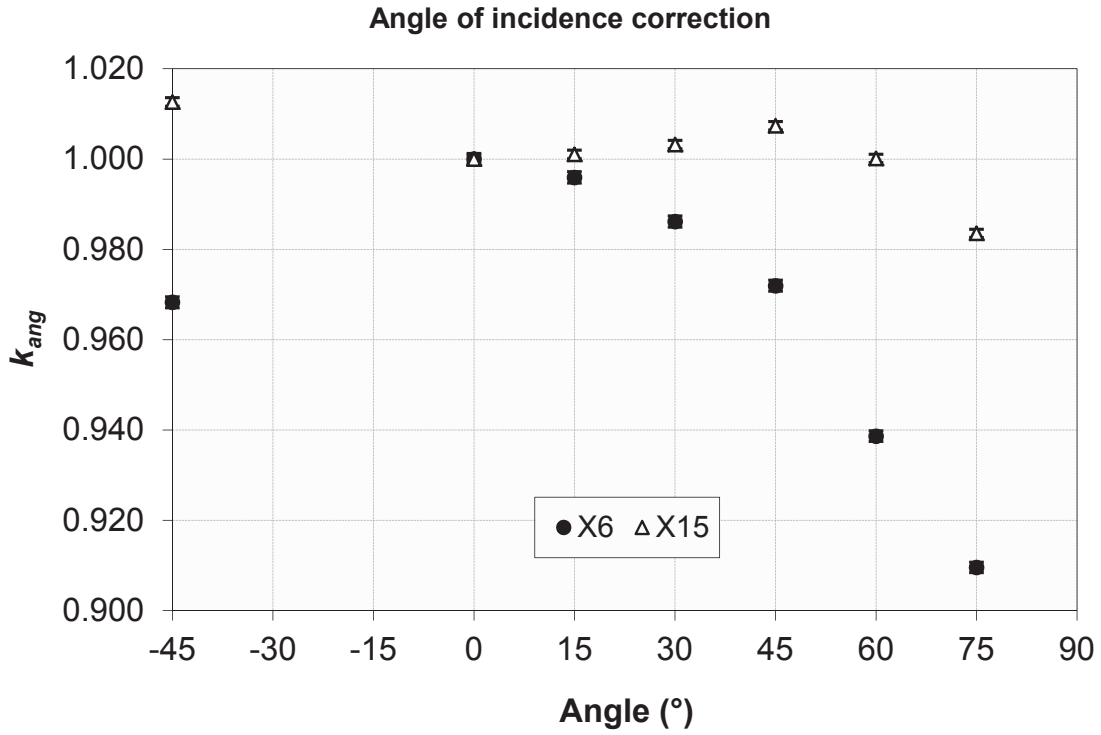

FIG. V–5. The k_{ang} for PTW diodes in 6 and 15 MV X ray beams.

TABLE V–3. SSD CORRECTION FACTORS

SSD (cm)	75	80	90	100	110
k_{SSD} (6 MV)	1.005	1.003	1.000	1.001	1.001
k_{SSD} (15 MV)	1.002	0.999	1.000	1.006	1.008

V–3.4.4. Wedge correction factor for diodes

The measurements were made under the reference conditions. The dosimeters were placed on the surface of the solid water phantom. The measurements were made for physical wedges of 15°, 30°, 45° and 60° and for open fields. For each measurement, 100 MU was delivered. Each measurement was repeated three times. The results are presented in the Table V–4.

V–3.4.5. Block and tray correction

The block and tray correction factors were not measured.

V–3.5. Clinical use of the measured corrections for diodes

In practice, three correction factors were applied for the angle, field and wedge — the k_{ang}, k_{field} and k_{wedge}. All other correction factors are in the range 0.99–1.01, and it was considered that there is no need to use them.

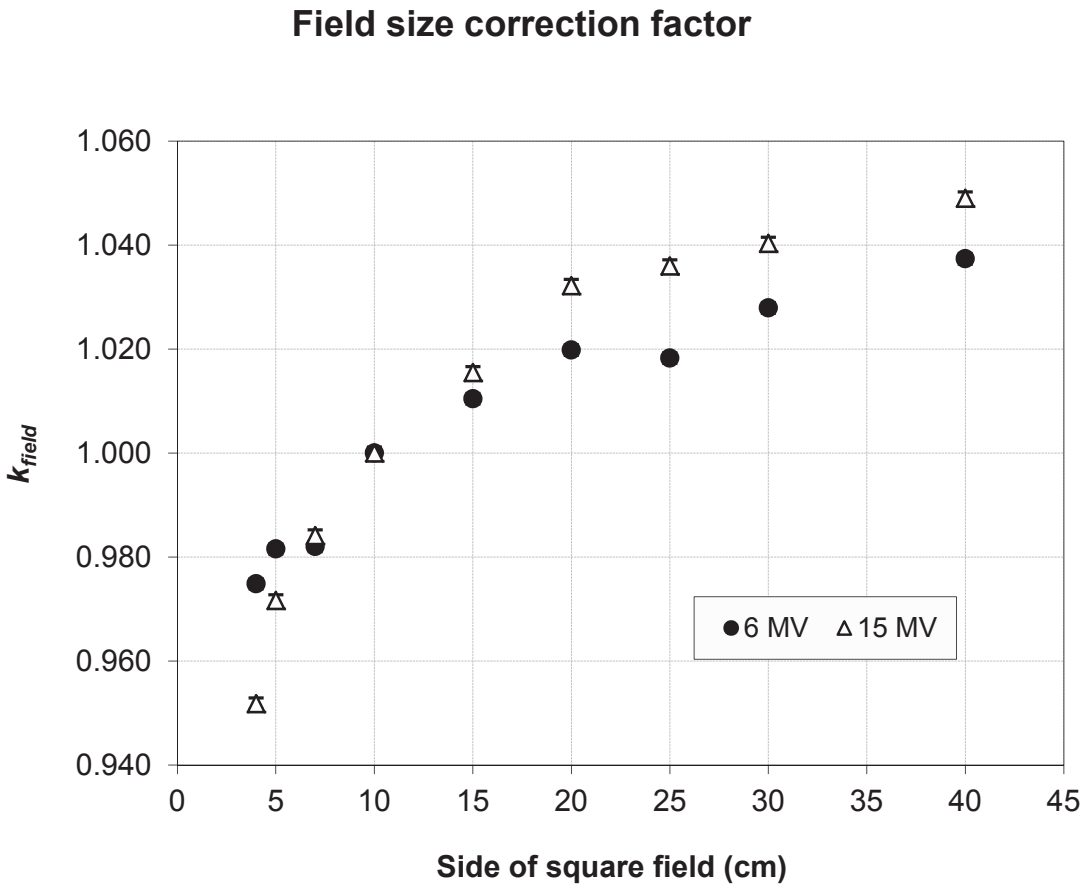

FIG. V–6. The k_{field} for PTW diodes in 6 and 15 MV X ray beams.

TABLE V–4. WEDGE CORRECTION FACTORS

Wedge angle (°)	0	15	30	45	60
k_{wedge} (6 MV)	1.000	1.004	0.999	0.992	0.990
k_{wedge} (15 MV)	1.000	0.987	0.986	0.975	0.981

V–3.5.1. Calculation of entrance dose at d_{max} from diode reading

Entrance dose for in vivo measurements is calculated as the product of the diode signal, calibration coefficient and correction factors. Entrance dose is given by:

$$D = M \cdot N_{cal} \cdot \left(\frac{SSD - d_s}{SSD + d_{max}} \right)^2 \cdot k_{ang} \cdot k_{field} \cdot k_{wedge} \qquad \text{(V–1)}$$

V–3.6. Alderson Rando phantom measurements with diodes

V–3.6.1. Pelvis

In all measurements, the three field technique and 15 MV X rays were used. Two treatment plans were used. The first one had open fields of 20 cm × 20 cm. Doses were calculated by the TPS to deliver 50 cGy to the isocentre. The second one was with a 20 cm × 20 cm open anterior field and two lateral 10 × 10 cm^2 wedged fields with 30° wedges. Doses were calculated with the Xio (CMS) TPS.

The measured doses were always larger than those calculated with the treatment planning system (the range was 0.7%–4.0% and the mean value was 2.5%). In comparison to the manually calculated doses at d_{max}, the differences were smaller. The differences were in the range 0.2–1.1%; the mean value was 0.8%.

V–3.6.2. Head and neck

The entrance dose was measured for the technique consisting of two parallel opposed 6 cm × 6 cm fields without wedges. Doses were calculated by the TPS XiO to deliver 100 cGy to the isocentre.

The measured doses were larger than the calculated ones by 2.3%. If the doses at d_{max} were calculated manually, smaller differences were obtained.

V–3.6.3. Breast

The entrance dose was measured for two tangential opposed 10 cm × 18 cm fields with 30° wedges. Doses were calculated by the TPS XiO to deliver 100 cGy to the isocentre.

The measured doses were larger than the calculated ones by 3.3% and 3.6%. If the doses at d_{max} were calculated manually, larger differences were obtained.

V–3.7. Patient measurements with diodes

V–3.7.1. Head and neck

The measurements were performed for 13 patients, and a total of 31 measurements were made. All patients were treated with 6 MV X rays with two wedge oblique or lateral opposed fields. The dose distributions were calculated with the XiO treatment planning system. Twenty-six of the measurements were made for wedged fields. The mean difference between measurements and calculations was +1.9%, with a standard deviation of 3.2%. In seven cases, the differences were larger than 5% and in only one case was the difference larger than 7%. All except one of these cases had wedged fields. 7% is the action level used in the HCC for wedged fields. In all cases where the action level was exceeded, a second measurement was made and in all cases, a satisfactory result was obtained. When the dose at dmax was calculated manually, the mean difference was 0.4%, with a standard deviation of 1.1%. The largest difference was −2.0% (the measured dose was smaller than the calculated one).

V–3.7.2. Pelvis

The measurements were performed for 14 patients, and a total of 39 measurements were made. All patients were treated with 15 MV X rays. The conformal box technique was mostly used. Fields were shaped with an MLC. The dose distributions were calculated with the XiO treatment planning system. A total of 22 measurements were made for wedged fields. The mean difference between measurements and calculations was 0.4%, with a standard deviation of 2.8%. In only two cases were the differences larger than 5%, and in only one case was the difference larger than 7%. In all the cases where the action level was exceeded, a second measurement was made and in all cases, satisfactory results were obtained. When the dose at d_{max} was calculated manually, the mean difference was 0.7%, with a standard deviation of 2.4%.

V–3.7.3. Breast

The measurements were performed for three patients, and a total of five measurements were made. All patients were treated with 6 MV X rays. The tangential wedge technique was used. The dose distributions were calculated with the XiO treatment planning system. In four cases, the difference was smaller then 2%. In one case, the difference was 12.8%. This measurement was repeated, and the difference was 3.1%.

V–3.8. Discussion

The diode in vivo dosimetry system is very simple to use, even for inexperienced users. What may cause some problems is the necessity of using different dosimeters for different energies. Our experience demonstrated that the validity of calculations of the dose at d_{max} should be checked before the system is used clinically. The extensive use of multileaf collimators introduces the problem of accurate estimation of the dose at d_{max} for MLC shaped fields. It seems very useful to measure the dose at d_{max} for a certain number of typical treatment fields.

For diodes, only correction factors for beam size, for the wedges for 15 MV and for the angle of incidence are important. The most pronounced is the beam size dependence. The correction factor should be calculated very accurately. For 6 MV X rays, the correction factor for incident angle for angles larger than about 20° plays an important role in the accuracy of the dose measurement. All other correction factors are smaller than 1%. The reproducibility of readings is very good. However, for very small doses at d_{max} (smaller than about 10 cGy), one may expect somewhat worse reproducibility.

The measurements performed with the Alderson Rando phantom showed that the system is ready for clinical use. However, for open fields applied to the pelvic region, differences between the expected and the measured doses were close to 3% (in one case even larger). These differences were observed for comparison made with the doses at d_{max} calculated with the TPS. Much smaller differences were obtained if the doses at d_{max} were calculated manually. It was concluded that the treatment planning system overestimated the doses at d_{max} for large field sizes.

The measurements for patients did not discover errors in patient data preparation for treatment. In the Holycross Cancer Center, the action levels are 5% for open fields and 7% for wedged fields. For the pelvis region, in one case, the action level was exceeded. This was for a 45° wedge. The result of the repeat measurement was within the acceptance level. If the CRP criteria were followed (5% action level), then in one more case, the action level would have been exceeded. For head and neck, in two cases, the action level was exceeded. The measurements were repeated, and the results were within the acceptance criteria. It should be noted that measurements for patients treated with tangential fields are less accurate due to the geometrical uncertainty of the dosimeter placement. Therefore, measurements made with wedges are less reliable. The conclusion of the HCC is to consider the use of two different action levels for open and wedged beams.

V–4. RESULTS FOR IN VIVO DOSIMETRY WITH MOSFET DOSIMETERS

The calibration coefficient and all correction factors were defined as described in the IAEA procedure for in vivo dosimetry with solid state detectors (Section 4). The MOSFET system has been used in the HCC for clinical applications since 2003.

V–4.1. MOSFET calibration (entrance dose)

In all measurements, 50 MU was delivered. Measurement set-up was the same as for diodes.

As for the diodes, measurements of D_0 and M were repeated three times. Measurements of D_0 were made with a PTW 30003 ion chamber and UNIDOS electrometer traceable to the Polish SSDL. The D_0 dose was recalculated to a depth of maximum dose using the per cent depth dose.

The calibration coefficients for 6 and 15 MV X rays were 0.349 ± 0.005 cGy/mV and 0.296 ± 0.003 cGy/mV, respectively. These calibration coefficients were calculated as the mean value for 65 dosimeters calibrated in the HCC since 2004. In Fig. V–7(a), calibration coefficients for 6 MV X rays for all 65 dosimeters are presented. In Fig. V–7(b), calibration coefficients for 15 MV X rays for all 65 dosimeters are presented.

(a)

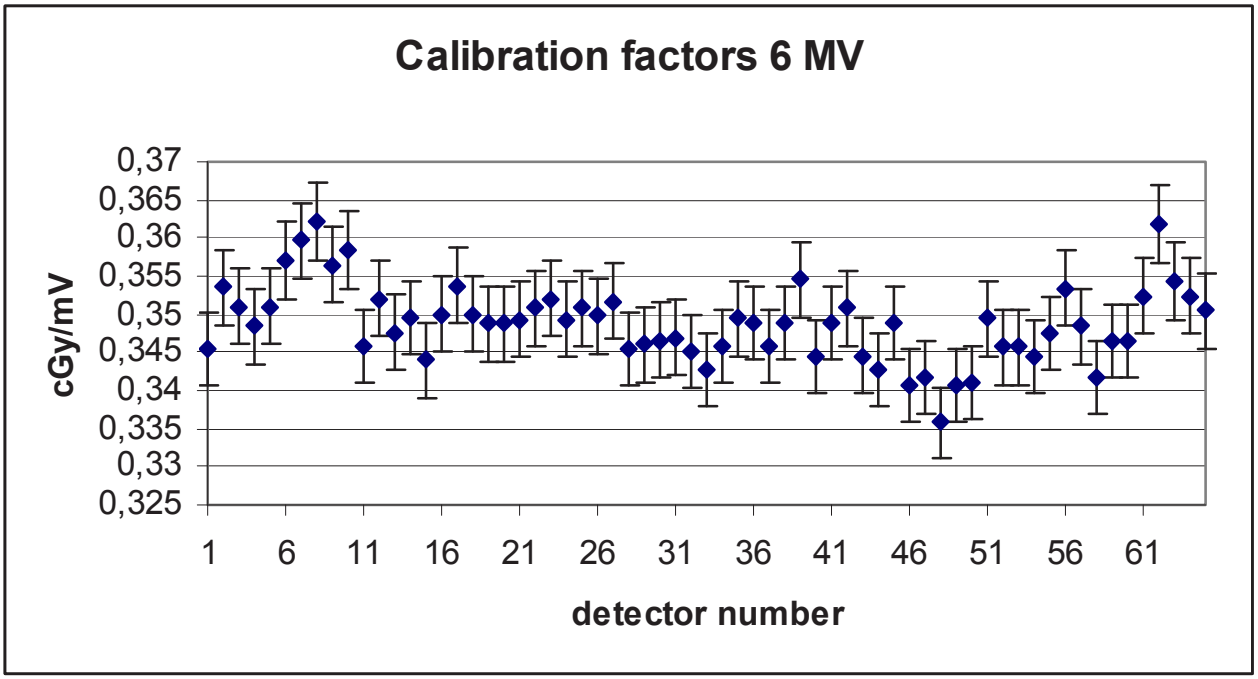

(b)

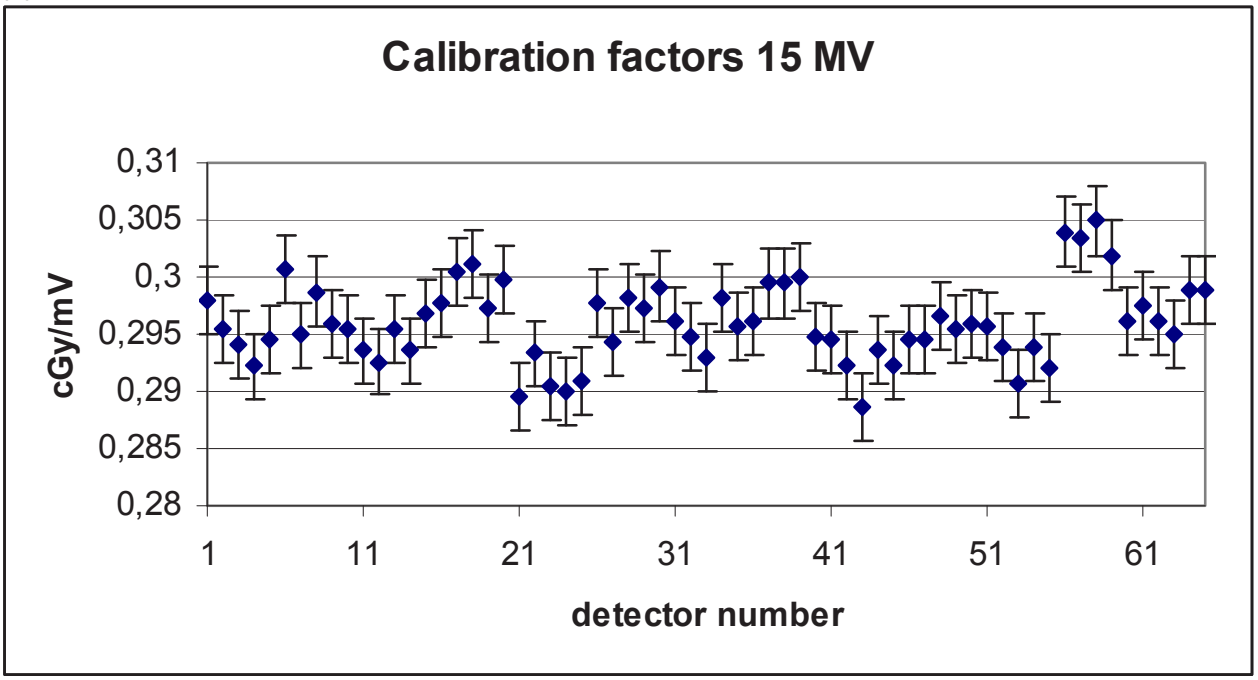

FIG. V–7. Calibration coefficients for MOSFET dosimeters for: (a) 6 MV X rays; (b) 15 MV X rays.

V–4.2. Intrinsic correction factors

V–4.2.1. Non-linearity dose response correction factor for MOSFET

The measurements of k_{lin} were performed under the reference conditions, in a similar way to the diode measurements. The MOSFET signal was measured for monitor units in the range of 25 to 200 MU in steps of 25 MU (the dose at d_{max} was in the range 40–300 cGy for 6 MV, and in the range 30–240 cGy for 15 MV). Results are shown in Table V–5.

TABLE V–5. THE NON-LINEARITY CORRECTION FACTOR FOR MOSFETs

MU	25	50	75	100	125	150	175	200
k_{lin} (6 MV)	1.006	0.999	1.000	1,000	0.995	0.994	0.990	0.980
k_{lin} (15 MV)	1.001	0.996	1.000	1.000	1.005	1.003	1.002	1.005

V–4.2.2. Energy correction factor

The energy correction factor was not measured. For each energy, a separate calibration coefficient was measured.

V–4.3. Beam dependent correction factors

V–4.3.1. Angle of incidence correction for MOSFET

A square field size of 30 cm was used. The signal was measured for 50 MU with the gantry at 45° (315°), 0°, 15°, 30°, 45°, 60° and 75°. For each angle, three measurements were made; M_0 and M_{ang} were the signals for 0° and the given angle.

The results are shown in Fig. V–8.

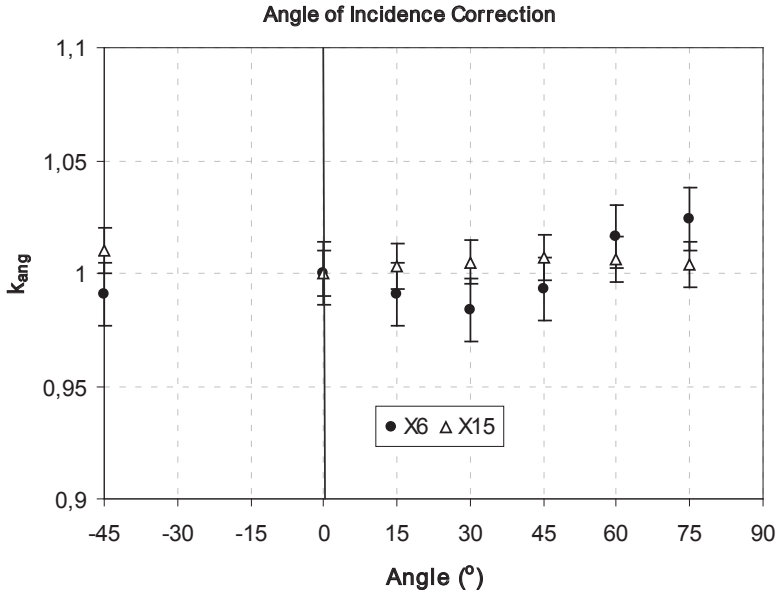

FIG. V–8. The k_{ang} for MOSFET dosimeters for 6 and 15 MV X ray beams.

V–4.3.2. SSD correction factor

Measurements were made for a 10 cm square field. 50 MU was delivered for each measurement. The dosimeters were placed on the solid water phantom. Measurements were made for six different source–surface distances: 75, 80, 90, 95, 100 and 110 cm.

For each SSD, measurements were repeated three times. Doses D_0 and D_{SSD} were calculated with the programme REF. The results are given in Table V–6.

TABLE V–6. MEASUREMENT AND CALCULATION RESULTS FOR SSD CORRECTION FACTORS

SSD (cm)	75	80	90	100	110
k_{SSD} (6 MV)	1.010	1.009	1.000	1.001	1.002
k_{SSD} (15 MV)	0.992	0.999	1.000	1.008	1.002

V–4.3.3. Field size correction factor for MOSFET

Measurements were made in the reference conditions. The dosimeters were placed on the surface of the solid phantom. Measurements were made for several square fields of 4, 5, 7, 10, 15, 20, 25, 30, 35 and 40 cm. 100 MU were delivered for each measurement. Three measurements were made for each field size. The results are given in Fig. V–9.

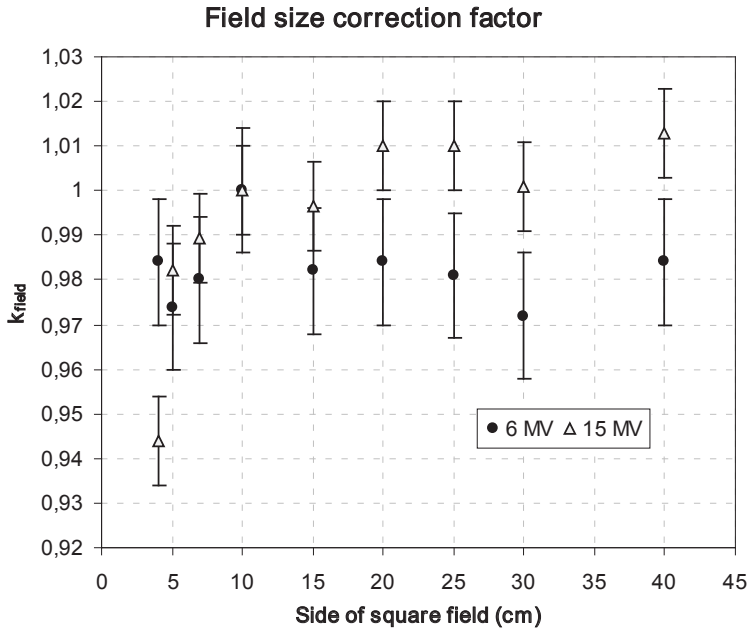

FIG. V–9. The k_{field} for MOSFET dosimeters for 6 and 15 MV X ray beams.

V–4.3.4. Wedge correction factor for MOSFET

Measurements were made in the reference conditions. The dosimeters were placed on the surface of the water solid phantom. Measurements were made for physical wedges of 15°, 30°, 45° and 60° and for an open field. For each measurement, 100 MU was delivered. Each measurement was repeated three times. The results are presented in Table V–7.

TABLE V–7. MEASUREMENT AND CALCULATION RESULTS FOR WEDGE CORRECTION FACTORS

Wedge angle (°)	0	15	30	45	60
k_{wedge} (6 MV)	1.000	1.012	1.008	1.000	1.007
k_{wedge} (15 MV)	1.000	1.008	1.004	1.009	1.010

V–4.3.5. Block and tray correction for MOSFET

The block and tray correction factors were not measured.

V–4.4. Clinical use of the measured corrections for MOSFET dosimeters

In practice, three correction factors were applied to MOSFET readings. All other correction factors are in the range 0.99–1.01, and there is no need to use them.

V–4.4.1. Calculation of entrance dose at d_{max} from MOSFET reading

The entrance dose for in vivo measurements is calculated as the product of the MOSFET signal, calibration coefficient and correction factor for field size only. The entrance dose is given by:

$$D = M \cdot N_{cal} \cdot k_{field} \tag{V–2}$$

V–4.5. Alderson Rando phantom measurements with MOSFETs

V–4.5.1. Pelvis

Entrance dose measurements were made for the three field geometry. Two treatment plans were used with the same beam arrangement as for diodes (see Section V–3.6).

The differences between the measured and TPS calculated doses were in the range 0.5–2.4%. The mean value of differences was 0.5%. In all cases, the manually calculated doses at d_{max} were smaller than the measured ones. The mean value of relative differences between the manually calculated doses and the MOSFET measured doses was −0.9%. In one case, the difference was larger than 3%.

V–4.5.2. Head and neck

The entrance dose was measured for the technique which used two parallel opposed 6 cm × 6 cm fields without wedges. Doses were calculated by the TPS XiO to deliver 100 cGy to the isocentre.

A very good agreement between the TPS calculations and measurements was obtained. The relative difference was always smaller then 1%. Similar results were obtained for computer and manual calculations.

V–4.5.3. Breast

The entrance dose was measured for two tangential opposed 10 cm × 18 cm fields with 30° wedges. Doses were calculated by the TPS XiO to deliver 100 cGy to the isocentre.

A very good agreement between the TPS calculations and measurements was obtained. The deviation was always smaller than 2%. Larger deviations between the manual calculations and measurements were obtained; however, they were smaller than 3%.

V–4.6. Patient measurements with MOSFETs

The results of in vivo measurements made in the year 2007 are presented for head and neck, thorax and pelvis. Because only a small number of patients with breast cancer were irradiated in 2007 (in our centre, mostly post-mastectomy patients are treated with the electron beam technique), the data for all patients treated in the thorax region are presented.

V–4.6.1. Head and neck measurements with MOSFETs

In total, 254 measurements with MOSFETs were made. All patients were treated with 6 MV X rays with conformal fields. The dose distributions were calculated with the XiO treatment planning system or with the TMS

Helax system. There were 100 and 154 measurements made for open and wedged fields, respectively. The mean difference between the measurements and calculations was −1.4%, with a standard deviation of 2.7%. In 23 cases, the deviations were larger than 5%. In this group, there were 18 cases where the wedge was used. In the HCC, the action level for wedged fields is 7%. This level was exceeded in two cases. In Fig. V–10, the distribution of deviations is shown.

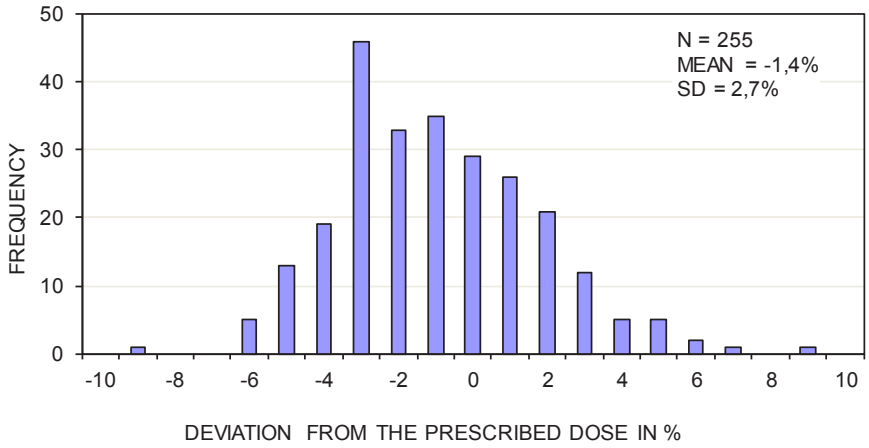

FIG. V–10. The deviation from the prescribed dose for head and neck patients measured with MOSFETs.

V–4.6.2. Thorax

MOSFET measurements were made for 155 fields. The data are presented for 15 MV X rays. All the patients were treated with conformal techniques. Almost all of the patients were suffering from lung cancer. The dose distributions were calculated with the XiO treatment planning system. There were 65 and 90 measurements made for open and wedged fields, respectively. The mean difference between the measurements and the calculations was −1.0%, with a standard deviation of 3.6%. In 19 cases, the deviations were larger than 5%. Wedge filters were used for 16 of these cases. The 7% wedge action level was exceeded in only one case. The distribution of deviations is shown in Fig. V–11.

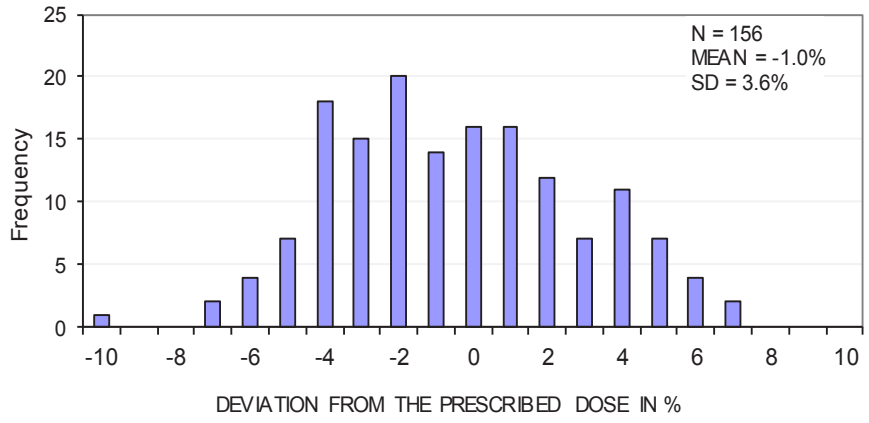

FIG. V–11. Deviations from the prescribed dose for thorax patients. Measurements were taken with MOSFETs.

V–4.6.3. Pelvis

In total, 1331 in vivo measurements were made with MOSFETs. The data are presented for 15 MV X rays. All patients were treated with conformal techniques, mostly with the box technique. Among this group there were patients with gynecological, rectal and prostate cancers. The dose distributions were calculated with the XiO treatment planning system. There were 684 and 647 measurements made for open and wedged fields, respectively. The mean difference between measurements and calculations was −0.4%, with a standard deviation of 3.6%. In 194 cases, the deviations were larger than 5%. In this group, the wedge was used in 167 cases. The action level for wedged fields of 7% was exceeded in 16 cases. In Fig. V–12, the distribution of deviations is shown.

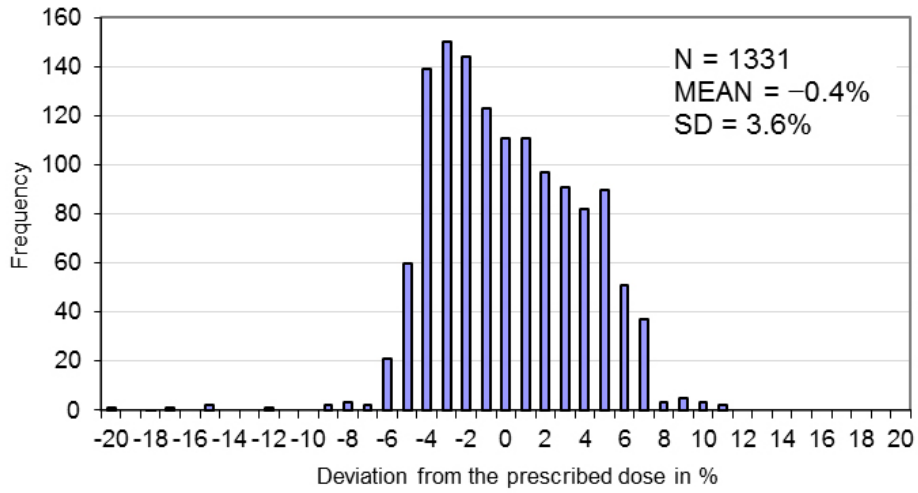

FIG. V–12. Deviation from the prescribed dose for patients treated in the pelvic region.

V–4.7. Discussion (MOSFET)

For more than four years, in vivo dosimetry with MOSFETs has been used as a method of checking the dose delivery. It is concluded that MOSFET dosimeters are good for in vivo measurements. Calibration is relatively simple, and the only correction factor needed is for field size. The correction factor for field size is pronounced only for very small fields. A disadvantage of this dosimeter is its relatively short lifespan. In HCC, a calibration of a new set of five dosimeters is carried out every three months. The procedure of calibration takes about three hours. Another disadvantage is its relatively large uncertainty, which increases when the measured signal is very small. It was also observed that for a typical signal measured, the uncertainty (1 SD) is about 1%. If the signal is smaller than 50 mV, the uncertainty increases to about 3%. For unknown reasons, the system gives erroneous readings from time to time.

The system is very simple to use and may even be used by inexperienced users. Due to their very small size, the MOSFET dosimeters may be used for other purposes, especially in high gradient regions.

Until now, more than 7000 measurements have been made at HCC. All patients were treated using the Lantis RV system. In six cases, a treatment preparation error was detected. All these errors occurred for procedures when the data for treatment were entered manually into the RV system. Two different action levels are used: the 5% for open and the 7% for wedged fields. The measurement data confirm the validity of using a larger action level for wedge fields. When a 7% rather than a 5% action level was used, the number of head and neck, thorax and pelvic patients whose measurements exceeded the action level reduced from 18 to 1, from 16 to 1 and from 167 to 16, respectively. It should be emphasized that no treatment preparation errors were detected in 2007.

V–5. RESULTS FOR IN VIVO DOSIMETRY IN BRACHYTHERAPY WITH MOSFET DOSIMETERS

In brachytherapy, the same Thomson & Nielsen MOSFET in vivo dosimetry system (TN-502 RD and MOSFET 20 reader) was used as for teletherapy so the characterization presented in this chapter of the report is limited to: (a) The calibration coefficients; (b) The temperature correction factor; and (c) The catheter correction factor.

V–5.1. MOSFET calibration

The calibration of MOSFET dosimeters was performed in the ^{60}Co beam and with the Ir-192 source. In each case, when the measurement was repeated several times, the result is represented by the mean value.

V–5.2. Calibration in a ^{60}Co beam

The calibration coefficients for ten MOSFET dosimeters (model TN-502 RD) were measured. The standard setting of the bias supply was used, i.e. the sensitivity of 1 mV/cGy. Measurements were made in the water phantom in the reference conditions. For each MOSFET dosimeter, two sets of measurements were made with the flat and with the bubble side towards the ^{60}Co beam. For each dosimeter, the measurements were repeated at least five times. The calibration coefficients *CF* were calculated from the equation:

$$CF = \frac{D_{10}}{M_{av}} \left[\frac{cGy}{mV}\right] \tag{V–3}$$

where D_{10} is the dose at 10 cm in the water phantom for a 10 cm × 10 cm field and M_{av} is the mean value of the MOSFET signal [mV]. Determination of D_{10} was made with a PTW 30003 ion chamber, and the UNIDOS electrometer was traceable to the Polish SSDL.

The CF values were calculated separately for the flat (CF_{flat}) and bubble (CF_{bubble}) sides. Finally, the calibration coefficient $N_{Co\text{-}60}$ for each single dosimeter was calculated as the average value of CF_{flat} and CF_{bubble}:

$$N_{Co-60} = \frac{CF_{flat} + CF_{bubble}}{2} \left[\frac{cGy}{mV}\right] \tag{V–4}$$

where CF_{flat} is the calibration coefficient for a MOSFET facing the flat side towards the beam, and CF_{bubble} is the calibration coefficient for a MOSFET facing the bubble side towards the beam.

In Fig. V–13, the calibration coefficients for all dosimeters are presented. The average values for flat and bubble sides were 0.897 ±0.010 and 0.853 ±0.010 cGy/mV, respectively. The calibration coefficient for the bubble side was 5% smaller than for the flat side. The standard deviation of the calibration coefficients calculated over all calibration coefficients was 0.023 cGy/mV.

V–5.3. Calibration with Ir-192 source

Calibration coefficients for the four MOSFET dosimeters (model TN-502 RD) were measured in the acrylic cylindrical afterloading phantom with an Ir-192 source. The standard setting of the bias supply was used, i.e. the sensitivity of 1 mV/cGy. The dosimeters were 8 cm from the source. The dose delivered to the dosimeters was measured with a Farmer ionization chamber connected to the UNIDOS dosimeter. The absorbed dose determined with ionizing chamber D_{IC} was calculated according to the procedure given in the manufacturer's instructions.

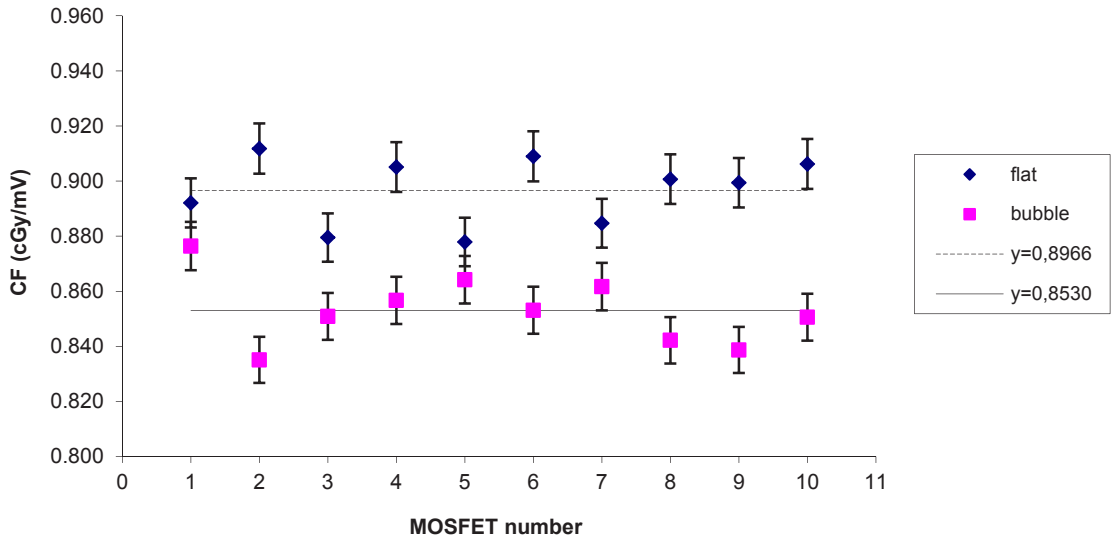

FIG. V–13. Calibration coefficients measured in the 60Co beam for 10 MOSFET dosimeters.

The measurements with MOSFETs were repeated three times. The measurements were taken with the MOSFET facing flat and the bubble side towards the source. The calibration coefficients were calculated with the following equation:

$$CF^{Ir} = \frac{D_{IC}^{Ir}}{M_{av}^{Ir}} \left[\frac{cGy}{mV}\right] \tag{V–5}$$

where D_{IC}^{Ir} is the dose measured with ionization chamber [cGy] and M_{av}^{Ir} is the average value of the MOSFET signal [mV].

The calibration coefficient for each dosimeter was calculated as the arithmetic average value of the calibration coefficients for both directions:

$$N_{Ir-192} = \frac{CF_{flat}^{Ir} + CF_{bubble}^{Ir}}{2} \left[\frac{cGy}{mV}\right] \tag{V–6}$$

where CF_{flat}^{Ir} is the calibration coefficient for a MOSFET with its flat side facing towards the source and CF_{bubble}^{Ir} is the calibration coefficient for a MOSFET with its bubble side facing towards the source.

Calibration coefficients for each dosimeter are shown in Table V–8.

TABLE V–8. CALIBRATION COEFFICIENTS FOR MOSFET DOSIMETERS MEASURED WITH THE ^{192}IR SOURCE

Dosimeter	A1	A2	A3	A4
Flat	0.854	0.715	0.869	0.833
Bubble	0.797	0.633	0.786	0.753
Average	0.825 ± 0.010	0.674 ± 0.010	0.8275 ± 0.010	0.793 ± 0.010

A much smaller calibration coefficient was obtained for dosimeter number A2. No explanation for this result was found. Therefore, for the comparison of the calibration coefficient for ^{60}Co and Iridium, this result was omitted. In Table V–9, the calibration coefficients for both energies are shown.

TABLE V–9. COMPARISON OF THE CALIBRATION COEFFICIENTS MEASURED IN THE Co-60 BEAM AND WITH THE IR-192 SOURCE

Dosimeter	A1	A3	A4
N Co-60 [cGy/mV]	0.884	0.865	0.881
N Ir-192 [cGy/mV]	0.826	0.828	0.792
Ratio	0.93	0.96	0.90

Note: The data for dosimeter 2 is omitted.

V–5.4. Temperature correction factor

The temperature dependence was determined in a wax phantom, which was initially heated to 38°C and after that cooled slowly. The measurements were performed in the ^{60}Co beam. The temperature dependence was measured for two dosimeters. The same treatment time was used throughout. For each temperature, three measurements were made. In Fig. V–14, the dependence of the signal on the temperature is shown.

In the range 36°C–38°C, the influence of the temperature on the MOSFET reading is negligible. This is consistent with the design of dual MOSFET dual bias detectors as described by Soubra et al. [V–1].

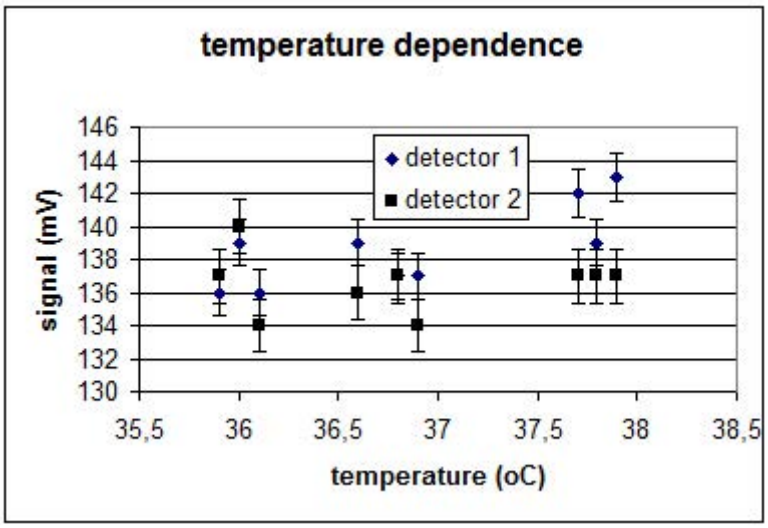

FIG. V–14. Temperature dependence of MOSFET dosimeters.

V–5.5. Catheter correction factor

For in vivo measurements in the rectum, dosimeters were placed in a plastic catheter (see Fig. V–3 in Section V–2.1.2). To determine the catheter correction factor, a series of measurements with and without the catheter were made. All the measurements were carried out in the water phantom using ^{60}Co radiation. The dosimeter was placed on the central axis of the beam at a depth of 10 cm in water. The SSD was 80 cm, and the

field was 10 × 10 cm^2. The dose delivered to the dosimeters was 100 cGy. The standard setting of the bias supply was used (sensitivity 1 mV/cGy). Two sets of six measurements for the situations with and without catheters were performed.

TABLE V–10. THE CATHETER CORRECTION FACTOR

B5 — flat	1	2	3	4	5	6	M_{av}	SD [mV]	K c
M without catheter	109	112	112	111	103	111	109.4	3.78	1.00
M with catheter	110	111	109	107	109	109	109.2	1.48	—

The catheter correction factor was calculated in an analogous way to the plastic-to-water correction factor (Eq. 4 in Section 4). The results of measurements of the catheter correction factor are shown in Table V–10. The influence of the catheter on the reading is negligible.

V–5.6. Phantom measurements

The measurements were carried out in a wax phantom using the interstitial applicators (needles) with the HDR ^{192}Ir source of the HDR Gammamed Plus. The measurements were repeated three times for three different rectal probes used in the treatment of the prostate. The position of the MOSFET dosimeters was defined radiographically. Two orthogonal radiographs, AP and LT, were made with the X ray mobile C-arm. The position of the dosimeters was reconstructed with the Abacus 3.1 treatment planning system, and the dose distribution was calculated. The measured values were compared with the calculated ones. The accuracy of the geometrical reconstruction of the position of the source and the dosimeter were estimated to be 1 mm. Therefore, the uncertainty of the dose calculation at the position of the source is approximately 10%. The results are shown in the Table V–11.

TABLE V–11. PERCENTAGE DIFFERENCE OF THE DOSES MEASURED WITH MOSFET DOSIMETERS AND CALCULATED DOSES

A–A1	A–A2	A–A3	B–B1	B–B2	B–B3	C–C1	C–C2	C–C3
4%	14%	1%	−1%	−7%	1%	20%	1%	13%

Note: The results are for three rectal probes, A, B and C, with three dosimeters each.

The ratios of the measured to calculated doses range from −7% to 20%, which is considered acceptable given the uncertainties involved.

V–5.7. Patient measurements

In the present report, measurement data for 25 patients are presented. In total, 121 measurements for 41 treatment fractions were performed with MOSFET dosimeters. The measurements were carried out for patients with prostate cancer treated with the HDR Gammamed Plus with ^{192}Ir sources. Comparison of MOSFET measurements and the dose calculated with the TPS Abacus 3.1 were performed for all measurements. The results presented in this report are for patients treated in 2004, 2005 and 2006.

The typical prescribed fraction dose was in the range 10 Gy to 15 Gy. Interstitial applicators (needles) were used for all cases. Three rectal probes with three MOSFET dosimeters were used. The average distance between needles and dosimeters was 2.3 cm. The position of the MOSFET dosimeters was obtained with two orthogonal radiographs, AP and LT, made with the mobile C-arm and Abacus 3.1 TPS. The radiographs are shown in Fig. V–15. Similar to the uncertainty of the phantom measurements, the uncertainty in distance between the radioactive source and the dosimeters was estimated to be 1 mm. Consequently, the uncertainty of the dose calculation at the

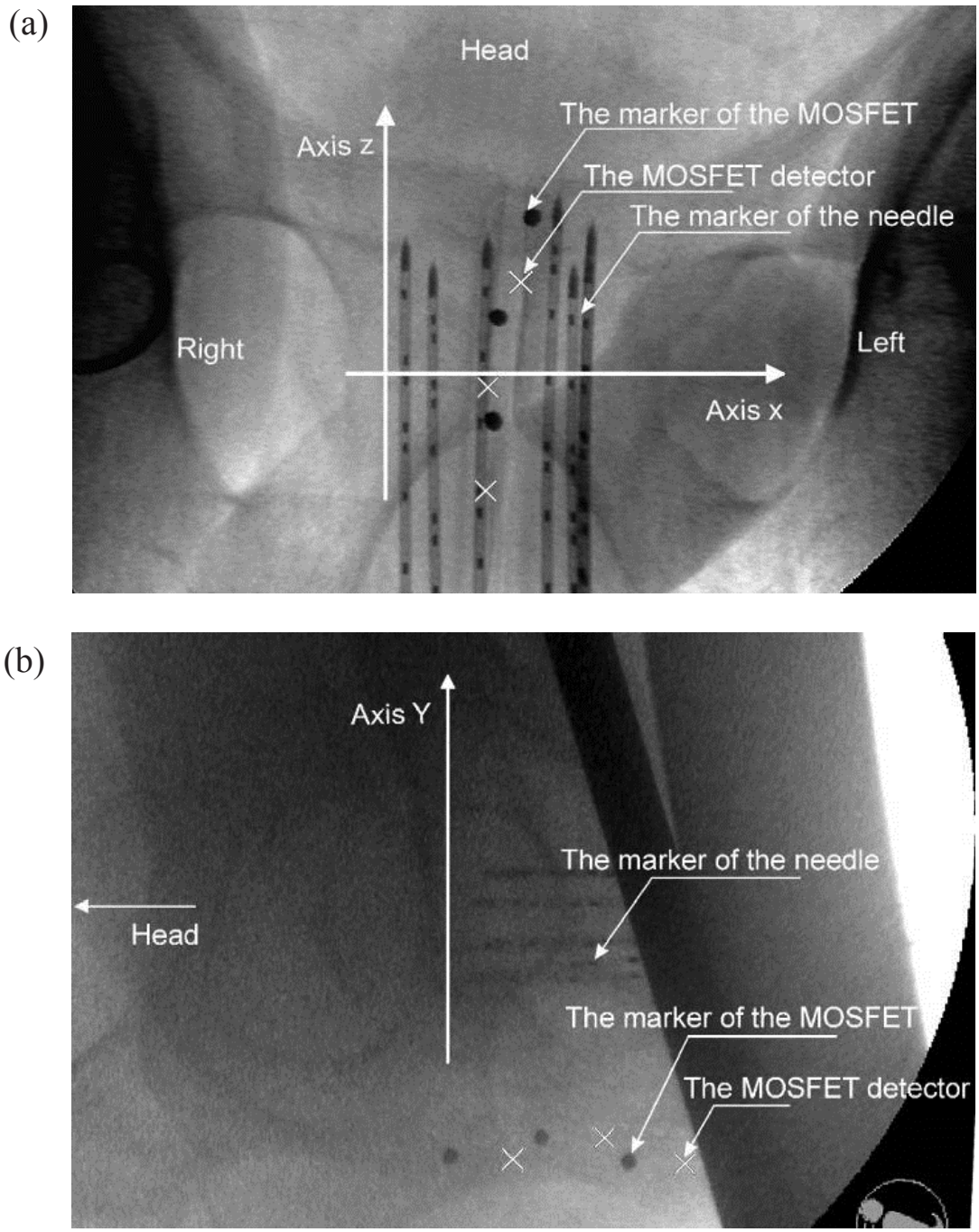

FIG. V–15. The AP and lateral (LT) radiograph.

position of a source is approximately 10%. The measured doses were compared with the calculated ones with the Abacus 3.1 treatment planning system. Only off-line comparisons were made.

V–5.7.1. Results

In Fig. V–16, the histogram of differences between measurements and calculations is presented.

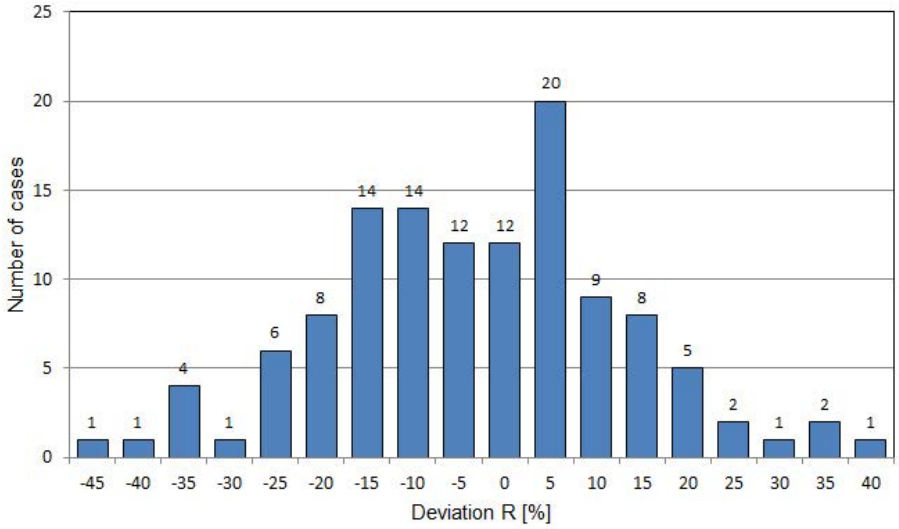

FIG. V–16. Histogram of differences between measurements and calculations.

The distribution of differences is symmetrical around zero with a mean value of 0.3%, so there was no systematic error. In approximately 50% of cases, the deviation was smaller than 10%, and in 80% of cases, the deviation was smaller than 20%. Only in 3 of the 120 cases was the deviation larger than 40%. In brachytherapy, the dose gradient is very steep, so much larger deviations may be expected than in teletherapy. Additionally, the position of the radioactive source with respect to the dosimeters was obtained from radiographs made before treatment. The actual position during treatment might not have been identical to the position at the time of the radiograph, which might have affected the measured dose. In Fig. V–17, the cumulative histogram of mean deviations (calculated over the three dosimeters from one probe) is shown.

In more than 15% of cases, the mean deviation between the measured and the calculated dose was larger than 20%. In less than 3% of the cases, the mean deviation was larger than 30%.

V–6. CONCLUSIONS

The MOSFET system has several characteristics well suited for in vivo dosimetry applied to brachytherapy applications. The main advantages are very high spatial resolution, fairly good angular characteristics and no temperature dependence. It allows the dose to be measured with an uncertainty of better than 3% (2 SD), which is well below the uncertainty required for brachytherapy. The disadvantages of the system used in this project are: (a) It does not allow the dose to be measured on-line; (b) The cost is relatively high due to the limited accumulated dose which may be measured with MOSFET dosimeters.

It is this group's opinion that at present there is no well-established procedure for in vivo measurements in brachytherapy, i.e. it is not clear what action levels should be used and what should be done if the action levels are exceeded. It is believed that research performed under this project will provide input to establish such procedures.

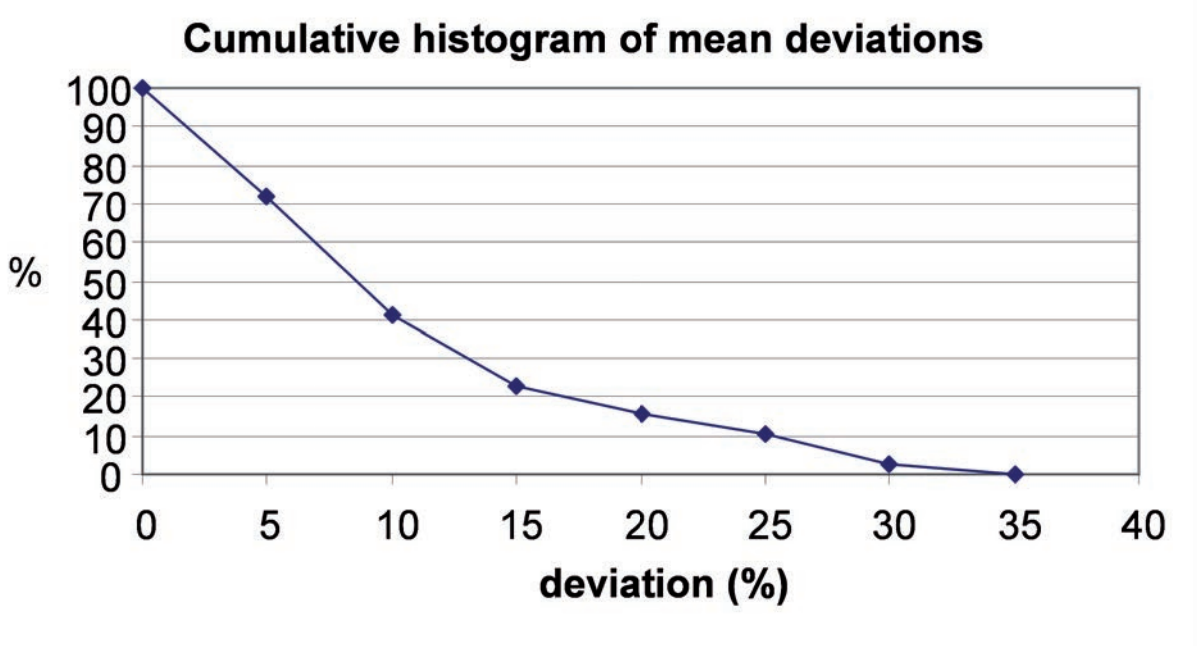

FIG. V–17. Cumulative histogram of mean deviations.

ACKNOWLEDGEMENTS

The authors gratefully acknowledge the PTW company for providing them with the VIVODOS system and dosimeters for the duration of this project. We also want to thank all colleagues participating in the project for their very good and friendly cooperation.

REFERENCE TO ANNEX V

[V–1] SOUBRA, M., CYGLER, J., MACKAY, G., Evaluation of dual bias dual metal oxide-silicon semiconductor field effect transistor detector as radiation dosimeter, Med. Phys. **21** (1994) 567–572.

Annex VI

UNITED KINGDOM — CHARACTERIZATION OF LANDAUER MICROSTAR OSL DOSIMETRY SYSTEM

M.J. AUSTIN, W.P.M. MAYLES
Clatterbridge Cancer Centre
Bebington, Merseyside, United Kingdom

Abstract

The commercial OSL system used in the CRP was investigated in terms of the dosimeter's early fading characteristic, the amount of stored dose lost per readout performed and the changeover between the two different stimulation light sources used to read low and high doses. It was found that 6 minutes must pass between irradiation and readout to allow for early fading of the OSL signal. Approximately 0.06% of the stored dose is lost per readout for dosimeters read out in the system's high dose mode. Finally, a steep transition was found in the OSL output when changing from one stimulation mode to the other. The system was found to be very simple and convenient to use, although reproducibility was found to be poor, and this was blamed on a possible mechanical problem with the dosimeter housing or the low power stimulation light that is used to read out dosimeters.

VI–1. INTRODUCTION

The Clatterbridge Cancer Centre (CCC) NHS Foundation Trust (Bebington, Wirral, UK) is the holder of a research agreement in relation to the CRP. The Centre has nine linear accelerators and a ^{60}Co unit that are used to treat around 6000 patients per year.

In vivo dosimetry has been used at Clatterbridge for many years for measurement of the dose to organs at risk and for total body irradiation. There is an ongoing programme to introduce routine in vivo dosimetry for QA purposes in order to comply with UK recommendations. Thermoluminescence (TL) dosimetry has been the primary dosimeter for organ at risk measurements, but diodes are being used for QA of treatments.

The in vivo programme is the responsibility of the physics department with both physicists and physics technicians being involved. Radiation therapy technologists operate the system for QA measurements, but other measurements are carried out by physics technicians.

An OSL reader was delivered to CCC for a short period of familiarization prior to being delivered to the participant in Croatia. This was to facilitate a more informed dialogue between the participants.

VI–2. MATERIALS AND METHODS

All experiments were carried out using the OSL system supplied by Landauer (Glenwood, Illinois, USA), consisting of a laptop for data acquisition, Landauer's fully portable Microstar OSL reader (manually operated model) and a set of Microstar 'Dot' dosimeters. The Dot dosimeters, as shown in Fig. VI–1, consist of a 7mm disc of α-Al_2O_3:C powder held between two sheets of plastic film and encased in a light-tight plastic housing measuring 25 mm × 12 mm × 2 mm.

The disc of powder is mounted on a sliding cassette, which is withdrawn from the housing once inside the reader and then illuminated by a bank of green LEDs for OSL measurement. To take a reading, a dosimeter is clipped into a plastic 'adapter', which is then placed into the reader drawer. The adapter is used to hold the dosimeter housing in position inside the reader as the sliding cassette is withdrawn and the LEDs are turned on.

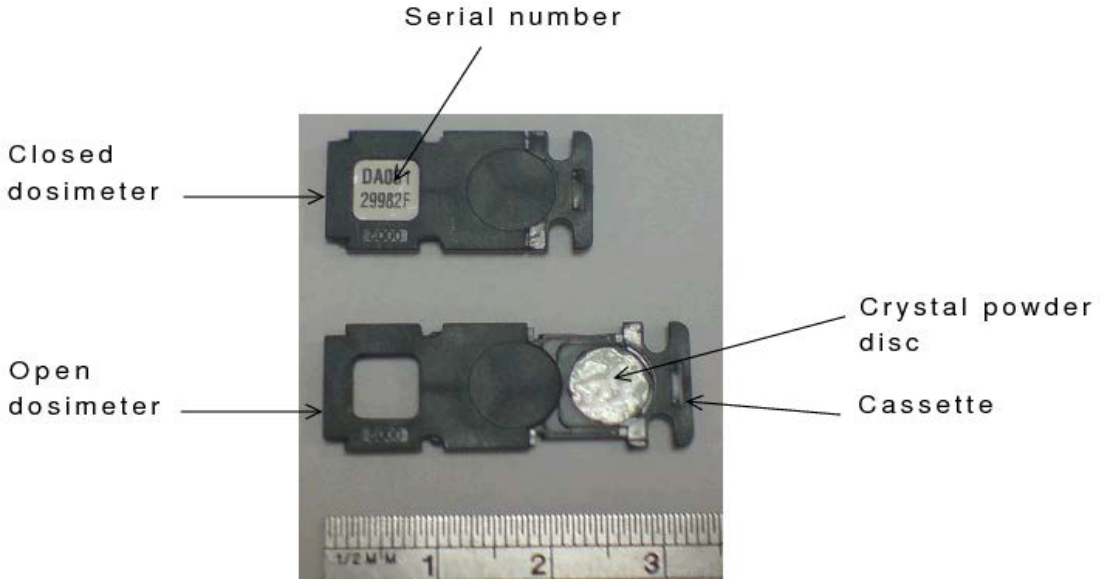

FIG. VI–1. Dot dosimeters. The upper dosimeter has its light tight casing closed, and the individual dosimeter serial number can be seen; the lower dosimeter has been opened to reveal the disc of α-Al_2O_3:C.

The reader has two modes of stimulation depending on whether a dosimeter has been given a high or low dose of ionizing radiation. All dosimeters are initially stimulated by a low power LED bank, and the initial OSL is monitored. If the dosimeter has absorbed a high dose, then this initial OSL will reach a certain threshold, and the low power stimulation light will then be used to take a full readout. If the dosimeter has only absorbed a low dose, then the initial OSL output will not reach the threshold, and the reader will switch on a higher power bank of LEDs so as to get a greater OSL signal from the dosimeter.

Different calibration coefficients are then used for each light source to convert output into a readout of dose. The calibration coefficients can be input into the reader by taking readouts from dosimeters with a range of known doses. However, without knowing details of any energy or dose dependency of the dosimeters, or, in fact, the dose below which the reader switches from using the low power to the high power stimulation, it was decided to use the system's default calibration and then calculate further calibration coefficients to be applied externally to the software.

After each irradiation and readout, another irradiation can be performed without annealing or bleaching the dosimeter. This means that the previously read out dose must be subtracted from each new readout to obtain a new dose.

All irradiations were performed at CCC using either the Theratron 780C ^{60}Co treatment unit or the Varian 2100c and Varian Clinac iX linear accelerators. All irradiations used 10 cm × 10 cm fields with solid phantoms with at least 10 cm of backscattering material and consisting of either stacked sheets of WT1 water equivalent material or Perspex at an SSD of 100 cm, as described by the common methodology in Section 4.

Where Perspex was used, a correction factor was applied to convert the dose to Perspex to a dose to water. The phantom was set up in each case so that the chamber inserted inside had its sensitive volume on the central axis of the beam, and the OSL dosimeters, placed on the phantom surface, were offset from the beam's central axis. The offset was decided on using pre-existing beam flatness scans so that the dosimeter was placed in an area where the beam at the surface was 'flat' relative to the central axis. Ionization chambers were set at depths according to the UK Institute of Physical Sciences in Medicine (IPSM) 1990 code of practice for photon dosimetry [VI–1] — that is, 5 cm for ^{60}Co γ rays, 6 MV X rays and 10 MV X rays and 7 cm for 15 MV X rays (some 6 MV irradiations were performed with the chamber at 7 cm due to availability of phantoms and in this instance an appropriate depth dose correction was used).

Buildup caps were supplied for analysis by the IAEA; 2 mm thick Al studs of diameter 9 mm were used for ^{60}Co γ irradiations and 2 mm thick Fe studs of diameter 9 mm were used for 6 MV X ray irradiations. X rays of energy 10 MV and 15 MV were also used in some experiments and these irradiations were performed at the relevant depth of dose maximum (d_{max}) under WT1 solid water sheets. In this case, 2 mm thick sheets of WT1 plastic water

were also placed at either side of the dosimeters to minimize scatter lost in the space between the WT1 sheets. This technique allowed two sides of the dosimeters to be bounded but left some gaps between the WT1 on the other sides. As a further measure to provide equal scatter conditions for all dosimeters with this set-up, an extra pair of dosimeters with buildup caps (or without, in the case of 10 MV and 15 MV irradiations) were placed at either end of each row of dosimeters. Correction factors, as described in the common methodology of Section 4, were applied where relevant.

Ionization chamber measurements were made by standard electrometers, and readings of charge were corrected by the absorbed dose to water factor $N_{D,w}$ for that chamber and electrometer (as supplied by the UK National Physical Laboratories (NPL) dosimetry chain). The temperature was monitored throughout experiments, and during no session did it leave the range 295–299 K.

At CCC, linear accelerators are calibrated to deliver 1 cGy per MU at d_{max} for a 10 cm × 10 cm field with 100 cm SSD. The tolerance on these measurements is generally ±2% and so to increase accuracy, a check on the machine output was performed before each experiment and the actual output 'on the day' used in all dose calculations.

It was discovered early on in the investigation that readouts appeared to be subject to significant random variations. To reduce this noise, it was decided that for each irradiation, five readouts would be taken and an average output calculated. Therefore, one of the most important factors to investigate was loss of dose stored in a dosimeter per readout performed. It was also found out at an early stage that when adapters were removed from the reader drawer, the dosimeters would be in slightly different positions, having become unclipped and slid by varying amounts out of the adapter (presumably when the dosimeter cassette was withdrawn inside the reader).

It was possible that these differences in the positioning of the dosimeters would contribute to signal variability; for example, if the dosimeter was not firmly clipped into the adapter, some of the dosimeter housing may obscure the powder disc from the light source or PMT. In the most extreme case, the entire dosimeter would completely slide out of the adapter when the reader tried to withdraw the cassette, and the stimulation light would only illuminate the dosimeter housing, hence giving a zero readout; this was observed frequently in a series of preliminary readouts. To solve this problem, it was decided that, even in between five successive readouts of the same dosimeter, the adapter would be withdrawn from the reader after each reading, and the dosimeter firmly clipped back in before being placed back in the reader drawer.

Before investigating the depletion of stored dose with readouts, it was necessary to find out how soon after irradiation a dosimeter could be read out. It was decided that it was important to separate early fading from the possibility of fading caused by repeated readouts, and so initially, 20 independent dosimeters were irradiated with 100 cGy using the Theratron ^{60}Co unit and then pairs of dosimeters were each read out once at various time intervals after irradiation. The time taken to irradiate and then retrieve the dosimeter meant that the earliest readout was at 40 seconds, and the experiment was continued until the final two dosimeters were read out at 36 minutes (2160 seconds).

To achieve a finer time resolution, pairs of dosimeters were irradiated, again with 100 cGy, and then successive readouts were performed on each dosimeter, allowing many readouts in a shorter time period. This experiment was repeated for four irradiation energies: ^{60}Co, 6 MV, 10 MV and 15 MV.

To investigate whether or not the readout process was non-destructive, two dosimeters were each irradiated with approximately 100 cGy of X rays at 6 MV. At least 85 successive readouts were then performed on each dosimeter. After one of the dosimeters had been read out 100 times, a 50 hour wait was observed before performing 20 further readouts, so as to rule out any fading effects coming from time rather than from the process of repeated readouts. Curves were fitted to the OSL output/readout data using robust non-linear regression analysis, made necessary by the occurrence of frequent outlying readings well below the trend. Results are only presented here for readings performed in high dose mode (i.e. with the low power stimulation light source).

The function used to model these data was of the form:

$$y = a \times b^x \tag{VI–1}$$

where y represents the OSL output after x readouts, a is the dose read at the first readout and $b = 1 – c$ where c is the proportion of dose lost per readout. This model comes from the work by Polf et al. [VI–2], who stated that the amount of charge stimulated from a trap in OSL is proportional to the amount of charge in that trap.

The changeover between the low and high power stimulation light sources was also investigated by irradiating groups of dosimeters in steps of 1 cGy of 6 MV X rays and taking a readout at each step. This allowed the average of three readouts per 1 cGy to be taken. The test was performed with doses from 1 cGy up to 20 cGy, at which point it was known that the system would have changed from high power to low power stimulation.

VI–3. RESULTS

VI–3.1. Early fading

Early fading of the OSL signal from Al_2O_3:C is not well documented in the literature. There is no indication from the OSL system's manufacturer of any need to wait after irradiation before reading a dosimeter, and only recently have reports emerged with evidence of early fading [VI–3].

Figure VI–2 shows preliminary results generated by reading independent dosimeters at varying times after irradiation with ^{60}Co γ rays.

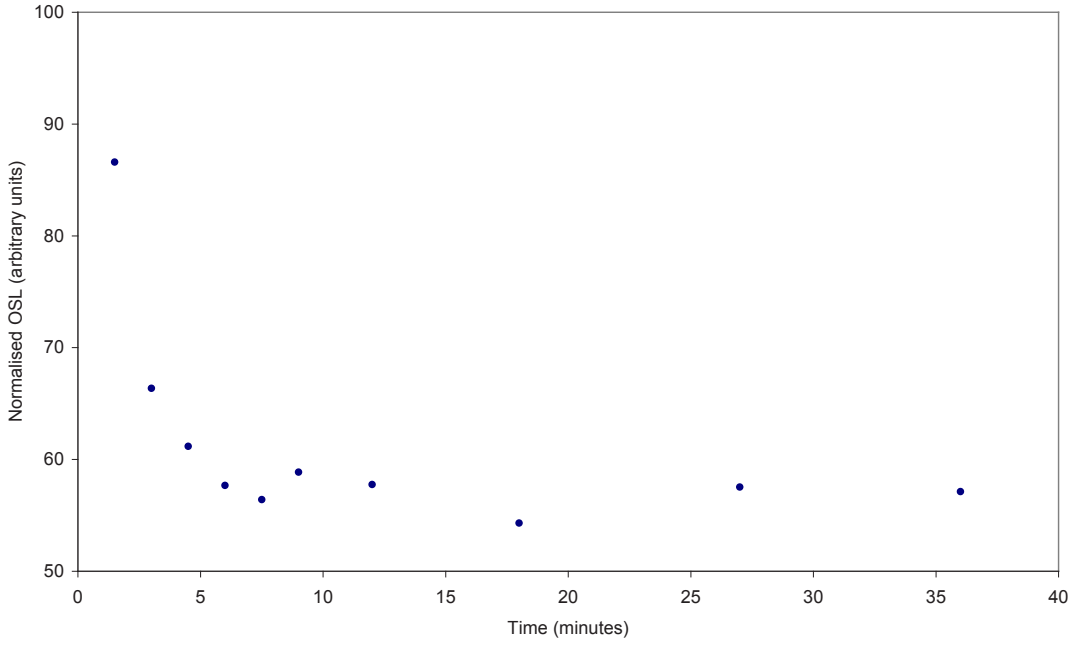

FIG. VI–2. Preliminary experiment on early fading with ^{60}Co irradiated dosimeters. Each point represents the average of two independent dosimeter readouts, which are normalized by the ionization chamber readout.

The graph clearly shows that the first readout, performed at 90 s after irradiation, is considerably higher than any subsequent readouts. The graph seems to suggest that a steady state value eventually settles after about six minutes. The variability of points after six minutes may suggest that there are sensitivity differences between dosimeters or that readouts are noisy. The value read out at 90 s is approximately 150% of the steady state value. These preliminary results, based on a single readout from different dosimeters, rule out the possibility that the profile is created by depleting the dose stored in the dosimeter by the readout process alone.

Assuming that the amount of charge located in shallow traps (responsible for early fading) decays exponentially, a function can be fitted to the early fading data with the form:

$$y = 1 + a \times e^{-\lambda x} \tag{VI–2}$$

where x is the time, a is a simple scalar value and y is the OSL output. The equation includes a + 1 term since the data are normalized to the steady state value. Non-linear regression using this function was performed for each

data set with starting values of $a = 1$ and $\lambda = 1/130$ s^{-1}. Regression analysis was used so that values at 90 s could be estimated for all cases and that an estimate of the half-life, $T_{1/2}$, of charge in shallow traps at room temperature could be calculated using:

$$T_{1/2} = \frac{\ln 2}{\lambda} \tag{VI–3}$$

These results are included at the end of this section.

To achieve a finer resolution on the time axis and to remove the possibility that different sensitivity values caused the higher readouts at early time points, single dosimeters were irradiated and read multiple times. Figure VI–3 shows successive readouts of two separate dosimeters irradiated with ^{60}Co γ rays.

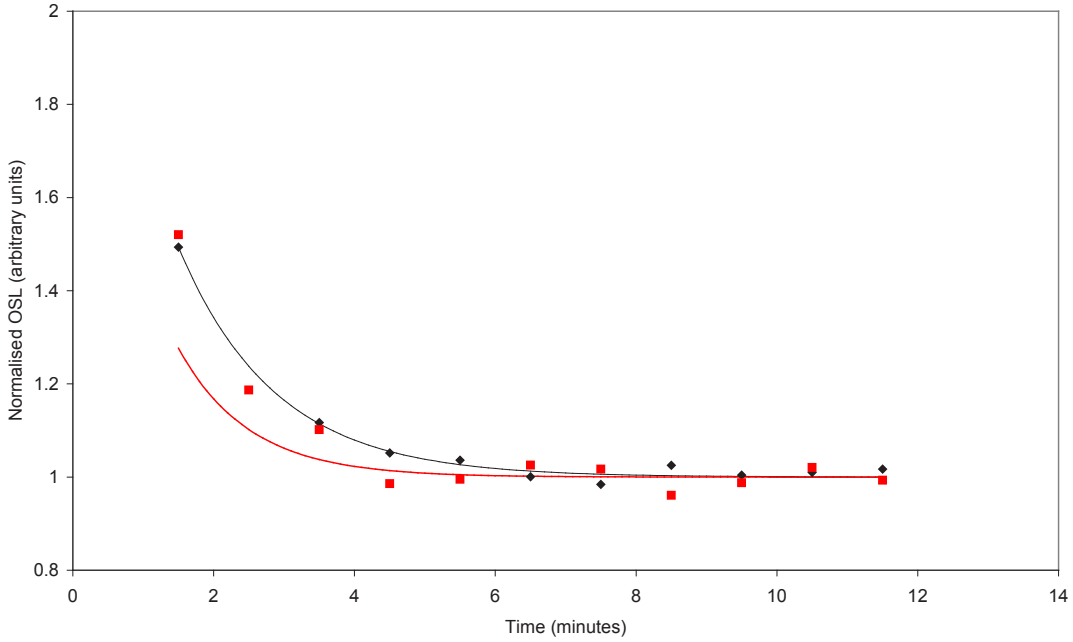

FIG. VI–3. Early fading from two independent dosimeters irradiated with ^{60}Co γ rays. Each point represents a single reading, normalized by the average of the final four values. Red data (squares), dosimeter A y = 1 + 2.317exp (−x/60.26); black data (diamonds), dosimeter B y = 1 + 1.477exp (−x/82.14).

The graph clearly shows the steady state value after approximately 360 s, which is around 66% of the 90 s readout (or, the 90 s readout is approximately 150% of the steady state). Dosimeter A had a value of 1.52 at 90 s and dosimeter B was 1.49. The datasets from each dosimeter show good agreement although both further demonstrate variability in readouts. Further experiments were conducted at different energies in case the effect of early fading had some energy dependence.

Figure VI–4 shows the same experiment performed with 6 MV X rays. It shows that the steady state value may, in this case, be achieved slightly earlier than 360 s although it is difficult to say exactly when, and a 360 s wait after irradiation would again seem appropriate. The agreement between the two different datasets is not particularly good in the early portion of the graph, with dosimeter C having lower readings in the region of early, rapid decay. This would suggest that this dosimeter trapped less charge in shallow states than dosimeter D, or less of the charge leaking away caused luminescence, although both dosimeters appear to achieve a steady state value at the same time. The 90 s readout from dosimeter C was estimated from the regression function as 1.22 and from dosimeter D as 1.37.

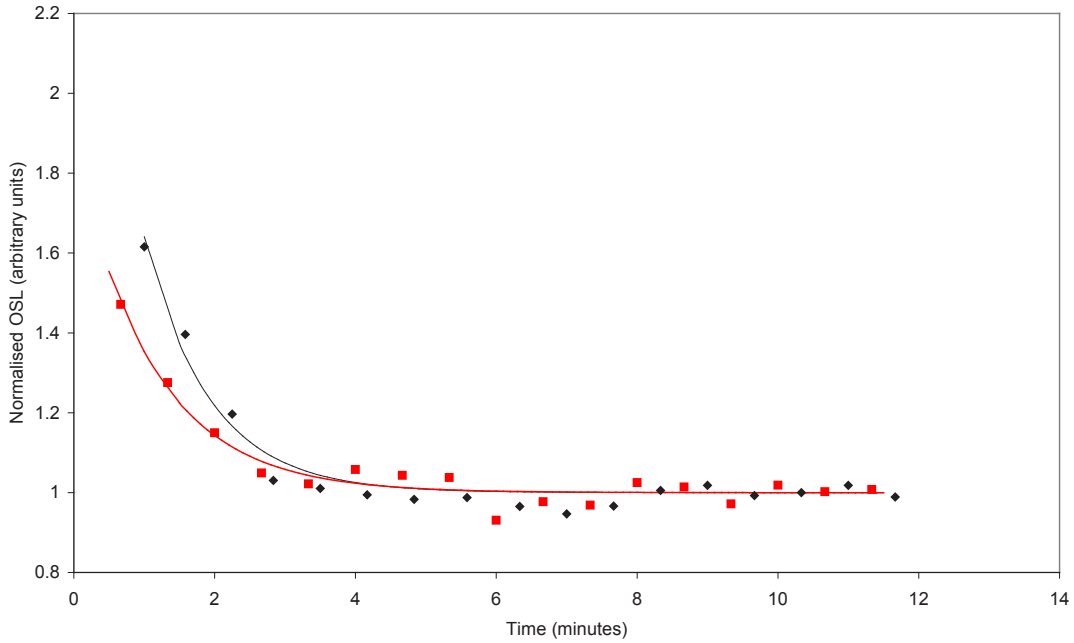

FIG. VI–4. Early fading from two independent dosimeters irradiated with 6 MV X rays. Each point represents a single reading, normalized by the average of the final four values. Red data (squares), dosimeter C y=1+0.8687exp(-x/66.57); black data (diamonds), dosimeter D y = 1 + 1.881exp(−x/55.70).

Figure VI–5 shows the early fading data from dosimeters irradiated at 10 MV. This graph suggests that 360 s would be a suitable time to wait before assuming that shallow trapped charge had disappeared. Unlike Fig. VI–4, the datasets match very well, and the regression functions are almost laid over one another. The 90 s readout from dosimeter F was estimated from the regression function as 1.41 and from dosimeter E as 1.43.

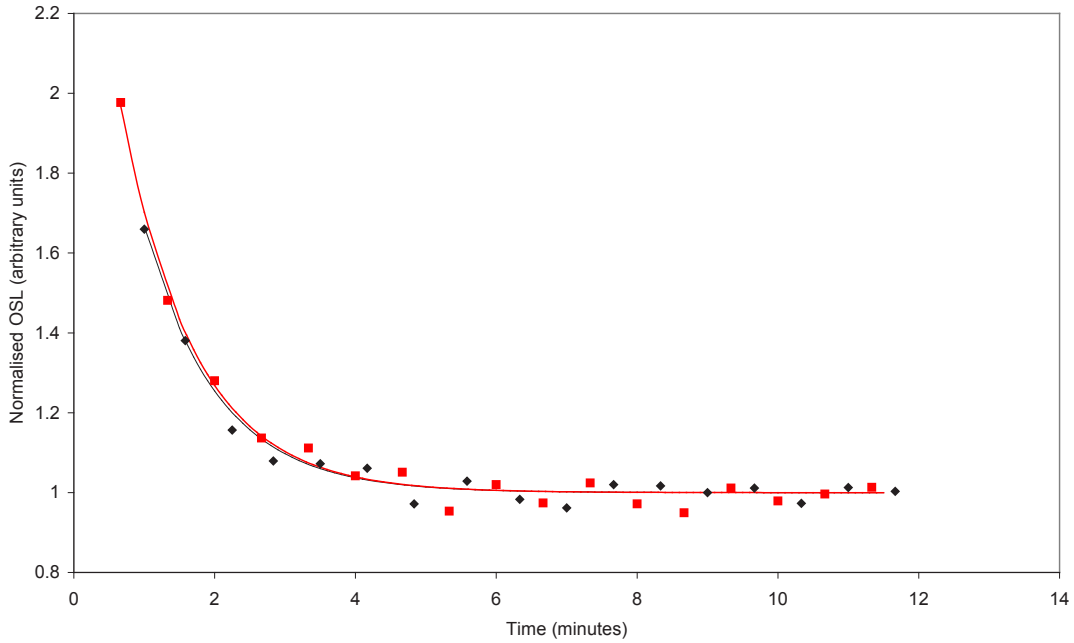

FIG. VI–5. Early fading from two independent dosimeters irradiated with 10 MV X rays. Each point represents a single reading, normalized by the average of the final four values. Red data (squares), dosimeter E y = 1 + 1.835exp(−x/62.47); black data (diamonds), dosimeter F y = 1 + 1.746exp(−x/62.33).

Figure VI–6 shows the data for dosimeters irradiated with 15 MV X rays. Once again, 360 s would seem like a suitable wait time after irradiation before performing any readouts. The fitted functions are in good agreement with one another. The 90 s readout from dosimeter G was estimated from the regression function as 1.47 and from dosimeter H as 1.47.

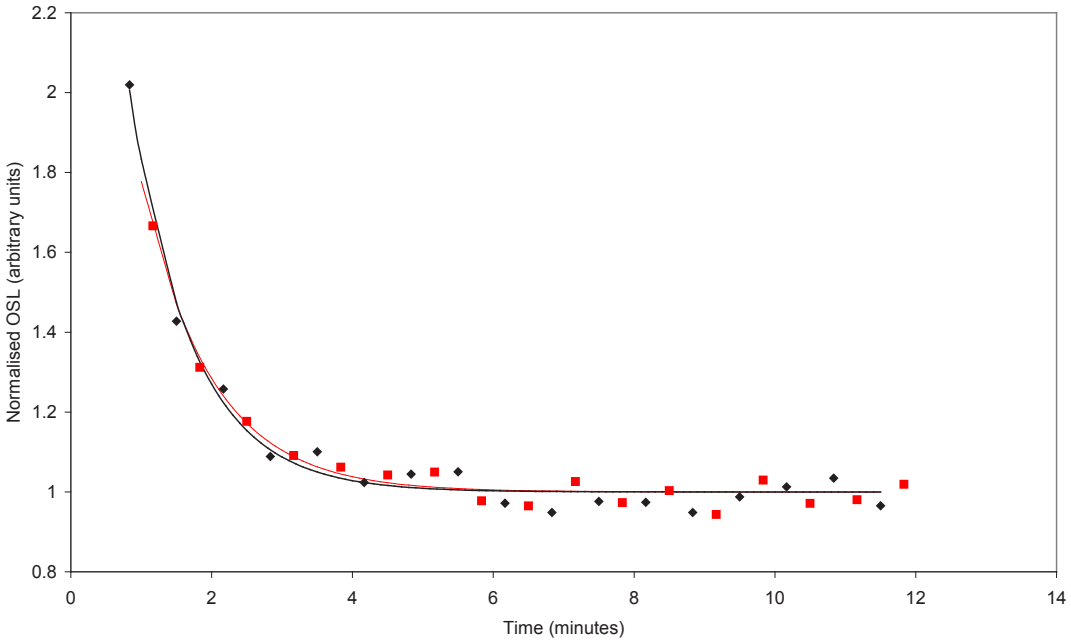

FIG. VI–6. Early fading from two independent dosimeters irradiated with 15 MV X rays. Each point represents a single reading, normalized by the average of the final four values. Red data (squares), dosimeter G $y = 1 + 2.125\exp(-x/59.67)$; black data (diamonds), dosimeter H $y = 1 + 2.573\exp(-x/53.25)$.

Table VI–1 summarizes the results from the early fading investigation. The value of *a* is an estimation by regression analysis of how much charge is trapped in the shallow traps at time zero. These values seem slightly erratic; for example, values for dosimeter A and B (both irradiated with ^{60}Co) are quite different. By referring back to Figure VI–3, the function for dosimeter A can be seen to be rather steeper than that for dosimeter B, possibly because of some particularly low values around 240–300 s, at the heel of the curve. The fact that each datapoint is just a single readout explains this variability, reflected in the width of the 95% confidence intervals for each value of *a*. Therefore, it is perhaps not prudent to draw serious conclusions from the values of *a*, although there is a suggestion that at 15 MV, there is a greater response from the shallow traps than at other energies.

VI–3.2. Dose depletion per readout

Figures VI–7 and VI–8 display graphs showing the OSL output from two independent dosimeters over a series of readouts with robust non-linear regression fits.

The raw data from these experiments was found to be skewed towards low readings; this can be seen by the large number of points below the main trend of values on each graph and few points above the main trend. Conventional least squares fitting of functions to non-normal data, especially severely skewed data as in this instance, is inappropriate. This is because the distance of outlying points from the mean is emphasized by the squaring operation and so the fitted function is biased towards outliers. Therefore, as already mentioned, robust non-linear regression was used, which places less emphasis on outlying values. An alternative approach would have been to linearize the data, but this method was not favoured since little was known about the true variability of the data.

TABLE VI–1. SUMMARY OF EARLY FADING RESULTS

	^{60}Co		6 MV	
Dosimeter	A	B	C	D
a	2.31	1.48	0.87	1.88
95% CI*	1.60–3.03	1.27–1.68	0.67–1.07	1.33–2.43
1/λ	60.26	82.4	66.57	55.7
95% CI	49.43–71.08	73.30–90.99	50.64–82.50	44.01–67.39
$T_{1/2}$ (s)	41.77	57.12	46.14	38.61
90s value	1.52	1.49	1.22	1.37
	10 MV		15 MV	
Dosimeter	E	F	G	H
a	1.75	1.83	2.12	2.57
95% CI	1.41–2.08	1.62–2.05	1.59–2.66	2.10–3.05
1/λ	62.33	62.47	59.67	53.25
95% CI	53.16–72.51	55.27–69.67	49.51–69.84	45.29–61.21
$T_{1/2}$ (s)	43.2	43.3	41.36	36.91
90s value	1.41	1.43	1.47	1.47

* CI — Confidence interval.

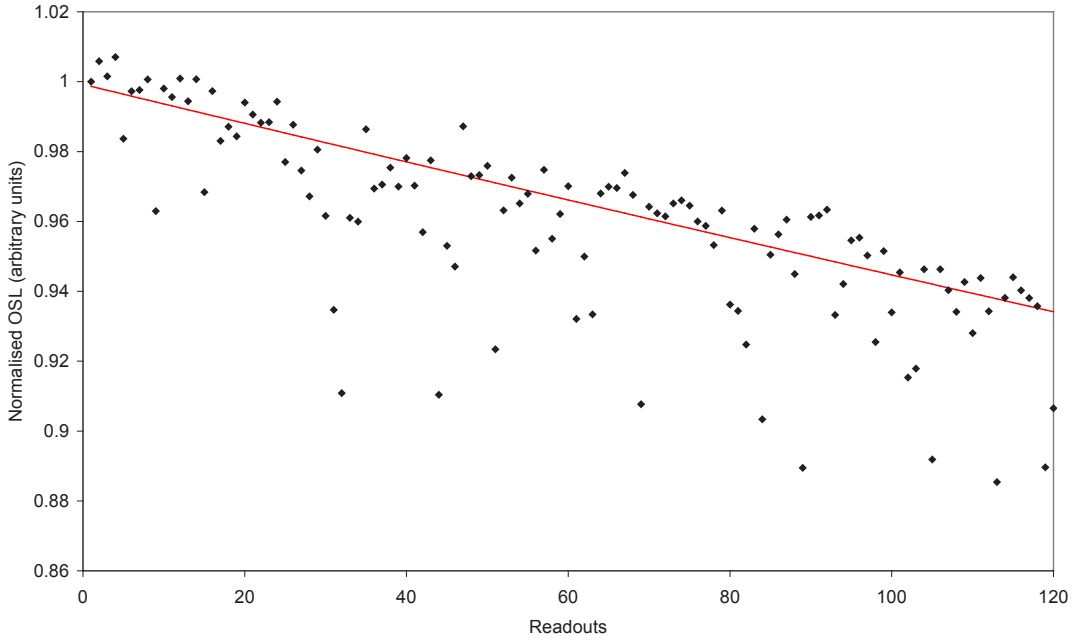

FIG. VI–7. Dosimeter X. OSL output over a series of 120 readouts. A 50 hour wait was observed between the 100th and 101st readout to exclude the possibility that the downward trend was caused by time based signal fading. Non-linear regression fit is $y = a \times b^x$ where a = 0.9992170 and b = 0.9994392.

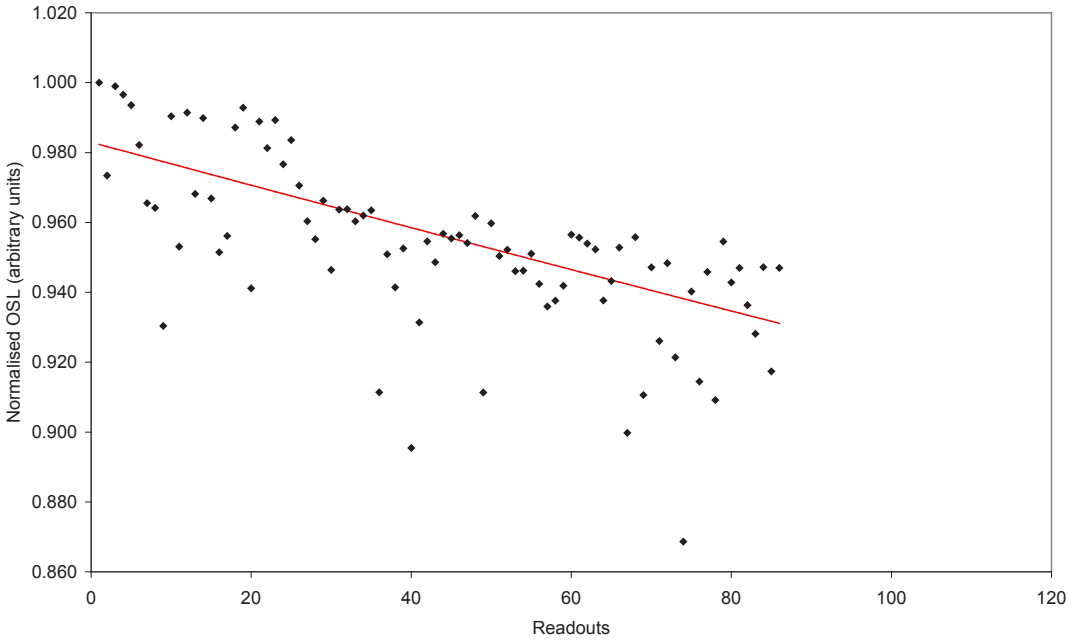

FIG. VI–8. Dosimeter Y. OSL output over a series of 85 readouts. Non-linear regression fit is $y = a \times b^x$ *where* $a = 0.9829452$ *and* $b = 0.9993703$.

The experiments give an approximate figure for the loss of dose as 0.06% per readout. Unfortunately, the robust algorithm does not allow for any statistical measures of accuracy, such as the standard error on the regression coefficients. It can be seen from the general appearance of the graph that the fit of the data to the model is not particularly good, although this seems more likely due to poor reproducibility of readouts than a poor model. Therefore, if dose depletion per readout is an important factor for a certain investigation, it should be ascertained more precisely.

One possible explanation for the negatively skewed results and poor reproducibility that has been observed so far is the occasional occurrence of 'bad' openings. These openings, where the disc of powder is partially obscured from the stimulation light and/or PMT by the dosimeter housing, would give low readouts and are known to occur. However, the frequency of occurrence is not known, and so it is unclear how significant a factor this is.

VI–3.3. Low and high power light source comparison

As previously mentioned, it was decided to use the reader's default calibration values for the two different stimulation light sources and apply extra calibration factors outside the system. However, it was not known at what point the calibration coefficients would differ. The default calibration coefficient is 1 for dosimeters irradiated with a low dose (and hence read out with the high power stimulation) and 15 for dosimeters irradiated with a large dose (read out with low power stimulation).

Figure VI–9 shows the continuity of reader output over a range of doses from 1 cGy to 20 cGy. Separate regression lines have been fitted above and below the step, and these were joined by a straight line to demonstrate the step more clearly.

The reader mode changed from low dose to high dose in between doses of 16 cGy and 17 cGy, although the boundary was not clear; one dosimeter irradiated with 16 cGy was read out four times in low dose mode and on the fifth occasion in high dose mode and two dosimeters irradiated with 17 Gy had their second and fourth readouts, respectively, performed in low dose mode.

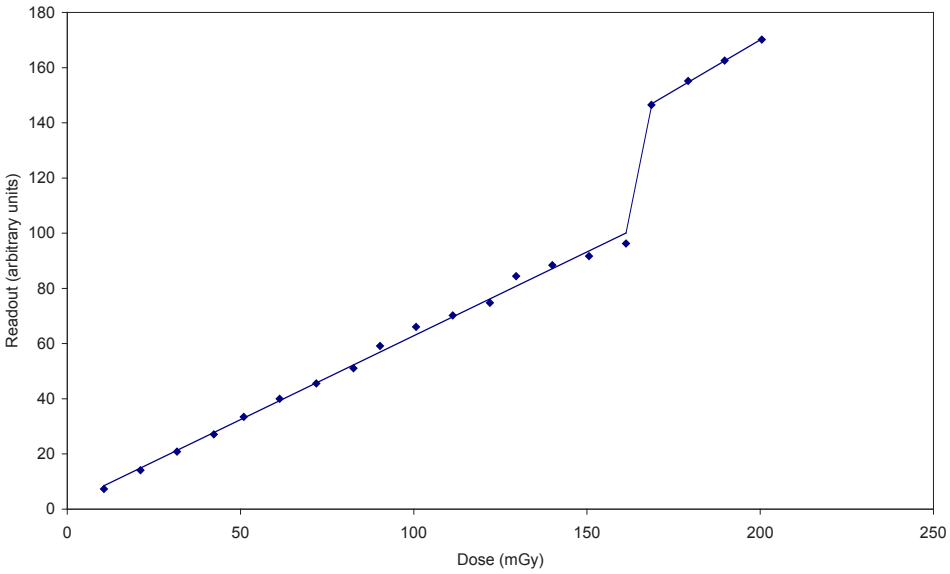

FIG. VI–9. Continuity of readouts from dosimeters irradiated with doses between 10 mGy and 200 mGy 6 MV X rays. The step in the response clearly shows where the stimulation switches from high power to low power and suggests that the default calibration coefficients are not matched between the stimuli for this energy of irradiation.

If the high dose calibration coefficient of 15 is removed, then the slope to the right hand side of the step would be smaller, and the absolute values would of course be less. This factor of 15 therefore makes the high dose dosimeters appear more sensitive: The gradient of the high dose mode linear regression was 0.80 (OSL/mGy), and the gradient of the low dose mode linear regression was 0.63 (OSL/mGy). If the factor of 15 is removed, giving a new gradient of 0.05, it can be estimated that the low dose stimulation light source is approximately 13 times more powerful than the high dose mode light source.

VI–4. DISCUSSION

VI–4.1. Characteristics of dosimeters

VI–4.1.1. Early fading

The early fading investigation showed the recently discovered [VI–3] characteristic of early fading from α-Al_2O_3:C when irradiated with megavoltage photons. This early fading effect means that at least 6 minutes must be allowed between irradiation and readout. The function used to model the early fading fitted the datapoints well and provided an approximate half-life of charge stored in the shallow traps responsible for early fading of 44 s.

The early fading is a result of charge either stored in (during irradiation) or transferred to (after irradiation) shallow trapping states, which allow the charge to leak away slowly at room temperature and recombine with F^+ centres to create F centre luminescence (wavelength 410 nm). It can be assumed that it is F centre luminescence being detected since the optical filtering in the reader should only allow wavelengths close to 410 nm to pass.

To learn more about the shallow traps, early fading could be investigated at different temperatures, since all results in this investigation were taken between 295 K and 299 K, and this was not considered a large enough range to alter the shallow trap characteristics. At higher temperatures of irradiation, the shallow traps would be less able to trap charge and so the magnitude of the fading would be less. Furthermore, the temperature during readout could be reduced to a point such that no early fading is observed. If the temperature of readout was increased, then an increase in the intensity of the fading signal may be observed due to an increase in probability of radiative recombination of exiting charge [VI–4].

The early fading does not depend on how many readouts are performed in the first 360 s after irradiation. This is known since stable signals have been read out after 360 s with no prior readouts. In fact, Polf et al. [VI–2] showed that there are shallow traps in Al_2O_3:C that are sensitive to thermal stimulation but not to optical stimulation.

It may be interesting to investigate the early fading of dose at a range of different doses. Kortov et al. [VI–5] found that a shallow trap with a TL peak at 350 K could store charge that was proportional to the dose up to 17 cGy, but then the trap appeared to saturate. The shallow trap observed in this investigation may be different from the 350 K TL trap or may be the low temperature tail of the same trap. If the trap could store charge proportionally to dose then the shallow trap itself could be used for dosimetry, meaning that measurements could be taken without the need for stimulating light. If the trap did saturate at a low dose, then this would only be useful for very small doses.

VI–4.1.2. Dose depletion per readout

The dose depletion investigation found estimates for the depletion of dose per readout in high dose mode. In high dose mode, approximately 0.06% of the overall dose is lost per readout. According to Polf et al. [VI–2], the depletion should be proportional to the laser power and so if the experiment were to be repeated with the reader in low dose mode, then a higher degree of depletion should be observed, and the difference between the stimulation powers was estimated as a factor of 13. However, different levels of noise on signals of different magnitudes may mean that this factor of 13 does not apply exactly.

To extend the study of dose depletion, successive readouts could have been performed on dosimeters irradiated with different doses. This would have tested the observation by Akselrod and McKeever [VI–6] that the same proportion of dose depletes per readout regardless of the overall dose. By examining the process of dosimeter sensitization with increasing dose, it can be rationalized that the proportion of dose depleted should be the same regardless of dose; The sensitization occurs when deep electron traps become full and so become less competitive with F^+ centres as recombination sites. This means that a greater signal is read out at higher doses because more of the charge leaving the main dosimetric trap (MDT) recombines radiatively and not because a different amount of charge leaves the MDT. The amount of charge leaving the MDT is effectively the magnitude of depletion, and so this should then be constant for constant stimulation power [VI–2]. The only factor that could change the dose depletion would be if the probability of optically stimulating the MDT changes according to how full the MDT is. This could perhaps be tested by Monte Carlo simulation, which may provide a more definitive depletion correction factor. A simpler way to increase accuracy would have been by performing a longer chain of successive readouts.

It was found via the dose depletion investigation that repeated readouts are not distributed normally around a regression function, with a strong negative skew of residual values. This was blamed on so-called bad openings, in which the dosimeter housing is not firmly clipped into position in an adapter insert and can come loose and obscure part of the dosimeter powder from the stimulation light and/or PMT (It is understood that Landauer have since improved this function). Robust regression was used, and this was very useful in fitting regression functions that could be seen to fit the majority of datapoints appropriately.

It would also be interesting to be able to open a dosimeter within the reader and take an OSL readout and then not close the dosimeter as normal but rather keep the powder disc in exactly the same position for a series of readout repetitions. This would remove any question of dosimeter placement being consistent and would also remove the effect of bad openings, allowing the true standard deviation of successive readouts to be established.

VI–4.1.3. Low and high power light source comparison

While it should be standard practice to calibrate the output of an in vivo dosimetry system (i.e. not use the default calibration coefficients), it is still important to know at what dose the calibration coefficients must change. Furthermore, the changeover from low dose mode to high dose mode was found to have a slightly blurred edge, with some dosimeters being automatically read out in different dose modes. This could be a problem if a dose is measured in the region of transition and this region, for 6 MV X ray irradiation, is between 16 cGy and 17 cGy. It is also important to recognize that the position of the step in Fig. VI–9 would change depending on the energy of irradiation or indeed any other factor that may change the sensitivity of the dosimeters.

The difference in the power of the stimulation light sources should also be identifiable by the amount of dose lost by a dosimeter per readout if a dosimeter irradiated with only a small dose were repeatedly read out. Compared to the previously discussed loss of dose, where high dose mode was used, dosimeters irradiated with a low dose will lose a greater proportion of their stored dose since the stimulation power is higher.

This raises the interesting question as to whether or not a higher powered light source should be used for all readings. This would come at the expense of non-destructive readouts but, since more charge would be stimulated from trapping levels within the dosimeter leading to greater luminescence intensity, then Poisson statistics would suggest that a more reproducible readout could be obtained.

VI–4.2. Resources

All measurements were performed out of hours on the clinical machines at CCC and took less than one month. The system used was loaned to the centre by Landauer Europe (Oxford, UK), a subsidiary of Landauer. The equipment is extremely easy to set up and use and, although this is not a case of routine use, it should not take an unreasonable time to integrate into routine use since it requires minimal training to operate.

The system benefits from its portable nature in that it can fit almost anywhere, including on a small office desktop. However, its disadvantage is that it has little automation, and so reading a number of dosimeters at a time can be a lengthy procedure and requires operator control throughout.

VI–5. CONCLUSION

Many thanks to the staff at Landauer and the IAEA for their provision of equipment and support during this investigation.

This investigation has provided some interesting and important points about using the OSL system despite only including measurements on non-anthropomorphic phantoms.

A minimum of 6 minutes must pass between irradiating a dosimeter and performing a readout to allow for the effects of charge leaking from room temperature unstable traps within the dosimeter crystal. This time does not change for irradiation energies between ^{60}Co and 15 MV.

It was also found that approximately 0.06% of stored dose is lost per readout performed in high dose mode. This has implications if dosimeters are to be repeatedly irradiated and read out and so needs to be kept in mind.

An unmatched transition between low and high dose mode was found in the region of 16 cGy to 17 cGy for 6 MV irradiated dosimeters. Although a transition like this can be dealt with easily by external calibration factors, care is required in the region of the change since some dosimeters may not be read out with the same stimulation light source on repeated readings.

Overall, the system was found to be extremely easy and quick to use, with the convenience of portability and low demands on space. However, in our hands the system had poor reproducibility, and it was suggested that this may be due to a mechanical problem with the dosimeter housing, where dosimeters do not attach securely enough to adapters that are used to hold them in the reader, and also due to the fact that only a small fraction of the overall dose is actually read each time, leading to poor Poisson counting statistics. As reported elsewhere, the reproducibility problems were improved during the course of the CRP by very careful operation of the reader dial and the use of five repeat readings. Some improvements to the adapter were made by Landauer.

REFERENCES TO ANNEX VI

[VI–1] LILLICRAP, S.C., OWEN, B., WILLIAMS, J.R., WILLIAMS, P.C., Code of practice for high-energy photon therapy dosimetry based on the NPL absorbed dose calibration service, Phys. Med. Biol. **35** (1990) 1355–1360.

[VI–2] POLF, J.C., YUKIHARA, E.G., AKSELROD, M.S., MCKEEVER, S.W.S., Real time luminescence from AL_2O_3 fibre dosimeters, Rad. Meas. **38** (2004) 227–240.

[VI–3] JURSINIC, P.A., Characterization of optically stimulated luminescent dosimeters, OSLDs, for clinical dosimetric measurement, Med. Phys. **34** (2007) 4594–4604.

[VI–4] MARKEY, B.G., MCKEEVER, S.W.S., AKSELROD, M.S. AND BØTTER-JENSEN, L., The temperature dependence of optically stimulated luminescence from Al_2O_3:C; Rad. Prot. Dos. **65** (1996) 185–189.

[VI–5] KORTOV, V.S., NIKIFOROV, S.V. AND SADYKOVA, É.Z., Competing processes with participation of shallow traps in anion-defective aluminium oxide, Rus. Phys. J. **49** (2006) 221–224.
[VI–6] AKSELROD, M.S. AND MCKEEVER, S.W.S., A radiation dosimetry method using pulsed optically stimulated luminescence, Rad. Prot. Dos. **81** (1999) 167–176.

CONTRIBUTORS TO DRAFTING AND REVIEW

Austin, M.J.	Clatterbridge Cancer Centre, United Kingdom
Bergstrand, E.S.	University of Oslo and the Norwegian Radium Hospital, Norway
Bokulic, T.	Sestre Milosrdnice University Hospital, Croatia
Campos de Araujo, A.M.	National Cancer Institute, Brazil
Cygler, J.E.	The Ottawa Hospital Regional Cancer Centre, Canada
Grey, J.E.	Landauer, United States of America
Heijmen, B.J.M.	Erasmus Medical Center Rotterdam, Netherlands
Izewska, J.	International Atomic Energy Agency
Jornet i Sala, N.	Hospital de la Santa Creu i Sant Pau, Spain
Kesner, A.	International Atomic Energy Agency
Kukolowicz, P.	Holycross Cancer Centre, Poland
Luo, S.	Chinese Centre for Disease Control and Prevention, China
Marinello, G.	Centre hospitalo-universitaire Henri Mondor, France
Mayles, P.	Clatterbridge Cancer Centre, United Kingdom
Mijnheer, B.	Netherlands Cancer Institute, Netherlands
Mrcela, I.	Sestre Milosrdnice University Hospital, Croatia
Van Dam, J.	University Hospital Gasthuisberg, Belgium
Viegas, C.C.B.	National Cancer Institute, Brazil
Wittych, J.	Holycross Cancer Centre, Poland
Yukihara, E.	Oklahoma State University, United States of America

Consultants Meetings

Vienna, Austria: 8−12 December 2003, 3−7 April 2006, 2−6 June 2008

Research Coordination Meetings

Vienna, Austria: 4−8 April 2005, 15−19 October 2007

IAEA
International Atomic Energy Agency

No. 23

ORDERING LOCALLY

In the following countries, IAEA priced publications may be purchased from the sources listed below, or from major local booksellers.

Orders for unpriced publications should be made directly to the IAEA. The contact details are given at the end of this list.

AUSTRALIA
DA Information Services
648 Whitehorse Road, Mitcham, VIC 3132, AUSTRALIA
Telephone: +61 3 9210 7777 • Fax: +61 3 9210 7788
Email: books@dadirect.com.au • Web site: http://www.dadirect.com.au

BELGIUM
Jean de Lannoy
Avenue du Roi 202, 1190 Brussels, BELGIUM
Telephone: +32 2 5384 308 • Fax: +32 2 5380 841
Email: jean.de.lannoy@euronet.be • Web site: http://www.jean-de-lannoy.be

CANADA
Renouf Publishing Co. Ltd.
Telephone: +1 613 745 2665 • Fax: +1 643 745 7660
5369 Canotek Road, Ottawa, ON K1J 9J3, CANADA
Email: order@renoufbooks.com • Web site: http://www.renoufbooks.com

Bernan Associates
4501 Forbes Blvd., Suite 200, Lanham, MD 20706-4391, USA
Telephone: +1 800 865 3457 • Fax: +1 800 865 3450
Email: orders@bernan.com • Web site: http://www.bernan.com

CZECH REPUBLIC
Suweco CZ, spol. S.r.o.
Klecakova 347, 180 21 Prague 9, CZECH REPUBLIC
Telephone: +420 242 459 202 • Fax: +420 242 459 203
Email: nakup@suweco.cz • Web site: http://www.suweco.cz

FINLAND
Akateeminen Kirjakauppa
PO Box 128 (Keskuskatu 1), 00101 Helsinki, FINLAND
Telephone: +358 9 121 41 • Fax: +358 9 121 4450
Email: akatilaus@akateeminen.com • Web site: http://www.akateeminen.com

FRANCE
Form-Edit
5, rue Janssen, PO Box 25, 75921 Paris CEDEX, FRANCE
Telephone: +33 1 42 01 49 49 • Fax: +33 1 42 01 90 90
Email: fabien.boucard@formedit.fr • Web site: http://www.formedit.fr

Lavoisier SAS
14, rue de Provigny, 94236 Cachan CEDEX, FRANCE
Telephone: +33 1 47 40 67 00 • Fax: +33 1 47 40 67 02
Email: livres@lavoisier.fr • Web site: http://www.lavoisier.fr

L'Appel du livre
99, rue de Charonne, 75011 Paris, FRANCE
Telephone: +33 1 43 07 50 80 • Fax: +33 1 43 07 50 80
Email: livres@appeldulivre.fr • Web site: http://www.appeldulivre.fr

GERMANY
Goethe Buchhandlung Teubig GmbH
Schweitzer Fachinformationen
Willstaetterstrasse 15, 40549 Duesseldorf, GERMANY
Telephone: +49 (0) 211 49 8740 • Fax: +49 (0) 211 49
Email: s.dehaan@schweitzer-online.de • Web site: http://www.goethebuch.de/

HUNGARY
Librotade Ltd., Book Import
PF 126, 1656 Budapest, HUNGARY
Telephone: +36 1 257 7777 • Fax: +36 1 257 7472
Email: books@librotade.hu • Web site: http://www.librotade.hu

INDIA
Allied Publishers Pvt. Ltd.
1st Floor, Dubash House, 15, J.N. Heredi Marg
Ballard Estate, Mumbai 400001, INDIA
Telephone: +91 22 42126969/31 • Fax: +91 22 2261 7928
Email: arjunsachdev@alliedpublishers.com • Web site: http://www.alliedpublishers.com

Bookwell
3/79 Nirankari, Dehli 110009, INDIA
Tel.: +91 11 2760 1283 • +91 11 27604536
Email: bkwell@nde.vsnl.net.in • Web site: http://www.bookwellindia.com/

ITALY
Libreria Scientifica "AEIOU"
Via Vincenzo Maria Coronelli 6, 20146 Milan, ITALY
Tel.: +39 02 48 95 45 52 • Fax: +39 02 48 95 45 48
Email: info@libreriaaeiou.eu • Web site: http://www.libreriaaeiou.eu/

JAPAN
Maruzen Co., Ltd.
1-9-18 Kaigan, Minato-ku, Tokyo 105-0022, JAPAN
Tel.: +81 3 6367 6047 • Fax: +81 3 6367 6160
Email: journal@maruzen.co.jp • Web site: http://maruzen.co.jp

NETHERLANDS
Martinus Nijhoff International
Koraalrood 50, Postbus 1853, 2700 CZ Zoetermeer, NETHERLANDS
Tel.: +31 793 684 400 • Fax: +31 793 615 698
Email: info@nijhoff.nl • Web site: http://www.nijhoff.nl

Swets
PO Box 26, 2300 AA Leiden
Dellaertweg 9b, 2316 WZ Leiden, NETHERLANDS
Telephone: +31 88 4679 263 • Fax: +31 88 4679 388
Email: tbeysens@nl.swets.com • Web site: www.swets.com

SLOVENIA
Cankarjeva Zalozba dd
Kopitarjeva 2, 1515 Ljubljana, SLOVENIA
Tel.: +386 1 432 31 44 • Fax: +386 1 230 14 35
Email: import.books@cankarjeva-z.si • Web site: http://www.mladinska.com/cankarjeva_zalozba

SPAIN
Diaz de Santos, S.A.
Librerias Bookshop • Departamento de pedidos
Calle Albasanz 2, esquina Hermanos Garcia Noblejas 21, 28037 Madrid, SPAIN
Telephone: +34 917 43 48 90
Email: compras@diazdesantos.es • Web site: http://www.diazdesantos.es/

UNITED KINGDOM
The Stationery Office Ltd. (TSO)
PO Box 29, Norwich, Norfolk, NR3 1PD, UNITED KINGDOM
Telephone: +44 870 600 5552
Email (orders): books.orders@tso.co.uk • (enquiries): book.enquiries@tso.co.uk • Web site: http://www.tso.co.uk

On-line orders:
DELTA International Ltd.
39, Alexandra Road, Addlestone, Surrey, KT15 2PQ, UNITED KINGDOM
Email: info@profbooks.com • Web site: http://www.profbooks.com

United Nations (UN)
300 East 42nd Street, IN-919J, New York, NY 1001, USA
Telephone: +1 212 963 8302 • Fax: +1 212 963 3489
Email: publications@un.org • Web site: http://www.unp.un.org

UNITED STATES OF AMERICA
Bernan Associates
4501 Forbes Blvd., Suite 200, Lanham, MD 20706-4391, USA
Tel.: +1 800 865 3457 • Fax: +1 800 865 3450
Email: orders@bernan.com • Web site: http://www.bernan.com

Renouf Publishing Co. Ltd.
812 Proctor Avenue, Ogdensburg, NY 13669, USA
Tel.: +800 551 7470 (toll free) • +800 568 8546 (toll free)
Email: orders@renoufbooks.com • Web site: http://www.renoufbooks.com

Orders for both priced and unpriced publications may be addressed directly to:

IAEA Publishing Section, Marketing and Sales Unit, International Atomic Energy Agency
Vienna International Centre, PO Box 100, 1400 Vienna, Austria
Telephone: +43 1 2600 22529 or 22488 • Fax: +43 1 2600 29302
Email: sales.publications@iaea.org • Web site: http://www.iaea.org/books

13-28371

INTERNATIONAL ATOMIC ENERGY AGENCY
VIENNA
ISBN 978–92–0–141610–0
ISSN 2074–7667